

# A trace metal perspective on biogeochemical processes in the North Sea

---

## **Dissertation**

with the aim of achieving a doctoral degree  
at the Faculty of Mathematics, Informatics and Natural Science

Department of Chemistry

Universität Hamburg

submitted by

**Anna Theresa Siems**

**09.07.2024**



1. Gutachter der Dissertation:

Dr. Daniel Pröfrock

Helmholtz-Zentrum Hereon - Anorganische Umweltchemie

2. Gutachter der Dissertation:

Prof. Dr. Michael Steiger

Universität Hamburg - Anorganische und Angewandte Chemie

Datum der Disputation:

11. Oktober 2024

Prüfungskommission der Disputation:

Prof. Dr. Michael Steiger

Prof. Dr. Florian Scholz

Assoc. Prof. DI Dr. Johanna Irrgeher





This thesis was accomplished from April 2021 to July 2024 in the Department of Inorganic Environmental Chemistry (KUA) and the Department of Aquatic Nutrient Cycles (KCN) at the Helmholtz-Zentrum Hereon in Geesthacht. The project was supervised by Dr. Daniel Pröfrock (KUA) and Dr. Tina Sanders (KCN). An advisory panel consisting of Prof. Dr. Michael Steiger (UHH), Dr. Daniel Pröfrock (KUA), Dr. Tina Sanders (KCN), Dr. Tristan Zimmermann (KUA), Dr. Kirstin Dähnke (KCN) and Assoz. Prof. Dr. Johanna Irrgeher (Montanuniversität Leoben, Austria) met once a year to discuss the progress of the thesis.



## List of peer-reviewed Publications

**Przibilla, A.**, Iwainki, S., Zimmermann, T., & Pröfrock, D. (2023). Impact of storage temperature and filtration method on dissolved trace metal concentrations in coastal water samples. *Water Environment Research*, 95(9), e10922. (<https://doi.org/10.1002/wer.10922>)

Spiegel, T., Dale, A. W., Lenz, N., Schmidt, M., Sommer, S., Kalapurakkal, H. T., **Przibilla, A.**, Lindhorst, S., & Wallmann, K. (2023). Biogenic silica cycling in the Skagerrak. *Frontiers in Marine Science*, 10, 1141448. (<https://doi.org/10.3389/fmars.2023.1141448>)

Hildebrandt, L., Fischer, M., Klein, O., Zimmermann, T., Fensky, F., **Siems, A.**, Zonderman, A., Hengstmann, E., Kirchgeorg, T. & Pröfrock, D. (2024). An analytical strategy for challenging members of the microplastic family: Particles from anti-corrosion coatings. *Journal of Hazardous Materials*, 134173. (<https://doi.org/10.1016/j.jhazmat.2024.134173>)

**Siems, A.**, Zimmermann, T., Sanders, T., & Pröfrock, D. (2024). Dissolved trace elements and nutrients in the North Sea—a current baseline. *Environmental Monitoring and Assessment*, 196(6), 539. (<https://doi.org/10.1007/s10661-024-12675-2>)

**Siems, A.**, Zimmermann, T., Sanders, T., Wieser, M. E. & Pröfrock, D. (under review). Trace metals in Skagerrak sediments – spatial distribution and release under changing oxygen conditions. Under review at *Biogeochemistry*.



# Table of Contents

|   |             |
|---|-------------|
| <b>List of peer-reviewed Publications .....</b>             | <b>I</b>    |
| <b>Table of Contents .....</b>                              | <b>III</b>  |
| <b>List of Abbreviations.....</b>                           | <b>VII</b>  |
| <b>List of Figures .....</b>                                | <b>IX</b>   |
| <b>List of Tables .....</b>                                 | <b>XIII</b> |
| <b>1 Zusammenfassung .....</b>                              | <b>1</b>    |
| <b>2 Abstract.....</b>                                      | <b>3</b>    |
| <b>3 Introduction.....</b>                                  | <b>5</b>    |
| 3.1 The North Sea as a study area .....                     | 5           |
| 3.2 Primary production and nutrients in the North Sea ..... | 7           |
| 3.3 Trace metals in the North Sea .....                     | 7           |
| 3.4 Analytical challenges of trace metal analysis.....      | 10          |
| <b>4 Aim of the Thesis.....</b>                             | <b>13</b>   |
| <b>5 Methods.....</b>                                       | <b>15</b>   |
| 5.1 Chemicals and Labware .....                             | 15          |
| 5.2 Experiments and sampling .....                          | 16          |
| 5.2.1 Filtration method comparison experiment .....         | 16          |
| 5.2.2 Seawater sampling .....                               | 16          |
| 5.2.3 Sediment sampling .....                               | 17          |
| 5.2.4 Sediment incubations .....                            | 18          |
| 5.3 Sample preparation and analysis .....                   | 19          |
| 5.3.1 Seawater filtration .....                             | 19          |
| 5.3.2 Seawater and incubation water analysis.....           | 20          |
| 5.3.3 Sediment analysis.....                                | 21          |
| 5.3.4 Porewater analysis.....                               | 22          |

|          |  |           |
|----------|--|-----------|
| 5.3.5    | Isotopic analysis.....   | 22        |
| 5.4      | Data evaluation.....   | 23        |
| 5.4.1    | Data processing.....   | 23        |
| 5.4.2    | Rare earth element data.....   | 23        |
| 5.4.3    | Principal component analysis .....   | 24        |
| 5.4.4    | Uncertainty calculation and detection limits.....  | 24        |
| <b>6</b> | <b>Results and Discussion .....</b>  | <b>27</b> |
| 6.1      | Effects of storage temperature and filtration method on dissolved trace metal concentrations.....            | 27        |
| 6.1.1    | Detection limits of the filtration setups.....   | 28        |
| 6.1.2    | Comparison of elemental concentrations between filtration setups.....  | 29        |
| 6.1.3    | Impact of storage temperatures on trace metal concentrations .....   | 32        |
| 6.1.4    | Conclusion .....   | 35        |
| 6.2      | Dissolved trace elements and nutrients in the North Sea .....  | 37        |
| 6.2.1    | Results for dissolved metals and nutrients in the North Sea.....   | 37        |
| 6.2.2    | Sources and biogeochemical interactions of trace metals and nutrients in the North Sea .....                 | 44        |
| 6.2.3    | Conclusion .....   | 52        |
| 6.3      | Trace metals in Skagerrak sediments – spatial distribution and release under changing redox conditions ..... | 53        |
| 6.3.1    | Redox conditions in Skagerrak sediments .....  | 54        |
| 6.3.2    | Anthropogenic trace metals in Skagerrak sediments .....  | 56        |
| 6.3.3    | Response of redox conditions in Skagerrak sediments to changing bottom water oxygen levels .....             | 59        |
| 6.3.4    | Response of anthropogenic trace metals in Skagerrak sediments to changing bottom water oxygen levels .....   | 63        |
| 6.3.5    | Conclusion .....   | 65        |

|           |  |            |
|-----------|--|------------|
| <b>7</b>  | <b>Summary and Outlook .....</b>                     | <b>69</b>  |
| <b>8</b>  | <b>References .....</b>                              | <b>71</b>  |
| <b>9</b>  | <b>Appendix.....</b>                                 | <b>87</b>  |
| 9.1       | List of hazardous substances .....                   | 87         |
| 9.2       | Table of peer-reviewed publications .....            | 91         |
| 9.3       | List of conference contributions .....               | 93         |
| 9.4       | List of published data sets .....                    | 95         |
| 9.5       | List of research cruises and sampling campaigns..... | 95         |
| 9.6       | Supplementary Figures .....                          | 97         |
| 9.7       | Supplementary Tables .....                           | 143        |
| <b>10</b> | <b>Danksagungen .....</b>                            | <b>151</b> |
| <b>11</b> | <b>Eidesstattliche Versicherung .....</b>            | <b>153</b> |





## List of Abbreviations

|                   |   |
|-------------------|---|
| BAC.....          | OSPAR background assessment concentration                 |
| BC .....          | OSPAR background concentration                            |
| BEC .....         | background equivalent concentration of ICP-MS measurement |
| CARBOSTORE .....  | project ‘Carbon Storage in German Coastal Seas’           |
| CDR.....          | carbon dioxide removal                                    |
| CTD.....          | conductivity, temperature and depth sensor                |
| DIN.....          | dissolved inorganic nitrogen                              |
| Gd/Gd* .....      | Gd anomaly calculated from Nd and Sm                      |
| $Gd_{anth}$ ..... | percentage of anthropogenic Gadolinium                    |
| GEOTRACES .....   | project on marine biogeochemical cycles of trace elements |
| HREE .....        | heavy rare earth elements (Dy, Er, Ho, Lu, Tb, Tm, Yb)    |
| ICP-MS .....      | inductively coupled plasma mass spectrometry              |
| ICP-MS/MS.....    | inductively coupled plasma tandem mass spectrometry       |
| IQR .....         | interquartile range                                       |
| LOD.....          | limit of detection  |
| LOQ.....          | limit of quantification                                   |
| LREE.....         | light rare earth elements (Ce, Eu, Gd, La, Nd, Pr, Sm)    |
| MAD .....         | median absolute deviation                                 |
| MRI .....         | magnetic resonance imaging                                |
| OSPAR.....        | Oslo and Paris Convention                                 |
| PAAS.....         | Post-Archean Australian Shale                             |
| PCA.....          | principal component analysis                              |
| REE .....         | rare earth elements                                       |
| SD.....           | standard deviation  |
| seaFAST.....      | online preconcentration system for seawater samples       |
| SPM.....          | suspended particulate matter                              |
| WWTP.....         | wastewater treatment plant                                |



## List of Figures

### Main text figures

|   |    |
|---|----|
| Figure 1 Map of sampling area, sampling stations and main currents in the North Sea.....  | 6  |
| Figure 2 Sediment sampling stations in the Skagerrak .....  | 17 |
| Figure 3 Setup and photo of the used filtration setups.....   | 19 |
| Figure 4 Concentrations of Ce, Cu and Mn in filtrates of each sample bottle for both filtration setups.....   | 30 |
| Figure 5 Recovery of filtrate A concentration in filtrate B per filtered bottle in percent ....   | 31 |
| Figure 6 Temporal trends of Ce, Co, Cu, La, Mn and Pb concentrations in the filtrates obtained using filtration setup B .....                                       | 33 |
| Figure 7 Recovery of original elemental concentration in filtrates of filtration setup B after 8, 15, 22, 63 days of storage at both investigated temperatures..... | 34 |
| Figure 8 Boxplots of salinity and dissolved Mo, NO <sub>3</sub> <sup>-</sup> , Cu, Gd and NH <sub>4</sub> <sup>+</sup> in the North Sea                             | 39 |
| Figure 9 Factor loadings of the analyzed variables for the four rotated components .....  | 40 |
| Figure 10 Surface concentrations and depth profiles of salinity, NO <sub>3</sub> <sup>-</sup> and Cu across two south-north and two east-west transects.....        | 41 |
| Figure 11 Correlation of inorganic nitrogen with PO <sub>4</sub> <sup>3-</sup> and percentage of Gd <sub>anth</sub> versus salinity .....                           | 47 |
| Figure 12 Depth profiles of Fe, Mn, Mo, δ <sup>98/95</sup> Mo for sediment and porewater.....   | 54 |
| Figure 13 Depth profiles of As, Cu, Ni, Pb for sediment and porewater profile for As .....  | 57 |
| Figure 14 Dissolved concentrations of Fe, Mn, and Mo as well as δ <sup>98/95</sup> Mo values for aerobic incubations .....  | 60 |
| Figure 15 Dissolved concentrations of Fe, Mn, and Mo as well as δ <sup>98/95</sup> Mo values for anaerobic incubations.....   | 61 |
| Figure 16 Release of Cd, Cu, Ni and Pb from sediments under aerobic and anaerobic conditions between months 0 and 12 .....  | 64 |

## Appendix figures

|   |     |
|---|-----|
| Figure A 1 Relative uncertainty ( $2*SD$ ) of the filtration triplicates for the respective elements and filtration methods ..... | 97  |
| Figure A 2 Concentrations of all investigated elements in filtrates of each sample bottle for both filtration setups .....        | 98  |
| Figure A 3 Temporal trend of all investigated elemental concentrations in the filtrates obtained using filtration setup B .....   | 99  |
| Figure A 4 Water sampling stations and regions for data interpretation in the North Sea   | 100 |
| Figure A 5 Surface concentrations and depth profiles of Cd.....   | 101 |
| Figure A 6 Surface concentrations and depth profiles of Ce.....   | 102 |
| Figure A 7 Surface concentrations and depth profiles of Co.....   | 103 |
| Figure A 8 Surface concentrations and depth profiles of Cu.....   | 104 |
| Figure A 9 Surface concentrations and depth profiles of Dy.....   | 105 |
| Figure A 10 Surface concentrations and depth profiles of Er.....  | 106 |
| Figure A 11 Surface concentrations and depth profiles of Eu.....  | 107 |
| Figure A 12 Surface concentrations and depth profiles of Fe.....  | 108 |
| Figure A 13 Surface concentrations and depth profiles of Ga.....  | 109 |
| Figure A 14 Surface concentrations and depth profiles of Gd.....  | 110 |
| Figure A 15 Surface concentrations and depth profiles of Gd <sub>anth</sub> .....   | 111 |
| Figure A 16 Surface concentrations and depth profiles of Ho.....  | 112 |
| Figure A 17 Surface concentrations and depth profiles of La .....   | 113 |
| Figure A 18 Surface concentrations and depth profiles of Lu .....   | 114 |
| Figure A 19 Surface concentrations and depth profiles of Mn.....  | 115 |
| Figure A 20 Surface concentrations and depth profiles of Mo.....  | 116 |
| Figure A 21 Surface concentrations and depth profiles of Nd.....  | 117 |
| Figure A 22 Surface concentrations and depth profiles of NH <sub>4</sub> <sup>+</sup> .....                                       | 118 |
| Figure A 23 Surface concentrations and depth profiles of Ni .....   | 119 |
| Figure A 24 Surface concentrations and depth profiles of NO <sub>2</sub> <sup>-</sup> .....                                       | 120 |
| Figure A 25 Surface concentrations and depth profiles of NO <sub>3</sub> <sup>-</sup> .....                                       | 121 |
| Figure A 26 Surface concentrations and depth profiles of Pb .....   | 122 |
| Figure A 27 Surface concentrations and depth profiles of PO <sub>4</sub> <sup>3-</sup> .....                                      | 123 |
| Figure A 28 Surface concentrations and depth profiles of Pr.....  | 124 |

|   |     |
|---|-----|
| Figure A 29 Surface concentrations and depth profiles of salinity .....   | 125 |
| Figure A 30 Surface concentrations and depth profiles of $\text{SiO}_4^{4-}$ .....                              | 126 |
| Figure A 31 Surface concentrations and depth profiles of Sm .....   | 127 |
| Figure A 32 Surface concentrations and depth profiles of Tb .....   | 128 |
| Figure A 33 Surface concentrations and depth profiles of Tm .....   | 129 |
| Figure A 34 Surface concentrations and depth profiles of U .....  | 130 |
| Figure A 35 Surface concentrations and depth profiles of V .....  | 131 |
| Figure A 36 Surface concentrations and depth profiles of W .....  | 132 |
| Figure A 37 Surface concentrations and depth profiles of Y .....  | 133 |
| Figure A 38 Surface concentrations and depth profiles of Yb.....  | 134 |
| Figure A 39 Surface concentrations and depth profiles of the sum of LREE.....                                   | 135 |
| Figure A 40 Surface concentrations and depth profiles of the sum of HREE .....                                  | 136 |
| Figure A 41 Boxplot of salinity and all analytes in the North Sea (total) and six regions of the North Sea..... | 137 |
| Figure A 42 Drift results for AL557 st.4 and HE586 st.26.....   | 138 |
| Figure A 43 Drift results for HE586 st.10 (left) and AL557 st.65 (right).....                                   | 139 |
| Figure A 44 Correlation plot of all dissolved analytes with salinity for the six regions of the North Sea.....  | 140 |
| Figure A 45 Dissolved concentrations of Cd, Cu, Ni and Pb in aerobic incubations .....                          | 141 |
| Figure A 46 Dissolved concentrations of Cd, Cu, Ni and Pb in anaerobic incubations ....                         | 141 |



## List of Tables

### Main text tables

Table 1 Anthropogenic sources of selected trace metals ..... 9

Table 2 Initial trace metal concentrations in the incubated Skagerrak sediments ..... 59

### Appendix tables

Table A 1 Blanks, LODs and LOQs for trace metal analysis in chapter 6.1 ..... 143

Table A 2 Validation of trace metal analysis in chapter 6.1 ..... 144

Table A 3 Bottle numbers, storage time and storage temperature for chapter 6.1 ..... 144

Table A 4 Validation, blanks, LOD and LOQ for trace metal analysis in chapter 6.2 ..... 145

Table A 5 Validation of nutrient analysis in chapter 6.2 ..... 146

Table A 6 Results of the PCA with varimax rotation in chapter 6.2 ..... 146

Table A 7 Metadata for the incubated sediments in chapter 6.3 ..... 147

Table A 8 Validation of trace metal analysis in sediments for chapter 6.3 ..... 148

Table A 9 Validation of trace metal analysis in seawater for chapter 6.3 ..... 148

Table A 10  $\delta^{98/95}\text{Mo}$  values for the analyzed reference materials in chapter 6.3 ..... 149

Table A 11 Validation of porewater analysis for chapter 6.3 ..... 149





# **1 Zusammenfassung**

Küstenmeere wie die Nordsee sind verschiedensten anthropogenen Stressoren von Land, Meer und der Atmosphäre ausgesetzt. Gleichzeitig sind die Küstenmeere aber auch ein wichtiger Kohlenstoffspeicher, insbesondere im Kampf gegen den Klimawandel. Da künstliche Verfahren zum Entziehen von Kohlendioxid aus der Atmosphäre das Risiko negativer Nebeneffekte und potenzieller zusätzlicher Verunreinigungen der Umwelt bergen können, wird innerhalb des Projektes CARBOSTORE die Verwundbarkeit und das Potenzial natürlicher Kohlenstoffspeicherprozesse in den deutschen Schelfmeeren untersucht. Im Rahmen von CARBOSTORE konzentriert sich diese Doktorarbeit auf die Untersuchung der Wechselwirkung von Spurenmetallen und Nährstoffen mit den biogeochemischen Prozessen der Kohlenstofffixierung und Remineralisierung. Spurenmetalle spielen eine wichtige Rolle als Mikronährstoffe bei der Remineralisierung, Fixierung und langfristigen Speicherung von Kohlenstoff im Meer. Insbesondere in Küstenregionen können hohe anthropogene Einträge allerdings auch einen negativen Effekt auf die biogeochemischen Prozesse haben.

Die Nordsee ist ein Schelfmeer mit dicht besiedelter Küste und wird durch den Eintrag von Spurenmetallen und Nährstoffen über Flüsse und Atmosphäre, sowie durch direkte anthropogene Eingriffe (z. B. Offshore-Plattformen, Schifffahrt, Fischerei) beeinflusst. Durch die vorwiegend zyklonische Strömung in der Nordsee sammeln sich die Schwebstoffe und (anthropogenen) Kontaminanten aus der gesamten Nordsee im Skagerrak zwischen Norwegen und Dänemark. Als tiefster Teil der Nordsee dient der Skagerrak als Archiv für organischen Kohlenstoff und anthropogene Schadstoffe. Künftige Änderungen der Zirkulationsmuster und Nährstoffeinträge könnten jedoch die Redoxbedingungen in den Sedimenten beeinflussen und damit auch das Speicherpotenzial der Skagerrak-Sedimente für Kohlenstoff und assoziierte Kontaminanten verändern. Um diese Prozesse abzuschätzen, ist eine detaillierte Untersuchung der Quellen und Senken von Spurenmetallen, sowie ihrer Wechselwirkungen mit Nährstoffen und Reaktion auf veränderte Randbedingungen erforderlich, die allerdings zuverlässige analytische Methoden erfordert.

Im Rahmen dieser Doktorarbeit wurden Wasserproben aus der gesamten Nordsee auf gelöste Spurenmetalle und Nährstoffe untersucht. Um die Reproduzierbarkeit und Vergleichbarkeit der Daten zu gewährleisten wurden zuvor zwei Filtrationsmethoden verglichen und die Effekte der gekühlten und gefrorenen Probenlagerung systematisch untersucht. Die entwickelte Filtrationsmethode wurde dann auf die Wasserproben aus der Nordsee

angewandt. Die erhaltenen Spurenmetall- und Nährstoffkonzentrationen wurden verwendet, um Senken, Quellen und ähnliches Verhalten der Analyten innerhalb der Nordsee zu identifizieren. Mit Hilfe statistischer Methoden wurden die Analyten Flusseinträgen, konservativem oder nährstoff-ähnlichem Verhalten zugeordnet. Außerdem ergaben die Daten, dass die Kontamination der Nordsee durch Gadolinium aus MRT-Kontrastmitteln zunimmt. Dies zeigt, dass gründliche Untersuchungen des Verhaltens und Verbleibs dieses und ähnlicher neu auftretender Schadstoffe nötig sind.

Zur Untersuchung der biogeochemischen Prozesse im Sediment wurden an drei Stellen im Skagerrak zusätzlich Sedimentkerne und Porenwasserproben genommen und die Spurenmetallkonzentrationen, sowie  $\delta^{98/95}\text{Mo}$ -Isotopenverhältnisse gemessen. Die Daten zeigten eine heterogene Verteilung von Redoxbedingungen und Kontaminanten innerhalb des Skagerraks. Obwohl die Metalle zwar wahrscheinlich aus anthropogenen Quellen stammten, akkumulierten sie abhängig von den Redoxbedingungen im Sediment. Aerobe und anaerobe Inkubationen der Skagerrak-Sedimente über einen Zeitraum von bis zu einem Jahr deuteten darauf hin, dass durch Veränderungen des Sauerstoffgehalts im Bodenwasser die im Sediment gebundenen Spurenmetalle remobilisiert werden. Darüber hinaus wurde eine starke  $\delta^{98/95}\text{Mo}$ -Fraktionierung in den anaeroben Wasserproben nachgewiesen, und die Inkubationen deuteten darauf hin, dass unter anaeroben Bedingungen Mangan-Reduktion in den Sedimenten von Eisen- und Sulfatreduktion abgelöst wird, selbst wenn noch ausreichend Mangan im Sediment verfügbar ist.

Im Rahmen von CARBOSTORE liefert diese Doktorarbeit die hochaufgelösten Spurenmetall- und Nährstoffdaten, die zur Modellierung von Kohlenstoffspeicherprozessen in der Nordsee nötig sind. Das Inkubationsexperiment hat gezeigt, wie die biogeochemischen Prozesse im Sediment auf Störungen, die im Zuge des Klimawandels zu erwarten sind, reagieren. Zusätzlich zur Nutzung in CARBOSTORE dient diese Arbeit als wichtiger Referenzpunkt für zukünftige Studien und wird helfen, Kontaminationen durch künstliche Kohlenstoffspeichermethoden abschätzen zu können.

## 2 Abstract

Coastal oceans, such as the North Sea, are exposed to various anthropogenic stressors originating from land, the ocean, and the atmosphere. At the same time, coastal oceans are an important carbon reservoir, especially to mitigate climate change. Since artificial carbon dioxide removal techniques harbor the risk of unintended side-effects and potential contamination of the environment, the CARBOSTORE project investigates the vulnerability and potential of natural carbon storage processes in the German shelf seas. As part of CARBOSTORE, this thesis focusses on the interaction of trace metals and nutrients with the biogeochemical processes of carbon fixation and remineralization. Trace metals play an important role as micronutrients for remineralization, fixation, and long-term storage of carbon in the marine environment. However, especially in coastal regions, high anthropogenic contamination may also have a negative effect on biogeochemical processes. The North Sea is a shelf sea with a highly populated coast and affected by direct anthropogenic action (e.g., offshore platforms, shipping, fishing, etc.), riverine trace metal and nutrient inflow and atmospheric deposition. Due to the mainly cyclonic circulation pattern, suspended matter and associated (anthropogenic) contaminants from the entire North Sea accumulate in the Skagerrak between Norway and Denmark. As the deepest part of the North Sea, the Skagerrak serves as an archive for organic carbon and anthropogenic contaminants. However, future changes in circulation patterns and eutrophication might influence sediment redox conditions and subsequently also the storage potential of the Skagerrak sediments for both carbon and buried anthropogenic contaminants. To investigate these processes, detailed knowledge of trace metal sources, sinks, interactions with nutrients and response to changing boundary conditions is needed but can only be achieved with reliable analytical methods.

In this thesis, water samples from the entire North Sea were analyzed for dissolved trace metals and nutrients. To gain reproducible and comparable data, two filtration methods were compared beforehand, and the effects of cooled and frozen sample storage were investigated systematically. The developed filtration method was then applied to the North Sea water samples. The obtained trace metal and nutrient concentrations were used to identify sinks, sources, and mutual behavior of the analytes within the North Sea. With the help of statistical analysis, the analytes were assigned to either the conservative, recycled or riverine group.

Further, the data showed that gadolinium contamination from MRI contrast agents in the North Sea is increasing, calling for thorough studies on behavior and fate of emerging contaminants in the North Sea.

To investigate the biogeochemical processes in the sediment, trace metal concentrations as well as  $\delta^{98/95}\text{Mo}$  isotopic ratios were measured in sediment cores and porewater samples from three locations within the Skagerrak. The data indicated a heterogeneous distribution of both redox conditions and contaminants throughout the Skagerrak. The contaminants were likely of anthropogenic origin but their accumulation depended on the sediment redox conditions. Aerobic and anaerobic incubations of Skagerrak sediments for up to one year indicated that changes in the bottom water oxygen levels will cause the remobilization of bound trace metals from the past decades. Further, a strong  $\delta^{98/95}\text{Mo}$  fractionation in anaerobic water samples was shown and the incubations indicated that under anaerobic conditions, manganese reduction in the sediments will be followed by iron and sulfate reduction, even if sufficient substrate might still be available.

Within the framework of CARBOSTORE, this thesis provides the high-resolution trace metal and nutrient data that is required to model carbon storage processes in the North Sea. The incubation experiment showed how the biogeochemical processes in the sediments respond to perturbations that are likely with a changing climate. In addition to their utilization within CARBOSTORE, the results from this study will be an important reference dataset for future studies and to track perturbations introduced by artificial carbon dioxide removal techniques which might be established in the future.

## 3 Introduction

Coastal oceans like the North Sea are strongly affected by anthropogenic pressure from land, ocean and atmosphere (Emeis et al., 2015). Rivers, atmospheric deposition and point sources like ships and offshore platforms introduce high loads of nutrients and trace metals to the North Sea (BSH, 2016; Byrnes & Dunn, 2020; Laane et al., 2013; OSPAR Commission, 2000; Pacyna et al., 2009). To combat climate change, also marine carbon storage is gaining importance (IPCC, 2022). However, carbon dioxide (CO<sub>2</sub>) removal techniques (CDR) such as ocean fertilization or alkalinity enhancement are controversial due to potential negative side-effects, high costs and complicated legislature (IPCC, 2022). Hence, the natural carbon storage capacity of the North Sea, as well as the processes involved need to be investigated to protect and enhance its natural storage capacity. Within the CARBOSTORE project, the basic principles of carbon uptake, storage and remineralization in the North Sea and Baltic Sea are investigated. Trace metals and nutrients are important players in both carbon uptake and remineralization but high-resolution concentration data as well as a detailed understanding of the key processes and responses to changing conditions are still missing. This thesis contributes to CARBOSTORE by investigating trace metal and nutrient distributions in the North Sea water column and sediments, as well as their response to changing oxygen conditions. The obtained data will be valuable for models and future management strategies, e.g. related to CDR approaches.

### 3.1 The North Sea as a study area

The North Sea is characterized by a mainly cyclonic circulation (Figure 1; OSPAR Commission (2000); Sündermann and Pohlmann (2011)): Currents move along the British coast to the southern North Sea where Atlantic water also enters via the English Channel (OSPAR Commission, 2000). These water masses are transported along the Dutch, German and Danish coast into the Skagerrak where they mix with Baltic Sea water and deep Atlantic water (OSPAR Commission, 2000). Additionally, water masses from the North Atlantic enter the northern North Sea and especially the Norwegian Trench and Skagerrak (OSPAR Commission, 2000). From the Skagerrak, the water masses are exported via the Norwegian Coastal Current to the North Atlantic (OSPAR Commission, 2000). This main circulation pattern is further influenced by the tidal wave that spreads into the North Sea from the North

Atlantic (OSPAR Commission, 2000), leading to water residence times between ~100 days and a few years (Meinte et al., 2001). Several large rivers drain into the North Sea with a mean run-off of 300 km<sup>3</sup> yr<sup>-1</sup> but with variability between regions and in terms of associated contaminants (OSPAR Commission, 2000).

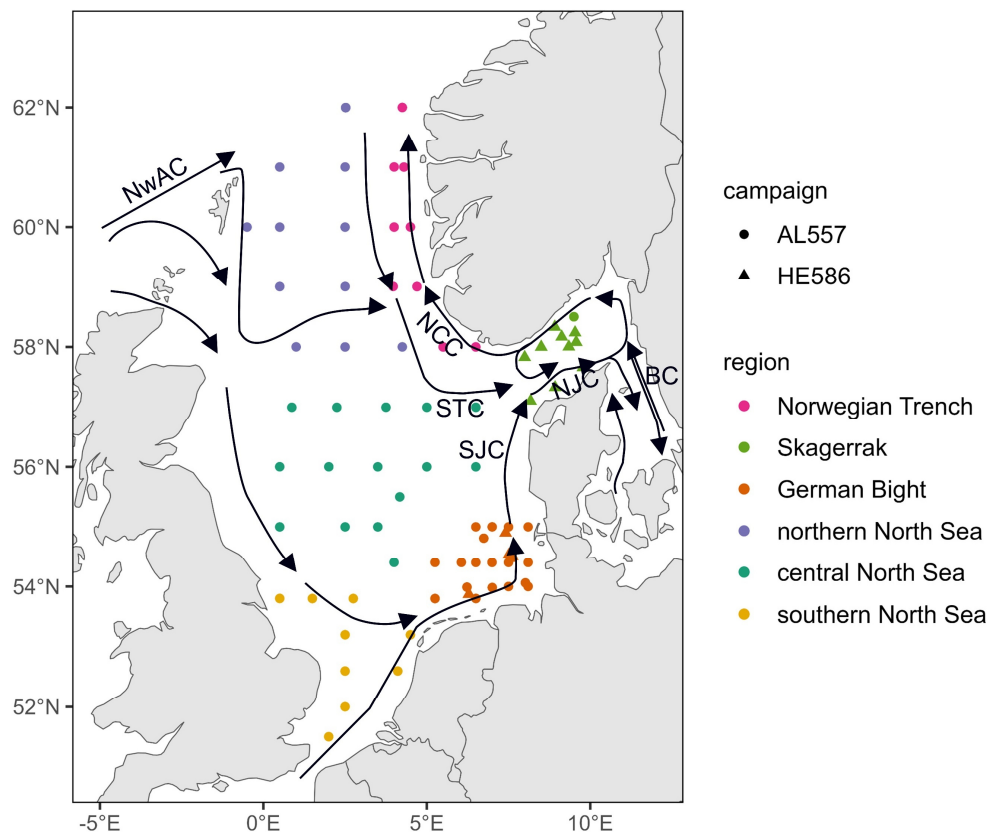


Figure 1 Map of sampling area, sampling stations and main currents in the North Sea. Currents are NwAC – Norwegian Atlantic Current, NCC – Norwegian Coastal Current, STC – Southern Trench Current, SJC – Southern Jutland Current, NJC – Northern Jutland Current, BC – Baltic Current. Currents are redrawn from Brückner and Mackensen (2006). The colored dots indicate the water sampling stations and regions for chapter 6.2 (Siems, Zimmermann, et al., 2024).

Most of the North Sea bottom sediments are sandy with low mud and organic matter contents (Bockelmann et al., 2018; Diesing et al., 2021). Fine-grained sediments from the entire North Sea reach the Skagerrak with the dominating currents. As the Skagerrak is the deepest part of the North Sea, it is the main depot center for fine-grained sediments (e.g., organic matter) and associated trace metals (Canfield, Thamdrup, et al., 1993; Diesing et al., 2021; Logemann et al., 2022). Other areas with fine-grained sediments within in the North Sea are the tidal flats along the Dutch, German and Danish coast, and the Helgoland mud area (Bockelmann et al., 2018; Diesing et al., 2021).

### 3.2 Primary production and nutrients in the North Sea

Marine phytoplankton serves as the basis of the marine food web and accounts for 46% of global carbon fixation by net primary production (Chavez et al., 2011; Field et al., 1998). Alongside light availability and temperature, nutrients are most important for phytoplankton growth (Chavez et al., 2011; Geider, 1987; Wiltshire et al., 2015). The ratio of available nutrient elements (nitrogen (N), phosphorus (P) and silicon (Si)) determines the growth rate of phytoplankton and its community structure (Burson et al., 2016; Redfield et al., 1963).

Nutrients for primary production enter the North Sea with the currents from the North Atlantic and are released during organic matter remineralization in the water column and sediments (Emeis et al., 2015; Pätsch & Kühn, 2008). In coastal regions, nutrients are mainly supplied via rivers with increased nutrient loads from anthropogenic eutrophication (Chaichana et al., 2019; Emeis et al., 2015; Jickells, 1998; Pätsch et al., 2004; Topcu et al., 2011) and especially nitrogen also reaches the North Sea via atmospheric transport (de Leeuw et al., 2003). While the open North Sea is rather N-limited, the coastal North Sea is mostly P-limited due to the high riverine N-inputs (Burson et al., 2016).

The northern North Sea is seasonally stratified while the water column of the southern, shallower North Sea is mainly mixed (Emeis et al., 2015). Due to the high nutrient loads and associated primary production, the southern North Sea acts as a seasonal carbon sink during the spring bloom but releases carbon during remineralization in the remaining seasons (Emeis et al., 2015; Macovei et al., 2021). In contrast, the central and northern North Sea act as carbon sinks year-round due to the remineralization of organic matter in the deeper layers which are exported to the North Atlantic (Bozec et al., 2005; Emeis et al., 2015; Thomas et al., 2004). However, Gröger et al. (2013) simulated that decreasing anthropogenic eutrophication and climate change-dependent change in ocean circulation might reduce nutrient supply and consequently reduce North Sea primary production by up to 35% during the 21<sup>st</sup> century. Thus, detailed knowledge on nutrient distributions in the North Sea is important to detect changes and trends as well as interactions with primary production and carbon storage.

### 3.3 Trace metals in the North Sea

In the open ocean, trace metals either originate from internal recycling or riverine run-off and atmospheric deposition. According to their main behavior in the water column, trace

metals are attributed to three main categories (Kremling et al., 1999): conservative, recycled or scavenged. Conservative elements (e.g., molybdenum (Mo)) are either available in non-reactive forms or present in sufficiently high concentrations to not be affected by biogeochemical processes and consequently correlate strongly with salinity. The concentration of scavenged elements (e.g., lead (Pb), manganese (Mn)) decreases from surface to bottom waters as they adsorb to particles and accumulate in the sediments. Thereby, particles and organic matter can function as a transport vector for these (toxic) metals. Recycled elements (e.g., cadmium (Cd), nickel (Ni)) behave like nutrients, as they are involved in biological cycles, incorporated into organic matter and released upon its remineralization. Hence, recycled elements are depleted in surface waters, but their concentration increases with water depth and increasing organic matter remineralization. Some elements (e.g., iron (Fe), copper (Cu)) exhibit a mixed behavior of scavenging and recycling. However, these open-ocean element profiles are often masked by deviating biogeochemical processes in the coastal regions of the North Sea. For example, nutrient-type behavior is often masked by high riverine input and e.g., Mo is adsorbed to organic matter and released during sediment resuspension in coastal regions (Dellwig et al., 2007).

Trace metals in the water column are of natural (marine, terrestrial) or anthropogenic origin. As these signals mix within the water column and sediments, the anthropogenic and natural contributions are often hard to distinguish. In the North Sea, natural trace metal input occurs by release from the bottom sediments during sediment resuspension or from biogeochemical processes, mixing with Atlantic or Baltic Sea water, wind erosion of soils, rock weathering and riverine input (Canfield, Jørgensen, et al., 1993; Dellwig et al., 2007; Nriagu, 1989; Schlesinger et al., 2017). Anthropogenic trace metals in the North Sea originate either from point sources or riverine run-off and atmospheric deposition (Bakker et al., 2009; BSH, 2016; Goldstein & Jacobsen, 1988; Kremling & Hydes, 1988; Laane et al., 2013; Pacyna et al., 2009; Schlesinger et al., 2017; Ussher et al., 2007). The anthropogenic sources for trace metals relevant within this study are given in Table 1. The main sources are combustion (fuel, coal, wood), industries, fertilizers, and agricultural dust, which release a diverse mixture of trace metals. However, there also are distinct point sources for certain elements like arsenic (As), gadolinium (Gd) and lead (Pb): For example, As was contained in warfare agents that were dumped in the Skagerrak after WWII and now release As from the rusting housings (Tørnes et al., 2002). Gd is used as a contrast agent for MRI exams but cannot be retained by wastewater treatment plants (WWTP) and thus reaches the North Sea via rivers



(Kulaksiz & Bau, 2007). Pb was used in anti-knocking fuel additives until the 1970s and 1980s and elevated concentrations are still found in North Sea sediments (Logemann et al., 2022; Pacyna et al., 2009). As the Skagerrak is the main depot center for particles from the North Sea, its sediments also accumulate the anthropogenic contaminants that reach the North Sea. The periods, in which certain contaminants were released into the environment are distinguishable in the undisturbed sediments of the deep Skagerrak (Logemann et al., 2022).

*Table 1 Anthropogenic sources of selected trace metals. Only those elements that are relevant for this study are shown.*

| anthropogenic source         | element                       | references  |
|------------------------------|-------------------------------|---|
| fuel, oil, coal combustion   | As, Cd, Cu, Mn, Mo, Ni, Pb, V | Nriagu and Pacyna (1988); Pacyna et al. (2009); Schlesinger et al. (2017); Wong et al. (2021) |
| gasoline combustion          | Pb                            | Pacyna et al. (2009)  |
| wood combustion              | As, Cd, Cu, Ni, Pb            | Nriagu and Pacyna (1988)  |
| metal industry               | As, Cd, Cu, Mn, Ni, Pb, V     | Nriagu and Pacyna (1988); Pacyna et al. (2009)  |
| cement production            | As, Cd, Ni, Pb                | Nriagu and Pacyna (1988)  |
| waste incineration           | As, Cd, Cu, Mn, Ni, Pb, V     | Nriagu and Pacyna (1988)  |
| phosphate fertilizer         | Cd, Cu, Ni, Pb, REE           | Nriagu and Pacyna (1988); Ramos et al. (2016)   |
| agricultural dust            | Mo                            | Wong et al. (2021)  |
| anti-fouling paints on ships | As, Cu, Pb                    | Byrnes and Dunn (2020)  |
| WWTP / MRI contrast agents   | Gd                            | Kulaksiz and Bau (2007)   |
| warfare agents               | As                            | Tørnes et al. (2002)  |

Trace metals are involved in various biogeochemical processes: Fe and Mn are required for carbon fixation, Cu, Fe and Mo are used in enzymes for N<sub>2</sub> fixation, nitrification, denitrification and calcification, whereas Cd is needed for silicate uptake in diatoms (Anderson et al., 2014; Morel et al., 2006; Morel & Price, 2003; Schulz et al., 2004). Therefore, the availability of certain trace metals can determine the phytoplankton community structure (Anderson et al., 2014; Sunda, 2012), but increased trace metal concentrations are also toxic for phytoplankton (e.g., Cd, Pb, Cu; Echeveste et al. (2012); Yang et al. (2019)). In the sediments, Fe and Mn oxides are important redox substrates for anaerobic organic matter remineralization (Canfield, Thamdrup, et al., 1993). After reduction of available Fe and Mn oxides, sulfate reduction and methanogenesis follow in the redox cascade, releasing sulfides and methane (Canfield, Thamdrup, et al., 1993). The prevailing redox conditions and availability of metal oxides or sulfides also determine the

mobility of other, potentially toxic, trace metals (Jonge et al., 2012; Neff, 1997; Tankere-Muller et al., 2007). Further, increasing sea surface temperature, decreasing seawater pH and expansion of hypoxic or anoxic zones might impact trace metal redox chemistry (Banks et al., 2012; Hoffmann et al., 2012). Hence, in addition to nutrient inputs, also the supply or absence of certain trace metals impact marine primary production, remineralization, and carbon burial.

#### 3.4 Analytical challenges of trace metal analysis

Since its first publication in 1980 (Houk et al., 1980), inductively coupled plasma mass spectrometry (ICP-MS) quickly developed to the state-of-the-art technique for multi-element analysis of trace metals. The quadrupole mass filter in combination with a collision/reaction cell enables for controlled reaction of the analyte ion and analysis of certain masses with only small interferences (Pröfrock & Prange, 2012). A second quadrupole mass filter before the collision/reaction cell (ICP-MS/MS; tandem mass spectrometry) even refines this result by allowing for two mass-filter steps (Pröfrock & Prange, 2012). With this setup, almost the entire periodic table can be analyzed precisely within only one analysis step and with low detection limits even for complicated matrices like sediment digests (Klein et al., 2021; Zimmermann et al., 2020). However, the high salinity of seawater samples still depresses the signal and causes interferences, both reducing the sensitivity. To avoid sample dilution and associated sensitivity loss, online pre-concentration systems were developed. The *seaFAST* (Elemental Scientific, USA) uses a buffer and two columns with chelating resin to preconcentrate the dissolved metals whilst removing the salt matrix (Sohrin et al., 2008; Wuttig et al., 2019). Thereby, detection limits of  $<1 \text{ ng L}^{-1}$  are reached in time-efficient routine analysis of seawater without manual chromatographic separation (Ebeling et al., 2022; Wuttig et al., 2019).

Although ICP-MS is a robust method, it requires sample preparation in the laboratory prior to analysis. Sediments are freeze-dried, milled, and digested. Although time-consuming, the sediment processing bears little sources for bias by contamination, redox reactions or evaporation, as trace metal contents are high and the total sediment is processed (Zimmermann et al., 2020). In contrast, seawater trace metal concentrations are lower (Bruland et al., 2014) and the water needs to be filtered before analysis of the dissolved concentrations. Adsorption, desorption, precipitation, and redox reactions easily bias the dissolved metal concentrations before and after filtration. Acidification of the filtered

samples prevents precipitation and redox reactions but is not applicable for fixation of unfiltered samples. Therefore, it would be convenient to filter the samples immediately after sampling. However, especially in coastal regions like the North Sea, time and space onboard research vessels are limited as a high spatial resolution of sampling (depths and stations) is required to map the high variability in dissolved trace metal patterns. Further, clean lab space is often not available onboard, causing high contamination risk. Filtration itself also biases the sample, on the one hand due to different definitions of the term “dissolved” (i.e., pore size), on the other hand because of possible contamination, different filter materials or bursting cells under pressure filtration. Considering the low detection limits of seaFAST-ICP-MS, a systematic investigation of the bias introduced by storage and filtration is overdue in order to exploit the full potential of recent analytical developments.



## 4 Aim of the Thesis

Trace metals are important players of the carbon cycle but also affected by anthropogenic perturbations through pollution, climate change and eutrophication. To investigate the interactions of trace metals with the carbon cycle in the North Sea under changing boundary conditions, the sources and sinks of trace metals in the North Sea and the response of the trace metals to changing boundary conditions need to be investigated. However, since there is no consistent method for storage and filtration of coastal water samples, a systematic evaluation of the method is required first. These challenges are addressed by three main research questions within this work:

1. What is needed to process and store seawater while maintaining the original dissolved trace metal concentrations?

The GEOTRACES program developed reliable protocols for open-ocean trace metal sampling (Cutter et al., 2017) but in coastal water sampling, the high concentrations, high sample resolution and limited lab-space call for different sampling methods and challenges. To reliably utilize the precise and sensitive ICP-MS methods available for trace metals in seawater, sampling and sample storage need to be equally reproducible. To increase reproducibility and comparability, different filtration methods and storage conditions will be investigated in this study.

2. What are the spatial distribution, sinks and sources of trace metals in the North Sea and how are they coupled to the nutrient cycle?

North Sea trace metal studies usually only cover certain regions or surface waters. To investigate coupled sources and biogeochemical processes in the water column, nutrient and trace metal data from the same locations are needed without temporal offset. Hence, water samples from the entire North Sea with a high spatial resolution will be analyzed for nutrient and trace metal concentrations to generate a data basis for future research on contamination, eutrophication, and biogeochemical interactions.

3. Do trace metals and redox conditions in the sediments interact and will they be mobilized under changing oxygen conditions?

To investigate climate change effects like changing oxygen supply on carbon burial and remineralization, more information on the vulnerability of sediment redox conditions and

trace metal mobility are needed. The Skagerrak is the main depot center of the North Sea with fine-grained sediments, high organic matter content and a large variety of sediment redox conditions. Thus, the key redox processes, trace metal storage and mobilization can be studied here in spatial vicinity. The information obtained from sediment cores and long-term incubations will form the basis for investigations of the response of carbon and nitrogen sequestration processes to changing redox conditions.

## 5 Methods

### 5.1 Chemicals and Labware

Preparatory laboratory work was performed in a class 10000 clean room inside a class 100 clean bench. Ultrapure water (type I reagent-grade water; resistivity: 18.2 M $\Omega$  cm) was produced by a Milli-Q Integral water purification system equipped with a QPod-Element (Merck Millipore, Germany). Nitric acid (HNO<sub>3</sub> ROTIPURAN<sup>®</sup>,  $w \geq 65\%$ , Carl Roth GmbH&Co. KG, Germany) and hydrochloric acid (HCl ROTIPURAN<sup>®</sup>,  $w = 37\%$ , Carl Roth GmbH&Co. KG, Germany) were further purified by double sub-boiling using PFA acid purification systems (DST4000 & DST-1000, Savillex, USA) operated under clean room conditions. The lower concentrated acids were diluted from the double sub-boiled acids with ultrapure water. Optima grade glacial acetic acid ( $w > 95\%$ , Fisher Scientific, Germany), Optima grade ammonia solution ( $w = 20\text{--}22\%$ , Fisher Scientific, Germany) and ultra-pure HBF<sub>4</sub> ( $w = 38\%$ , Chem-Lab, Belgium) were used without further purification.

*DigiTUBE*<sup>™</sup>s (50 mL and 100 mL, SCP Science, Canada) were rinsed three times with ultrapure water, filled with HNO<sub>3</sub> ( $w = 1.3\%$ ) and allowed to stand for at least one week. Afterwards, they were rinsed three times with ultrapure water and directly used. For Mo isotopic analysis, the *DigiTUBE*<sup>™</sup>s were used directly from the bag. Bottles for sample storage (0.5 L, LDPE, Nalgene<sup>™</sup>, Thermo Scientific<sup>™</sup>, USA; 1 L, LDPE, Brand, Germany) were leached twice with HCl ( $w = 0.3\%$ ) for one week, two weeks with HNO<sub>3</sub> ( $w = 0.3\%$ ) and stored with HNO<sub>3</sub> ( $w = 0.1\%$ ) until use. Before use, they were rinsed thoroughly with ultrapure water and sample water. Canisters (25 L, HDPE, Kautex Textron, Germany) for the large-volume sample (chapter 6.1) were leached with HCl ( $w = 0.3\%$ ) for a week and rinsed thoroughly with ultrapure water and sample water before use. Centrifuge tubes (PP, 15 mL Labcon<sup>®</sup>, USA; 50 mL Greiner Bio-one, Germany) were used for nutrient samples without rinsing.

*DigiFILTER*<sup>™</sup>s (0.45  $\mu$ m, 50 mL, SCP Science, Canada) and Nuclepore<sup>™</sup> polycarbonate filters (0.4  $\mu$ m, 47 mm diameter, Whatman<sup>®</sup>, UK) were acid cleaned in a PTFE or PFA container as follows: after rinsing them three times with ultrapure water, they were stored in HCl ( $w = 0.1\%$ ) for one day, rinsed and stored in HCl ( $w = 0.1\%$ ) for another day. Afterwards, the filters were rinsed and stored in ultrapure water for two days and rinsed again. Then, the *DigiFILTER*<sup>™</sup>s were stored in ultrapure water until use. The Nuclepore<sup>™</sup> filters were

separated into acid-cleaned petri dishes (PS, Greiner Bio-One, Germany) and dried in a laminar flow hood. The PFA filtration bombs and PFA frits (both Savillex, USA) for pressure filtration were mechanically cleaned after use, rinsed with ultrapure water, and leached in HCl ( $w=0.15\%$ ) for three days. Prior to usage, the filtration bombs were rinsed several times with ultrapure water.

## 5.2 Experiments and sampling

### 5.2.1 Filtration method comparison experiment

For chapter 6.1, two 25 L water samples were taken around high tide on June 27<sup>th</sup>, 2022, 11:58 am with a submersible pump at the COSYNA stationary FerryBox system located in Cuxhaven (Germany; 53.877°N, 8.705°E). The pump is protected by a cage made of Cu to reduce unwanted biofilm growth. Indeed, due to the high impact of terrestrial and anthropogenic contaminations in coastal areas, trace-metal clean sampling was not necessary for the experiment. The sample was directly transported to the laboratory and the upper 10 L from both canisters were mixed into a third canister to reduce the sediment content originating from tidal sediment resuspension, which ensured homogeneity of the stored aliquots. From this well-mixed sample, 18 aliquots were filled into the pre-cleaned 1 L LDPE bottles. Eight aliquots were stored frozen (-18 °C), eight aliquots were stored cooled (4 °C), and two aliquots were filtered directly. After storage for 8, 15, 22 and 63 days, aliquots of two cooled and two frozen samples were filtered with filtration setups A and B (see chapter 5.3.1). The frozen samples were thawed at room temperature in a laminar flow bench one night before the filtration was conducted. Before filtration, the samples were again homogenized by shaking for some minutes. All aliquots were chosen randomly.

### 5.2.2 Seawater sampling

The water samples for chapter 6.2 were taken during two cruises in June and October 2021. The cruise in June covered the entire North Sea (RV Alkor, AL557), while the cruise in October (RV Heincke, HE586) focused on the Skagerrak and the German and Danish coast. Sampling stations are shown in Figure 1, additional information on locations, water depths, bottom depths and sampling dates is given in Figure A 4 and PANGEA (Badewien et al., 2022; Siems, Nantke, et al., 2024; Siems, Sanders, et al., 2024). The water samples were taken at several depths with Niskin bottles attached to a CTD (conductivity, temperature, and depth sensor). The ship was positioned against the currents and the Niskin bottles were rinsed



with ambient water during the downcast. For trace element analysis, the water was directly filled into two pre-cleaned 0.5 L bottles during AL557 and into one pre-cleaned 1 L bottle during HE586. Samples were frozen immediately (-20 °C) onboard the ship and filtered with filtration setup B (chapter 5.3.1) in the land-based laboratory under clean room conditions in triplicates. For nutrient analysis, the samples were filtered with cellulose acetate syringe filters (0.47 µm, Minisart, Sartorius, Germany) on AL557 and with glass fiber filters (0.7 µm, 47 mm, Whatman™, USA) on HE586 onboard the ships. The nutrient samples were frozen immediately after filtration until analysis.

### 5.2.3 Sediment sampling

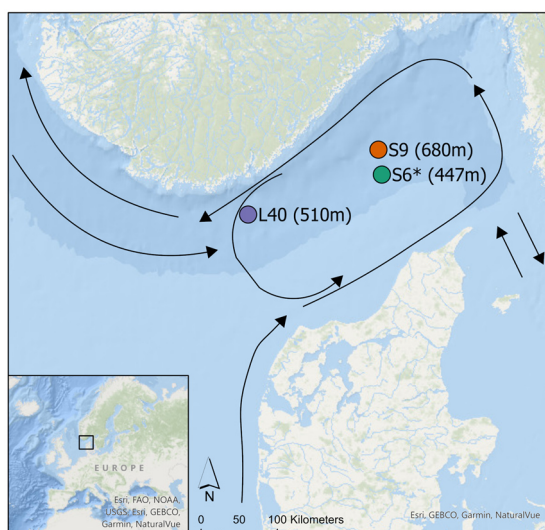


Figure 2 Sediment sampling stations in the Skagerrak. Currents are adapted from Brückner and Mackensen (2006).

Three stations in the Skagerrak were sampled during cruise HE586 (October 2021) with the research vessel Heincke. The station letters and numbers were adopted from earlier publications to avoid confusion: While station S9 (58.2349°N, 9.5346°E) corresponds to earlier studies by Canfield et al., station S6\* (58.0799°N, 9.5746°E) was approximately 3.5 km north of S6 (Canfield, Thamdrup, et al., 1993). Station L40 (57.8304°N, 7.9981°E) corresponds to sampling station 40 from Logemann et al. (2022) (Figure 2). The sediment cores were taken with a Multicorer (Oktopus Kiel) equipped with pre-cleaned transparent acrylic (Poly(methyl methacrylate)) core liners (10 cm inner diameter, 60 cm length). Directly after sampling, the cores were cut into 1 cm slices, stored in pre-cleaned DigiTUBE™s (100 mL) and frozen immediately (-20°C). The samples for the incubation experiment were stored in PP containers (120 mL, ratiolab, Germany) and cooled (4 °C) until

the start of the incubation experiment. Porewaters were extracted from intact cores with rhizon samplers (0.15  $\mu\text{m}$  pore size; Rhizosphere Research Products, Netherlands) and frozen immediately after sampling (2 mL PP cryo vials).

### 5.2.4 Sediment incubations

For the incubations, sediment cores from stations S6\*, S9 and L40 (Figure 2) were used. The upper, middle, and bottom third of each sediment core were well-mixed and subsamples for initial analysis were taken. These layers correspond approximately to fresh, intermediate and old organic material, as the sediments in the Skagerrak are in general undisturbed (Logemann et al., 2022). For the aerobic incubations, glass bottles (100 mL, SCHOTT Duran, Germany) were filled with ~6 g sediment and 65 mL low-nutrient seawater (prepared from artificial low-nutrient seawater (OSIL, UK) and North Sea water). The lid was screwed on loosely to allow for air-exchange and the samples were incubated on a horizontal shaker (110 rpm) in the dark until harvesting after 1-12 months. For anaerobic incubations, glass bottles (125 mL, DWK Life Science, Germany) were filled with ~15 g sediment, filled to the top with low-nutrient seawater and crimp-sealed. The anaerobic bottles were incubated in the dark until harvesting without shaking. For each oxygen condition, core, depth category and time point, a triplicate sample was prepared. The sampling dates, times, coordinates as well as depths that were used for each incubation and the mass of sediments used for each replicate are given in Table A 7.

Upon harvesting after 1, 3, 6 and 12 months, a Helium headspace of 30 mL was added through the seal of the anaerobic bottles. The replaced water was collected with a plastic syringe (50 mL, B. Braun, Germany) while the aerobic samples were taken with a syringe through the open lid. The water was filtered (0.45  $\mu\text{m}$ , Minisart syringe filter, Sartorius, Germany) and acidified to 0.1% (*w/w*)  $\text{HNO}_3$ . Afterwards, the sediment was resuspended in the remaining water, transferred into centrifuge tubes (50 mL) and centrifuged. The settled sediments were transferred into *DigiTUBE*<sup>™</sup>s (100 mL) and frozen immediately. Process blanks (ultrapure water) of the bottles and harvesting process were taken for analytical quality control.

## 5.3 Sample preparation and analysis

### 5.3.1 Seawater filtration

Within this study, two filtration methods were used for dissolved trace metal analysis in seawater: The first setup consisted of custom-made PFA filtration bombs (Savillex, USA) and excess pressure of nitrogen or argon (5.0 purity or better) as shown in Figure 3. For filtration, the acid-cleaned bombs and Nuclepore™ polycarbonate filters (0.4 μm, 47 mm diameter, Whatman®, UK) were assembled and rinsed with 500 mL HCl ( $w=0.3\%$ ), followed by 500 mL ultrapure water. Afterwards, the homogenized sample was filled into the bomb and after discarding a few mL of filtrate, the filtrate was collected into a pre-cleaned *DigiTUBE™* by PFA tubing attached to a lid to prevent unfiltered sample getting into the sample. The rinsing solutions and sample were filtered with a pressure of up to 3 bar. After filtration, the bombs and frits were first rinsed with ultrapure water, afterwards HCl ( $w=0.3\%$ ) and ultrapure water were filtered through the setup. Each day, one filtration blank (ultrapure water) was filtered with each of the three available filtration bombs. This setup will be referred to as setup A throughout the study.

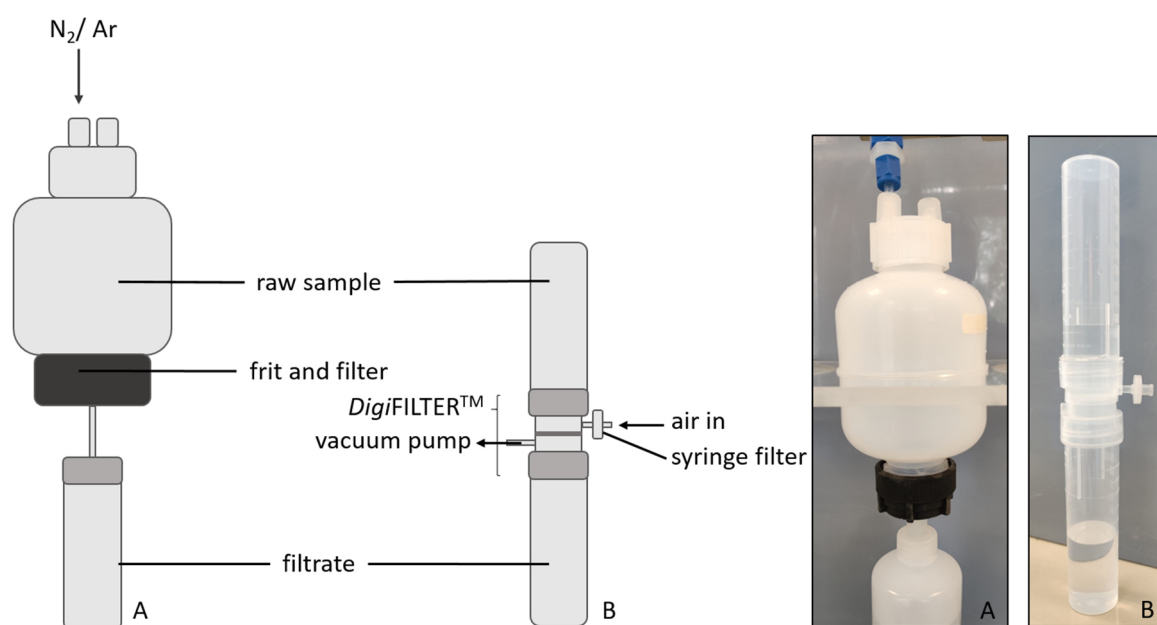


Figure 3 Setup and photo of the used filtration setups. Filtration setup A is on the left and setup B on the right in both the schematic drawing and the photo.

The second filtration method used pre-cleaned *DigiFILTER™*s which were screwed onto two pre-cleaned *DigiTUBE™*s (50 mL) as shown in Figure 3. The air inlet of the *DigiFILTER™*s was equipped with a PTFE syringe filter (Acrodisc, 0.2 μm, 13 mm

diameter, Pall, USA) to minimize potential contamination from airborne dust during vacuum filtration. For rinsing, the upper *DigiTUBE*<sup>TM</sup> was filled with HCl ( $w=0.1\%$ ), screwed onto the filter and attached to a second *DigiTUBE*<sup>TM</sup>. The setup was turned upside down and attached to a manifold connected to a vacuum pump. The filtered acid was discarded, the tube filled with 50 mL homogenized sample and the sample filtered. The manifold allows for parallel filtration of up to 12 samples. Each day, filtration blanks (HCl,  $w=0.1\%$ ) were conducted with one or two *DigiFILTER*<sup>TM</sup>s. This setup will be referred to as setup B throughout the study. For chapter 6.2 samples, the sample tubes were rinsed with a small volume of sample that was discarded before the sample was filtered. Additionally, a few mL of sample were filtered through the *DigiFILTER*<sup>TM</sup> and discarded before the sample was collected.

Both filtration methods were operated under cleanroom conditions and the filtrates were acidified with  $\text{HNO}_3$  to  $0.13\%$  ( $w/w$ ) and stored at  $4\text{ }^\circ\text{C}$  until analysis.

### 5.3.2 Seawater and incubation water analysis

The filtered water samples were preconcentrated online on a *seaFAST* SP2 (Elemental Scientific, USA), coupled to either a collision cell ICP-MS (Agilent 7900, Agilent Technologies, Japan) or an ICP-MS/MS (Agilent 8900, Agilent Technologies, Japan). The *seaFAST* was equipped with two Nobias chelate-PA1 resin columns (HITACHI High-Tech Fielding Corporation, Japan) and the pH was adjusted online with ammonia acetate buffer ( $4\text{ mol L}^{-1}$ ,  $\text{pH } 6.0 \pm 0.2$ ). On the columns, the samples were preconcentrated by a factor of 20 and eluted with  $1.5\text{ mol L}^{-1}\text{ HNO}_3$ . Two external calibration solutions, stabilized in diluted  $\text{HNO}_3$  ( $w=0.14\%$ ), containing 20 and  $1000\text{ ng L}^{-1}$  of each analyte were prepared from custom-made multi-element standards (traceable to NIST standards; Inorganic Ventures, USA). For the external calibration, the syringe module of the *seaFAST* automatically diluted the multi-element solutions to 1, 5, 10, 50, 100, 500 and  $1000\text{ ng L}^{-1}$ . For the analysis in chapter 6.1, additionally a  $5000\text{ ng L}^{-1}$  standard was used in the external calibration. A niobium solution ( $1\text{ }\mu\text{g L}^{-1}$ ) was dosed online to every sample as an internal standard, allowing for drift correction if necessary.  $\text{HNO}_3$  ( $w=0.07\%$ ) wash blanks were measured after each sample triplicate to monitor potential carry-over effects. The *seaFAST* method was used according to Ebeling et al. (2022). The ICP-MS/MS was operated in single-quadrupole mode and both instruments were operated with  $\text{He}/\text{H}_2$  ( $4.0\text{ mL min}^{-1}$ ,  $0.5\text{ mL min}^{-1}$ ) as cell gasses. To maintain a reliable batch-to-batch performance, the instruments were tuned in a weekly

routine with a tuning solution containing lithium (Li), cobalt (Co), yttrium (Y), cerium (Ce) and Thallium (Tl). Potential signal drift was tracked with an in-house multi-element standard solution, measured repeatedly throughout the measurement, containing 250 or 2500 ng L<sup>-1</sup> Fe and Zn and 25 or 250 ng L<sup>-1</sup> of all other analytes. The method was validated with certified seawater reference material (NASS-7, NRC, Canada). Due to the efficient matrix removal of the seaFAST system, this setup allowed for a constant operation over one week. The limits of detection (LOD), limits of quantification (LOQ) and recoveries for reference materials are listed in Table A 1, Table A 2, Table A 4 and Table A 9.

For the determination of the dissolved nutrients, standard colorimetric techniques (Hansen & Koroleff, 2007) and a continuous flow auto analyzer (AA3, SEAL Analytical, Germany) were used. The calibration range was 0-15 µmol L<sup>-1</sup> for ammonium (NH<sub>4</sub><sup>+</sup>), 0-2 µmol L<sup>-1</sup> for NO<sub>2</sub><sup>-</sup> (nitrite), 0-22 µmol L<sup>-1</sup> for NO<sub>3</sub><sup>-</sup> + NO<sub>2</sub><sup>-</sup> (nitrate + nitrite), 0-3 µmol L<sup>-1</sup> for PO<sub>4</sub><sup>3-</sup> (phosphate) and 0-10 µmol L<sup>-1</sup> for SiO<sub>4</sub><sup>4-</sup> (silicate). The samples were measured in duplicates and the analysis was validated with the VKI standards QC SW3.1B and QC SW3.2B (Eurofins, Denmark; 2 µmol L<sup>-1</sup> PO<sub>4</sub><sup>3-</sup> and NH<sub>4</sub><sup>+</sup>, 15 µmol L<sup>-1</sup> SiO<sub>4</sub><sup>4-</sup>, 10 µmol L<sup>-1</sup> NO<sub>3</sub><sup>-</sup> + NO<sub>2</sub><sup>-</sup>, 1 µmol L<sup>-1</sup> NO<sub>2</sub><sup>-</sup>). LODs, LOQs and measured concentrations of the standards are given in Table A 5. Nutrient analysis was performed by the department of Aquatic Nutrient Cycles at the Helmholtz-Zentrum Hereon.

### 5.3.3 Sediment analysis

All sediments were freeze-dried (Christ Gamma, Christ, Germany), sieved (<2 mm) and homogenized by grinding in a planetary ball mill (15 min, 300 rpm, 2 cm agate balls; Retsch, Germany). For trace element analysis, 50 mg aliquots were digested with a mixture of 5 mL HNO<sub>3</sub>, 2 mL HCl and 1 mL HBF<sub>4</sub> in TFM digestion vessels (35 mL, CEM Corp., Germany). The digestion was done at 180°C for 360 min with a MARS 6 microwave (CEM Corp., Germany). Afterwards, the digests were transferred into *DigiTUBE*<sup>™</sup>s (50 mL, SCP Science, Canada) and diluted to 50 mL total volume with ultrapure water. Two reference materials (BCR-2, USGS, USA; GBW07311, CNRM, China) as well as blanks were digested with the samples to validate the method. The sediment digests were measured on an ICP-MS/MS (Agilent 8800, Agilent Technologies, Japan) with He, H<sub>2</sub> and N<sub>2</sub>O as cell/reaction gasses (Klein et al., 2021; Zimmermann et al., 2020). The calibration was prepared daily from custom-made multi-element standards (traceable to NIST standards; Inorganic Ventures, USA) and ranged between 0.1 µg L<sup>-1</sup> and 100 µg L<sup>-1</sup>. Potential signal drift was

tracked with an in-house multi-element standard solution, measured repeatedly throughout the measurement, containing 250  $\mu\text{g L}^{-1}$  Fe and As and 25  $\mu\text{g L}^{-1}$  of all other analytes. An internal standard (Iridium (Ir), Rhodium (Rh)) was dosed online to every sample to allow for drift correction if necessary. Measured isotopes, blanks, LODs, LOQs as well as recoveries of the reference materials and the in-house multi-element standard are given in Table A 8.

### 5.3.4 Porewater analysis

The porewater samples were acidified with 100  $\mu\text{L HNO}_3$  ( $w=65\%$ ) and diluted 10-fold with  $\text{HNO}_3$  ( $w=1.3\%$ ). The diluted porewater samples were measured on an ICP-MS/MS (Agilent 8800, Agilent Technologies, Japan) with  $\text{H}_2$  and  $\text{N}_2\text{O}$  as cell/reaction gases. The calibration was prepared daily from custom-made multi-element standards (traceable to NIST standards; Inorganic Ventures, USA) and ranged between 0.01  $\mu\text{g L}^{-1}$  and 100  $\mu\text{g L}^{-1}$ . Potential signal drift was tracked with an in-house multi-element standard solution, measured repeatedly throughout the measurement, containing 250  $\mu\text{g L}^{-1}$  Fe and As and 25  $\mu\text{g L}^{-1}$  of all other analytes. An internal standard (Ir, Rh) was dosed online to every sample to allow for drift correction if necessary. CASS-6 (NRC, Canada) and SLRS-6 (NRC, Canada) were measured as reference materials. Since the diluted porewater samples still contained high portions of salt, the signal only stabilized slowly. Therefore, the first two data points from triplicate measurements of the same tube were discarded and only the third injection was evaluated. The uncertainty was calculated from four measurements per injection. LODs, LOQs and recoveries for reference materials are given in Table A 11.

### 5.3.5 Isotopic analysis

For the analysis of  $\delta^{98/95}\text{Mo}$  isotopic ratios, equivalents of 75-200 ng total Mo of the sediment digests, water and porewater samples were dried down in *DigiTUBE*<sup>TM</sup>s. Porewater samples were pooled to gain enough Mo. Additionally, IAPSO standard seawater, SRM3134 (NIST, USA), GBW07311 (CNRM, China) digests and BCR-2 (USGS, USA) digests were prepared in the same manner to validate the method. At the university of Calgary, the sediment and water samples were redissolved in 4 mL or 2 mL 3 mol  $\text{L}^{-1}$   $\text{HNO}_3$ , respectively. A  $^{92/98}\text{Mo}$  double spike was added and the sample was dried down in an evaporation unit (*DigiPrep*<sup>TM</sup> Jr, SCP Science, Canada). To homogenize the double spike and prepare the sample for ion exchange, the sample was sequentially redissolved and dried down in 4 mL  $\text{HCl}$  (4 mol  $\text{L}^{-1}$ ) and 100  $\mu\text{L HCl}$  (concentrated) before redissolution in 4 mL 4 mol  $\text{L}^{-1}$   $\text{HCl}$ . For the ion

exchange, Analytical Grade Anion Exchange Resin (1x8, 100-200 mesh, Chloride form, eichrom, USA) and Cation Exchange Resin (100-200 mesh, 50Wx8, Hydrogen form, eichrom, USA) were used. The resins were rinsed with 5 mol L<sup>-1</sup> HNO<sub>3</sub>, ultrapure water and 4 mol L<sup>-1</sup> HCl directly before use. 1 mL glass columns were used for ion exchange. More information on the ion exchange procedure is available in Wieser et al. (2007).

Mo isotope-amount ratios were measured on a Neptune MC ICP-MS (Thermo Fisher Scientific, Germany) operated in low mass resolution mode. Samples were introduced with an ESI SC2-DX autosampler (Elemental Scientific, USA) through a Teflon spray chamber (Elemental Scientific, USA) into a quartz torch. Eight Faraday cups (10<sup>11</sup> Ω resistors) were used to simultaneously measure the ion beams of <sup>91</sup>Zr, <sup>92</sup>Mo, <sup>94</sup>Mo, <sup>95</sup>Mo, <sup>96</sup>Mo, <sup>97</sup>Mo, <sup>98</sup>Mo, <sup>100</sup>Mo. Sample measurements consisted of one acquisition block with 20 measurements. Data reduction was done with a custom-written python script (Mayer & Wieser, 2014; Rudge et al., 2009). The results for the reference materials are given in Table A 10.

## 5.4 Data evaluation

### 5.4.1 Data processing

Multi-element data from ICP-MS and ICP-MS/MS analysis was preprocessed using MassHunter version 4.6 (Agilent Technologies, Japan) and a custom-written Excel spreadsheet. A Dean–Dixon outlier test was performed for all trace element data. Statistics and plots were generated with the free programming language R (R Core Team, 2022), using the package tidyverse (Wickham et al., 2019). The significant number of digits is given according to GUM and EURACHEM guidelines, whereby the uncertainty determines the significant number of digits to be presented with the value (Ellison & Williams, 2012; Magnusson et al., 2015).

### 5.4.2 Rare earth element data

Due to their mutual behavior, the rare earth elements (REE) were summarized as light rare earth elements (LREE; Ce, europium (Eu), Gd, lanthanum (La), neodymium (Nd), praseodymium (Pr), samarium (Sm); Kulaksiz and Bau (2007)) and heavy rare earth elements (HREE; dysprosium (Dy), erbium (Er), holmium (Ho), lutetium (Lu), terbium (Tb), thulium (Tm), ytterbium (Yb)) according to Kulaksiz and Bau (2007). The Gd anomaly (Gd/Gd\*) was calculated from Nd and Sm concentrations and describes the ratio of the measured Gd concentration to the expected Gd concentration (Gd\*), both normalized to the

Post-Archean Australian Shale (PAAS; Kulaksiz and Bau (2007); McLennan (1989)). From this anomaly, the percentage of anthropogenic Gd ( $Gd_{anth}$ ) was estimated (Kulaksiz & Bau, 2007). However, the value can be overestimated by anomalies in Nd and Sm and the natural Gd anomaly of seawater.

### 5.4.3 Principal component analysis

For the PCA (principal component analysis) with varimax rotation in chapter 6.2, the R package psych (Revelle, 2017) was used. To increase the robustness to outliers and account for the different orders of magnitude of the analytes, the data was rank-transformed and then scaled and centered prior to the PCA. For stability testing, the PCA was repeated with the upper and lower values of the measurement uncertainties of each variable. The REE were summarized as LREE and HREE to reduce their impact in the PCA.

### 5.4.4 Uncertainty calculation and detection limits

For the data in chapter 6.1, the background equivalent concentration (BEC) was calculated based on the calibration blanks and the slope of the calibration curve using the MassHunter software (Agilent Technologies, Japan). The given uncertainties of the samples represent twice the standard deviation ( $2*SD$ ) of the filtration replicates. The LOD ( $blank+3*SD$ ) and LOQ ( $LOQ, blank+10*SD$ ) were calculated from the filtration blanks ( $n=14$  and  $n=8$  for setup A and B, respectively) of both filtration setups (MacDougall et al., 1980).

The uncertainties for dissolved trace metals in chapter 6.2 represent  $2*SD$  of the filtration replicates. The LODs and LOQs were calculated from the filtration blanks. Since the filtration blanks were not normally distributed, the median and the median absolute deviation (MAD) of the filtration blanks ( $n=35$ ) were used instead of the mean and the SD to calculate the LOD ( $median+3*MAD$ ) and LOQ ( $median+10*MAD$ ) according to MacDougall et al. (1980). In case the LOD was lower than the BEC of one analysis run, the LOD was set to this value. The LODs and LOQs are given in Table A 4. For the calculation of the median concentrations in chapter 6.2, also the values below the LOD and LOQ were included. For the nutrient concentrations, the uncertainty corresponds to the SD of the duplicate measurement and the LOD and LOQ were calculated based on the error of the calibration line according to the German DIN (DIN32645, 1994) for each campaign separately (Table A 5).



The given uncertainties in chapter 6.3 represent the expanded uncertainty  $U(k=2)$  as a combination of measurement uncertainty and variability between distinct incubation bottles or sediment digests. The expanded uncertainty for the  $\delta^{98/95}\text{Mo}$  analysis was calculated from repeated measurement of a double spike-SRM3134 mixture ( $n=15$ ) and process blanks for the respective matrix. LODs and LOQs are given in Table A 8, Table A 9, Table A 11. The LOD and LOQ of dissolved trace metals in the incubation samples were calculated from the mean and SD of the incubation blanks ( $n=3$ ) for each oxygen condition. The sediment trace metal LOD and LOQ were calculated from the digestion blanks ( $n=42$ ). For the porewater analysis, the LOD and LOQ were calculated from the measurement blanks ( $n=3$ ) and the calibration curve as these were higher than the values calculated from the rhizon blanks.



## 6 Results and Discussion

### 6.1 Effects of storage temperature and filtration method on dissolved trace metal concentrations

Since dissolved trace metals are transported furthest within water masses and organisms take up dissolved metals (Morel & Price, 2003), it is crucial to remove all particles prior to analysis. Filtration is the most common separation method for dissolved trace metals but different pore sizes between 0.2-04  $\mu\text{m}$  are used (Almeida et al., 2023; Bruland et al., 2014; Cutter et al., 2017; Padhi et al., 2013). However, both fractions ( $<0.2 \mu\text{m}$ ,  $<0.4 \mu\text{m}$ ) contain colloidal and not only truly dissolved metals (Bergquist et al., 2007; Dai et al., 1995; Fitzsimmons & Boyle, 2012; Waeles et al., 2008; Wu et al., 2001; Wu & Luther, 1994). This might include clay minerals, Fe and Mn oxides, organic and inorganic metal complexes and humic acids in addition to the free metal ions (Hall et al., 1996). There are various filter membranes (e.g., PTFE, PES, cellulose-nitrate, polycarbonate), pressure or vacuum filtration, single-use and reusable setups (Almeida et al., 2023; Bersuder et al., 2021; BSH, 2016; Cutter et al., 2017; Danielsson, 1982; Hedberg et al., 2011; Park, Choi, Jang, Joe, & Park, 2020; Sohrin et al., 2008; Zhang et al., 2018). Although filter diameter, type and even suspended matter content impact the filtration results by varying adsorption processes or reducing the effective pore size, often only the pore size is reported in literature (Hall et al., 1996; Horowitz et al., 1996a).

For open-ocean cruises, detailed protocols for the filtration of trace metal samples are available (Cutter et al., 2017). In coastal areas, higher trace metal concentrations (Bruland et al., 2014; Harnesa et al., 2022) allow for smaller sample volumes, but diverse biogeochemical processes require higher spatial and depth resolution. The research vessels used for coastal sampling often do not provide sufficient clean lab space. Due to the limited space and time, a decision must be made whether to store samples until processing in land-based laboratories or filter them onboard with lower quality standards. If processed on land, precipitation, adsorption, desorption, and ongoing biological processes during cooled or frozen sample storage prior to filtration are often neglected and require for systematic investigations. Further, open-ocean filtration methods (AcroPak<sup>TM</sup> filter cartridges; Cutter et al. (2017)) are expensive, require elaborate preparation and are hence not suitable for the

high sample-throughput in coastal regions and suspended particulate matter (SPM) collection from the filtered water is not possible with them.

In this chapter, two filtration methods that are suitable for the high number but small volume of water samples that are taken in coastal areas were compared with the aim to find a cost-efficient, reliable, and fast filtration method. In parallel, the effect of storage time and temperature on dissolved trace metal concentrations was investigated systematically. By dividing a large-volume water sample into aliquots that were cooled or frozen for up to 63 days, the storage effects on 22 elements were analyzed.

### 6.1.1 Detection limits of the filtration setups

The LODs for the filtration with pressure bombs and Nuclepore™ polycarbonate filters (setup A, chapter 5.2.1) ranged between 0.007 ng L<sup>-1</sup> for Ho and 2400 ng L<sup>-1</sup> for zinc (Zn; Table A 1). For the filtration with DigiFILTER™s (setup B, chapter 5.2.1), LODs ranged between 0.004 ng L<sup>-1</sup> for Ho and 700 ng L<sup>-1</sup> for Zn (Table A 1). The LODs obtained from the filtration blanks were higher than the LOQs calculated for the seaFAST method (Table A 1). Hence, the elemental concentrations in the filtration blanks originated from the filtration method and were not caused by the analysis method. In general, setup B achieved lower LODs for all analyzed elements except for Mo, uranium (U), vanadium (V) and tungsten (W). The higher LODs for setup A were caused both by the higher mean blank concentration and by the higher SDs between the blanks which were due to randomly distributed elevated blank concentrations. This indicates that setup B is more robust and has a higher repeatability, likely due to the more challenging cleaning procedure and higher risk of contamination for setup A compared to the single-use setup of filtration B. Elevated blank concentrations of Cu and Zn have also been reported by other studies (Gardner & Comber, 1997; Hedberg et al., 2011), partly independent of the pre-cleaning procedure and attributed to contaminations from the membrane, possibly mobilized by the pre-cleaning acid (Hedberg et al., 2011).

Most studies only give the blank values of the analysis method (pre-concentration, ICP-MS; Biller and Bruland (2012); Lagerström et al. (2013); Quéroué et al. (2014)). Thus, the blank concentrations given in this study may be higher than in recently published literature using pre-concentration systems for seawater analysis (Jackson et al., 2018; Samanta et al., 2021; Tonnard et al., 2020). Nevertheless, it is important to monitor all possible contamination sources from sampling to analysis, which is why procedural blanks are given here. Compared

to the filtration blanks presented here, the filtration blanks in other studies of estuarine water were higher for Cd, Cu, Fe, Mn, Pb, Zn ( $1 \pm 0 \text{ ng L}^{-1}$ ,  $360 \pm 60 \text{ ng L}^{-1}$ ,  $1230 \pm 60 \text{ ng L}^{-1}$ ,  $390 \pm 30 \text{ ng L}^{-1}$ ,  $30 \pm 10 \text{ ng L}^{-1}$ ,  $610 \pm 100 \text{ ng L}^{-1}$ ; Zhang et al. (2018)). Except for Pb and Zn in filtration setup A, all LODs of the procedural blanks were sufficiently low to interpret the dissolved elemental concentrations in the analyzed water sample of this study (Table A 1), as well as coastal and estuarine concentrations reported by other studies (BSH, 2016; Harmesa et al., 2022). This indicates that at least filtration setup B is suitable for dissolved trace metal analysis in coastal and estuarine water samples.

### 6.1.2 Comparison of elemental concentrations between filtration setups

The dissolved concentrations of the investigated metals in the directly processed filtrates ( $day=0$ ) using filtration setup B ranged from  $0.29 \pm 0.03 \text{ ng L}^{-1}$  for Tb to  $9320 \pm 50 \text{ ng L}^{-1}$  for Cu and are listed in Table A 1. The concentrations were within the range expected from literature for mean seawater concentrations (La, W, Y; Bruland et al. (2014)), samples taken in the German Bight (Cd, Co, Mn, Pb, Zn; BSH, 2016; Kremling and Hydes (1988)), the sampling station Cuxhaven (Ce, Dy, Er, Eu, Ho, Nd, Pr, Sm, Tb; Petersen et al. (2015)) or mixing experiments for the Elbe river (Mo, V; Schneider et al. (2016)). However, Cu concentrations ( $9320 \pm 50 \text{ ng L}^{-1}$ ) were more than twice as high as reported for the German Bight ( $4000 \text{ ng kg}^{-1}$ ; Kremling and Hydes (1988)). This was most likely caused by the protective Cu cage on the sampling pump as well as the sampling location, which is influenced by riverine input from the German Elbe River. Comparing the results to other studies, similar concentrations of Cd, Co, Fe, Mn, Pb, Zn and even the elevated Cu concentrations were found in other coastal and estuarine waters around Mexico and Asia (Harmesa et al., 2022; Park, Choi, Jang, Joe, Park, et al., 2020; Zhang et al., 2018). Therefore, despite potential contamination of the analyzed sample, the Cu concentrations were still within a realistic range.

To compare both filtration setups in terms of measured elemental concentrations, samples from a well-mixed bottle were filtered with both setups in triplicates. The dissolved concentrations of Ce, Cu and Mn in the filtrates from each bottle are shown in Figure 4 for both setups. The concentrations ranged between  $3.2 \pm 0.5 \text{ ng L}^{-1}$  to  $14.7 \pm 1.2 \text{ ng L}^{-1}$  for Ce,  $8600 \pm 150 \text{ ng L}^{-1}$  to  $11400 \pm 600 \text{ ng L}^{-1}$  for Cu and  $170 \pm 70 \text{ ng L}^{-1}$  to  $3200 \pm 500 \text{ ng L}^{-1}$  for Mn. The Cu concentrations of both filtration setups matched within uncertainty for each filtered bottle. The dissolved concentrations of Mn and even more pronounced Ce were

higher in filtrates of setup A than of setup B and also had higher uncertainties for setup A (Figure 4, Figure A 1). This pattern was independent of the elemental concentration in the analyzed aliquots.

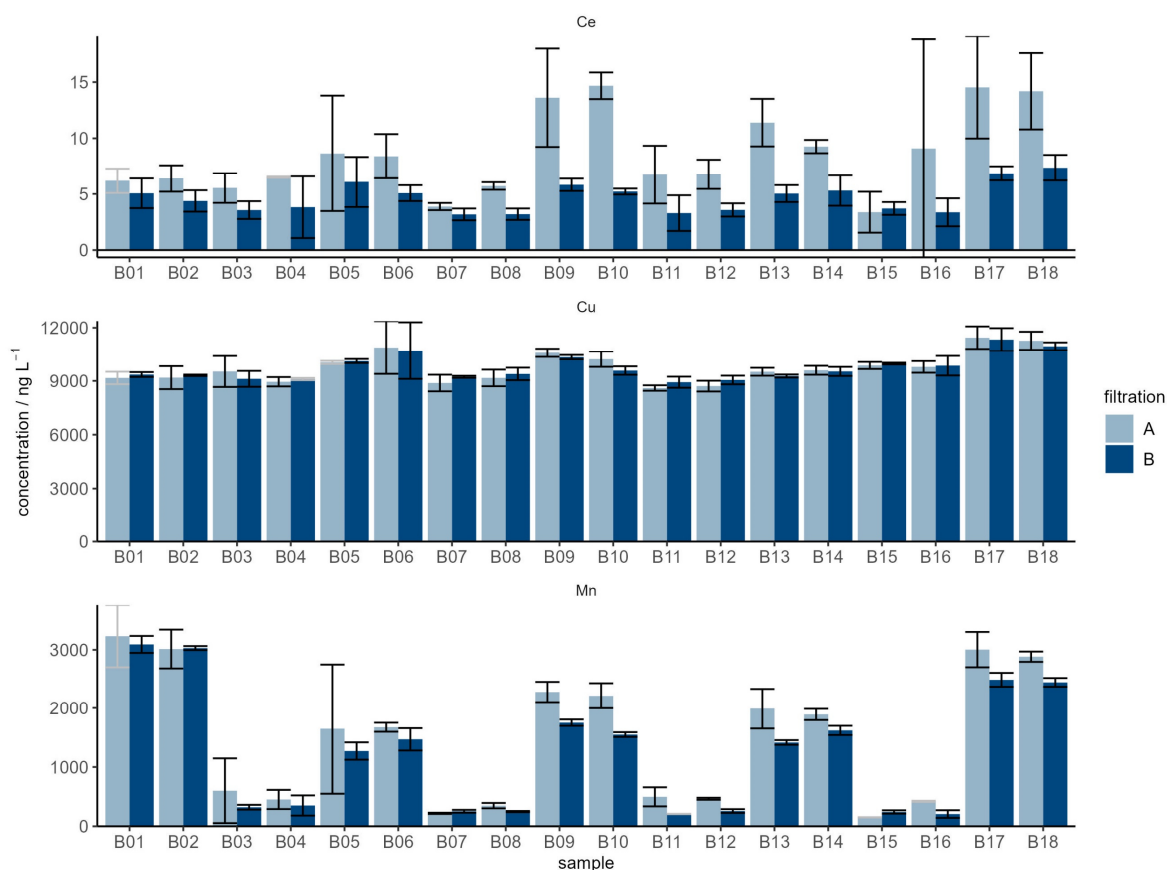


Figure 4 Concentrations of Ce, Cu and Mn in filtrates of each sample bottle for both filtration setups. Each pair of bars corresponds to one sample bottle that was either directly filtered (B01, B02), cooled or frozen (B03-B18) before filtration (Przibilla et al., 2023). Error bars correspond to  $2*SD$  ( $n=3$ , except for grey error bars with  $n=2$  after Dean-Dixon test). Description of samples for respective bottle numbers are listed in Table A 3. Bar plots for all other elements are shown in Figure A 2.

For each analyzed element, the recovery of its concentration in filtrate A in filtrate B is summarized in Figure 5 with one data point per bottle. Values around 100% indicate similar concentrations in the filtrates of setup A and B (Cd, Co, Cu, Dy, Er, Ho, Mo, U, V, W, Y, Zn; median 98% for V to 110% for Dy), while values  $>100\%$  indicate that the elemental concentration was higher in filtrate A than in filtrate B (Ce, Eu, Fe, La, Mn, Nd, Pb, Pr, Sm, Tb; median 120% for Tb to 410% for Fe). The size of the box illustrates whether the similarity between both setups was found for most samples: A small box indicates that the concordance of the two setups was apparent in most samples (e.g., Cd, Cu, Mo, U, V, W), while a large box indicates varying deviations between both setups (e.g., Ce, Fe, Mn, Pb).

The statistical significance of differences between both setups was tested with a paired t-test ( $\alpha=0.05$ , colors in Figure 5). The small deviations between the setups for Cd, Cu, Mo, U, V, W and Zn in all samples were not significant, indicating that both filtration setups had no or the same impact on these elements. Except for Zn, all elements of this group showed relative uncertainties of <20% between filtration triplicates for most samples (Figure A 1). Zn had higher relative uncertainties for both setups, likely caused by the contamination issue which was also reported by other studies (Gardner & Comber, 1997; Hedberg et al., 2011). This indicates that both setups are appropriate to generate repeatable and consistent results for dissolved Cd, Cu, Mo, U, V and W in coastal water samples.

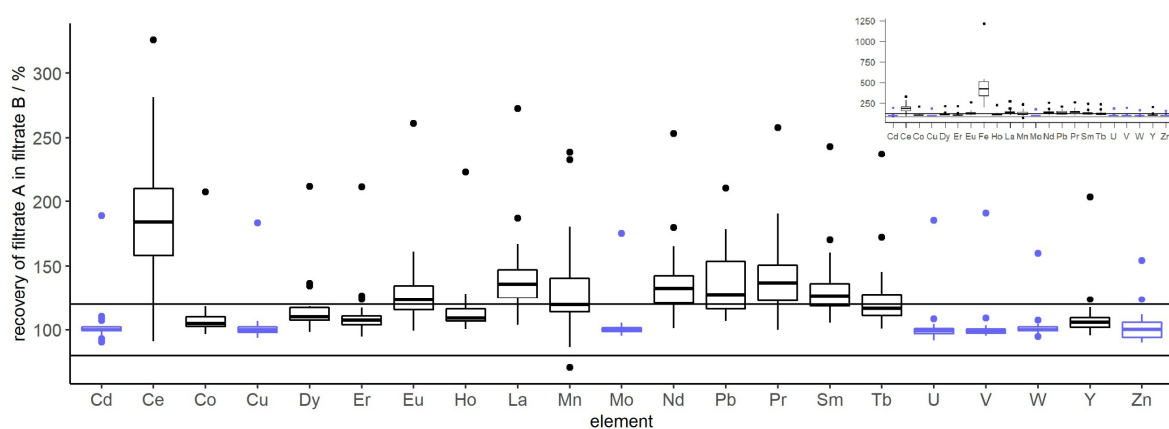


Figure 5 Recovery of filtrate A concentration in filtrate B per filtered bottle in percent. Each data point was calculated from three filtration replicates per setup. Values larger than 100% indicate that filtrates from filtration setup A had higher concentrations than filtrates from filtration setup B. Blue boxes represent elements that do not differ significantly (paired t-test,  $\alpha=0.05$ ,  $n=18$ ) between filtration setup A and B. The small graph has a larger y-axis and includes Fe (Przibilla et al., 2023).

For Ce, Co, Dy, Er, Eu, Fe, Ho, La, Mn, Nd, Pb, Pr, Sm, Tb and Y, filtration setup A yielded significantly higher dissolved concentrations than filtration setup B (Figure 5). Only for Co, Dy, Er, Ho and Y, the recovery of filtrate A in filtrate B was between 80% and 120% for most samples (Figure 5). For Fe, the median recovery of filtrate A in filtrate B was 410% (Figure 5). The significant difference of around 900 ng L<sup>-1</sup> Fe was unlikely caused by contamination from the setup, as the highest blank for Fe was 180 ng L<sup>-1</sup> for setup A. Consequently, reasons for the higher concentrations in filtrate A than filtrate B must have either been adsorption of the mentioned elements to the filter of setup B or different behavior of colloidal forms in both setups (Danielsson, 1982; Horowitz et al., 1992). Horowitz et al. (1992) assumed that the higher pressure of pressure filtration might force colloids through the filter. The different filter diameters (47 mm and 28 mm for filtration A and B, respectively), filter thickness and material might also have played a role, as they affect dead

volume, sorption processes and equilibration of elements on the filter (Horowitz et al., 1992). Clogging of the filter as observed by several other studies (Danielsson, 1982; Horowitz et al., 1992; Karlsson et al., 1994) is unlikely, as the flow rate did not change during filtration and only small volumes (50 mL) were filtered for this study. Since the “true” concentration of the elements with significant differences between the setups is unknown for the analyzed sample, it is not possible to decide which filtration setup gave the more precise results. However, the relative uncertainty of filtration triplicates was mostly higher for setup A (Figure A 1), indicating that setup B is more robust than setup A. In follow-up studies, the processes leading to the differences between both methods could be investigated in more detail by digestion of filters and total water samples as well as comparison with other methods for direct determination of dissolved metal concentrations (e.g., stripping voltammetry; Hedberg et al. (2011)).

### 6.1.3 Impact of storage temperatures on trace metal concentrations

Since filtration setup B (*DigiFILTER*<sup>TM</sup>) yielded lower blank concentrations for most elements and in general lower uncertainties between the filtration replicates than setup A, the impact of storage conditions was evaluated on filtrates from setup B only. To investigate the effects of storage conditions, aliquots of a large-volume sample were frozen (-18 °C) and cooled (4 °C) for 8, 15, 22 and 63 days before filtration and analysis.

In Figure 6, the dissolved concentrations of Ce, Co, Cu, La, Mn and Pb are shown for frozen and cooled samples after different storage durations. The data basis is the same as for Figure 4 and shows the same concentration ranges but the Dean-Dixon outlier test was performed on the six replicates per temperature and day. The assignment of temperature and day to the bottles is given in Table A 3. Within nine weeks, the concentrations of dissolved Co, Mn and Pb in the cooled samples significantly decreased to 36%, 7%, and 37% of the initial dissolved concentration, respectively (Figure 6). In open waters, dissolved Pb is very particle-reactive and removed by scavenging, while dissolved Mn is removed from the water column by oxidation (e.g., by bacteria), with Co co-precipitating or being taken up by organisms (Krauskopf, 1956; Mellett et al., 2018). These processes might also take place during cool storage. A decrease in Pb concentrations during storage was also observed by (Mart, 1979). In contrast, the dissolved concentrations in the frozen samples remained within the uncertainty of the initial concentration for Co and Pb but fluctuated and decreased to 81% of the initial concentration after nine weeks for Mn (Figure 6). The higher final concentration



of dissolved Mn in the frozen samples together with the more constant Co and Pb concentrations support the hypothesis of co-precipitation in the cooled samples. Apparently, the observed problems for Co and Pb can be tackled by freezing the samples while for Mn, either the equilibrium between Mn, SPM and the oxidation process during freezing/thawing caused this pattern or the processes were too heterogeneous to be monitored by the number of analyzed samples.

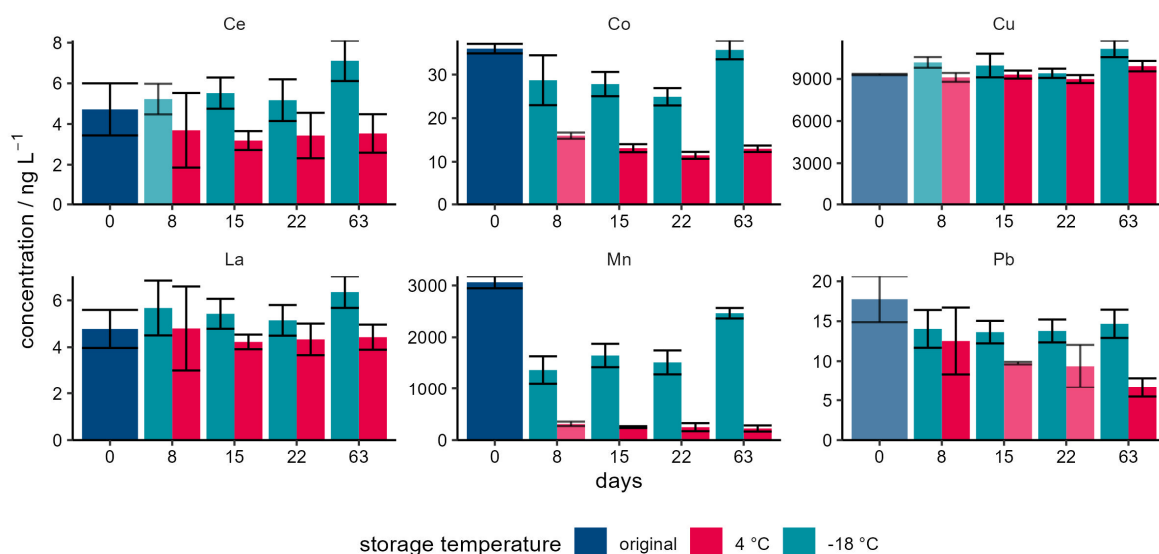


Figure 6 Temporal trends of Ce, Co, Cu, La, Mn and Pb concentrations in the filtrates obtained using filtration setup B. Error bars correspond to  $2*SD$  with  $n=6$  (except for pale-colored bars with  $n=5$  after Dean-Dixon test). Please note that the x-axis is not chronologically spaced (Przibilla et al., 2023). Data for all other investigated elements is shown in Figure A 3.

The recoveries of the elemental concentration of the initially filtered sample (100%) in the filtrates of the cooled and frozen samples was calculated based on the data shown in Figure 6 and Figure A 3 and is summarized in the boxplot of Figure 7. Each box summarizes the data after storage for 8, 15, 22 and 63 days for the respective metal. For most metals, the recoveries ranged between 80-120%, indicating that changes during storage were covered by the measurement uncertainty and sample heterogeneity. For Co, Mn and Pb, the recoveries were lower than 80% for at least one storage temperature (Figure 7), indicating that these elements were not stable in dissolved phase during storage as discussed before. In literature, Cd is described to be removed from the water column by adsorption (Krauskopf, 1956), but in this experiment the Cd recovery was close to 120% for all storage days (Figure 7). As no clear temporal trend and impact of storage temperature on dissolved Cd concentrations was visible (Figure A 3), the initial concentration might have been negatively biased. Despite the affinity of Mo to Mn oxides (Berrang & Grill, 1974), Mo, U, V and W exhibit rather

conservative behaviors in the ocean (Bruland et al., 2014; Graßhoff et al., 1999; Ku et al., 1977; Shiller & Boyle, 1987). The dissolved concentrations of these metals were close to 100% recovery both in the frozen and in the cooled samples with only small deviations. Fe and Zn concentrations seem to have decreased slightly during storage, but all changes were within the uncertainties of these analytes (Figure A 3).

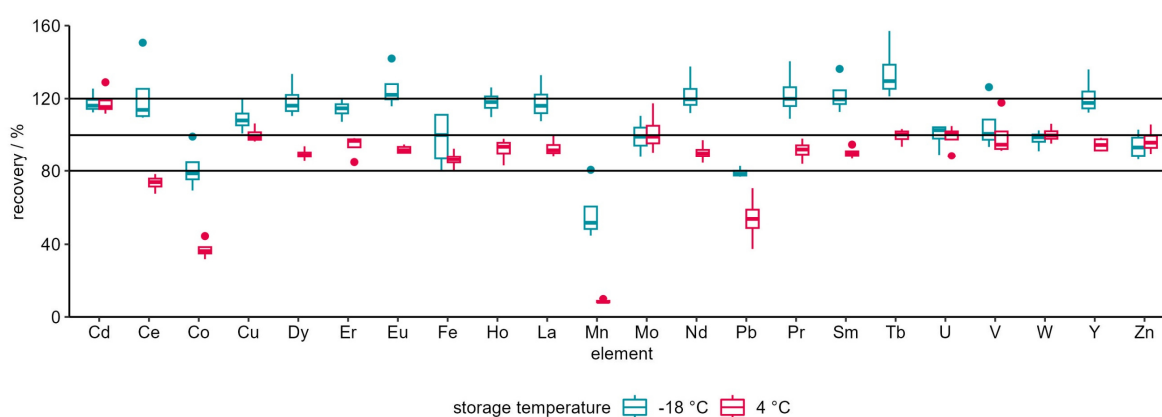


Figure 7 Recovery of original elemental concentration in filtrates of filtration setup B after 8, 15, 22, 63 days of storage at both investigated temperatures ( $n=4$ ) (Przibilla et al., 2023).

The concentrations of dissolved Ce and La decreased within the uncertainty range in the cooled samples and increased by more than the uncertainty range in the frozen samples (Figure 6). The high uncertainties were caused by the general low elemental concentrations. The decrease in Ce concentrations might have been caused by oxidation and precipitation of dissolved Ce, which predominantly takes place on Mn-oxyhydroxides (de Baar et al., 1991; Sholkovitz et al., 1994). Adsorption of REE to particles removes them from the dissolved phase (Byrne & Kim, 1990) and these elements are also involved in biological processes (Cotruvo Jr, 2019). The increase in Ce and La concentrations in the frozen samples might have been caused by desorption from SPM, as changes in pH, temperature or biological/chemical processes can change their sorption equilibrium (Byrne & Kim, 1990). Further, bursting phytoplankton cells during the freezing/unfreezing process might release additional dissolved metals (Batley & Gardner, 1977). The same trends as for Ce and La also apply for the other analyzed REE (Dy, Er, Eu, Ho, Nd, Pr, Sm, Tb, Y; Figure 7). For Cu, also a slight increase in the frozen samples was observed but cooled samples remained constant (Figure 6, Figure 7).

Overall, the results of the storage experiment imply that samples should be filtered directly after sampling. If immediate filtration of the samples is not possible, frozen storage should

be preferred but the effect of storage conditions on each investigated element needs to be considered during evaluation.

#### 6.1.4 Conclusion

Emphasizing other authors' results (Hedberg et al., 2011; Horowitz et al., 1992; Horowitz et al., 1996b), this chapter highlights the importance of giving a detailed description of the filtration method when publishing dissolved metal concentrations. Based on the results, the single-use *DigiFILTER*<sup>TM</sup>s are recommended for coastal water samples as they are easy to handle, very time-efficient (12 samples can be handled at once) and less prone to contamination from the surrounding atmosphere or potential carry-over from previously filtered samples. To further improve their robustness, the sample tubes should be rinsed with a small volume of sample that is discarded before the sample is filtered. Additionally, a few mL of sample should be filtered through the *DigiFILTER*<sup>TM</sup> and discarded before the sample is collected. The application of the *seaFAST*-ICP-MS/MS setup allowed to study the impact of the different tested parameters on a variety of metals simultaneously. However, although most studies only report the measurement blank of the analysis method, it was shown that it is crucial to report a method blank that was exposed to the same processes (e.g., filtration) as the samples.

Even though sample storage is often unavoidable due to limited space and time during sampling campaigns, its effect on the samples is often neglected. The storage experiment showed that cooled and frozen storage of unfiltered coastal water samples introduces large bias to the dissolved concentrations of certain elements like Co, Mn, Pb or REE. The bias is variable and different for each element, likely also dependent on the non-dissolved sample composition (colloids, SPM content and grain size; Horowitz et al. (1992)). Therefore, water samples should be filtered directly after sampling in a metal-free lab space, preferably under clean room conditions or in a clean bench. In the lack of clean lab space, the samples should be frozen and filtered as soon as possible after sampling. In that case, it needs to be considered that the analysis results do not necessarily reflect the original dissolved concentration.

The issues addressed in this chapter are not limited to coastal water samples, but similar effects of storage and filtration are possible for all types of water samples (e.g., river water, surface water, groundwater, open ocean water) and analytes. Therefore, these effects need to be investigated and minimized for different dissolved constituents and matrices.

As a result of the work carried out during this thesis, the paper “Impact of storage temperature and filtration method on dissolved trace metal concentrations in coastal water samples” was published in *Water Environment Research* by A. Przibilla, S. Iwainki, T. Zimmermann, and D. Pröfrock (<https://doi.org/10.1002/wer.10922>).

### **Author Contributions**

S. Iwainki and A. Siems performed all analytical chemistry work. A. Siems conducted the data analysis and prepared the initial draft of the paper. T. Zimmermann contributed to drafting and editing the paper. D. Pröfrock obtained funding, provided supervision and guidance on writing and final drafting the paper.

## 6.2 Dissolved trace elements and nutrients in the North Sea

The North Sea is an important sink for CO<sub>2</sub> which is bound physically and by primary production (Bozec et al., 2005; Chaichana et al., 2019; Thomas et al., 2004). Primary producers rely not only on the typical nutrient elements N, P and Si but also on trace elements like Co, Cu, Cd, Fe, Mn and Ni, e.g., for the synthesis of enzymes related to nutrient and carbon uptake or nitrogen sequestration (Croot et al., 2002; Morel, 2008; Morel & Price, 2003; Pinedo-González et al., 2015; Redfield et al., 1963; Schulz et al., 2004). However, increased metal concentrations can also hamper phytoplankton growth (Echeveste et al., 2012; Yang et al., 2019) and the effects of recently introduced new anthropogenic metal contaminants like Gd or other REE are still not sufficiently investigated. As the available elements and their concentrations strongly affect the phytoplankton community structure and productivity (Sunda, 2012), they also affect carbon fixation, its export and long-term storage. Thorough data sets of combined nutrient and trace metal data with high resolution (spatial, depth) are required to determine the combined effects of these analytes on primary production, to track future changes and to perform model calculations. Although both trace metals and nutrients have been thoroughly monitored in the North Sea (Bozec et al., 2005; BSH, 2016; Chaichana et al., 2019; Frigstad et al., 2020; Hydes & Kremling, 1993; Raabe & Wiltshire, 2009), no North Sea wide combined data set is available and monitoring cruises often only cover a small number of elements.

To investigate the spatial distribution, sinks and sources of trace metals in the North Sea and their interaction with the nutrient cycle, 337 North Sea water samples from two cruises were analyzed for dissolved nutrients and 26 dissolved trace elements. Despite seasonal differences between the two cruises, a PCA was applied to the data set to reveal mutual behavior of the analytes.

### 6.2.1 Results for dissolved metals and nutrients in the North Sea

In total, 337 water samples with salinities >28.5 psu were analyzed for the concentration of 26 elements (Cd, Ce, Co, Cu, Dy, Er, Eu, Fe, Gd, Ho, La, Lu, Mn, Mo, Nd, Ni, Pb, Pr, Sm, Tb, Tm, U, V, W, Y, Yb) and for the nutrients NH<sub>4</sub><sup>+</sup>, NO<sub>2</sub><sup>-</sup>, NO<sub>3</sub><sup>-</sup>, PO<sub>4</sub><sup>3-</sup> and SiO<sub>4</sub><sup>4-</sup>. Salinity, water depth, coordinates and concentrations are published in PANGEA (Badewien et al., 2022; Siems, Nantke, et al., 2024; Siems, Sanders, et al., 2024). Surface concentrations and depth profiles for each analyte as well as for the sums of LREE and HREE are given in

Figure A 5 to Figure A 40. The samples had to be frozen and filtered later in the land-based laboratory since no clean lab space was available on board.

Due to the size of the data set, a PCA was performed to identify major trends. To give an overview of the data set, analytes that represent each component are summarized in Figure 8 and will be described before the results of the PCA (Figure 9) are discussed. For a better understanding of trends in the data set, the sampling stations were divided into six groups (Figure 1, Figure A 4) by means of their geographic location: The southern, central and northern North Sea were subdivided along the 54° and 57° latitude. Additionally, the regions Skagerrak, German Bight and Norwegian Trench were approximated as they are influenced by either water mass mixing or riverine input (Topcu et al., 2011; Winther & Johannessen, 2006) and were thus expected to show a deviating behavior. Where applicable, the samples were further divided into the deepest (bottom), shallowest (surface) and all intermediate samples per station.

### 6.2.1.1 *Trace metal and nutrient concentrations*

The salinity ranged from 28.9 psu at a surface station in the Skagerrak to 35.3 psu at intermediate depth in the northern North Sea (Figure 8a, Figure 10a). The northern North Sea showed the highest median salinity (35.1 psu) and the lowest variability, as illustrated by the interquartile range (IQR; 0.23 psu), while the German Bight had the lowest median salinity (33.0 psu, IQR=1.0 psu). The Skagerrak showed the highest variability (IQR=2.7 psu; Figure 8a) due to the low surface salinity from Baltic Sea inflow compared to intermediate and bottom water samples. The salinity increased with depth and to the Northwest, while especially in the German Bight, Skagerrak and Norwegian Trench, low-salinity surface water was found (Figure 10a).

Mo concentrations were homogeneously distributed (IQR between 700 and 1500 ng L<sup>-1</sup>) between all regions and showed both minimum ( $4700 \pm 2300$  ng L<sup>-1</sup>) and maximum ( $10700 \pm 2500$  ng L<sup>-1</sup>) concentrations within the Skagerrak (Figure 8b). The highest median Mo concentrations (8500 ng L<sup>-1</sup>) occurred in the Norwegian Trench and the lowest median Mo concentration was found for the central North Sea (8050 ng L<sup>-1</sup>, Figure 8b).

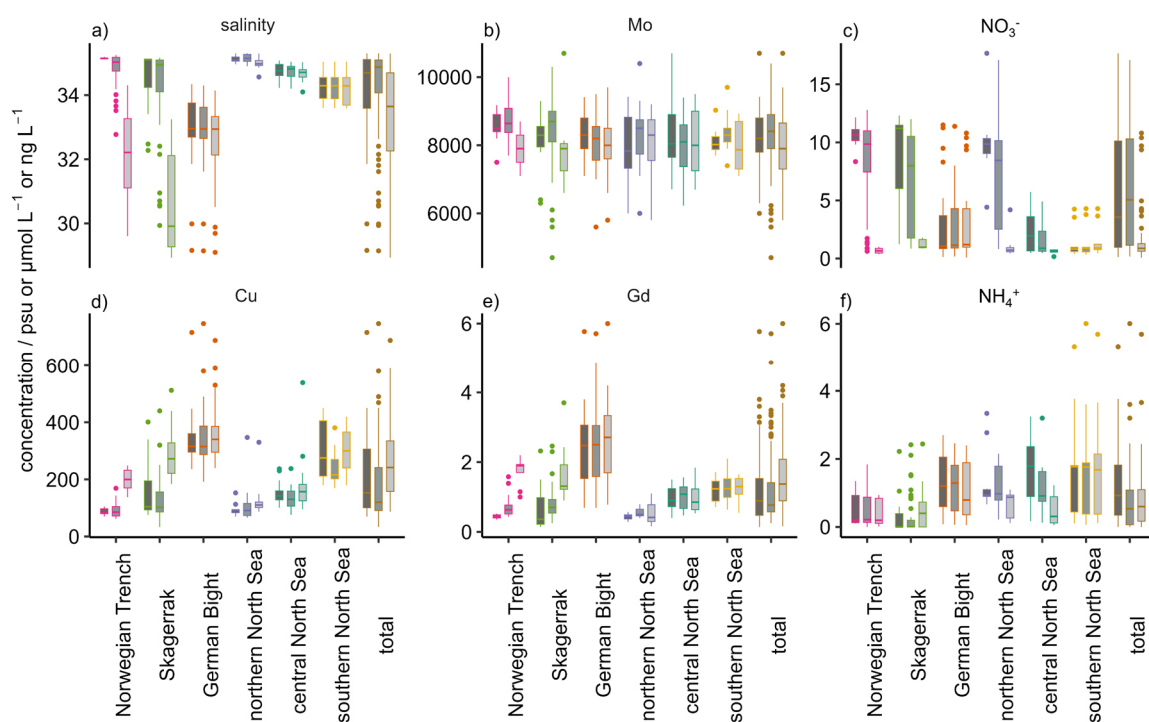


Figure 8 Boxplots of salinity and dissolved Mo,  $\text{NO}_3^-$ , Cu, Gd and  $\text{NH}_4^+$  in the North Sea. Salinity (a) and concentrations of Mo (b),  $\text{NO}_3^-$  (c), Cu (d), Gd (e),  $\text{NH}_4^+$  (f) are given for the total North Sea and split into six regions of the North Sea according to their location (see text for more information). The three boxplots per region indicate bottom (dark grey), intermediate depth (medium grey) and surface (light grey) samples (Siems, Zimmermann, et al., 2024). Boxplots of all investigated parameters are shown in Figure A 41.

The concentration of  $\text{NO}_3^-$  ranged between  $<0.17 \mu\text{mol L}^{-1}$  in the German Bight and  $17.67 \pm 0.23 \mu\text{mol L}^{-1}$  in the northern North Sea.  $\text{NO}_3^-$  concentrations showed a high variation within all regions (IQR 3-9  $\mu\text{mol L}^{-1}$ ), except for the southern and central North Sea (IQR 0.5 and 1.7  $\mu\text{mol L}^{-1}$ , respectively) which also showed lowest median  $\text{NO}_3^-$  concentrations (0.9 and 0.7  $\mu\text{mol L}^{-1}$ , respectively; Figure 8c). Surface concentrations of  $\text{NO}_3^-$  were below 4  $\mu\text{mol L}^{-1}$  throughout most of the North Sea but reached more than 10  $\mu\text{mol L}^{-1}$  in the German Bight where they correlated negatively with salinity (Figure 10b, S41).  $\text{NO}_3^-$  concentrations increased with depth towards the Skagerrak and North Atlantic where the maximum concentration occurred (Figure 10b).

Cu concentrations ranged from  $33.6 \pm 1.8 \text{ ng L}^{-1}$  in the Skagerrak to  $749 \pm 8 \text{ ng L}^{-1}$  in the German Bight (Figure 8d). The median Cu concentrations ranged between 90 and 140  $\text{ng L}^{-1}$  for the Skagerrak, Norwegian Trench, central and northern North Sea, while median concentrations were higher in the southern North Sea (260  $\text{ng L}^{-1}$ ) and German Bight (320  $\text{ng L}^{-1}$ ; Figure 8d). This trend was also visible for the east-west and south-north transects (Figure 10c): Only in the German Bight and southern North Sea, elevated Cu concentrations were found and decreased towards the deeper waters of the central and

northern North Sea. Elevated Cu concentrations were found in Skagerrak surface waters close to the Norwegian coast ( $512 \pm 5 \text{ ng L}^{-1}$ ) and in the water column close to the Danish coast (up to  $440 \pm 50 \text{ ng L}^{-1}$ ; Figure 10c). In general, Cu concentrations correlated negatively with salinity (Figure A 44).

Gd concentrations ranged between  $0.141 \pm 0.013 \text{ ng L}^{-1}$  in the Skagerrak and  $6.0 \pm 2.3 \text{ ng L}^{-1}$  in the German Bight (Figure 8e). Median Gd concentrations ranged between 0.5 and  $1.3 \text{ ng L}^{-1}$  for most regions but reached up to  $2.6 \text{ ng L}^{-1}$  in the German Bight (Figure 8e). These elevated surface concentrations decreased from the German Bight towards the Northwest and towards deeper waters (Figure 8e, Figure A 14) and correlated negatively with salinity (Figure A 44).

$\text{NH}_4^+$  concentrations were below the LOD in most surface samples and in deep water samples from the Skagerrak, for which the median  $\text{NH}_4^+$  concentration was the lowest ( $<0.11 \text{ } \mu\text{mol L}^{-1}$ ; Figure 8f). The maximum  $\text{NH}_4^+$  concentration ( $6.0070 \pm 0.0010 \text{ } \mu\text{mol L}^{-1}$ ) occurred within the southern North Sea which also showed the highest median  $\text{NH}_4^+$  concentration ( $1.8 \text{ } \mu\text{mol L}^{-1}$ ; Figure 8f). Overall, quantifiable  $\text{NH}_4^+$  concentrations were found mostly in the southern North Sea and in the coastal waters of the Skagerrak and German Bight (Figure A 22).

For the PCA, only samples for which both nutrient and elemental data was available, were used (262 samples from 79 stations) and all concentrations below the LOD were set to the LOD. For the REE, only the sums of LREE (Ce, Eu, Gd, La, Nd, Pr, Sm) and HREE (Dy, Er, Ho, Lu, Tb, Tm, Yb) were included in the PCA to reduce their impact on the PCA. Four rotated components were chosen after varimax rotation as they explained 75% of the sample variance. Factor loadings of all input variables larger than 0.5 are shown in Figure 3, numbers are given in Table A 6. Stability testing additionally assigned Mn positively and  $\text{PO}_4^{3-}$  negatively to component 3 while all other analytes were considered stable (Table A 6).

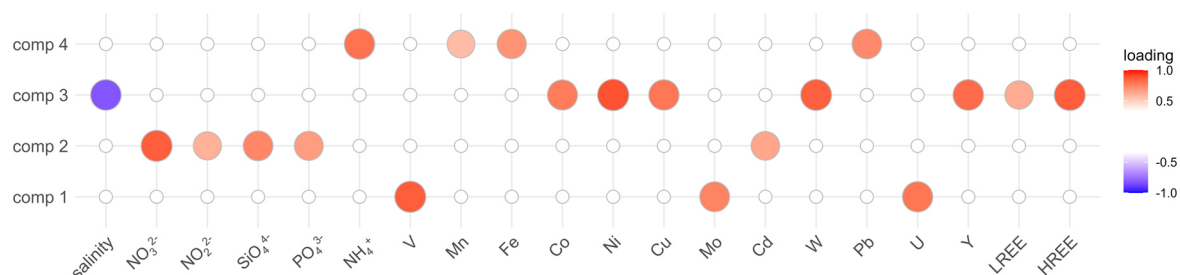


Figure 9 Factor loadings of the analyzed variables for the four rotated components. Note that only loadings larger than 0.5 are shown (Siems, Zimmermann, et al., 2024). The loadings for all analytes are given in Table A 6.



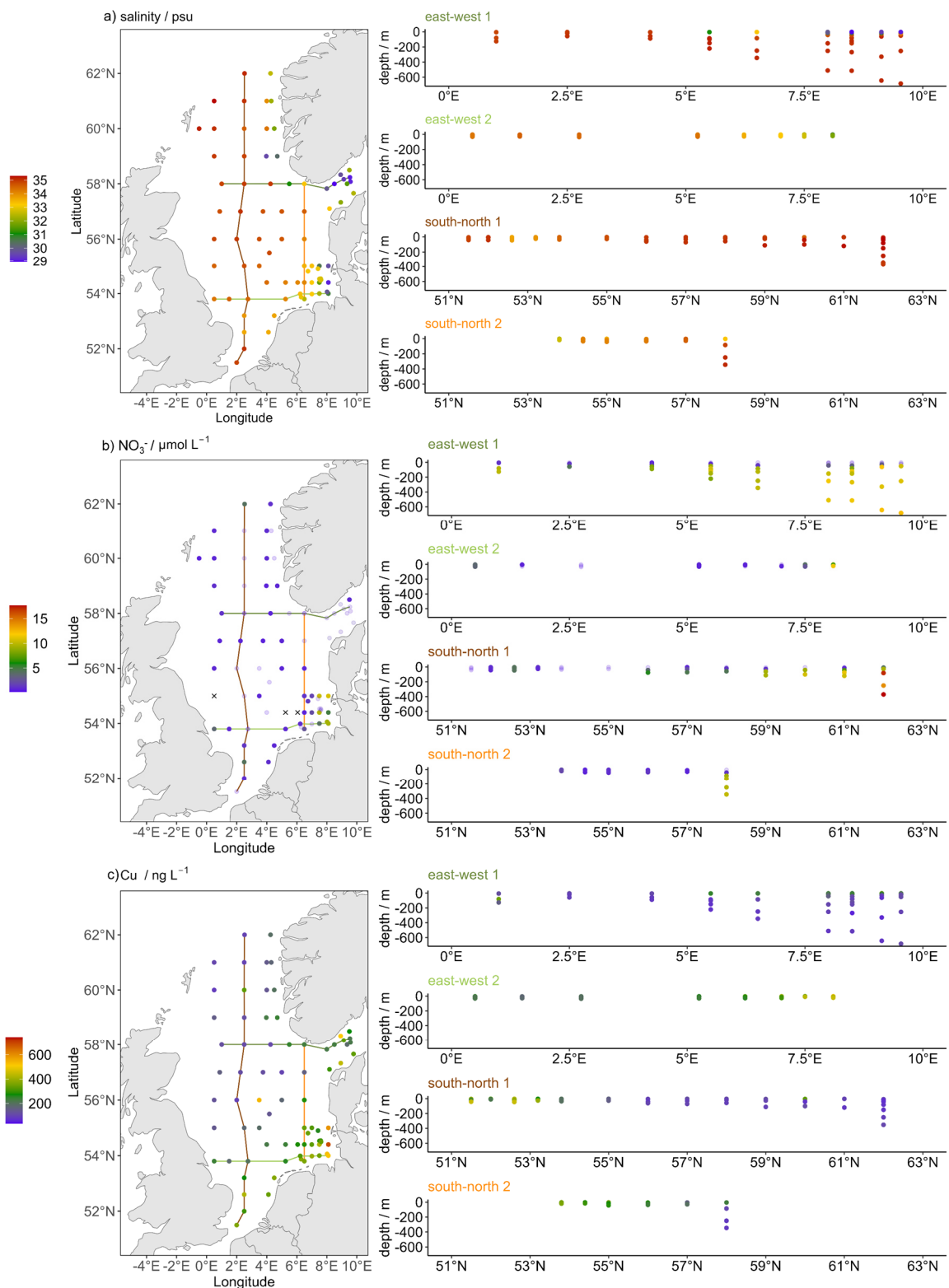


Figure 10 Surface concentrations and depth profiles of salinity,  $\text{NO}_3^-$  and  $\text{Cu}$  across two south-north and two east-west transects. The northernmost transect is east-west 1 and the westernmost transect is south-north 1 (Siems, Zimmermann, et al., 2024). *x* indicates that concentrations were below the LOD, faint points indicate that concentrations were between LOD and LOQ.

#### 6.2.1.2 *Component 1 – Mo, U, V*

Component 1 correlated positively with Mo, U and V (0.74, 0.80, 0.86) and explained 15% of the sample variance. U showed a similarly homogeneous distribution ( $1100 \pm 500$  to  $4100 \pm 500$  ng L<sup>-1</sup>) as Mo. The lowest surface concentrations and lowest median concentrations for U were observed in the German Bight and Skagerrak ( $2400$  ng L<sup>-1</sup>) and median concentrations ranged between  $2800$  and  $3000$  ng L<sup>-1</sup> in all other regions with the maximum occurring at HE586 st.26 close to the Danish coast (Figure A 34, Figure A 41). V concentrations ranged from  $800 \pm 400$  ng L<sup>-1</sup> to  $2060 \pm 5$  ng L<sup>-1</sup> with the lowest median concentration ( $1300$  ng L<sup>-1</sup>) and lowest surface concentrations in the German Bight and highest median concentrations in the northern North Sea ( $1800$  ng L<sup>-1</sup>). For V and U, the concentrations declined towards the bottom waters of the Skagerrak (Figure A 34, Figure A 35).

#### 6.2.1.3 *Component 2 – NO<sub>3</sub><sup>-</sup>, NO<sub>2</sub><sup>-</sup>, SiO<sub>4</sub><sup>4-</sup>, PO<sub>4</sub><sup>3-</sup>, Cd*

Component 2 correlated positively with the major nutrients (NO<sub>3</sub><sup>-</sup>, NO<sub>2</sub><sup>-</sup>, SiO<sub>4</sub><sup>4-</sup>, PO<sub>4</sub><sup>3-</sup>; 0.85, 0.60, 0.73, 0.66) and Cd (0.65). This component explained 15% of the sample variance. The distribution patterns of PO<sub>4</sub><sup>3-</sup> and SiO<sub>4</sub><sup>4-</sup> were comparable to NO<sub>3</sub><sup>-</sup> and ranged from  $<0.007$  to  $0.977 \pm 0.005$  μmol L<sup>-1</sup> for PO<sub>4</sub><sup>3-</sup> and  $<0.4$  to  $10.50 \pm 0.04$  μmol L<sup>-1</sup> for SiO<sub>4</sub><sup>4-</sup> with low surface concentrations and highest concentrations in Skagerrak bottom waters (Figure A 27, Figure A 30). PO<sub>4</sub><sup>3-</sup> additionally correlated negatively with component 3 (-0.48, Table A 6). NO<sub>2</sub><sup>-</sup> concentrations were comparably low throughout the North Sea (median  $0.03$  μmol L<sup>-1</sup>, LOD  $0.03$  μmol L<sup>-1</sup>) and reached maximum concentrations ( $0.760 \pm 0.001$  μmol L<sup>-1</sup>) in the deeper waters of the northern North Sea (Figure A 24). Cd showed a similar distribution as NO<sub>3</sub><sup>-</sup> with the lowest values at the surface of the northern North Sea ( $4.4 \pm 0.9$  ng L<sup>-1</sup>) and a maximum concentration ( $25 \pm 12$  ng L<sup>-1</sup>) at the northernmost station (Figure A 5).

#### 6.2.1.4 *Component 3 – salinity, Cu, Co, Ni, W, Y, LREE, HREE*

Component 3 described 31% of the overall sample variance and correlated negatively with salinity (-0.81) and positively with Cu, Co, Ni, W, Y, LREE, HREE (0.79, 0.76, 0.89, 0.84, 0.83, 0.72, 0.84). Co ( $0.67 \pm 0.08$  to  $47 \pm 4$  ng L<sup>-1</sup>), Ni ( $90 \pm 40$  to  $661 \pm 4$  ng L<sup>-1</sup>) and W ( $3.7 \pm 1.8$  to  $17 \pm 5$  ng L<sup>-1</sup>) showed a similar distribution as Cu with maximum concentrations in the German Bight (Figure A 7, Figure A 23, Figure A 36). However, W also showed distinctly increased concentrations close to the Danish coast. HREE ranged

between  $<0.01 \text{ ng L}^{-1}$  for Tb and  $2.71 \pm 0.30 \text{ ng L}^{-1}$  for Dy (Figure A 9-Figure A 38). They showed a similar trend as Cu with highest concentrations in the German Bight (AL557 st.4;  $2.45 \pm 0.07$ ,  $2.199 \pm 0.022$ ,  $0.638 \pm 0.005$ ,  $0.45 \pm 0.03$ ,  $0.330 \pm 0.008$ ,  $0.35461 \pm 0.00022$ ,  $2.480 \pm 0.005 \text{ ng L}^{-1}$  for Dy, Er, Ho, Lu, Tb, Tm, Yb) and in a surface sample close to the Norwegian coast (HE586, st.10;  $2.71 \pm 0.30$ ,  $2.05 \pm 0.22$ ,  $0.63 \pm 0.06$ ,  $0.32 \pm 0.04$ ,  $0.42 \pm 0.04$ ,  $0.296 \pm 0.024$ ,  $2.06 \pm 0.29 \text{ ng L}^{-1}$  for Dy, Er, Ho, Lu, Tb, Tm, Yb). Although Y concentrations were higher throughout the analyzed samples ( $2.03 \pm 0.05$  to  $29.88 \pm 0.13 \text{ ng L}^{-1}$ ) than for the HREE, Y is often associated with the HREE and showed similar trends with hotspots in the German Bight ( $29.88 \pm 0.13 \text{ ng L}^{-1}$ ) and the Skagerrak ( $28.51 \pm 0.04 \text{ ng L}^{-1}$ ). The LREE ranged from  $<0.0097 \text{ ng L}^{-1}$  for Eu to  $16.47 \pm 0.04 \text{ ng L}^{-1}$  for La (Figure A 6-Figure A 31) with maximum concentrations for all elements at the surface of a station close to the Norwegian coast (HE586 st.10;  $14.5 \pm 1.6$ ,  $0.39 \pm 0.05$ ,  $3.7 \pm 0.6$ ,  $16.47 \pm 0.04$ ,  $13.2 \pm 1.1$ ,  $3.24 \pm 0.30$ ,  $2.49 \pm 0.24 \text{ ng L}^{-1}$  for Ce, Eu, Gd, La, Nd, Pr, Sm). The LREE further showed increased surface concentrations in the Norwegian Trench (Figure A 39).

#### 6.2.1.5 Component 4 – Fe, Mn, Pb, $\text{NH}_4^+$

Component 4 correlated positively with Fe, Mn, Pb and  $\text{NH}_4^+$  (0.70, 0.57, 0.73, 0.80) and explained 15% of the sample variance. As for  $\text{NH}_4^+$ , the concentrations of Fe, Mn and Pb were highest in the German Bight and southern North Sea.

Mn showed the highest median concentrations within the southern North Sea ( $2025 \text{ ng L}^{-1}$ ) and German Bight ( $2190 \text{ ng L}^{-1}$ ) and significantly lower median concentrations ( $<800 \text{ ng L}^{-1}$ ) in all other regions (Figure A 19, Figure A 41). The maximum Mn concentration was found in the surface water of AL557 st.4 in the German Bight ( $12287 \pm 23 \text{ ng L}^{-1}$ ) and the lowest in the Norwegian Trench ( $55 \pm 17 \text{ ng L}^{-1}$ ). Mn also correlated with component 3 (0.48, Table A 6). Pb values ranged from  $<3.5 \text{ ng L}^{-1}$  to  $86 \pm 16 \text{ ng L}^{-1}$  with the highest median concentration ( $18.6 \text{ ng L}^{-1}$ ) in the southern North Sea and lowest median concentrations in the Norwegian Trench ( $4.85 \text{ ng L}^{-1}$ ) and Skagerrak ( $5.8 \text{ ng L}^{-1}$ ; Figure A 41). Median Fe concentrations were highest in the German Bight ( $310 \text{ ng L}^{-1}$ ) and southern North Sea ( $300 \text{ ng L}^{-1}$ ) and lowest in the northern North Sea ( $<230 \text{ ng L}^{-1}$ , Figure A 41).

## 6.2.2 Sources and biogeochemical interactions of trace metals and nutrients in the North Sea

### 6.2.2.1 Tracers for seawater and oxygen conditions

The salinity distribution was in good agreement with the dominant currents in the North Sea (Figure 1, Figure 10a; Brückner and Mackensen (2006)). The median salinities decreased from the northern to the southern North Sea with decreasing impact of North Atlantic water and increasing freshwater impact (Figure 8a). In the Skagerrak, the surface waters had low salinities due to mixing with Baltic Sea water, while the deeper waters featured higher salinities due to the inflow of Atlantic and central North Sea deep water (Figure 10a). The low salinity in the German Bight (Figure 10a) was caused by riverine discharge.

Mo, U and V (component 1) concentrations are high in oxygenated seawater but decrease during mixing with river water in the North Sea (Schneider et al., 2016; Tribovillard et al., 2006). This was illustrated by the lowest median concentrations of U and V in the German Bight and Skagerrak where seawater mixes with lower-salinity water originating from rivers and the Baltic Sea. However, for Mo, the trend was not as clear as for U and V and component 1 only correlated weakly with salinity (0.43, Table A 6). Hence, also other processes than conservative mixing with North Atlantic, Baltic Sea and river water played a role. Mo concentrations in the German Bight were in the same range as previously reported by Dellwig et al. (2007). However, Mo concentrations were higher in October (HE586) than in June (AL557), indicating the release of Mo that was adsorbed to organic matter during summer which is typical for Mo in coastal regions (Dellwig et al., 2007; Kowalski et al., 2013). Mo and V may also have anthropogenic sources and reach the ocean by atmospheric deposition (Schlesinger et al., 2017; Schneider et al., 2016; Wong et al., 2021), but there was no clear evidence for this in this data set.

The bottom waters of the Skagerrak are only renewed every two to three years while oxygen is continuously consumed by the degradation of organic matter (Brückner & Mackensen, 2006; Johannessen & Dahl, 1996). This likely leads to a depletion of U and V in Skagerrak bottom waters under suboxic conditions (Figure A 34, Figure A 35). Although Mo and V are involved in microbial processes of the nitrogen cycle and primary production (Butler, 1998; Meisch & Bielig, 1975; Morel & Price, 2003; Rehder, 2015) and correlate with primary production in the open Atlantic Ocean (Pinedo-González et al., 2015), they are sufficiently high concentrated in oxic seawater to not be limiting for phytoplankton growth in the North Sea (Rehder, 2015). However, due to climate warming and anthropogenic inputs, oxygen

minimum zones and regions with anoxic sediments might expand in the future, removing dissolved Mo, U and V from the water column (Emerson & Husted, 1991). Consequently, an impact on phytoplankton growth might be observed in the future.

#### 6.2.2.2 *Nutrients and nutrient-like analytes*

The measured nutrient concentrations were in the same range as reported for the North Sea by previous studies (Andersson, 1996; Chaichana et al., 2019; Wiltshire et al., 2010). The increasing concentrations of  $\text{NO}_3^-$ ,  $\text{PO}_4^{3-}$  and  $\text{SiO}_4^{4-}$  with increasing water depth and towards the North Atlantic (Figure 10b, Figure A 27, Figure A 30) reflect the remineralization of organic matter in the deeper waters of the open North Sea and the export of nutrients into the North Atlantic (Thomas et al., 2004). The nutrient concentrations in the German Bight were in the same range as reported for summer and autumn 2011 (BSH, 2016) and in the Skagerrak comparable to those reported for July 1997 for the upper 50 m (Croot et al., 2002). In the Skagerrak, the nutrient concentrations were lowest in surface waters with higher fractions of low-salinity Baltic Sea water (Croot et al., 2002). The cruise in June (AL557) likely took place after an algae bloom, while for the autumn cruise (HE586), the increased  $\text{PO}_4^{3-}$  and  $\text{SiO}_4^{4-}$  concentrations in the German Bight indicated nutrient recycling (Figure A 44). This was not evident for  $\text{NO}_3^-$  (Figure A 44), likely due to high riverine inputs during summer and the high variability of biogeochemical processes in this region. Nevertheless, the data was in good agreement with monitoring data from the German Bight which indicates high seasonal and year-to-year variability of nutrients (BSH, 2016). In the German Bight, nutrients are mainly supplied by rivers, whereas deeper waters of the North Sea are influenced by recycling of organic matter and mixing with high-nutrient Atlantic water (Chaichana et al., 2019; Jickells, 1998; Topcu et al., 2011). In the central and southern North Sea, Atlantic water inflow with lower N:P ratios is more important than terrestrial input (Burson et al., 2016) and recycled nutrients are directly consumed, leading to low nutrient concentrations. In addition to riverine input, atmospheric deposition can act as another source of nutrients (Jickells et al., 2016; Mahowald et al., 2008). Atmospheric nitrogen inputs to the North Sea were estimated to be as high as 36% of riverine input and are mainly deposited in the southern North Sea and German Bight (de Leeuw et al., 2003; Pätsch & Kühn, 2008). However, since most samples in the southern North Sea and German Bight were taken in summer, possible atmospheric inputs of nutrients were likely quickly consumed.

For primary production, the ratio of dissolved inorganic nitrogen (DIN;  $\text{NO}_2^-$ ,  $\text{NO}_3^-$ ,  $\text{NH}_4^+$ ) and  $\text{PO}_4^{3-}$  should be close to 16:1 (*n/n*; Redfield et al. (1963)) and is typically found in seawater where biomass recycling is followed by nutrient uptake. Most samples from the Skagerrak, Norwegian Trench, northern and central North Sea followed this ratio (median 15-17 (*n/n*); Figure 11a). However, the samples from the German Bight and southern North Sea deviated from this distribution with a high median N:P ratio of 50 (*n/n*; IQR=130) for the German Bight and 30 (*n/n*; IQR=60) for the southern North Sea. This was due to high  $\text{NO}_3^-$  concentrations during June (up to  $11.5 \pm 0.5 \mu\text{mol L}^{-1}$ ), indicating a significant surplus of  $\text{NO}_3^-$  compared to  $\text{PO}_4^{3-}$ . Comparable N:P ratios were found for the major tributaries of the North Sea (van Beusekom et al., 2019) and for the bottom waters of the coastal German Bight ( $>50$  (*n/n*)) during the winter seasons of 2008-2011 but with a high year-to-year variability (BSH, 2016).  $\text{NO}_3^-$  concentrations of the German Bight correlated negatively with salinity during June ( $R^2=0.8$ ), indicating a strong  $\text{NO}_3^-$  input from terrestrial sources (e.g., agriculture) with distinct seasonal variability (Pätsch et al., 2004). In contrast, in October (HE586), the  $\text{NO}_3^-$  concentrations were lower and the  $\text{PO}_4^{3-}$  concentrations were slightly higher in the German Bight compared to June (Figure 11a). This indicated less anthropogenic nitrogen input and more nutrient recycling during autumn. Although most of the samples were taken in June, this showed the increasing P-limitation of the German Bight and southern North Sea that is caused by the regulation of riverine P inputs despite high nitrogen inputs during the past decades (Balkoni et al., 2023; Burson et al., 2016; Pätsch et al., 2004).

$\text{NO}_2^-$  is an intermediate product of nitrification and denitrification but easily oxidized to  $\text{NO}_3^-$  under oxic conditions and reduced under anoxic conditions (Zhang et al., 2020). Therefore, its concentration was mostly below the LOD in this study.  $\text{NH}_4^+$  is also produced during organic matter remineralization and quickly oxidized (Zhang et al., 2020). Hence, local hotspots for both analytes might occur during the remineralization of organic matter. The PCA attributed  $\text{NH}_4^+$  to component 4, indicating that  $\text{NH}_4^+$  was not only influenced by organic matter remineralization but also by redox processes or atmospheric deposition (de Leeuw et al., 2003). The increased  $\text{NH}_4^+$  concentrations in the coastal waters of the Skagerrak, German Bight and southern North Sea were probably caused by remineralization of decaying phytoplankton blooms (Chaichana et al., 2019; Johnson et al., 2007). The highest median  $\text{NH}_4^+$  concentrations ( $1.8 \mu\text{mol L}^{-1}$ , IQR  $1.6 \mu\text{mol L}^{-1}$ ) were found in the southern North Sea where it significantly contributed to high surface N:P ratios. This might have been

caused by atmospheric deposition or decoupling of remineralization and primary production (Chaichana et al., 2019; de Leeuw et al., 2003).

Various studies revealed contrasting effects of eutrophication and climate change on the North Sea: Especially for the beginning of the spring bloom, the winter reserve from internal nutrient recycling and light availability are more important in the North Sea than riverine input (Frigstad et al., 2020; Leote et al., 2016; McQuatters-Gollop et al., 2007; Wiltshire et al., 2015). However, riverine input is important for the duration of the bloom and phytoplankton growth, especially in coastal regions (Frigstad et al., 2020; Gross et al., 2022; Skogen et al., 2004). Limitations of specific nutrients can cause a shift in the phytoplankton community, due to different demands of the species (Gross et al., 2022; Grosse et al., 2017; Gypens et al., 2017). Thus, unbalanced nutrient inputs support toxic algae blooms (Emeis et al., 2015; Lefebvre & Dezecache, 2020) and especially in coastal regions, diatom growth can also be limited by  $\text{SiO}_4^{4-}$  availability (Burson et al., 2016; Lefebvre & Dezecache, 2020).

As climate change might reduce the vertical water mass mixing in the Atlantic Ocean, nutrient concentrations of the water entering the North Sea from the North Atlantic might decrease (Gröger et al., 2013). In case riverine inputs remain P-limited, this might lead to further changes in the phytoplankton community within the North Sea and related processes.

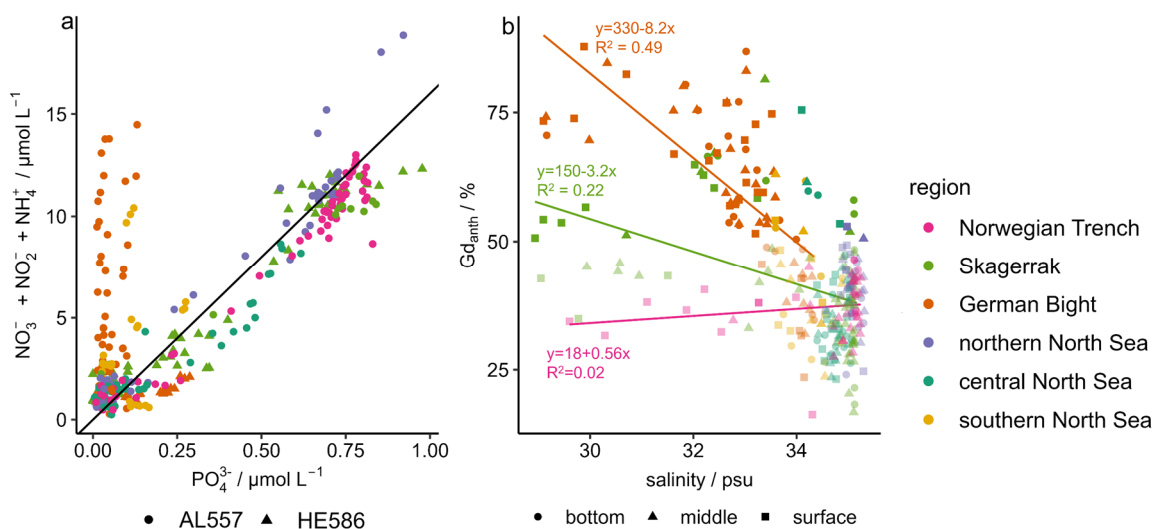


Figure 11 Correlation of inorganic nitrogen with  $\text{PO}_4^{3-}$  and percentage of  $Gd_{anth}$  versus salinity. The correlation of inorganic nitrogen with  $\text{PO}_4^{3-}$  (a) is given for AL557 (circle) and HE586 (triangle). The diagonal line (a) indicates the N:P ratio of 16 (n/n). The percentage of  $Gd_{anth}$  versus salinity (b) is given for bottom (circle), middle (triangle) and surface (square) samples. Pale points indicate the samples with  $Gd$  anomalies  $< 2$  (b) (Siems, Zimmermann, et al., 2024).

In addition to the traditional nutrients, Cd also correlated positively with component 2. Cd is needed by diatoms for  $\text{CO}_2$  sequestration (Lane et al., 2005) and has a nutrient-like depth

profile in the North Atlantic (Kremling et al., 1999; Pinedo-González et al., 2015). Higher Cd concentrations in the deeper waters of the northern North Sea might therefore be due to recycling of organic matter that contained or adsorbed Cd. The maximum Cd concentrations reported in this study were lower than the maximum of 51 ng L<sup>-1</sup> Cd reported for the open North Sea by Laslett (1995). Over the past decades, riverine and atmospheric inputs were the main Cd sources (Laane et al., 2013; Pacyna et al., 2009), but it seems that anthropogenic Cd contamination of the coastal regions decreased drastically, making the North Atlantic a source of Cd to the North Sea.

### 6.2.2.3 *Tracers of riverine input*

Co, Cu, Ni, and W were summarized by component 3 which correlated negatively with salinity (Figure 9, Figure A 7-Figure A 36, Figure A 44). The main source for these elements is riverine input and they are diluted with increasing distance to the river mouths in the German Bight and southern North Sea (BSH, 2016; Hydes & Kremling, 1993; Kremling et al., 1999; Kulaksiz & Bau, 2007; Mart et al., 1985; Sohrin et al., 1987). In the open ocean, these elements are prone to scavenging or biological uptake (Kremling et al., 1999; Sohrin et al., 1987). However, due to the scattering of the sampling points in this study, only conservative mixing with North Sea water was observed, except for a positive correlation of Co with salinity in the German Bight (Figure A 44). The higher concentrations of these analytes in the Skagerrak surface waters originated from Baltic Sea water (Croot et al., 2002; Kremling & Petersen, 1978), as well as transport of German Bight water to the Skagerrak via the southern Jutland current (Figure 1). During the winters of 2008-2011, maximum Cu and Ni concentrations in the Elbe river mouth were 800 ng L<sup>-1</sup> and decreased with increasing distance within the German Bight, which is in good agreement with the findings of this study (BSH, 2016). Co and Cu concentrations in the Skagerrak were in the same order of magnitude as for a transect measured in July 1997, with the highest Co concentrations at the coastal station (Croot et al., 2002). Co, Cu, Fe, Mn, and Ni are required for the nitrogen cycle and other processes within marine phytoplankton (Morel & Price, 2003; Twining & Baines, 2013). Since the elemental requirements vary between species, Co, Cu and Mn availability can affect the phytoplankton community structure (Sunda, 2012). However, increased Cu and Ni concentrations might also be toxic or increase P-limitation by complexation (Thomas et al., 1980; Yang et al., 2019). Dissolved Cu might inhibit growth at concentrations above 65 ng L<sup>-1</sup> for some species while most species have a significantly higher tolerance and are



mostly harmed by  $\text{Cu}^{2+}$  which usually features low concentrations in seawater (Yang et al., 2019). Nevertheless, this indicates that anthropogenic Cu inputs need to be limited, especially since it is also supplied by atmospheric deposition (Paytan et al., 2009). To cover the year-to-year variability of these elements, as shown for the German Bight (BSH, 2016), further studies are required to monitor trends in anthropogenic inputs.

The REE and Y are mainly supplied by rivers and behave inversely to salinity, but LREE might also adsorb to organic matter and be released upon remineralization (Goldstein & Jacobsen, 1988; Sutorius et al., 2022). This was reflected by the high median concentrations of all REE in the German Bight and the high concentrations of the REE in Norwegian Trench surface waters compared to deeper water samples (Figure A 41). The REE concentrations at AL557 st.2 and st.8, closest to the Elbe and Weser rivers were comparable to those described by Kulaksiz and Bau (2007) a few km south at similar salinities. The high REE concentrations in the surface waters of the Norwegian Trench were likely due to freshwater inputs with low anthropogenic impact, e.g., from fjords.

For most REE, the median concentrations were highest in the German Bight. However, for Gd, a large discrepancy between the German Bight and all other regions was found (Figure 8e, Figure A 41). REE and Y share a very similar biogeochemistry, resulting in consistent ratios of these elements throughout marine and terrestrial environments. Deviations of certain elements from this behavior (anomalies), e.g., by anthropogenic impact or distinct chemical processes can be revealed by normalization to a reference material like the PAAS (Kulaksiz & Bau, 2007). A Gd anomaly of 1.6 (Gd/Gd\*) is natural in the North Atlantic but anthropogenic inputs in coastal regions exceed this value (Kulaksiz & Bau, 2007). Within the aquatic environment, magnetic resonance imaging (MRI) contrast agents are the main source of anthropogenic Gd (Kulaksiz & Bau, 2007). As the contained Gd complexes have a high solubility and stability, they are not removed during wastewater treatment but reach the oceans via rivers, making Gd a suitable tracer for anthropogenic riverine input (Kulaksiz & Bau, 2007). From the Gd anomaly,  $Gd_{anth}$  was calculated and is shown in Figure 11b and Figure A 15. To account for the natural seawater Gd anomaly and the uncertainties associated with the calculation of  $Gd_{anth}$ , only samples with anomalies  $>2$  ( $\sim 50\%$   $Gd_{anth}$ ) will be discussed for anthropogenic input. Up to 88% of the Gd in the samples was of anthropogenic origin and in general, an increase in  $Gd_{anth}$  with decreasing salinity was evident for the Skagerrak and German Bight (Figure 11b, Figure A 15). For 2005, (Kulaksiz & Bau, 2007), reported anomalies of 5-7 for the Weser river ( $\sim 85\%$   $Gd_{anth}$ , 3-7 psu), decreasing within the

estuary (anomaly of 4, ~75%  $Gd_{anth}$ , 14-20 psu) towards an anomaly of 1.6-2 (~40-50%  $Gd_{anth}$ , 32 psu) off the East Frisian Islands. The AL557 and HE586 sampling did not cover the rivers and estuaries, but highest  $Gd_{anth}$  values were found in the surface waters of the German Bight and decreased towards the Northwest. The maximum values of  $82 \pm 8\%$  and  $70 \pm 4\%$   $Gd_{anth}$  at the southernmost stations in the German Bight (AL557 st.2 and st.8) were significantly higher than those estimated by Kulaksiz and Bau (2007) for similar locations and salinities nearly two decades ago. This indicates that the high  $Gd_{anth}$  that was reported for the Weser estuary by Kulaksiz and Bau (2007) is propagating into the German Bight from the main river estuaries and is in good agreement with the doubling of MRI exams in Germany between 2005 and 2021 (OECD, 2016). However, more samples are needed as the applied calculation has in high uncertainties. Elevated  $Gd_{anth}$  values were also calculated for the Danish coast (up to 80%, Figure A 15). These likely originated from the German Bight, as a surface water drift model<sup>1</sup> (Callies et al., 2021) indicated the northward transport of these water masses via the southern Jutland current (Figure A 42). The low fractions of  $Gd_{anth}$  in the surface waters of the Norwegian Trench support the hypothesis that the elevated REE concentrations here originated from freshwater inputs with low anthropogenic disturbance (Figure A 15). Up to now, there are no studies available on the effects of Gd on phytoplankton but recent studies with higher marine organisms suggest negative effects of Gd on marine life (Trapasso et al., 2021).

Two stations showed noticeably elevated elemental concentrations: One surface water sample close to the Norwegian coast off Arendal (HE586, st.10) with significantly higher REE concentrations and all samples of AL557 st.4 in the German Bight with higher concentrations of Cd, Cu, Fe, Mn, Ni, W and all HREE, while LREE remained low (Figure A 5-Figure A 39). Sediment resuspension or submarine groundwater input was unlikely for both stations as the maximum concentrations occurred at the surface. For the surface sample near Arendal, the salinity was lower (30 psu) than the deeper and surrounding samples (33-35 psu), indicating that this water mass might have originated from the Kattegat (Aure et al., 1998; Kristiansen & Aas, 2015). This was supported by a surface drift model<sup>1</sup> (Callies et al., 2021) showing that the water mass originated from the eastern Skagerrak during HE586, while the currents were different during AL557 (Figure A 43). In contrast, for AL557

---

<sup>1</sup> [hcdc.hereon.de/drift-now/](https://hcdc.hereon.de/drift-now/)

st.4, the surface drift model<sup>1</sup> (Figure A 42; Callies et al. (2021)) showed that the water mass has been moving in the region due to tidal activity but might have originated from the Eider or Elbe estuary. This is supported by the low salinity of this sample (Figure 10a).

Fe, Mn and Pb are also supplied mainly from rivers and therefore discussed in this section (BSH, 2016; Laane et al., 2013; Ussher et al., 2007). However, although Mn was also assigned to component 3 during stability testing, Fe, Mn and Pb were best represented by component 4 (Figure 9, Table A 6). This was likely caused by atmospheric deposition (e.g., from dust or anthropogenic sources) and scavenging by organic matter or other particles that is known for these elements (Jickells et al., 2016; Kremling et al., 1999; Pacyna et al., 2009; Ussher et al., 2007). Pb concentrations were highest in the southern and central North Sea and in the German Bight, likely due to riverine input and atmospheric deposition (Pacyna et al., 2009) but sediment resuspension might also have played a role (Tappin et al., 1995). This patchiness is in good agreement with monitoring results for the winters of 2008-2011 in the German Bight (BSH, 2016). However, except for one water sample from AL557 st.53 ( $86 \pm 16 \text{ ng L}^{-1}$ ), Pb concentrations were lower in this study than the reported hotspot concentrations ( $\sim 50\text{-}100 \text{ ng L}^{-1}$ ; BSH (2016)), likely due to scavenging of Pb on fresh organic matter during summer. In general, the Pb concentrations found for the North Sea were significantly lower than toxic concentrations for Atlantic Ocean phytoplankton ( $20 \mu\text{g L}^{-1}$ ; Echeveste et al. (2012)). As a high year-to-year variability was observed for Pb before (BSH, 2016), further studies are needed to monitor the development of Pb concentrations in the North Sea.

Dissolved Fe and Mn are quickly oxidized and precipitated when they are introduced to oxygenated seawater. Hence, their concentrations correlated well with salinity in the German Bight with high river discharge (Figure A 44). Except for AL557 st.4 and st.9, the Mn concentrations in the German Bight were in the same range as those found for the winters 2008-2011, decreasing from the river mouths to the open North Sea (BSH, 2016). In the Skagerrak, the trend was not as clear because low-salinity Baltic water, from which Fe and Mn might have already precipitated, mixes with high-salinity water. Mn and Fe are important for phytoplankton growth and Fe often acts as a limiting micronutrient (Sunda, 2012; Twining & Baines, 2013). However, due to high blank concentrations, no significant spatial or seasonal differences were found for Fe in this study. Further, the samples had been stored frozen for a year before filtration. As shown in chapter 6.1, this might have biased the results but not the trends between stations.

Mn concentrations are most likely not limiting in the North Sea, as concentrations were mostly higher than in the open ocean due to the terrestrial input (Sunda, 2012). However, Mn availability might impact the phytoplankton community structure (Sunda, 2012). With increasing sea surface temperature, metal oxidation will increase, while decreasing seawater pH will increase metal reduction (Hoffmann et al., 2012) and thereby might change the availability of these redox-active, scavenged elements.

### 6.2.3 Conclusion

This chapter gave a comprehensive overview of dissolved trace element and nutrient concentrations for the entire North Sea with a high sampling resolution. Although biogeochemical processes are highly variable and underlay interannual and seasonal changes, the concentrations were in the same range as in previous studies. The PCA confirmed that metal and nutrient concentrations in the North Sea are mainly dependent on river run-off, water mass mixing and recycling of organic matter but also atmospheric deposition might play a role. Therefore, anthropogenic inputs and their regulation remain important. Especially the effects of increasing input of new contaminants like Gd must be investigated in more detail. Future studies should also cover the speciation of selected elements like Fe and Cu to determine their bioavailability and additionally expand the presented data set to cover year-to-year and seasonal differences. However, the aim of this thesis was to provide a first comprehensive data set which is needed to outline those areas that are most important for further investigations related to carbon cycling and long-term storage.

As a result of the work carried out during this thesis, the paper “Dissolved trace elements and nutrients in the North Sea – a current baseline” was published in *Environmental Monitoring and Assessment* by A. Siems, T. Zimmermann, T. Sanders, and D. Pröfrock (<https://doi.org/10.1007/s10661-024-12675-2>).

### Author Contributions

A. Siems took and processed the samples onboard HE586, measured the trace elements, conducted the data analysis, and prepared the initial draft of the paper. T. Zimmermann and T. Sanders contributed to drafting and editing the paper. T. Sanders and D. Pröfrock obtained funding, provided laboratory resources and supervision on writing and drafting the paper.

### 6.3 Trace metals in Skagerrak sediments – spatial distribution and release under changing redox conditions

The Skagerrak is the main depot center for organic matter and associated contaminants from the entire North Sea (Diesing et al., 2021; Logemann et al., 2022). Consequently, the metals that are introduced to the North Sea by rivers and scavenged by suspended matter or taken-up as nutrients by organisms will end up in the Skagerrak sediments. Indeed, the sequence of anthropogenic contamination in the North Sea over the past decades can be tracked in Skagerrak sediment profiles (Logemann et al., 2022). These trace metals and metalloids are redox-sensitive and/or affected by reduction of Fe and Mn oxide phases, sulfide production and oxidation or remineralization of the organic matter to which they are adsorbed (Kelderman & Osman, 2007; Neff, 1997; Rinklebe & Shaheen, 2017). In the Skagerrak, the sediment redox conditions are very heterogeneous (Canfield, Jørgensen, et al., 1993) and follow the reverse redox cascade from sulfate to Fe to Mn reduction with increasing water depth and distance to the coast (Canfield, Jørgensen, et al., 1993; Rysgaard et al., 2001). However, the zones of the reduction reactions overlap due to different stabilities of oxide minerals and secondary (abiotic) reduction and precipitation reactions (Canfield, Thamdrup, et al., 1993; Thibault de Chanvalon et al., 2023; van der Zee & Van Raaphorst, 2004).

The bottom water oxygen levels of the Skagerrak highly depend on water mass circulation. Due to the changing climate, the circulation pattern and subsequently bottom water oxygen in the Skagerrak might change in the future and affect sedimentary carbon remineralization, storage, and trace metal mobility.  $\delta^{98/95}\text{Mo}$  isotopic signatures are a helpful tool to track changes in oxygen and redox conditions in sediments: While preferably light Mo isotopes adsorb to Mn and Fe oxides under aerobic conditions, thiomolybdates are scavenged quantitatively with almost no fractionation under anaerobic conditions (Goldberg et al., 2009; Goldberg et al., 2012; Scholz et al., 2013; Siebert et al., 2006).

Within this chapter, the spatial distribution of trace metals in Skagerrak sediments and porewaters were investigated to find connections between redox conditions and anthropogenic trace metals. Further, the sediments were incubated under aerobic and anaerobic conditions for up to one year to investigate the effect of changes in bottom water oxygen conditions on redox conditions and mobility of anthropogenic trace metals. For the sediment cores and incubations,  $\delta^{98/95}\text{Mo}$  isotopic ratios were used as tracers for redox conditions.

## 6.3.1 Redox conditions in Skagerrak sediments

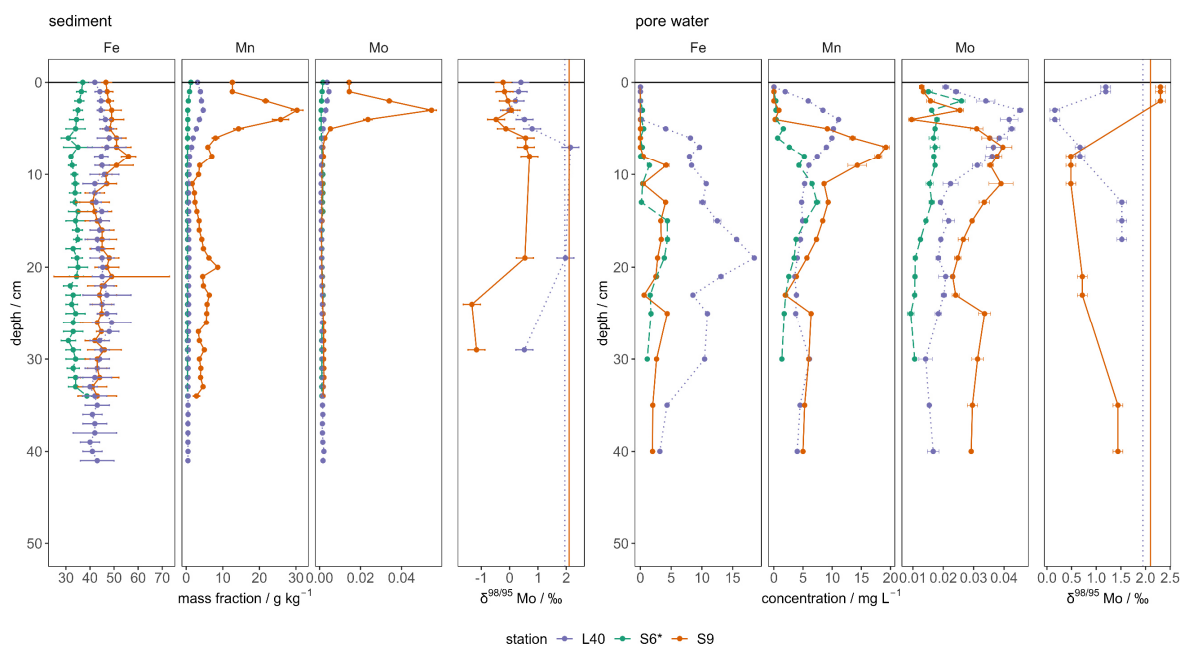


Figure 12 Depth profiles of Fe, Mn, Mo,  $\delta^{98/95}\text{Mo}$  for sediment and porewater. Sediment profiles are given on the left and porewater on the right. The vertical line in  $\delta^{98/95}\text{Mo}$  values indicates the bottom water value for the respective stations. Error bars correspond to the expanded uncertainty  $U(k=2)$ .

The redox conditions within the sediment cores were determined by Fe, Mn, and Mo sediment and porewater concentrations and  $\delta^{98/95}\text{Mo}$  values (Figure 12). The sediment Fe mass fractions were similar for all investigated stations, ranging between  $31 \pm 3 \text{ g kg}^{-1}$  and  $56 \pm 3 \text{ g kg}^{-1}$  (Figure 12), while differences in depth profiles and between stations were observed for Mn and Mo with highest mass fractions at S9 ( $30.3 \pm 1.6 \text{ g kg}^{-1}$  Mn and  $54.6 \pm 2.4 \text{ mg kg}^{-1}$  Mo at 3 cm depth) and lowest mass fractions at S6\* ( $0.338 \pm 0.016 \text{ g kg}^{-1}$  Mn and  $0.78 \pm 0.11 \text{ mg kg}^{-1}$  Mo; Figure 12). The porewater concentrations ranged between  $<0.0016 \text{ mg L}^{-1}$  to  $18.53 \pm 0.25 \text{ mg L}^{-1}$  Fe,  $<0.00004 \text{ mg L}^{-1}$  to  $19.2 \pm 0.6 \text{ mg L}^{-1}$  Mn and  $9.3 \pm 1.1 \text{ } \mu\text{g L}^{-1}$  to  $45.3 \pm 9 \text{ } \mu\text{g L}^{-1}$  Mo which is comparable to other studies in the Skagerrak region (Goldberg et al., 2012; Magnusson et al., 1996).

The range of porewater  $\delta^{98/95}\text{Mo}$  at L40 and S9 ( $0.16 \pm 0.10\text{‰}$  to  $1.95 \pm 0.10\text{‰}$  and  $0.48 \pm 0.10\text{‰}$  to  $2.30 \pm 0.10\text{‰}$ ) was comparable to the  $\sim 0.4$  to  $3.5\text{‰}$  found in the Gullmar Fjord that drains into the Skagerrak (Goldberg et al., 2012). Sedimentary  $\delta^{98/95}\text{Mo}$  values ranged between  $0.15 \pm 0.10\text{‰}$  and  $2.30 \pm 0.10\text{‰}$  which was in good agreement with other studies on Mn-rich sediments (Goldberg et al., 2012; Siebert et al., 2006). From the core data, the redox zonation at stations L40 and S9 developed with depth as follows:

In the upper 6 cm of the cores, sedimentary Mn and Mo mass fractions were highest ( $4.65 \pm 0.12 \text{ g kg}^{-1}$  Mn and  $4.6 \pm 0.4 \text{ mg kg}^{-1}$  Mo at L40,  $30.3 \pm 1.6 \text{ g kg}^{-1}$  Mn and  $54.6 \pm 2.4 \text{ mg kg}^{-1}$  Mo at S9), accompanied by low sediment  $\delta^{98/95}\text{Mo}$  values ( $-0.0 \pm 0.3\text{‰}$  and  $-0.5 \pm 0.3\text{‰}$  at L40 and S9, respectively). The low sediment  $\delta^{98/95}\text{Mo}$  values indicated adsorption of light Mo to Mn and Fe oxides in the sediment and were in good agreement with  $0.24\text{‰}$  at the surface of a sediment core from Gullmar Fjord with similar Mn and Fe mass fractions (Barling & Anbar, 2004; Goldberg et al., 2009; Goldberg et al., 2012). In this study, the maximum Mn and Mo mass fractions were found a few cm below the surface, likely due to the upward diffusion of reduced Mn that was oxidized and precipitated at the boundary of the aerobic layer (Goldberg et al., 2012; Siebert et al., 2006). Porewater Mn and Mo concentrations were highest at 3-4 cm depth at L40 ( $11.08 \pm 0.28 \text{ mg L}^{-1}$  and  $45.3 \pm 0.9 \text{ } \mu\text{g L}^{-1}$ , respectively) and at 7 cm depth at S9 ( $19.2 \pm 0.6 \text{ mg L}^{-1}$  and  $39.6 \pm 3.0 \text{ } \mu\text{g L}^{-1}$ ), indicating reductive dissolution of Mn oxides accompanied by release of the adsorbed Mo. This was confirmed by the minimum porewater  $\delta^{98/95}\text{Mo}$  values of  $0.16 \pm 0.10\text{‰}$  and  $0.49 \pm 0.10\text{‰}$  which were in good agreement with those found for the zone of Mn reduction in the Gullmar Fjord (Goldberg et al., 2012). Although the  $\delta^{98/95}\text{Mo}$  value of Mo released from Mn oxides would theoretically be lower (Wasylenki et al., 2008), these values represent a combined signal of the pooled samples, diffusion and mixing with seawater Mo in the porewater as well as secondary adsorption processes (Goldberg et al., 2012). Below the layer with high Mn reduction, the sediment Mn and Mo mass fractions at L40 decreased and the sediment  $\delta^{98/95}\text{Mo}$  value rose to seawater values ( $2.14 \pm 0.35\text{‰}$ ; 7 cm), indicating that less Mn oxides with adsorbed light Mo were available and isotopically heavier Mo was adsorbed to Fe oxides (Barling & Anbar, 2004; Goldberg et al., 2009). In this zone, the porewater Fe concentrations at L40 increased to  $18.53 \pm 0.25 \text{ mg L}^{-1}$  (19 cm), indicating Fe reduction due to a decreasing sedimentary Mn stock with depth. Fe oxides adsorb isotopically heavier Mo than Mn oxides (Barling & Anbar, 2004; Goldberg et al., 2009), leading to an increase in porewater  $\delta^{98/95}\text{Mo}$  during Fe reduction which was also observed for the Gullmar Fjord (Goldberg et al., 2012). The decrease in sedimentary  $\delta^{98/95}\text{Mo}$  values down to  $0.5 \pm 0.3\text{‰}$  (29 cm) at L40 coincided with decreasing porewater Mo concentrations and increasing  $\delta^{98/95}\text{Mo}$  values and was also observed for the Gullmar Fjord where it was attributed to adsorption of porewater Mo under iron-reducing or sulfidic conditions (Goldberg et al., 2012). In contrast, at station S9, the sedimentary  $\delta^{98/95}\text{Mo}$  value only increased to  $0.7 \pm 0.3\text{‰}$  (19 cm) below the zone of Mn reduction and porewater Fe

concentrations only increased slightly ( $4.363 \pm 0.029 \text{ mg L}^{-1}$ ; 25 cm), indicating low Fe reduction and ongoing Mn reduction. Around 25 cm depth, an increase in porewater Fe, Mn and Mo occurred at S9, coinciding with decreasing sediment  $\delta^{98/95}\text{Mo}$  ( $-1.3 \pm 0.3\%$ ). This might have indicated Fe reduction followed by abiotic Mn reduction and re-adsorption of the released Mo to freshly formed Fe oxides. However, this process cannot be resolved since the porewater  $\delta^{98/95}\text{Mo}$  samples had to be pooled and porewater results only present a snapshot of the ongoing processes (Goldberg et al., 2012). At S6\*, porewater concentrations indicated Fe reduction around 15 cm depth and Mn reduction between 7 cm and 15 cm depth but no  $\delta^{98/95}\text{Mo}$  values are available for this station (Figure 12).

Overall, the porewater and sediment results were in good agreement with other studies that attributed >90% of carbon oxidation at S9 to Mn reduction and found Fe and sulfate reduction with secondary, abiotic Mn reduction to dominate S6 (Canfield, Jørgensen, et al., 1993; Wang & Van Cappellen, 1996). For L40, no previous studies on remineralization processes are available, but it is likely that dissimilatory Mn reduction took place in the upper part and dissimilatory Fe reduction dominated at 19 cm depth. This coincides with the decreasing reactivity of organic matter with increasing water depth and distance to land and the redox activity developing vice versa (Kristensen et al., 2018).

### 6.3.2 Anthropogenic trace metals in Skagerrak sediments

The OSPAR Commission (Oslo and Paris Convention) gives background concentrations (BC) and background assessment concentrations (BAC), below which trace metal concentrations are assumed to be close to the natural background (OSPAR Commission, 2014). The BCs and BACs are given with the sediment profiles for As, Cu, Ni and Pb in Figure 13. Due the low concentration of trace metals in porewater and the small available sample volume, only As porewater profiles were analyzable (Figure 13).

At stations L40 and S9, the sediment As mass fractions were highest within the upper 10 cm, reaching up to  $43 \pm 3 \text{ mg kg}^{-1}$  and  $94 \pm 6 \text{ mg kg}^{-1}$  (Figure 13), exceeding the OSPAR BC ( $15 \text{ mg kg}^{-1}$ ; OSPAR Commission (2014)) three- and sixfold. Below 10 cm depth, the As mass fractions ranged around the OSPAR BC. The depth distribution as well as the mass fractions at station L40 very well reproduced the results from Logemann et al. (2022) at the same location four years earlier. At station S6\*, As mass fractions were lower (max.  $24.8 \pm 1.4 \text{ mg kg}^{-1}$ ) and ranged between the OSPAR BC and BAC ( $25 \text{ mg kg}^{-1}$ ; OSPAR Commission (2014)). A main source for anthropogenic As in the Skagerrak are warfare



agents on scuttled ships from WWII (Beldowski et al., 2020; Logemann et al., 2022; Tørnes et al., 2002). In the vicinity of the wrecks, sediment As reaches  $480 \text{ mg kg}^{-1}$  (Tørnes et al., 2002) and station S9 which had highest sediment As values is closest to the wreck positions (Tørnes et al., 2006).

In contrast to the sediment As contents, the maximum porewater As concentrations at L40 ( $63 \pm 7 \mu\text{g L}^{-1}$ ) were higher than at S9 ( $37 \pm 3 \mu\text{g L}^{-1}$ ) but both showed highest values between 6-19 cm depth. S6\* As porewater concentrations reached a maximum of  $20.3 \pm 2.2 \mu\text{g L}^{-1}$  at 15 cm depth. The concentrations at L40 were similar to the  $73 \mu\text{g L}^{-1}$  found at a Mn-rich station in the Skagerrak before (Magnusson et al., 1996). Although the As in the sediments likely originates from warfare agents, the distribution indicates that their accumulation depends on Mn and Fe oxides to which the As is adsorbed in marine sediments and released to the porewater upon their dissolution (Neff, 1997).

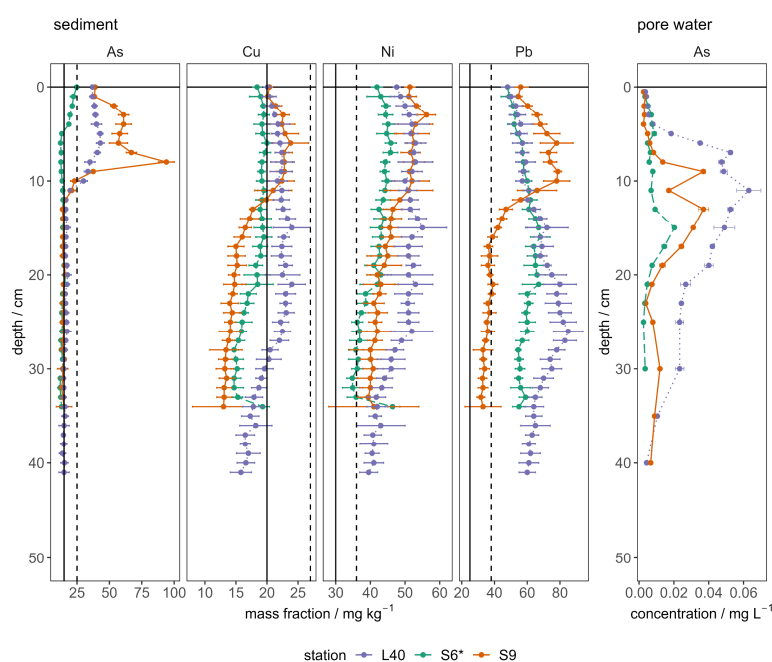


Figure 13 Depth profiles of As, Cu, Ni, Pb for sediment and porewater profile for As. Sediment profiles are given on the left and porewater on the right. The vertical lines in sediment profiles represent OSPAR BAC and BC values (OSPAR Commission, 2014). Error bars correspond to the expanded uncertainty  $U(k=2)$ .

The Cu mass fractions at station L40 ranged between  $15.8 \pm 1.7 \text{ mg kg}^{-1}$  and  $24 \pm 3 \text{ mg kg}^{-1}$  with maximum values between 14 and 21 cm depth, exceeding the OSPAR BC but in good agreement with the sediment profiles from (Logemann et al., 2022). In the surface sediments of S9, the maximum concentration ( $23.8 \pm 2.9 \text{ mg kg}^{-1}$ ) was comparable to station L40 and exceeded the OSPAR BC. However, below 11 cm depth, the Cu mass fractions decreased to

$13 \pm 5 \text{ mg kg}^{-1}$  at S9. At station S6\*, Cu showed the lowest variability with depth and ranged between  $14.7 \pm 0.7 \text{ mg kg}^{-1}$  and  $20.0 \pm 0.8 \text{ mg kg}^{-1}$ . These values are comparable to previous studies in the Skagerrak (Dave & Dennegård, 1994). Cu is likely scavenged with organic matter to the sediment surface and released during remineralization (Kelderman & Osman, 2007; Kremling et al., 1999). Although all Cu mass fractions were below the OSPAR BAC (OSPAR Commission, 2014), the increased Cu mass fractions at L40 and S9 might originate from anthropogenic sources like combustion, steel production and anti-fouling paint on ships (Byrnes & Dunn, 2020; Logemann et al., 2022; Nriagu & Pacyna, 1988).

In contrast to As and Cu, Ni showed low variability with depth at all stations. At L40, maximum Ni mass fractions occurred at 15 cm depth ( $55 \pm 7 \text{ mg kg}^{-1}$ ), while at S9, maximum Ni mass fractions occurred close to the surface ( $56.2 \pm 2.6 \text{ mg kg}^{-1}$ ). At S6\*, the Ni mass fractions ranged between  $34.8 \pm 1.6 \text{ mg kg}^{-1}$  and  $46.4 \pm 2.1 \text{ mg kg}^{-1}$ . Although the depth distribution was similar, the Ni values at L40 were higher than the maximum of  $43.6 \pm 0.9 \text{ mg kg}^{-1}$  reported by Logemann et al. (2022) and also exceeded the 3-43  $\text{mg kg}^{-1}$  reported for Skagerrak and Kattegat surface sediments (Dave & Dennegård, 1994) and OSPAR BC and BAC values. Anthropogenic Ni sources are combustion, fertilizers, steel manufacturing and waste (Nriagu & Pacyna, 1988; Rathor et al., 2014) but the availability of Ni at changing redox conditions depends on its adsorption to organic matter as well as Fe and Mn oxides (Rinklebe & Shaheen, 2017; Shaheen et al., 2014).

The Pb distribution pattern differed significantly between L40 and S6\* compared to S9. The depth distribution and mass fractions at station L40 reproduced the results from Logemann et al. (2022) with highest mass fractions at 26 cm depth ( $85 \pm 9 \text{ mg kg}^{-1}$ ). The distribution was similar at S6\* with the maximum at 15 cm depth ( $68 \pm 6 \text{ mg kg}^{-1}$ ). In contrast, at station S9, the maximum Pb mass fractions (up to  $78.7 \pm 2.3 \text{ mg kg}^{-1}$ ) occurred between 2-12 cm depth and decreased to  $31.7 \pm 2.4 \text{ mg kg}^{-1}$  below. Hence, S9 was the only station with Pb mass fractions below the OSPAR BAC. The Pb values found in the other sediments were significantly higher than the up to  $37 \text{ mg kg}^{-1}$  Pb found for the Skagerrak and Kattegat surface sediments by previous studies, likely because these only sampled superficial sediments and not the deepest part of the Skagerrak (Dave & Dennegård, 1994; Kuijpers et al., 1993). Pb is prone to scavenging and binds to various kinds of particles (Kelderman & Osman, 2007; Kremling et al., 1999). The increased Pb likely originated from the long-term utilization of Pb-based fuel additives, mining, and metal production (Logemann et al., 2022; Nriagu & Pacyna, 1988; Pacyna et al., 2009). The different depth profiles at the stations

might indicate higher sedimentation rates at L40 and S6\* compared to S9 which accumulates the high anthropogenic Pb input only in the upper part of the core and serves undisturbed sediments below. While sedimentation rates are actually higher at S6\* than at S9 (Diesing et al., 2021), this is not true compared to station L40, thus redox conditions likely were the driving factor at S9.

### 6.3.3 Response of redox conditions in Skagerrak sediments to changing bottom water oxygen levels

Surface (i.e. fresh) and deeper (i.e. intermediate and old) sediments from each station were incubated under aerobic and anaerobic conditions for up to 12 months to investigate the effect of bottom water oxygen levels on the sediment redox conditions. The incubation of fresh and older sediments from different locations covers a range of different metal contents, redox states, and likely also microbial communities. Initial mass fractions and  $\delta^{98/95}\text{Mo}$  values for the incubated sediments are given in Table 2. Due to the high mass fractions of the elements in the sediment phase, changes in the water phase are evaluated to track processes during the incubations.

Table 2 Initial trace metal concentrations in the incubated Skagerrak sediments.

|     |              | Fe /<br>mg kg <sup>-1</sup> | Mn /<br>mg kg <sup>-1</sup> | Mo /<br>mg kg <sup>-1</sup> | $\delta^{98/95}\text{Mo}$<br>/ % | Cd /<br>$\mu\text{g kg}^{-1}$ | Cu /<br>mg kg <sup>-1</sup> | Ni /<br>mg kg <sup>-1</sup> | Pb /<br>mg kg <sup>-1</sup> |
|-----|--------------|-----------------------------|-----------------------------|-----------------------------|----------------------------------|-------------------------------|-----------------------------|-----------------------------|-----------------------------|
| L40 | fresh        | 41300 ±<br>2100             | 2000 ±<br>110               | 1.85 ±<br>0.16              | 0.9 ± 0.4                        | 560 ±<br>110                  | 17.1 ±<br>0.9               | 39.4 ±<br>1.8               | 68.1 ±<br>1.4               |
|     | intermediate | 39900 ±<br>1800             | 1170 ±<br>100               | 1.21 ±<br>0.15              | -                                | 610 ±<br>150                  | 17.6 ±<br>1.5               | 40 ± 3                      | 79 ± 6                      |
|     | old          | 40000 ±<br>4000             | 690 ± 80                    | 1.29 ±<br>0.23              | -                                | 600 ±<br>130                  | 18.2 ±<br>2.8               | 42 ± 6                      | 87 ± 11                     |
| S6* | fresh        | 33000 ±<br>4000             | 680 ± 70                    | 1.14 ±<br>0.17              | 1.2 ± 0.4                        | 580 ±<br>120                  | 15.7 ±<br>1.8               | 37 ± 4                      | 60 ± 6                      |
|     | intermediate | 36000 ±<br>5000             | 430 ± 70                    | 1.47 ±<br>0.21              | -                                | 600 ±<br>190                  | 16.1 ±<br>2.3               | 39 ± 6                      | 67 ± 9                      |
|     | old          | 31000 ±<br>4000             | 410 ± 40                    | 1.55 ±<br>0.17              | -                                | 600 ±<br>150                  | 15.4 ±<br>1.4               | 37 ± 4                      | 72 ± 6                      |
| S9  | fresh        | 45000 ±<br>3000             | 13600 ±<br>700              | 10.7 ±<br>0.7               | -<br>0.4 ± 0.4                   | 640 ±<br>120                  | 17.8 ±<br>1.1               | 46 ± 3                      | 83 ± 5                      |
|     | intermediate | 41400 ±<br>2700             | 5740 ±<br>290               | 1.31 ±<br>0.11              | -<br>1.2 ± 0.4                   | 690 ±<br>180                  | 14.1 ±<br>0.6               | 42.4 ±<br>1.6               | 54.1 ±<br>2.7               |
|     | old          | 42500 ±<br>2200             | 4580 ±<br>270               | 1.94 ±<br>0.21              | -<br>0.1 ± 0.4                   | 690 ±<br>140                  | 13.1 ±<br>0.8               | 43 ± 3                      | 40.9 ±<br>2.4               |

In the aerobic incubations, Fe and Mn ranged between  $0.54 \pm 0.10 \mu\text{g L}^{-1}$  to  $10 \pm 30 \mu\text{g L}^{-1}$  and  $0.15 \pm 0.04 \mu\text{g L}^{-1}$  to  $3 \pm 4 \mu\text{g L}^{-1}$  with no significant changes throughout the incubations and between setups (Figure 14). This indicates that neither Fe nor Mn reduction took place in the aerobic incubations. As the metals were likely primarily present in the sediments in oxidized form, no considerable dissolution but equilibration between adsorbed metals and

the overlying water phase was expected. The large error bars reflect the natural variability of this process between the replicate bottles and might for month 1 indicate that one bottle was insufficiently oxygenated. Dissolved Mo concentrations increased at the beginning of the incubation, reaching up to  $40 \pm 9 \mu\text{g L}^{-1}$  for S6\* old sediments but remained stable within uncertainty afterwards (Figure 14). The  $\delta^{98/95}\text{Mo}$  values of the dissolved Mo decreased from  $\sim 2\text{‰}$  at the beginning to  $-0.51 \pm 0.10\text{‰}$  and  $-0.31 \pm 0.10\text{‰}$  after one month for S9 intermediate and old sediments, indicating desorption of light Mo which was likely associated with Fe and Mn oxides before (Figure 14). Since this was caused by equilibration between the continuously shaken sediments and the overlying water phase, the  $\delta^{98/95}\text{Mo}$  values remained low throughout the following months. The dissolved  $\delta^{98/95}\text{Mo}$  values in the fresh sediment incubations from S9, L40 and S6\* only reached minimum values of  $1.36 \pm 0.10\text{‰}$ . This was caused by the higher initial sediment  $\delta^{98/95}\text{Mo}$  value at L40 and S6\* and likely by the high initial Mo content of S9 sediments.

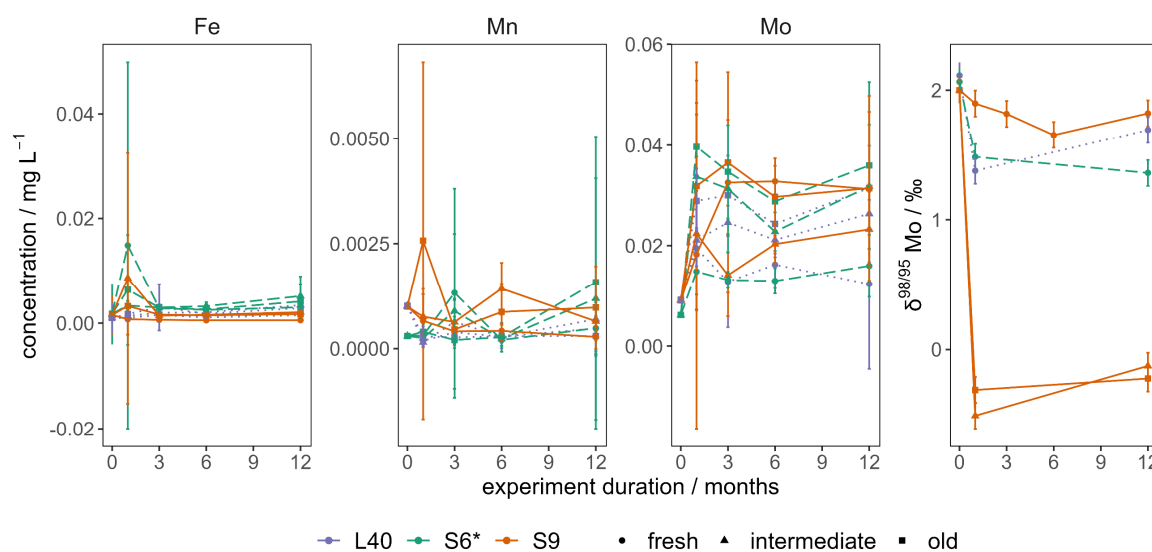


Figure 14 Dissolved concentrations of Fe, Mn, and Mo as well as  $\delta^{98/95}\text{Mo}$  values for aerobic incubations. Error bars correspond to the expanded uncertainty  $U(k=2)$ .

In contrast to the aerobic incubations, the anaerobic incubations released significant amounts of Fe, Mn, and Mo (Figure 15), indicating more complex redox processes and corresponding  $\delta^{98/95}\text{Mo}$  signatures.

The fresh sediment incubations from station L40 indicate constant Fe reduction by releasing Fe almost linearly between month 1 ( $14 \pm 4 \mu\text{g L}^{-1}$ ) and month 12 ( $21 \pm 4 \text{mg L}^{-1}$ ). In contrast, Mn increased between months 1-3 but then reached a plateau with a maximum at month 12 ( $30 \pm 6 \text{mg L}^{-1}$ ), indicating initial Mn reduction that either was replaced by Fe

reduction after month 3 or continued but with the released Mn being bound again in the sediments. The reduced Mn could have either adsorbed to the sediments (Canfield, Thamdrup, et al., 1993) or formed Mn carbonates which is typical for anaerobic conditions (Lee et al., 2011; Lenstra et al., 2021; Novotnik et al., 2019). If reduced Mn was trapped in the sediments, Mo concentrations would have been expected to continuously increase and  $\delta^{98/95}\text{Mo}$  values to decrease. However, Mo also reached a plateau with the maximum concentration at the end of the incubation ( $52 \pm 11 \mu\text{g L}^{-1}$ ) and the  $\delta^{98/95}\text{Mo}$  value decreased to  $0.34 \pm 0.10\text{‰}$  after one month but did not change significantly afterwards. Hence, Fe reduction likely dominated over Mn reduction after month 3, probably because the remaining sedimentary Mn was more refractory or the microorganisms that rely on Fe reduction developed metabolic advantages.

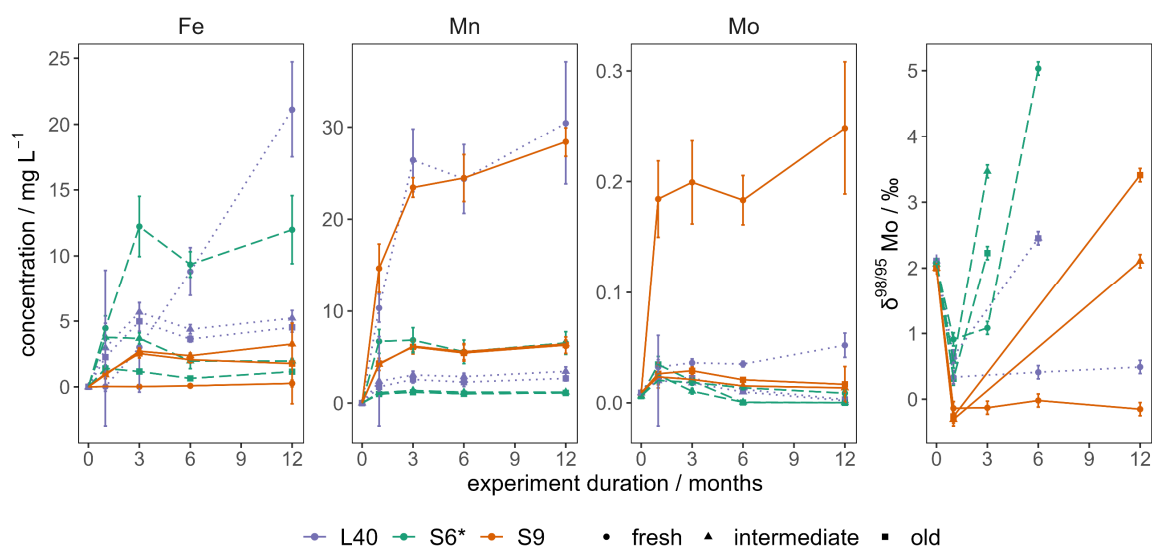


Figure 15 Dissolved concentrations of Fe, Mn, and Mo as well as  $\delta^{98/95}\text{Mo}$  values for anaerobic incubations. Error bars correspond to the expanded uncertainty  $U(k=2)$ .

In S9 fresh sediment incubations, Fe concentrations reached  $0.26 \pm 0.25 \text{ mg L}^{-1}$  after 12 months but were within uncertainty throughout the incubation, indicating no significant Fe reduction. Mn and Mo concentrations increased within the first three months but also reached a plateau afterwards ( $28.4 \pm 1.6 \text{ mg L}^{-1}$  and  $0.25 \pm 0.06 \text{ mg L}^{-1}$ ).  $\delta^{98/95}\text{Mo}$  values initially decreased to  $-0.13 \pm 0.10\text{‰}$  but did not decrease further, indicating that also the Mo isotopic composition equilibrated. As for L40, these results do not indicate adsorption or carbonate formation for Mn after month 3 but as almost no Fe reduction was detected here, a different redox process (e.g., sulfate reduction) might have been taking place that was not detectable with the applied methods. The absence of Fe reduction was on the one hand likely

caused by the abundant sedimentary Mn which the dominant microorganisms in the sediment were specialized in and on the other hand by the inhibition of sulfate reduction by molybdate (Canfield, Thamdrup, et al., 1993). The impact of sulfate reduction might increase slowly if the sediments stay entirely anaerobic.

In the fresh S6\* incubations, the dissolved  $\delta^{98/95}\text{Mo}$  also decreased within the first month ( $0.91 \pm 0.10\text{‰}$ ) but then increased significantly, reaching  $5.03 \pm 0.10\text{‰}$  after 12 months. Since the trend was similar for all intermediate and old incubations, these are discussed together. Within the first 1-3 months, dissolved Fe, Mn, and Mo concentrations increased to  $12.2 \pm 2.3 \text{ mg L}^{-1}$ ,  $6.8 \pm 1.4 \text{ mg L}^{-1}$  and  $35 \pm 7 \text{ } \mu\text{g L}^{-1}$  (Figure 15). Together with the decrease in  $\delta^{98/95}\text{Mo}$  values, this indicates reductive dissolution of Fe and Mn in the beginning of the incubations. While the Fe and Mn concentrations remained around this level, Mo concentrations decreased again between months 1 to 12 in parallel to the increasing  $\delta^{98/95}\text{Mo}$  values which were not analyzable at very low Mo concentrations (Figure 15). This indicates that different processes than Fe and Mn reduction occurred, likely sulfate reduction, as indicated by a sulfidic smell and black precipitates on the bottle lids. Under sulfidic conditions, Mo is expected to be removed quantitatively from the water phase since thiomolybdates adsorb strongly to Fe sulfides and organic matter, leading to the same isotopic signature in the sediments as was present in the overlying water (Siebert et al., 2003). In the incubation experiments, the  $\delta^{98/95}\text{Mo}$  value even exceeded the overlying water value, likely due to fractionation of the very low dissolved Mo concentration remaining in the dissolved phase after precipitation of thiomolybdates. As Fe concentrations also reached a plateau for these samples, it is possible that Fe and sulfate reduction occurred simultaneously and were balanced, continuously forming Fe sulfide (Bethke et al., 2011). In the Skagerrak, sulfate reduction occurs at the depth of Fe reduction and sulfate-reducing bacteria contribute to Fe-reduction, likely by secondary abiotic reactions (Reyes et al., 2017). Only the S9 intermediate and old sediments showed higher Mn than Fe concentrations and later production of sulfide, indicating that the Mn reduction dominated over Fe reduction.

The presented results differ from in-situ sediments as bioturbation and the sedimentation of new substrates were excluded. In the aerobic incubations, the initial redox conditions only influenced  $\delta^{98/95}\text{Mo}$  values and only aerobic respiration occurred but even at high bottom water oxygen concentrations, the sediments will become anaerobic at a certain depth. In the anaerobic incubations, the sediments were initially dominated by the same redox process as in-situ (Fe and Mn reduction at L40, Mn reduction at S9, Fe reduction at S6\*; Canfield,

Jørgensen, et al. (1993); Wang and Van Cappellen (1996)). This was especially true for the incubated surface sediments. However, the incubation setups moved down the redox cascade (Mn-Fe-sulfate reduction) at different paces, likely depending on the dominant microbial community and the availability of accessible redox partners but also on the remineralization of organic matter (Lentini et al., 2012). If metal oxides become less bioavailable, sulfate reducers might become dominant despite high Fe mass fractions (Lentini et al., 2012). In the field, sulfate reduction might further increase with increasing temperature and organic matter supply but is likely buffered by abiotic Fe reduction as long as labile Fe oxides are available (Hargrave et al., 2008; Sanz-Lázaro et al., 2011).

#### 6.3.4 Response of anthropogenic trace metals in Skagerrak sediments to changing bottom water oxygen levels

Fe and Mn oxyhydroxides as well as organic matter adsorb several trace metals, export them into the sediments and release them upon reductive dissolution or remineralization (Hart, 1982; Tankere-Muller et al., 2007; Tribovillard et al., 2006). Under aerobic conditions, trace metal mobility also increases after sulfide oxidation (Jonge et al., 2012). The burial or release of Cd, Cu, Ni and Pb from the sediments within 12 months were calculated from the dissolved concentrations and the incubated sediment mass (Figure 16). Monthly concentrations are given in Figure A 45 and Figure A 46. The initial dissolved concentrations of Cd, Cu and Ni for stations S9 and L40 were higher than typical coastal North Sea concentrations due to the incubated artificial seawater. The masses of released Cd, Cu, Ni and Pb show large error bars, indicating that the results were heterogeneous between the incubated bottles (Figure 16).

Cd was released from the sediments under aerobic conditions with a maximum of  $5 \pm 6 \text{ ng g}^{-1}$  (S6\* old sediments), while under anaerobic conditions the sediments acted as a Cd sink ( $-0.20 \pm 0.14 \text{ ng g}^{-1}$  for S9 intermediate incubations; Figure 16). Although the uncertainties exceeded the release/burial for most incubations, the results indicate that Cd was released under aerobic conditions due to the dissolution of sulfides and remineralization of organic matter which strongly bind Cd (Jonge et al., 2012; Tankere-Muller et al., 2007). Therefore, the highest Cd release occurred from the sulfidic, shallow S6\* sediments (Figure 16). In contrast, under anaerobic conditions, equilibration with the increased initial Cd concentrations in the artificial seawater as well as sulfide formation decreased the dissolved Cd concentrations.

Significant release of Cu from all sediments occurred under aerobic conditions ( $110 \pm 70 \text{ ng g}^{-1}$  for fresh S9 sediments to  $170 \pm 60 \text{ ng g}^{-1}$  for intermediate L40 sediments; Figure 16), while under anaerobic conditions, the sediments acted as a sink for Cu ( $-27 \pm 13 \text{ ng g}^{-1}$  for S9 intermediate sediments). Although this was mostly caused by the increased initial Cu concentrations for L40 and S9, it indicates that the sediments “cleaned” the water column under anaerobic conditions. The magnitude of Cu burial depended on the initial concentrations as the lower Cu burial at S6\* compared to the other stations was caused by the lower initial Cu concentrations in the incubated water.

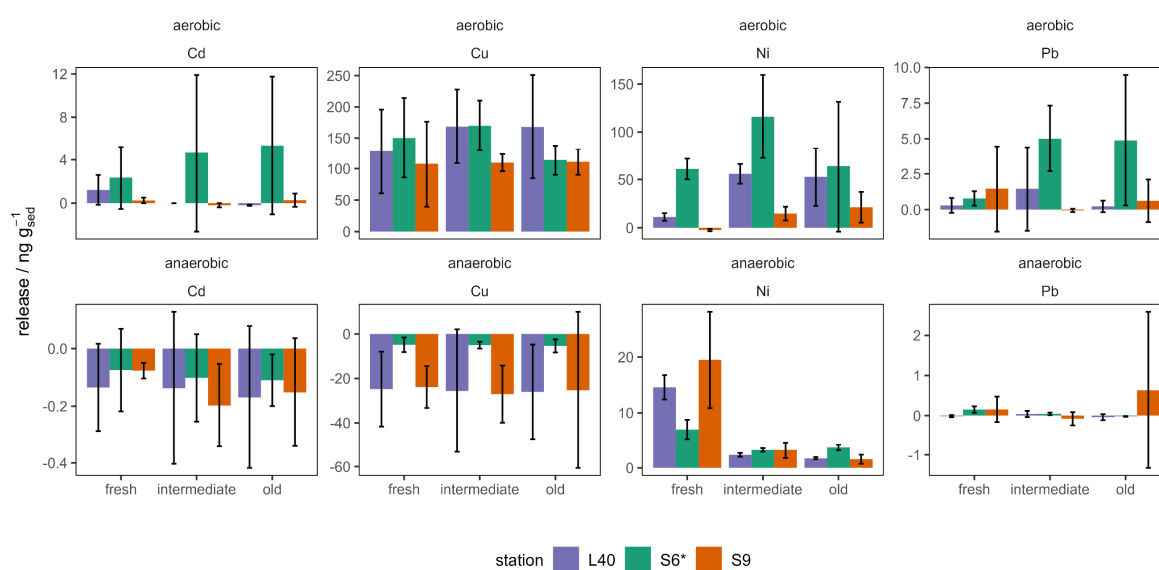


Figure 16 Release of Cd, Cu, Ni and Pb from sediments under aerobic and anaerobic conditions between months 0 and 12. Error bars for aerobic (top) and anaerobic (bottom) incubations correspond to the expanded uncertainty  $U(k=2)$ .

Dissolved Ni concentrations increased initially in all incubations but declined or formed a plateau after the initial 1-3 months in the anaerobic incubations (Figure A 45, Figure A 46). Over the 12 months of incubation, the sediments however were a net source for Ni under both aerobic and anaerobic conditions, releasing up to  $120 \pm 40 \text{ ng g}^{-1}$  Ni from aerobic S6\* sediments. Only the fresh S9 sediments, which had the highest initial Ni mass fractions (Table 2) removed Ni from the water column under aerobic conditions ( $-2.3 \pm 1.3 \text{ ng g}^{-1}$ ) while they released  $19 \pm 9 \text{ ng g}^{-1}$  Ni under anaerobic conditions (Figure 16). As Ni is associated with both organic matter and Fe oxides (Grybos et al., 2007; Tribovillard et al., 2006), its release depends on the remineralization of organic matter and on the reductive dissolution of Fe oxides. Under aerobic conditions, the organic matter remineralization was likely highest for S6\* as the station is closest to the coast and has the freshest organic



material. Under anaerobic conditions, the surface (i.e. fresh) sediments from all stations released most Ni, probably because of the high reductive dissolution rate of Fe and Mn oxides.

A significant Pb release (up to  $5.0 \pm 2.3 \text{ ng g}^{-1}$ ) occurred only from S6\* sediments under aerobic conditions, while for the other sediments, the uncertainty was  $>100\%$ . The Pb was likely bound in sulfide form in the initial sediments and released after oxidation under aerobic conditions. Since S6\* was the most sulfidic station, the effect was largest for S6\* sediments and covered by the heterogeneity of the sediments for the other stations. Under anaerobic conditions, Pb concentrations increased initially but then decreased again, causing a maximum net release of  $0.6 \pm 2.0 \text{ ng g}^{-1}$  Pb from old S9 sediments which had the lowest initial Pb mass fractions (Figure 16, Figure A 46). This was likely caused by initial oxidation of sulfides followed by sulfide formation which then scavenged Pb again.

The incubations indicate that under aerobic conditions, Cd and Cu can be released from formerly not fully oxygenated sediments while these metals are rather bound in the sediments under anaerobic conditions. Pb and Ni seem to be more dependent on other processes as they were released both under aerobic and anaerobic conditions but with high uncertainties. The released trace metals might impact microbial processes in the sediments (e.g., nitrification) but to evaluate the effect of the released trace metals, speciation is needed, as bulk concentrations are not meaningful in terms of bioavailability and potential toxicological effects (Tessier & Campbell, 1987). Although only operationally defined, sequential extractions (Hamzeh et al., 2014; Tessier & Campbell, 1987) or X-ray analysis of the sediments (Retschko et al., 2023) in the beginning and end of the incubations will give more information on the mineral phases to which the metals are bound and the processes that dominate the release.

### 6.3.5 Conclusion

Fe, Mn, Mo as well as  $\delta^{98/95}\text{Mo}$  isotopic values are heterogeneously distributed within the cores and between stations, reflecting the heterogeneous redox conditions within the Skagerrak sediments. While As, Cu, Ni and Pb peaks are likely caused by anthropogenic inputs, their distribution in sediments and porewater is highly dependent on sediment redox conditions. Hence, it is important to monitor redox conditions and contaminants together to get a realistic picture of the contamination status of sediments.

If the bottom water oxygen concentration in the Skagerrak changes, sediment redox conditions are immediately affected. Under aerobic conditions, the sediments switched to aerobic respiration, independent of the formerly dominant redox metabolism. With decreasing oxygen supply, which might occur due to diminishing bioturbation, water mass exchange or increasing eutrophication, the dominant anaerobic remineralization process initially persisted in the experiment. However, Fe and sulfate reduction became more important at all stations during the incubation, indicating that the release of sulfides and reduced Fe would increase with decreasing oxygen concentrations.

If formerly anaerobic sediments are oxygenized, they release significant amounts of Cu, Cd, Ni and Pb, depending on the initial conditions in the sediments. Under anaerobic conditions the sediments also released Ni but acted as a sink for Cu. These processes only occur during the transition of the sediments to more aerobic or anaerobic conditions as they are likely coupled to changes in the redox status and will diminish upon equilibration. Nevertheless, these are important factors for the remobilization of legacy pollutants. To assess the bioavailability and distinguish adsorbed and precipitated metals, sequential sediment extractions and chemical speciation analysis should be applied to the sediments in future studies (Anschutz et al., 2005; Lenstra et al., 2021; Oldham et al., 2017). Although these methods are more time-consuming than bulk sediment analysis, they should be considered to add even more value to the data.

$\delta^{98/95}\text{Mo}$  analysis was a useful tool to determine differences between equilibrium and redox processes in the incubations, especially as it was not possible to measure oxygen concentrations or redox potential in-situ. However, to confirm the hypothesized redox processes and get a deeper insight into the microbial processes taking place, analysis of bacterial DNA in the sediments and dissolved  $\text{CO}_2$  and  $\text{CH}_4$  in the anaerobic incubations is needed. The incubation experiments showed that long-term incubations can contribute to closing the knowledge gap of future changes in the ocean which cannot be assessed with typical incubations lasting only days to weeks.

As a result of the work carried out during this thesis, the paper “Trace metals in Skagerrak sediments – spatial distribution and release under changing oxygen conditions” was submitted to *Biogeochemistry* by A. Siems, T. Zimmermann, M. E. Wieser, and D. Pröfrock (under review).

### **Author Contributions**

A. Siems took and processed the samples onboard HE586, measured all trace element samples, conducted the data analysis and prepared the manuscript. A. Siems and T. Sanders set up and sampled the incubations. T. Zimmermann contributed to drafting and editing the paper. M. E. Wieser, T. Sanders and D. Pröfrock obtained funding, provided laboratory resources, supervision and guidance on writing and final drafting the paper.



## 7 Summary and Outlook

This thesis spans the arc from water sampling methods to water and sediment trace metal concentrations and the effects of changing oxygen conditions on trace metal behavior. The three research questions of the thesis were answered as follows:

1. What is needed to process and store seawater while maintaining the original dissolved trace metal concentrations?

The filtration experiment showed that awareness for possible sample biases is needed and that thorough method blanks, covering all preparational steps are as crucial as a detailed reporting of the entire setup including rinsing steps, filter membrane materials and pore size. Further, especially cooled sample storage should be avoided to prevent sample alteration by precipitation or adsorption. *DigiFILTER*<sup>TM</sup>s are a fast and cost-efficient filtration method which reduces contamination and increases reproducibility of trace metal samples. Thus, they are the perfect option for coastal and estuarine trace metal sampling campaigns with large sample batches. Although Niskin bottles attached to a CTD rosette were used during AL557 and HE586 and yielded sufficiently low blanks, it stays important to adapt GEOTRACES strategies also for the coastal region. Trace-metal free equipment should be used but needs to supply sufficient sample volume and water depths from the same station to measure all parameters from the same water sample.

2. What are the spatial distribution, sinks and sources of trace metals in the North Sea and how are they coupled to the nutrient cycle?

Trace metal and nutrient samples from the entire North Sea indicate a clear riverine nutrient and trace metal input in coastal regions. With increasing distance to the coast, water mass mixing, remineralization and primary production become more important driving factors for combined trace metal and nutrient distributions. In the future, new emerging contaminants like REE in electronics or pharmaceuticals will occur in the North Sea due to missing recycling and wastewater purification methods. The present data set will serve as a future reference for these inputs but also as baseline for North Sea models. However, further data is needed to reflect seasonal and year-to-year changes and to track atmospheric deposition in comparison to riverine input.

3. Do trace metals and redox conditions in the sediments interact and will they be mobilized under changing oxygen conditions?

The Skagerrak samples and incubation experiments showed that anthropogenic contaminants accumulate in the sediments, and that their distribution depends both on sources and redox conditions. Upon both increasing and decreasing oxygen supply, these contaminants might be remobilized, depending on their mineral and binding form and this likely also applies for other emerging contaminants. In contrast to known contaminants like Pb or Cu, little is known on the biogeochemical effects of recently emerging contaminants, but they might as well interact with or affect benthic remineralization pathways. Therefore, it is crucial to study the potential effects of these elements (e.g., REE and other metals used in pharmaceuticals or electronics) in the marine environment in parallel to removal and recycling techniques.

The trace metal and nutrient data obtained in this thesis can serve as input data for a North Sea model within CARBOSTORE. However, more seasonal data as well as knowledge on interaction mechanisms is needed for an improved estimate of primary production, remineralization, and carbon export. Here, especially laboratory or mesocosm studies are needed to investigate the combined effects of various contaminants or nutrients on carbon storage and subsequently develop management methods for processes with highest vulnerability or carbon storage potential. The results from this thesis will also serve future studies on biogeochemical processes in the North Sea when combined with chlorophyll, alkalinity or dissolved inorganic carbon data. In case that CDR techniques are applied in the North Sea in the future, this thesis sets a valuable reference point to monitor contamination and unintended negative side-effects. As the incubation experiment showed that remineralization processes in the sediment are very complex and can be affected by small perturbations, close supervision and monitoring of effects are needed in case of CDR application. To prevent negative effects from the outset, long-term incubations as applied in this study would be a great tool to assess negative side-effects of CDR on North Sea biogeochemical processes.

## 8 References

- Almeida, J. M., Palma, C., Félix, P. M., & Brito, A. C. (2023). Long-term variation of dissolved metals and metalloid in the waters of an Atlantic mesotidal estuary (Sado Estuary, Portugal). *Marine Pollution Bulletin*, 188, 114615. <https://doi.org/10.1016/j.marpolbul.2023.114615>
- Anderson, R. F., Mawji, E., Cutter, G. A., Measures, C. I., & Jeandel, C. (2014). GEOTRACES: changing the way we explore ocean chemistry. *Oceanography*, 27(1), 50-61.
- Andersson, L. (1996). Trends in nutrient and oxygen concentrations in the Skagerrak-Kattegat. *Journal of Sea Research*, 35(1-3), 63–71. [https://doi.org/10.1016/S1385-1101\(96\)90735-2](https://doi.org/10.1016/S1385-1101(96)90735-2)
- Anschutz, P., Dedieu, K., Desmazes, F., & Chaillou, G. (2005). Speciation, oxidation state, and reactivity of particulate manganese in marine sediments. *Chemical Geology*, 218(3-4), 265-279. <https://doi.org/10.1016/j.chemgeo.2005.01.008>
- Aure, J., Danielssen, D., & Svendsen, E. (1998). The origin of Skagerrak coastal water off Arendal in relation to variations in nutrient concentrations. *ICES Journal of Marine Science*, 55(4), 610–619. <https://doi.org/10.1006/jmsc.1998.0395>
- Badewien, T. H., Hoppmann, M., & Tippenhauer, S. (2022). *Physical oceanography during RV HEINCKE cruise HE586 PANGAEA*. <https://doi.org/10.1594/PANGAEA.940830>
- Bakker, J., Lüerßen, G., Marencic, H., & Jung, K. (2009). Hazardous Substances. In H. Marencic & J. de Vlas (Eds.), *Wadden Sea Ecosystem No. 25*. Common Wadden Sea Secretariat, Trilateral Monitoring and Assessment Group, Wilhelmshaven, Germany.
- Balkoni, A., Guignard, M. S., Boersma, M., & Wiltshire, K. H. (2023). Evaluation of different averaging methods for calculation of ratios in nutrient data. *Fundamental and Applied Limnology*. <https://doi.org/10.1127/fal/2023/1487>
- Banks, J. L., Ross, D. J., Keough, M. J., Eyre, B. D., & Macleod, C. K. (2012). Measuring hypoxia induced metal release from highly contaminated estuarine sediments during a 40 day laboratory incubation experiment. *The Science of the total environment*, 420, 229-237. <https://doi.org/10.1016/j.scitotenv.2012.01.033>
- Barling, J., & Anbar, A. D. (2004). Molybdenum isotope fractionation during adsorption by manganese oxides. *Earth and Planetary Science Letters*, 217(3), 315-329. [https://doi.org/10.1016/S0012-821X\(03\)00608-3](https://doi.org/10.1016/S0012-821X(03)00608-3)
- Batley, G. E., & Gardner, D. (1977). Sampling and storage of natural waters for trace metal analysis. *Water research*, 11(9), 745–756. [https://doi.org/10.1016/0043-1354\(77\)90042-2](https://doi.org/10.1016/0043-1354(77)90042-2)
- Beldowski, J., Brenner, M., & Lehtonen, K. K. (2020). Contaminated by war: A brief history of sea-dumping of munitions. *Marine Environmental Research*, 162, 105189. <https://doi.org/10.1016/j.marenvres.2020.105189>
- Bergquist, B. A., Wu, J., & Boyle, E. A. (2007). Variability in oceanic dissolved iron is dominated by the colloidal fraction. *Geochimica et Cosmochimica Acta*, 71(12), 2960–2974. <https://doi.org/10.1016/j.gca.2007.03.013>
- Berrang, P. G., & Grill, E. V. (1974). The effect of manganese oxide scavenging on molybdenum in saanich inlet, British Columbia. *Marine Chemistry*, 2(2), 125–148. [https://doi.org/10.1016/0304-4203\(74\)90033-4](https://doi.org/10.1016/0304-4203(74)90033-4)

- Bersuder, P., Amouroux, I., Belzunce-Segarra, M. J., Bolam, T., Caetano, M., Carvalho, I., . . . Zhang, H. (2021). Concurrent sampling of transitional and coastal waters by Diffusive Gradient in Thin-films (DGT) and spot sampling for trace metals analysis. *Methodsx*, 8, 101462. <https://doi.org/10.1016/j.mex.2021.101462>
- Bethke, C. M., Sanford, R. A., Kirk, M. F., Jin, Q., & Flynn, T. M. (2011). The thermodynamic ladder in geomicrobiology. *American Journal of Science*, 311(3), 183-210. <https://doi.org/10.2475/03.2011.01>
- Biller, D. V., & Bruland, K. W. (2012). Analysis of Mn, Fe, Co, Ni, Cu, Zn, Cd, and Pb in seawater using the Nobias-chelate PA1 resin and magnetic sector inductively coupled plasma mass spectrometry (ICP-MS). *Marine Chemistry*, 130-131(3), 12–20. <https://doi.org/10.1016/j.marchem.2011.12.001>
- Bockelmann, F.-D., Puls, W., Kleeberg, U., Müller, D., & Emeis, K.-C. (2018). Mapping mud content and median grain-size of North Sea sediments – A geostatistical approach. *Marine Geology*, 397, 60-71. <https://doi.org/10.1016/j.margeo.2017.11.003>
- Bozec, Y., Thomas, H., Elkalay, K., & de Baar, H. J. W. (2005). The continental shelf pump for CO<sub>2</sub> in the North Sea—evidence from summer observation. *Marine Chemistry*, 93(2-4), 131-147. <https://doi.org/10.1016/j.marchem.2004.07.006>
- Brückner, S., & Mackensen, A. (2006). Deep-water renewal in the Skagerrak during the last 1200 years triggered by the North Atlantic Oscillation: evidence from benthic foraminiferal  $\delta^{18}O$ . *The Holocene*, 16(3), 331. <https://doi.org/10.1191/0959683605hl931r>
- Bruland, K. W., Middag, R., & Lohan, M. C. (2014). Controls of Trace Metals in Seawater. In *Treatise on Geochemistry* (Second edition ed., Vol. 35, pp. 19–51). Elsevier. <https://doi.org/10.1016/B978-0-08-095975-7.00602-1>
- BSH. (2016). *Nordseezustand 2008-2011* (Berichte des BSH, Issue. <https://www.bsh.de/download/Berichte-des-BSH-54.pdf>
- Burson, A., Stomp, M., Akil, L., Brussaard, C. P. D., & Huisman, J. (2016). Unbalanced reduction of nutrient loads has created an offshore gradient from phosphorus to nitrogen limitation in the North Sea. *Limnology and Oceanography*, 61(3), 869–888. <https://doi.org/10.1002/lno.10257>
- Butler, A. (1998). Acquisition and Utilization of Transition Metal Ions by Marine Organisms. *Science*, 281(5374), 207-209. <https://doi.org/10.1126/science.281.5374.207>
- Byrne, R. H., & Kim, K.-H. (1990). Rare earth element scavenging in seawater. *Geochimica et Cosmochimica Acta*, 54(10), 2645–2656. [https://doi.org/10.1016/0016-7037\(90\)90002-3](https://doi.org/10.1016/0016-7037(90)90002-3)
- Byrnes, T. A., & Dunn, R. J. K. (2020). Boating- and Shipping-Related Environmental Impacts and Example Management Measures: A Review. *Journal of Marine Science and Engineering*, 8(11). <https://doi.org/10.3390/jmse8110908>
- Callies, U., Kreuz, M., Petersen, W., & Voynova, Y. G. (2021). On using lagrangian drift simulations to aid interpretation of in situ monitoring data. *Frontiers in Marine Science*, 8, 666653. <https://doi.org/10.3389/fmars.2021.666653>
- Canfield, D. E., Jørgensen, B. B., Fossing, H., Glud, R., Gundersen, J., Ramsing, N. B., . . . Hall, P. O. J. (1993). Pathways of organic carbon oxidation in three continental margin sediments. *Marine Geology*, 113(1-2), 27-40. [https://doi.org/10.1016/0025-3227\(93\)90147-N](https://doi.org/10.1016/0025-3227(93)90147-N)
- Canfield, D. E., Thamdrup, B., & Hansen, J. W. (1993). The anaerobic degradation of organic matter in Danish coastal sediments: Iron reduction, manganese reduction,



- and sulfate reduction. *Geochimica et Cosmochimica Acta*, 57(16), 3867-3883. [https://doi.org/10.1016/0016-7037\(93\)90340-3](https://doi.org/10.1016/0016-7037(93)90340-3)
- Chaichana, S., Jickells, T., & Johnson, M. (2019). Interannual variability in the summer dissolved organic matter inventory of the North Sea: implications for the continental shelf pump. *Biogeosciences*, 16(5), 1073–1096. <https://doi.org/10.5194/bg-16-1073-2019>
- Chavez, F. P., Messié, M., & Pennington, J. T. (2011). Marine primary production in relation to climate variability and change. *Annual review of marine science*, 3, 227-260. <https://doi.org/10.1146/annurev.marine.010908.163917>
- Cotruvo Jr, J. A. (2019). The chemistry of lanthanides in biology: recent discoveries, emerging principles, and technological applications. *ACS central science*, 5(9), 1496-1506. <https://doi.org/10.1021/acscentsci.9b00642>
- Croot, P. L., Karlson, B., Wulff, A., Linares, F., & Andersson, K. (2002). Trace metal/phytoplankton interactions in the Skagerrak. *Journal of Marine Systems*, 35(1-2), 39–60. [https://doi.org/10.1016/S0924-7963\(02\)00044-1](https://doi.org/10.1016/S0924-7963(02)00044-1)
- Cutter, G., Casciotti, K., Croot, P., Geibert, W., Heimbürger, L.-E., Lohan, M., . . . van de Flierdt, T. (2017). Sampling and Sample-handling Protocols for GEOTRACES Cruises. Version 3, August 2017. 178. <https://doi.org/10.25607/OBP-2>
- Dai, M., Martin, J.-M., & Cauwet, G. (1995). The significant role of colloids in the transport and transformation of organic carbon and associated trace metals (Cd, Cu and Ni) in the Rhône delta (France). *Marine Chemistry*, 51(2), 159–175. [https://doi.org/10.1016/0304-4203\(95\)00051-R](https://doi.org/10.1016/0304-4203(95)00051-R)
- Danielsson, L. G. (1982). On the use of filters for distinguishing between dissolved and particulate fractions in natural waters. *Water research*, 16(2), 179–182. [https://doi.org/10.1016/0043-1354\(82\)90108-7](https://doi.org/10.1016/0043-1354(82)90108-7)
- Dave, G., & Dennegård, B. (1994). Sediment toxicity and heavy metals in the Kattegat and Skagerrak. *Journal of Aquatic Ecosystem Health*, 3, 207-219. <https://doi.org/10.1007/BF00043242>
- de Baar, H., Schijf, J., & Byrne, R. H. (1991). Solution chemistry of the rare earth elements in seawater. *European Journal of Solid State and Inorganic Chemistry*(28), 357–373.
- de Leeuw, G., Skjøth, C. A., Hertel, O., Jickells, T., Spokes, L., Vignati, E., . . . Kunz, G. J. (2003). Deposition of nitrogen into the North Sea. *Atmospheric Environment*, 37, 145-165. [https://doi.org/10.1016/S1352-2310\(03\)00246-2](https://doi.org/10.1016/S1352-2310(03)00246-2)
- Dellwig, O., Beck, M., Lemke, A., Lunau, M., Kolditz, K., Schnetger, B., & Brumsack, H. J. (2007). Non-conservative behaviour of molybdenum in coastal waters: Coupling geochemical, biological, and sedimentological processes. *Geochimica et Cosmochimica Acta*, 71(11), 2745–2761. <https://doi.org/10.1016/j.gca.2007.03.014>
- Diesing, M., Thorsnes, T., & Bjarnadóttir, L. R. (2021). Organic carbon densities and accumulation rates in surface sediments of the North Sea and Skagerrak. *Biogeosciences*, 18(6), 2139-2160. <https://doi.org/10.5194/bg-18-2139-2021>
- DIN32645. (1994). Nachweis-, Erfassungs- und Bestimmungsgrenze. In: Beuth Verlag, Berlin.
- Ebeling, A., Zimmermann, T., Klein, O., Irrgeher, J., & Pröfrock, D. (2022). Analysis of Seventeen Certified Water Reference Materials for Trace and Technology-Critical Elements. *Geostandards and Geoanalytical Research*, 46(2), 351–378. <https://doi.org/10.1111/ggr.12422>
- Echeveste, P., Agustí, S., & Tovar-Sánchez, A. (2012). Toxic thresholds of cadmium and lead to oceanic phytoplankton: Cell size and ocean basin–dependent effects.

- Environmental toxicology and chemistry*, 31(8), 1887-1894.  
<https://doi.org/10.1002/etc.1893>
- Ellison, S. L. R., & Williams, A. (2012). *Eurachem/CITAC Guide: Quantifying Uncertainty in Analytical Measurement*.
- Emeis, K.-C., van Beusekom, J., Callies, U., Ebinghaus, R., Kannen, A., Kraus, G., . . . Zorita, E. (2015). The North Sea — A shelf sea in the Anthropocene. *Journal of Marine Systems*, 141, 18-33. <https://doi.org/10.1016/j.jmarsys.2014.03.012>
- Emerson, S. R., & Husted, S. S. (1991). Ocean anoxia and the concentrations of molybdenum and vanadium in seawater. *Marine Chemistry*, 34(3-4), 177-196. [https://doi.org/10.1016/0304-4203\(91\)90002-E](https://doi.org/10.1016/0304-4203(91)90002-E)
- Field, C. B., Behrenfeld, M. J., Randerson, J. T., & Falkowski, P. (1998). Primary Production of the Biosphere: Integrating Terrestrial and Oceanic Components. *Science*, 281(5374), 237-240. <https://doi.org/10.1126/science.281.5374.237>
- Fitzsimmons, J. N., & Boyle, E. A. (2012). An intercalibration between the GEOTRACES GO-FLO and the MITESS/Vanes sampling systems for dissolved iron concentration analyses (and a closer look at adsorption effects). *Limnology and Oceanography: Methods*, 10(6), 437-450. <https://doi.org/10.4319/lom.2012.10.437>
- Frigstad, H., Kaste, O., Deininger, A., Kvalsund, K., Christensen, G., Bellerby, R. G. J., . . . King, A. L. (2020). Influence of Riverine Input on Norwegian Coastal Systems. *Frontiers in Marine Science*, 7. <https://doi.org/10.3389/fmars.2020.00332>
- Gardner, M., & Comber, S. (1997). Sample filtration as a source of error in the determination of trace metals in marine waters. *The Analyst*, 122(10), 1029-1032. <https://doi.org/10.1039/A704527A>
- Geider, R. J. (1987). Light and temperature dependence of the carbon to chlorophyll a ratio in microalgae and cyanobacteria: implications for physiology and growth of phytoplankton. *New Phytologist*, 1-34.
- Goldberg, T., Archer, C., Vance, D., & Poulton, S. W. (2009). Mo isotope fractionation during adsorption to Fe (oxyhydr)oxides. *Geochimica et Cosmochimica Acta*, 73(21), 6502-6516. <https://doi.org/10.1016/j.gca.2009.08.004>
- Goldberg, T., Archer, C., Vance, D., Thamdrup, B., McAnena, A., & Poulton, S. W. (2012). Controls on Mo isotope fractionations in a Mn-rich anoxic marine sediment, Gullmar Fjord, Sweden. *Chemical Geology*, 296-297, 73-82. <https://doi.org/10.1016/j.chemgeo.2011.12.020>
- Goldstein, S. J., & Jacobsen, S. B. (1988). Rare earth elements in river waters. *Earth and Planetary Science Letters*, 89(1), 35-47. [https://doi.org/10.1016/0012-821X\(88\)90031-3](https://doi.org/10.1016/0012-821X(88)90031-3)
- Graßhoff, K., Kremling, K., Anderson, L. G., & Ehrhardt, M. (Eds.). (1999). *Methods of seawater analysis* (3rd, completely rev. and extended ed. ed.). Wiley-VCH. <https://doi.org/10.1002/9783527613984>.
- Gröger, M., Maier-Reimer, E., Mikolajewicz, U., Moll, A., & Sein, D. (2013). NW European shelf under climate warming: implications for open ocean-shelf exchange, primary production, and carbon absorption. *Biogeosciences*, 10(6), 3767-3792. <https://doi.org/10.5194/bg-10-3767-2013>
- Gross, E., Di Pane, J., Boersma, M., & Meunier, C. L. (2022). River discharge-related nutrient effects on North Sea coastal and offshore phytoplankton communities. *Journal of Plankton Research*, 44(6), 959-972. <https://doi.org/10.1093/plankt/fbac049>

- Grosse, J., van Breugel, P., Brussaard, C. P. D., & Boschker, H. T. S. (2017). A biosynthesis view on nutrient stress in coastal phytoplankton. *Limnology and Oceanography*, 62(2), 490–506. <https://doi.org/10.1002/lno.10439>
- Grybos, M., Davranche, M., Gruau, G., & Petitjean, P. (2007). Is trace metal release in wetland soils controlled by organic matter mobility or Fe-oxyhydroxides reduction? *Journal of Colloid and Interface Science*, 314(2), 490-501. <https://doi.org/10.1016/j.jcis.2007.04.062>
- Gypens, N., Borges, A. V., & Ghyoot, C. (2017). How phosphorus limitation can control climate-active gas sources and sinks. *Journal of Marine Systems*, 170, 42–49. <https://doi.org/10.1016/j.jmarsys.2017.02.002>
- Hall, G. E. M., Bonham-Carter, G. F., Horowitz, A. J., Lum, K., Lemieux, C., Quemerais, B., & Garbarino, J. R. (1996). The effect of using different 0.45 µm filter membranes on ‘dissolved’ element concentrations in natural waters. *Applied Geochemistry*, 11(1-2), 243–249. [https://doi.org/10.1016/0883-2927\(96\)00059-5](https://doi.org/10.1016/0883-2927(96)00059-5)
- Hamzeh, M., Ouddane, B., Daye, M., & Halwani, J. (2014). Trace Metal Mobilization from Surficial Sediments of the Seine River Estuary. *Water, Air, & Soil Pollution*, 225(3), 175. <https://doi.org/10.1007/s11270-014-1878-0>
- Hansen, H. P., & Koroleff, F. (2007). Determination of nutrients. Methods of Seawater Analysis: Third, Completely Revised and Extended Edition. In: Weinheim, Germany: Wiley-VCH Verlag GmbH.
- Hargrave, B. T., Holmer, M., & Newcombe, C. P. (2008). Towards a classification of organic enrichment in marine sediments based on biogeochemical indicators. *Marine Pollution Bulletin*, 56(5), 810-824. <https://doi.org/10.1016/j.marpolbul.2008.02.006>
- Harmesa, Wahyudi, A. a. J., Lestari, & Taufiqurrahman, E. (2022). Variability of trace metals in coastal and estuary: Distribution, profile, and drivers. *Marine Pollution Bulletin*, 174, 113173. <https://doi.org/10.1016/j.marpolbul.2021.113173>
- Hart, B. T. (1982). Uptake of trace metals by sediments and suspended particulates: a review. *Hydrobiologia*, 91(1), 299-313. <https://doi.org/10.1007/BF02391947>
- Hedberg, Y., Herting, G., & Wallinder, I. O. (2011). Risks of using membrane filtration for trace metal analysis and assessing the dissolved metal fraction of aqueous media--a study on zinc, copper and nickel. *Environmental pollution (Barking, Essex : 1987)*, 159(5), 1144–1150. <https://doi.org/10.1016/j.envpol.2011.02.014>
- Hoffmann, L. J., Breitbarth, E., Boyd, P. W., & Hunter, K. A. (2012). Influence of ocean warming and acidification on trace metal biogeochemistry. *Marine Ecology Progress Series*, 470, 191-205. <https://doi.org/10.3354/meps10082>
- Horowitz, A. J., Elrick, K. A., & Colberg, M. R. (1992). The effect of membrane filtration artifacts on dissolved trace element concentrations. *Water research*, 26(6), 753–763. [https://doi.org/10.1016/0043-1354\(92\)90006-P](https://doi.org/10.1016/0043-1354(92)90006-P)
- Horowitz, A. J., Lum, K. R., Garbarino, J. R., Hall, G. E. M., Lemieux, C., & Demas, C. R. (1996a). The effect of membrane filtration on dissolved trace element concentrations. *Water, Air, & Soil Pollution*, 90(1-2), 281–294. <https://doi.org/10.1007/BF00619288>
- Horowitz, A. J., Lum, K. R., Garbarino, J. R., Hall, G. E. M., Lemieux, C., & Demas, C. R. (1996b). Problems Associated with Using Filtration To Define Dissolved Trace Element Concentrations in Natural Water Samples. *Environmental science & technology*, 30(3), 954–963. <https://doi.org/10.1021/es950407h>
- Houk, R. S., Fassel, V. A., Flesch, G. D., Svec, H. J., Gray, A. L., & Taylor, C. E. (1980). Inductively coupled argon plasma as an ion source for mass spectrometric determination of trace elements. *Analytical chemistry*, 52(14), 2283-2289. <https://doi.org/10.1021/ac50064a012>

- Hydes, D. J., & Kremling, K. (1993). Patchiness in dissolved metals (Al, Cd, Co, Cu, Mn, Ni) in North Sea surface waters: seasonal differences and influence of suspended sediment. *Continental Shelf Research*, 13(10), 1083–1101. [https://doi.org/10.1016/0278-4343\(93\)90042-V](https://doi.org/10.1016/0278-4343(93)90042-V)
- IPCC. (2022). *Climate Change 2022: Mitigation of Climate Change. Contribution of Working Group III to the Sixth Assessment Report of the Intergovernmental Panel on Climate Change* (P. R. Shukla, J. Skea, R. Slade, A. A. Khoualdjje, R. v. Diemen, D. McCollum, M. Pathak, S. Some, P. Vyas, R. Fradera, M. Belkacemi, A. Hasija, G. Lisboa, S. Luz, & J. Malley, Eds.). Cambridge University Press. <https://doi.org/doi:10.1017/9781009157926>
- Jackson, S. L., Spence, J., Janssen, D. J., Ross, A. R. S., & Cullen, J. T. (2018). Determination of Mn, Fe, Ni, Cu, Zn, Cd and Pb in seawater using offline extraction and triple quadrupole ICP-MS/MS [10.1039/C7JA00237H]. *Journal of Analytical Atomic Spectrometry*, 33(2), 304-313. <https://doi.org/10.1039/C7JA00237H>
- Jickells, T. D. (1998). Nutrient biogeochemistry of the coastal zone. *Science*, 281(5374), 217-222. <https://doi.org/10.1126/science.281.5374.217>
- Jickells, T. D., Baker, A. R., & Chance, R. (2016). Atmospheric transport of trace elements and nutrients to the oceans. *Philosophical Transactions of the Royal Society A: Mathematical, Physical and Engineering Sciences*, 374(2081), 20150286. <https://doi.org/10.1098/rsta.2015.0286>
- Johannessen, T., & Dahl, E. (1996). Declines in oxygen concentrations along the Norwegian Skagerrak coast, 1927-1993: A signal of ecosystem changes due to eutrophication? *Limnology and Oceanography*, 41(4), 766–778. <https://doi.org/10.4319/lo.1996.41.4.0766>
- Johnson, M., Sanders, R., Avgoustidi, V., Lucas, M., Brown, L., Hansell, D., . . . Jickells, T. (2007). Ammonium accumulation during a silicate-limited diatom bloom indicates the potential for ammonia emission events. *Marine Chemistry*, 106(1), 63-75. <https://doi.org/10.1016/j.marchem.2006.09.006>
- Jonge, M., Teuchies, J., Meire, P., Blust, R., & Bervoets, L. (2012). The impact of increased oxygen conditions on metal-contaminated sediments part I: effects on redox status, sediment geochemistry and metal bioavailability. *Water research*, 46(7), 2205-2214. <https://doi.org/10.1016/j.watres.2012.01.052>
- Karlsson, S., Peterson, A., Håkansson, K., & Ledin, A. (1994). Fractionation of trace metals in surface water with screen filters. *Science of The Total Environment*, 149(3), 215–223. [https://doi.org/10.1016/0048-9697\(94\)90180-5](https://doi.org/10.1016/0048-9697(94)90180-5)
- Kelderman, P., & Osman, A. A. (2007). Effect of redox potential on heavy metal binding forms in polluted canal sediments in Delft (The Netherlands). *Water research*, 41(18), 4251-4261. <https://doi.org/10.1016/j.watres.2007.05.058>
- Klein, O., Zimmermann, T., & Pröfrock, D. (2021). Improved determination of technologically critical elements in sediment digests by ICP-MS/MS using N<sub>2</sub>O as a reaction gas. *Journal of Analytical Atomic Spectrometry*, 36(7), 1524-1532. <https://doi.org/10.1039/D1JA00088H>
- Kowalski, N., Dellwig, O., Beck, M., Gräwe, U., Neubert, N., Nägler, T. F., . . . Böttcher, M. E. (2013). Pelagic molybdenum concentration anomalies and the impact of sediment resuspension on the molybdenum budget in two tidal systems of the North Sea. *Geochimica et Cosmochimica Acta*, 119(3–4), 198-211. <https://doi.org/10.1016/j.gca.2013.05.046>



- Krauskopf, K. B. (1956). Factors controlling the concentrations of thirteen rare metals in seawater. *Geochimica et Cosmochimica Acta*, 9(1-2), 1-B32. [https://doi.org/10.1016/0016-7037\(56\)90055-2](https://doi.org/10.1016/0016-7037(56)90055-2)
- Kremling, K., Andreae, M. O., Brüggemann, L., Van den Berg, C. M. G., Prange, A., Schirmacher, M., . . . Kus, J. (1999). Determination of trace elements. *Methods of seawater analysis*, 253-364. <https://doi.org/10.1002/9783527613984.ch12>
- Kremling, K., & Hydes, D. (1988). Summer distribution of dissolved Al, Cd, Co, Cu, Mn and Ni in surface waters around the British Isles. *Continental Shelf Research*, 8(1), 89–105. [https://doi.org/10.1016/0278-4343\(88\)90026-X](https://doi.org/10.1016/0278-4343(88)90026-X)
- Kremling, K., & Petersen, H. (1978). The distribution of Mn, Fe, Zn, Cd and Cu in Baltic seawater; a study on the basis of one anchor station. *Marine Chemistry*, 6(2), 155-170. [https://doi.org/10.1016/0304-4203\(78\)90025-7](https://doi.org/10.1016/0304-4203(78)90025-7)
- Kristensen, E., Røy, H., Debrabant, K., & Valdemarsen, T. (2018). Carbon oxidation and bioirrigation in sediments along a Skagerrak-Kattegat-Belt Sea depth transect. *Marine Ecology Progress Series*, 604, 33-50. <https://doi.org/10.3354/meps12734>
- Kristiansen, T., & Aas, E. (2015). Water type quantification in the Skagerrak, the Kattegat and off the Jutland west coast. *Oceanologia*, 57(2), 177–195. <https://doi.org/10.1016/j.oceano.2014.11.002>
- Ku, T.-L., Mathieu, G. G., & Knauss, K. G. (1977). Uranium in open ocean: concentration and isotopic composition. *Deep Sea Research*, 24(11), 1005–1017. [https://doi.org/10.1016/0146-6291\(77\)90571-9](https://doi.org/10.1016/0146-6291(77)90571-9)
- Kuijpers, A., Dennegård, B., Albinsson, Y., & Jensen, A. (1993). Sediment transport pathways in the Skagerrak and Kattegat as indicated by sediment Chernobyl radioactivity and heavy metal concentrations. *Marine Geology*, 111(3), 231-244. [https://doi.org/10.1016/0025-3227\(93\)90133-G](https://doi.org/10.1016/0025-3227(93)90133-G)
- Kulaksiz, S., & Bau, M. (2007). Contrasting behaviour of anthropogenic gadolinium and natural rare earth elements in estuaries and the gadolinium input into the North Sea. *Earth and Planetary Science Letters*, 260(1-2), 361–371. <https://doi.org/10.1016/j.epsl.2007.06.016>
- Laane, R., Vethaak, A. D., Gandrass, J., Vorkamp, K., Kohler, A., Larsen, M. M., & Strand, J. (2013). Chemical contaminants in the Wadden Sea: Sources, transport, fate and effects. *Journal of Sea Research*, 82, 10–53. <https://doi.org/10.1016/j.seares.2013.03.004>
- Lagerström, M. E., Field, M. P., Séguret, M., Fischer, L., Hann, S., & Sherrell, R. M. (2013). Automated on-line flow-injection ICP-MS determination of trace metals (Mn, Fe, Co, Ni, Cu and Zn) in open ocean seawater: Application to the GEOTRACES program. *Marine Chemistry*, 155, 71–80. <https://doi.org/10.1016/j.marchem.2013.06.001>
- Lane, T. W., Saito, M. A., George, G. N., Pickering, I. J., Prince, R. C., & Morel, F. M. M. (2005). A cadmium enzyme from a marine diatom. *Nature*, 435(7038), 42-42. <https://doi.org/10.1038/435042a>
- Laslett, R. E. (1995). Concentrations of dissolved and suspended particulate Cd, Cu, Mn, Ni, Pb and Zn in surface waters around the coasts of England and Wales and in adjacent seas. *Estuarine Coastal and Shelf Science*, 40(1), 67–85. [https://doi.org/10.1016/0272-7714\(95\)90014-4](https://doi.org/10.1016/0272-7714(95)90014-4)
- Lee, J. H., Kennedy, D. W., Dohnalkova, A., Moore, D. A., Nachimuthu, P., Reed, S. B., & Fredrickson, J. K. (2011). Manganese sulfide formation via concomitant microbial manganese oxide and thiosulfate reduction. *Environmental Microbiology*, 13(12), 3275-3288. <https://doi.org/10.1111/j.1462-2920.2011.02587.x>

- Lefebvre, A., & Dezechache, C. (2020). Trajectories of Changes in Phytoplankton Biomass, *Phaeocystis globosa* and Diatom (incl. *Pseudo-nitzschia* sp.) Abundances Related to Nutrient Pressures in the Eastern English Channel, Southern North Sea. *Journal of Marine Science and Engineering*, 8(6). <https://doi.org/10.3390/jmse8060401>
- Lenstra, W. K., Klomp, R., Molema, F., Behrends, T., & Slomp, C. P. (2021). A sequential extraction procedure for particulate manganese and its application to coastal marine sediments. *Chemical Geology*, 584, 120538. <https://doi.org/10.1016/j.chemgeo.2021.120538>
- Lentini, C. J., Wankel, S. D., & Hansel, C. M. (2012). Enriched iron (III)-reducing bacterial communities are shaped by carbon substrate and iron oxide mineralogy. *Frontiers in Microbiology*, 3, 404. <https://doi.org/10.3389/fmicb.2012.00404>
- Leote, C., Mulder, L. L., Philippart, C. J. M., & Epping, E. H. G. (2016). Nutrients in the Western Wadden Sea: Freshwater Input Versus Internal Recycling. *Estuaries and Coasts*, 39(1), 40–53. <https://doi.org/10.1007/s12237-015-9979-6>
- Logemann, A., Reininghaus, M., Schmidt, M., Ebeling, A., Zimmermann, T., Wolschke, H., . . . Witt, G. (2022). Assessing the chemical anthropocene - Development of the legacy pollution fingerprint in the North Sea during the last century. *Environmental pollution*, 302, 119040. <https://doi.org/10.1016/j.envpol.2022.119040>
- MacDougall, D., Crummett, W. B., & al., e. (1980). Guidelines for data acquisition and data quality evaluation in environmental chemistry. *Analytical chemistry*, 52(14), 2242–2249. <https://doi.org/10.1021/ac50064a004>
- Macovei, V. A., Voynova, Y. G., Becker, M., Triest, J., & Petersen, W. (2021). Long-term intercomparison of two p CO<sub>2</sub> instruments based on ship-of-opportunity measurements in a dynamic shelf sea environment. *Limnology and Oceanography: Methods*, 19(1), 37-50. <https://doi.org/10.1002/lom3.10403>
- Magnusson, B., Ellison, S. L. R., & Örnemark, U. (2015). *Eurachem Guide: Template for Eurachem Guides – A Guide for Guide Editors*. [www.eurachem.org](http://www.eurachem.org)
- Magnusson, K., Ekelund, R., Dave, G., Granmo, A., Forlin, L., Wennberg, L., . . . Brorstrom-Lunden, E. (1996). Contamination and correlation with toxicity of sediment samples from the Skagerrak and Kattegat. *Journal of Sea Research*, 35(1-3), 223–234. [https://doi.org/10.1016/S1385-1101\(96\)90749-2](https://doi.org/10.1016/S1385-1101(96)90749-2)
- Mahowald, N., Jickells, T. D., Baker, A. R., Artaxo, P., Benitez-Nelson, C. R., Bergametti, G., . . . Tsukuda, S. (2008). Global distribution of atmospheric phosphorus sources, concentrations and deposition rates, and anthropogenic impacts. *Global Biogeochemical Cycles*, 22(4). <https://doi.org/10.1029/2008GB003240>
- Mart, L. (1979). Prevention of contamination and other accuracy risks in voltammetric trace metal analysis of natural waters. *Fresenius' Zeitschrift für analytische Chemie*, 296(5), 350–357. <https://doi.org/10.1007/BF00479972>
- Mart, L., Nürnberg, H. W., & Rützel, H. (1985). Levels of heavy metals in the tidal Elbe and its estuary and the heavy metal input into the sea. *Science of The Total Environment*, 44(1), 35-49. [https://doi.org/10.1016/0048-9697\(85\)90049-X](https://doi.org/10.1016/0048-9697(85)90049-X)
- Mayer, A. J., & Wieser, M. E. (2014). The absolute isotopic composition and atomic weight of molybdenum in SRM 3134 using an isotopic double-spike. *Journal of Analytical Atomic Spectrometry*, 29(1), 85-94. <https://doi.org/10.1039/C3JA50164G>
- McLennan, S. M. (1989). Chapter 7. Rare Earth Elements in Sedimentary Rocks: Influence of Provenance and Sedimentary Processes. In B. R. Lipin & G. A. McKay (Eds.), *Geochemistry and Mineralogy of Rare Earth Elements* (pp. 169-200). De Gruyter. <https://doi.org/doi:10.1515/9781501509032-010>

- McQuatters-Gollop, A., Raitos, D. E., Edwards, M., Pradhan, Y., Mee, L. D., Lavender, S. J., & Attrill, M. J. (2007). A long-term chlorophyll data set reveals regime shift in North Sea phytoplankton biomass unconnected to nutrient trends. *Limnology and Oceanography*, 52(2), 635–648. <https://doi.org/10.4319/lo.2007.52.2.0635>
- Meinte, B., David, K., & Huib, E. d. S. (2001). Large-scale circulation and flushing characteristics of the North Sea under various climate forcings. *Climate Research*, 18(1-2), 47-54. <https://www.int-res.com/abstracts/cr/v18/n1-2/p47-54/>
- Meisch, H.-U., & Bielig, H.-J. (1975). Effect of vanadium on growth, chlorophyll formation and iron metabolism in unicellular green algae. *Archives of microbiology*, 105(1), 77-82. <https://doi.org/10.1007/bf00447117>
- Mellet, T., Brown, M. T., Chappell, P. D., Duckham, C., Fitzsimmons, J. N., Till, C. P., . . . Buck, K. N. (2018). The biogeochemical cycling of iron, copper, nickel, cadmium, manganese, cobalt, lead, and scandium in a California Current experimental study. *Limnology and Oceanography*, 63(S1), 23. <https://doi.org/10.1002/lno.10751>
- Morel, F., Milligan, A., & Saito, M. (2006). Marine Bioinorganic Chemistry: The. *The oceans and marine geochemistry*, 6, 113.
- Morel, F. M. M. (2008). The co-evolution of phytoplankton and trace element cycles in the oceans. *Geobiology*, 6(3), 318–324. <https://doi.org/10.1111/j.1472-4669.2008.00144.x>
- Morel, F. M. M., & Price, N. M. (2003). The biogeochemical cycles of trace metals in the oceans. *Science (New York, N.Y.)*, 300(5621), 944–947. <https://doi.org/10.1126/science.1083545>
- Nadeau, K., Brophy, C., Yang, L., Grinberg, P., Pihillagawa Gedara, I., Meija, J., . . . Mester, Z. (2016). NASS-7: Seawater Certified Reference Material for Trace Metals and other Constituents. <https://doi.org/10.4224/crm.2016.nass-7>
- Neff, J. M. (1997). Ecotoxicology of arsenic in the marine environment. *Environmental toxicology and chemistry*, 16(5), 917-927. <https://doi.org/10.1002/etc.5620160511>
- Novotnik, B., Zorz, J., Bryant, S., & Strous, M. (2019). The effect of dissimilatory manganese reduction on lactate fermentation and microbial community assembly. *Frontiers in Microbiology*, 10, 1007. <https://doi.org/10.3389/fmicb.2019.01007>
- Nriagu, J. O. (1989). A global assessment of natural sources of atmospheric trace metals. *Nature*, 338(6210), 47-49. <https://doi.org/10.1038/338047a0>
- Nriagu, J. O., & Pacyna, J. M. (1988). Quantitative assessment of worldwide contamination of air, water and soils by trace metals. *Nature*, 333(6169), 134-139. <https://doi.org/10.1038/333134a0>
- OECD. (2016). *Health care utilisation* <https://doi.org/10.1787/data-00542-en>
- Oldham, V. E., Jones, M. R., Tebo, B. M., & Luther Iii, G. W. (2017). Oxidative and reductive processes contributing to manganese cycling at oxic-anoxic interfaces. *Marine Chemistry*, 195, 122-128. <https://doi.org/10.1016/j.marchem.2017.06.002>
- OSPAR Commission. (2000). Quality Status Report 2000, Region II – Greater North Sea. OSPAR Commission, London.
- OSPAR Commission. (2014). Levels and trends in marine contaminants and their biological effects - CEMP Assessment report 2013.
- Pacyna, J. M., Pacyna, E. G., & Aas, W. (2009). Changes of emissions and atmospheric deposition of mercury, lead, and cadmium. *Atmospheric Environment*, 43(1), 117-127. <https://doi.org/10.1016/j.atmosenv.2008.09.066>
- Padhi, R. K., Biswas, S., Mohanty, A. K., Prabhu, R. K., Satpathy, K. K., & Nayak, L. (2013). Temporal distribution of dissolved trace metal in the coastal waters of southwestern

- Bay of Bengal, India. *Water environment research*, 85(8), 696-705. <https://doi.org/10.2175/106143012x13560205144975>
- Park, S., Choi, M., Jang, D., Joe, D., & Park, K. (2020). Distribution and sources of dissolved and particulate heavy metals (Mn, Co, Ni, Cu, Zn, Cd, Pb) in Masan Bay, Korea. *Ocean Science Journal*, 55(1), 49-67. <https://doi.org/10.1007/s12601-020-0001-2>
- Park, S., Choi, M., Jang, D., Joe, D., Park, K., Lee, H., . . . Park, J. (2020). Spatiotemporal distribution of dissolved heavy metals in Gyeonggi Bay, Korea. *Ocean Science Journal*, 55, 69-84. <https://doi.org/10.1007/s12601-020-0002-1>
- Pätsch, J., & Kühn, W. (2008). Nitrogen and carbon cycling in the North Sea and exchange with the North Atlantic—A model study. Part I. Nitrogen budget and fluxes. *Continental Shelf Research*, 28(6), 767-787. <https://doi.org/10.1016/j.csr.2007.12.013>
- Pätsch, J., Lenhart, H.-J., & Schütt, M. (2004). *Daily loads of nutrients, total alkalinity, dissolved inorganic carbon and dissolved organic carbon of the European continental rivers for the years 1977-2002*. Inst.. für Meereskunde.
- Paytan, A., Mackey, K. R. M., Chen, Y., Lima, I. D., Doney, S. C., Mahowald, N., . . . Post, A. F. (2009). Toxicity of atmospheric aerosols on marine phytoplankton. *Proceedings of the National Academy of Sciences*, 106(12), 4601-4605. <https://doi.org/10.1073/pnas.0811486106>
- Petersen, J., Pröfrock, D., Paschke, A., Broekaert, J. A. C., & Prange, A. (2015). Laboratory calibration and field testing of the Chemcatcher-Metal for trace levels of rare earth elements in estuarine waters. *Environmental science and pollution research international*, 22(20), 16051–16059. <https://doi.org/10.1007/s11356-015-4823-x>
- Pinedo-González, P., West, A. J., Tovar-Sánchez, A., Duarte, C. M., Marañón, E., Cermeño, P., . . . Fernández, A. (2015). Surface distribution of dissolved trace metals in the oligotrophic ocean and their influence on phytoplankton biomass and productivity. *Global Biogeochemical Cycles*, 29(10), 1763-1781. <https://doi.org/10.1002/2015GB005149>
- Pröfrock, D., & Prange, A. (2012). Inductively Coupled Plasma–Mass Spectrometry (ICP-MS) for Quantitative Analysis in Environmental and Life Sciences: A Review of Challenges, Solutions, and Trends. *Applied Spectroscopy*, 66(8), 843-868. <https://doi.org/10.1366/12-06681>
- Przibilla, A., Iwanski, S., Zimmermann, T., & Pröfrock, D. (2023). Impact of storage temperature and filtration method on dissolved trace metal concentrations in coastal water samples. *Water environment research*, 95(9), e10922. <https://doi.org/10.1002/wer.10922>
- Quéroué, F., Townsend, A., van der Merwe, P., Lannuzel, D., Sarthou, G., Bucciarelli, E., & Bowie, A. (2014). Advances in the offline trace metal extraction of Mn, Co, Ni, Cu, Cd, and Pb from open ocean seawater samples with determination by sector field ICP-MS analysis [10.1039/C3AY41312H]. *Analytical Methods*, 6(9), 2837-2847. <https://doi.org/10.1039/C3AY41312H>
- R Core Team. (2022). *R: A language and environment for statistical computing*. In *R Foundation for Statistical Computing, Vienna, Austria* <https://www.R-project.org>
- Raabe, T., & Wiltshire, K. H. (2009). Quality control and analyses of the long-term nutrient data from Helgoland Roads, North Sea. *Journal of Sea Research*, 61(1-2), 3–16. <https://doi.org/10.1016/j.seares.2008.07.004>
- Ramos, S. J., Dinali, G. S., de Carvalho, T. S., Chaves, L. C., Siqueira, J. O., & Guilherme, L. R. G. (2016). Rare earth elements in raw materials and products of the phosphate fertilizer industry in South America: Content, signature, and crystalline phases.



- Journal of Geochemical Exploration*, 168, 177-186.  
<https://doi.org/10.1016/j.gexplo.2016.06.009>
- Rathor, G., Chopra, N., & Adhikari, T. (2014). Nickel as a Pollutant and its Management. *Int Res J Environ Sci*, 3(10), 94-98.
- Redfield, A. C., Ketchum, B. H., & Richards, F. A. (1963). The influence of organisms on the composition of seawater. *The sea*, 2, 26-77.
- Rehder, D. (2015). The role of vanadium in biology. *Metallomics : integrated biometal science*, 7(5), 730–742. <https://doi.org/10.1039/c4mt00304g>
- Retschko, A.-K., Vosteen, P., Plass, A., Welter, E., & Scholz, F. (2023). Comparison of sedimentary iron speciation obtained by sequential extraction and X-ray absorption spectroscopy. *Marine Chemistry*, 252, 104249. <https://doi.org/10.1016/j.marchem.2023.104249>
- Revelle, W. R. (2017). psych: Procedures for personality and psychological research.
- Reyes, C., Schneider, D., Thürmer, A., Kulkarni, A., Lipka, M., Szejtjenszus, S. Y., . . . Friedrich, M. W. (2017). Potentially Active Iron, Sulfur, and Sulfate Reducing Bacteria in Skagerrak and Bothnian Bay Sediments. *Geomicrobiology Journal*, 34(10), 840-850. <https://doi.org/10.1080/01490451.2017.1281360>
- Rinklebe, J., & Shaheen, S. M. (2017). Redox chemistry of nickel in soils and sediments: A review. *Chemosphere*, 179, 265-278. <https://doi.org/10.1016/j.chemosphere.2017.02.153>
- Rudge, J. F., Reynolds, B. C., & Bourdon, B. (2009). The double spike toolbox. *Chemical Geology*, 265(3-4), 420-431. <https://doi.org/10.1016/j.chemgeo.2009.05.010>
- Rysgaard, S., Fossing, H., & Jensen, M. M. (2001). Organic matter degradation through oxygen respiration, denitrification, and manganese, iron, and sulfate reduction in marine sediments (the Kattegat and the Skagerrak). *Ophelia*, 55(2), 77-91. <https://doi.org/10.1080/00785236.2001.10409475>
- Samanta, S., Cloete, R., Looek, J., Rossouw, R., & Roychoudhury, A. N. (2021). Determination of Trace Metal (Mn, Fe, Ni, Cu, Zn, Co, Cd and Pb) Concentrations in Seawater Using Single Quadrupole ICP-MS: A Comparison between Offline and Online Preconcentration Setups. *Minerals*, 11(11). <https://doi.org/10.3390/min11111289>
- Sanz-Lázaro, C., Valdemarsen, T., Marín, A., & Holmer, M. (2011). Effect of temperature on biogeochemistry of marine organic-enriched systems: Implications in a global warming scenario. *Ecological Applications*, 21(7), 2664-2677. <https://doi.org/10.1890/10-2219.1>
- Schlesinger, W. H., Klein, E. M., & Vengosh, A. (2017). Global biogeochemical cycle of vanadium. *Proceedings of the National Academy of Sciences*, 114(52), E11092-E11100. <https://doi.org/10.1073/pnas.1715500114>
- Schneider, A. B., Koschinsky, A., Kiprotich, J., Poehle, S., & do Nascimento, P. C. (2016). An experimental study on the mixing behavior of Ti, Zr, V and Mo in the Elbe, Rhine and Weser estuaries. *Estuarine Coastal and Shelf Science*, 170, 34–44. <https://doi.org/10.1016/j.ecss.2015.12.002>
- Scholz, F., McManus, J., & Sommer, S. (2013). The manganese and iron shuttle in a modern euxinic basin and implications for molybdenum cycling at euxinic ocean margins. *Chemical Geology*, 355, 56-68. <https://doi.org/10.1016/j.chemgeo.2013.07.006>
- Schulz, K. G., Zondervan, I., Gerringa, L. J. A., Timmermans, K. R., Veldhuis, M. J. W., & Riebesell, U. (2004). Effect of trace metal availability on coccolithophorid calcification. *Nature*, 430(7000), 673–676. <https://doi.org/10.1038/nature02631>

- Shaheen, S. M., Rinklebe, J., Frohne, T., White, J. R., & DeLaune, R. D. (2014). Biogeochemical Factors Governing Cobalt, Nickel, Selenium, and Vanadium Dynamics in Periodically Flooded Egyptian North Nile Delta Rice Soils. *Soil Science Society of America Journal*, 78(3), 1065-1078. <https://doi.org/10.2136/sssaj2013.10.0441>
- Shiller, A. M., & Boyle, E. A. (1987). Dissolved vanadium in rivers and estuaries. *Earth and Planetary Science Letters*, 86(2-4), 214–224. [https://doi.org/10.1016/0012-821X\(87\)90222-6](https://doi.org/10.1016/0012-821X(87)90222-6)
- Sholkovitz, E. R., Landing, W. M., & Lewis, B. L. (1994). Ocean particle chemistry: The fractionation of rare earth elements between suspended particles and seawater. *Geochimica et Cosmochimica Acta*, 58(6), 1567–1579. [https://doi.org/10.1016/0016-7037\(94\)90559-2](https://doi.org/10.1016/0016-7037(94)90559-2)
- Siebert, C., McManus, J., Bice, A., Poulson, R., & Berelson, W. M. (2006). Molybdenum isotope signatures in continental margin marine sediments. *Earth and Planetary Science Letters*, 241(3-4), 723-733. <https://doi.org/10.1016/j.epsl.2005.11.010>
- Siebert, C., Nägler, T. F., von Blanckenburg, F., & Kramers, J. D. (2003). Molybdenum isotope records as a potential new proxy for paleoceanography. *Earth and Planetary Science Letters*, 211(1-2), 159-171. [https://doi.org/10.1016/S0012-821X\(03\)00189-4](https://doi.org/10.1016/S0012-821X(03)00189-4)
- Siems, A., Nantke, C., Neumann, A., Sanders, T., & Pröfrock, D. (2024). *Nutrient and trace metal data distribution from water samples of ALKOR cruise AL557 PANGAEA*. <https://doi.pangaea.de/10.1594/PANGAEA.967370>
- Siems, A., Sanders, T., & Pröfrock, D. (2024). *Nutrient and trace metal data distribution from water samples of HEINCKE cruise HE586 PANGAEA*. <https://doi.pangaea.de/10.1594/PANGAEA.967369>
- Siems, A., Zimmermann, T., Sanders, T., & Pröfrock, D. (2024). Dissolved trace elements and nutrients in the North Sea—a current baseline. *Environmental Monitoring and Assessment*, 196(6), 539. <https://doi.org/10.1007/s10661-024-12675-2>
- Skogen, M. D., Soiland, H., & Svendsen, E. (2004). Effects of changing nutrient loads to the North Sea. *Journal of Marine Systems*, 46(1-4), 23–38. <https://doi.org/10.1016/j.jmarsys.2003.11.013>
- Sohrin, Y., Isshiki, K., Kuwamoto, T., & Nakayama, E. (1987). Tungsten in north pacific waters. *Marine Chemistry*, 22(1), 95-103. [https://doi.org/10.1016/0304-4203\(87\)90051-X](https://doi.org/10.1016/0304-4203(87)90051-X)
- Sohrin, Y., Urushihara, S., Nakatsuka, S., Kono, T., Higo, E., Minami, T., . . . Umetani, S. (2008). Multielemental determination of GEOTRACES key trace metals in seawater by ICPMS after preconcentration using an ethylenediaminetriacetic acid chelating resin. *Analytical chemistry*, 80(16), 6267–6273. <https://doi.org/10.1021/ac800500f>
- Sunda, W. G. (2012). Feedback interactions between trace metal nutrients and phytoplankton in the ocean. *Frontiers in Microbiology*, 3. <https://doi.org/10.3389/fmicb.2012.00204>
- Sündermann, J., & Pohlmann, T. (2011). A brief analysis of North Sea physics. *Oceanologia*, 53(3), 663-689. <https://doi.org/10.5697/oc.53-3.663>
- Sutorius, M., Mori, C., Greskowiak, J., Boettcher, L., Bunse, C., Dittmar, T., . . . Pahnke, K. (2022). Rare earth element behaviour in seawater under the influence of organic matter cycling during a phytoplankton spring bloom – A mesocosm study [Original Research]. *Frontiers in Marine Science*, 9. <https://www.frontiersin.org/articles/10.3389/fmars.2022.895723>
- Tankere-Muller, S., Zhang, H., Davison, W., Finke, N., Larsen, O., Stahl, H., & Glud, R. N. (2007). Fine scale remobilisation of Fe, Mn, Co, Ni, Cu and Cd in contaminated

- marine sediment. *Marine Chemistry*, 106(1-2), 192-207. <https://doi.org/10.1016/j.marchem.2006.04.005>
- Tappin, A. D., Millward, G. E., Statham, P. J., Burton, J. D., & Morris, A. W. (1995). Trace Metals in the Central and Southern North Sea. *Estuarine, Coastal and Shelf Science*, 41(3), 275–323. [https://doi.org/10.1006/S0272-7714\(85\)70068-7](https://doi.org/10.1006/S0272-7714(85)70068-7)
- Tessier, A., & Campbell, P. G. C. (1987). Partitioning of trace metals in sediments: relationships with bioavailability. *Hydrobiologia*, 149, 43-52. <https://doi.org/10.1007/BF00048645>
- Thibault de Chanvalon, A., Luther, G. W., Estes, E. R., Necker, J., Tebo, B. M., Su, J., & Cai, W. J. (2023). Influence of manganese cycling on alkalinity in the redox stratified water column of Chesapeake Bay. *Biogeosciences*, 20(14), 3053-3071. <https://doi.org/10.5194/bg-20-3053-2023>
- Thomas, H., Bozec, Y., Elkalay, K., & De Baar, H. J. (2004). Enhanced open ocean storage of CO<sub>2</sub> from shelf sea pumping. *Science*, 304(5673), 1005-1008. <https://doi.org/10.1126/science.1095491>
- Thomas, W. H., Hollibaugh, J. T., Seibert, D. L. R., & Wallace Jr, G. T. (1980). Toxicity of a mixture of ten metals to phytoplankton. *Marine Ecology Progress Series*, 2(3), 212-220. <https://doi.org/10.3354/meps002213>
- Tonnard, M., Planquette, H., Bowie, A. R., van der Merwe, P., Gallinari, M., Desprez de Gésincourt, F., . . . Sarthou, G. (2020). Dissolved iron in the North Atlantic Ocean and Labrador Sea along the GEOVIDE section (GEOTRACES section GA01). *Biogeosciences*, 17(4), 917-943. <https://doi.org/10.5194/bg-17-917-2020>
- Topcu, D., Behrendt, H., Brockmann, U., & Claussen, U. (2011). Natural background concentrations of nutrients in the German Bight area (North Sea). *Environmental Monitoring and Assessment*, 174(1), 361-388. <https://doi.org/10.1007/s10661-010-1463-y>
- Tørnes, J. A., Opstad, A. M., & Johnsen, B. A. (2006). Determination of organoarsenic warfare agents in sediment samples from Skagerrak by gas chromatography-mass spectrometry. *Science of The Total Environment*, 356(1), 235-246. <https://doi.org/10.1016/j.scitotenv.2005.03.031>
- Tørnes, J. A., Voie, Ø. A., Ljønes, M., Opstad, A. M., Bjerkeseth, L. H., & Hussain, F. (2002). Investigation and risk assessment of ships loaded with chemical ammunition scuttled in Skagerrak. <https://www.ffi.no/en/publications-archive/investigation-and-risk-assessment-of-ships-loaded-with-chemical-ammunition-scuttled-in-skagerrak>
- Trapasso, G., Chiesa, S., Freitas, R., & Pereira, E. (2021). What do we know about the ecotoxicological implications of the rare earth element gadolinium in aquatic ecosystems? *The Science of the total environment*, 781, 146273. <https://doi.org/10.1016/j.scitotenv.2021.146273>
- Tribovillard, N., Algeo, T. J., Lyons, T., & Riboulleau, A. (2006). Trace metals as paleoredox and paleoproductivity proxies: an update. *Chemical Geology*, 232(1-2), 12-32. <https://doi.org/10.1016/j.chemgeo.2006.02.012>
- Twining, B. S., & Baines, S. B. (2013). The trace metal composition of marine phytoplankton. *Annual review of marine science*, 5, 191-215. <https://doi.org/10.1146/annurev-marine-121211-172322>
- Ussher, S. J., Worsfold, P. J., Achterberg, E. P., Laes, A., Blain, S., Laan, P., & Baar, H. J. W. (2007). Distribution and redox speciation of dissolved iron on the European continental margin. *Limnology and Oceanography*, 52(6), 2530–2539. <https://doi.org/10.4319/lo.2007.52.6.2530>

- van Beusekom, J. E. E., Carstensen, J., Dolch, T., Grage, A., Hofmeister, R., Lenhart, H., . . . Ruiters, H. (2019). Wadden Sea Eutrophication: Long-Term Trends and Regional Differences. *Frontiers in Marine Science*, 6. <https://doi.org/10.3389/fmars.2019.00370>
- van der Zee, C., & Van Raaphorst, W. (2004). Manganese oxide reactivity in North Sea sediments. *Journal of Sea Research*, 52(2), 73-85. <https://doi.org/10.1016/j.seares.2003.10.005>
- Waeles, M., Tanguy, V., Lespes, G., & Riso, R. D. (2008). Behaviour of colloidal trace metals (Cu, Pb and Cd) in estuarine waters: An approach using frontal ultrafiltration (UF) and stripping chronopotentiometric methods (SCP). *Estuarine, Coastal and Shelf Science*, 80(4), 538-544. <https://doi.org/10.1016/j.ecss.2008.09.010>
- Wang, Y., & Van Cappellen, P. (1996). A multicomponent reactive transport model of early diagenesis: Application to redox cycling in coastal marine sediments. *Geochimica et Cosmochimica Acta*, 60(16), 2993-3014. [https://doi.org/10.1016/0016-7037\(96\)00140-8](https://doi.org/10.1016/0016-7037(96)00140-8)
- Wasylenki, L. E., Rolfe, B. A., Weeks, C. L., Spiro, T. G., & Anbar, A. D. (2008). Experimental investigation of the effects of temperature and ionic strength on Mo isotope fractionation during adsorption to manganese oxides. *Geochimica et Cosmochimica Acta*, 72(24), 5997-6005. <https://doi.org/10.1016/j.gca.2008.08.027>
- Wickham, H., Averick, M., Bryan, J., Chang, W., McGowan, L., François, R., . . . Yutani, H. (2019). Welcome to the Tidyverse. *Journal of Open Source Software*, 4(43), 1686. <https://doi.org/10.21105/joss.01686>
- Wieser, M. E., De Laeter, J. R., & Varner, M. D. (2007). Isotope fractionation studies of molybdenum. *International Journal of Mass Spectrometry*, 265(1), 40-48. <https://doi.org/10.1016/j.ijms.2007.05.010>
- Wiltshire, K. H., Boersma, M., Carstens, K., Kraberg, A. C., Peters, S., & Scharfe, M. (2015). Control of phytoplankton in a shelf sea: Determination of the main drivers based on the Helgoland Roads Time Series. *Journal of Sea Research*, 105, 42-52. <https://doi.org/10.1016/j.seares.2015.06.022>
- Wiltshire, K. H., Kraberg, A., Bartsch, I., Boersma, M., Franke, H.-D., Freund, J., . . . Wichels, A. (2010). Helgoland Roads, North Sea: 45 Years of Change. *Estuaries and Coasts*, 33(2), 295-310. <https://doi.org/10.1007/s12237-009-9228-y>
- Winther, N. G., & Johannessen, J. A. (2006). North Sea circulation: Atlantic inflow and its destination. *Journal of Geophysical Research: Oceans*, 111(C12). <https://doi.org/10.1029/2005JC003310>
- Wong, M. Y., Rathod, S. D., Marino, R., Li, L., Howarth, R. W., Alastuey, A., . . . Mahowald, N. M. (2021). Anthropogenic Perturbations to the Atmospheric Molybdenum Cycle. *Global Biogeochemical Cycles*, 35(2), e2020GB006787. <https://doi.org/10.1029/2020GB006787>
- Wu, J., Boyle, E., Sunda, W., & Wen, L. S. (2001). Soluble and colloidal iron in the oligotrophic North Atlantic and North Pacific. *Science (New York, N.Y.)*, 293(5531), 847-849. <https://doi.org/10.1126/science.1059251>
- Wu, J., & Luther, G. W. (1994). Size-fractionated iron concentrations in the water column of the western North Atlantic Ocean. *Limnology and Oceanography*, 39(5), 1119-1129. <https://doi.org/10.4319/lo.1994.39.5.1119>
- Wuttig, K., Townsend, A. T., van der Merwe, P., Gault-Ringold, M., Holmes, T., Schallenberg, C., . . . Bowie, A. R. (2019). Critical evaluation of a seaFAST system for the analysis of trace metals in marine samples. *Talanta*, 197, 653-668. <https://doi.org/10.1016/j.talanta.2019.01.047>

- 
- Yang, T., Chen, Y., Zhou, S., & Li, H. (2019). Impacts of Aerosol Copper on Marine Phytoplankton: A Review. *Atmosphere*, 10(7). <https://doi.org/10.3390/atmos10070414>
- Zhang, J., Zhou, F., Chen, C., Sun, X., Shi, Y., Zhao, H., & Chen, F. (2018). Spatial distribution and correlation characteristics of heavy metals in the seawater, suspended particulate matter and sediments in Zhanjiang Bay, China. *PLoS One*, 13(8), e0201414. <https://doi.org/10.1371/journal.pone.0201414>
- Zhang, X., Ward, B. B., & Sigman, D. M. (2020). Global Nitrogen Cycle: Critical Enzymes, Organisms, and Processes for Nitrogen Budgets and Dynamics. *Chemical reviews*, 120(12), 5308-5351. <https://doi.org/10.1021/acs.chemrev.9b00613>
- Zimmermann, T., Au, M., Reese, A., Klein, O., Hildebrandt, L., & Pröfrock, D. (2020). Substituting HF by HBF<sub>4</sub>- an optimized digestion method for multi-elemental sediment analysis via ICP-MS/MS. *Analytical methods : advancing methods and applications*, 12(30), 3778-3787. <https://doi.org/10.1039/d0ay01049a>



## 9 Appendix







### 9.1 List of hazardous substances

| Substance                      | GHS-Symbols | Hazard statements            | Precautionary statements  |
|--------------------------------|-------------|------------------------------|---|
| acetic acid (>95% w/w)         |             | H226<br>H314                 | P210<br>P280<br>P301+P330+P331<br>P303+P361+P353<br>P305+P351+P338<br>P310      |
| acetone                        |             | H225<br>H319<br>H336         | P210<br>P305+P351+P338<br>P403+P233   |
| ammonia<br>(20-22% w/w)        |             | H314<br>H355                 | P280<br>P301+P330+P331<br>P304+P340<br>P305+P351+P338<br>P310<br>P303+P361+P353 |
| ammonium chloride              |             | H302<br>H319                 | P270<br>P305+P351+P338  |
| ammonium molybdate             |             | H302<br>H315<br>H319<br>H335 | P280<br>P302+P352<br>P305+P351+P338<br>P337+P313                                |
| antimony potassium<br>tartrate |             | H302+H332<br>H411            | P261<br>P273<br>P301+P312+P330<br>P304+P340+P312<br>P391<br>P501                |
| disodium tetraborate           |             | H319<br>H360FD               | P201<br>P305+P351+P338<br>P308+P313   |
| ethanol (96% w/w)              |             | H225<br>H319                 | P210<br>P233<br>P305+P351+P338  |



| Substance                                | GHS-Symbols | Hazard statements                            | Precautionary statements   |
|--|-------------|--|--|
| hydrochloric acid<br>(35% w/w)           |             | H290   | P234<br>P390<br>P406   |
|  |             | H290<br>H314<br>H317<br>H350<br>H373<br>H411 | P201<br>P227<br>P280<br>P301+P330+P331<br>P302+P352<br>P305+P351+P338<br>P308+P310 |
| ICP-multi-element<br>standard solutions  |             | H315<br>H319<br>335                          | P261<br>P280<br>P302+P352<br>P305+P351+P338<br>P312<br>P403+P233<br>P501           |
|  |             | H315<br>H319<br>335                          | P210<br>P220<br>P280<br>P303+P361+P353<br>P304+P340+P310<br>P305+P351+P338         |
| naphthylethylendiamin<br>dihydrochloride |             | H315<br>H319<br>335                          | P261<br>P280<br>P302+P352<br>P305+P351+P338<br>P312<br>P403+P233<br>P501           |
| nitric acid<br>(65% w/w)                 |             | H272<br>H290<br>H303<br>H314                 | P210<br>P220<br>P280<br>P303+P361+P353<br>P304+P340+P310<br>P305+P351+P338         |
|  |             | H272<br>H290<br>H303<br>H314                 | P210<br>P220<br>P280<br>P303+P361+P353<br>P304+P340+P310<br>P305+P351+P338         |
| oxalic acid                              |             | H302+H312<br>H318                            | P264<br>P280<br>P301+P312<br>P302+P352+P312<br>P305+P351+P338<br>P362+P364         |
|  |             | H302+H312<br>H318                            | P264<br>P280<br>P301+P312<br>P302+P352+P312<br>P305+P351+P338<br>P362+P364         |



| Substance                          | GHS-Symbols   | Hazard statements | Precautionary statements |
|------------------------------------|---|-------------------|--------------------------|
| phthalaldehyde                     |    | H301              | P260                     |
|                                    |   | H314              | P273                     |
|                                    |   | H317              | P280                     |
|                                    |   | H318              | P303+P361+P353           |
|                                    |   | H335              | P304+P340+P310           |
|                                    |   | H400              | P305+P351+P338           |
|                                    |   | H410              |                          |
| phosphoric acid<br>(85% w/w)       |    | H290              | P260                     |
|                                    |   | H302              | P280                     |
|                                    |   | H314              | P303+P361+P353           |
|                                    |   | H318              | P305+P351+P338           |
|                                    |   |                   | P390                     |
| sodium dodecyl sulfate             |  | H228              | P210                     |
|                                    |   | H302+H332         | P273                     |
|                                    |   | H315              | P280                     |
|                                    |   | H318              | P301+P312                |
|                                    |   | H335              | P304+P340+P312           |
|                                    |   | H412              | P305+P351+P338           |
| SRM 3134<br>(molybdenum)           |  | H290              | P234                     |
|                                    |   | H315              | P246                     |
|                                    |   | H318              | P280                     |
|                                    |   |                   | P302+P352                |
| sulfuric acid (96%<br>w/w)         |  | H290              | P234                     |
|                                    |   | H314              | P246                     |
|                                    |   | H318              | P280                     |
|                                    |   |                   | P302+P352                |
|                                    |   |                   | P305+P351+P338           |
| tetrafluoroboric acid<br>(38% w/w) |  | H314              | P280                     |
|                                    |   |                   | P305+P351+P338           |
|                                    |   |                   | P310                     |



## 9.2 Table of peer-reviewed publications

| Title  | Journal  | Authors   | Impact Factor | Reads / Citations |
|--|--|---|---------------|-------------------|
| Impact of storage temperature and filtration method on dissolved trace metal concentrations in coastal water samples | Water Environment Research (2023)              | Przibilla, A., Iwainki, S., Zimmermann, T., Pröfrock, D.  | 3.1           | 521 / 0           |
| Biogenic silica cycling in the Skagerrak   | Frontiers in Marine Science (2023)             | Spiegel, T., Dale, A. W., Lenz, N., Schmidt, M., Sommer, S., Kalapurakkal, H. T., Przibilla, A., Lindhorst, S., Wallmann, K.                | 3.7           | 1400 / 3          |
| An analytical strategy for challenging members of the microplastic family: Particles from anti-corrosion coatings    | Journal of Hazardous Materials (2024)          | Hildebrandt, L., Fischer, M., Klein, O., Zimmermann, T., Fensky, F., Siems, A., Zonderman, A., Hengstmann, E., Kirchgeorg, T., Pröfrock, D. | 13.6          | 13 / 0            |
| Dissolved trace elements and nutrients in the North Sea—a current baseline   | Environmental Monitoring and Assessment (2024) | Siems, A., Zimmermann, T., Sanders, T., Pröfrock, D.  | 3.0           | 825 / 1           |
| Trace metals in Skagerrak sediments – spatial distribution and release under changing oxygen conditions              | Biogeochemistry (under review)                 | Siems, A., Zimmermann, T., Sanders, T., Wieser, M. E., Pröfrock, D.   | 4.0           |                   |



### 9.3 List of conference contributions

**Siems, A.**, Sanders, T., Zimmermann, T., Wieser, M. E., Proefrock, D. (2024): Release and turn-over of carbon, nitrogen and metals under oxic and suboxic conditions in long-term incubations of Skagerrak sediments. EGU General Assembly 2024. Wien (AUT), 14.04. – 19.04.2024. *This poster was awarded the OSPP (outstanding student poster presentation) award of EGU.*

**Przibilla, A.**, Zimmermann, T., Sanders, T., Wieser, M. E., Proefrock, D. (2023):  $\delta^{98/95}\text{Mo}$  as tracer for past and current redox conditions in sediment samples from the Skagerrak. 7th PhD Seminar of the German Working Group for Analytical Spectroscopy (DAAS) in the GDCh Division of Analytical Chemistry. Berlin (DEU), 15.11.2023 – 17.11.2023.

**Przibilla, A.**, Sanders, T., Zimmermann, T., Schulz, G., Nantke, C., Proefrock, D. (2023): Response of metal contaminated Skagerrak sediments to changing oxygen conditions. Goldschmidt Conference 2023. Lyon (FRA), 09.07. – 14.07.2023.

Rohrweber, A., **Przibilla, A.**, Ebeling, A., Zimmermann, T., Proefrock, D. (2023): The spatial distribution of trace metals in North Sea and Baltic Sea – defining a baseline to study effects of potential ocean alkalinity enhancement activities. Goldschmidt Conference 2023. Lyon (FRA), 09.07. – 14.07.2023.

Proefrock, D., **Przibilla, A.**, Klein, O., Hildebrandt, L., Ebeling, A., el Gareb, F., Rohrweber, A., Witthoff, C., Zimmermann, T. (2023): New Applications of ICP-MS/MS and MC ICP-MS to study the chemical Anthropocene. European Winter Conference on Plasma Spectrochemistry. Ljubljana (SVN), 29.01. – 03.02.2023.

**Przibilla, A.**, Iwainki, S., Zimmermann, T., Nantke, C., Proefrock, D. (2023): Analysis of dissolved trace metals in North Sea water: How to obtain reliable data using ICP-MS/MS? 54<sup>th</sup> annual conference of the DGMS. Dortmund (DEU), 14.05. – 17.05.2023.

**Przibilla, A.**, Iwainki, S., Zimmermann, T., Proefrock, D. (2022): Aufbereitung von Meerwasserproben für die Messung der Metallgehalte mittels seaFAST-ICP-MS: Einfluss

von Filtrationsmethode und Lagerung auf die Ergebnisse. ICP-MS Anwender\*innen Treffen. Leoben (AUT), 05.09.2022 – 08.09.2022.

Pröfrock, D., **Przibilla, A.**, Klein, O., Hildebrandt, L., Ebeling, A., El Gareb, F., Zimmermann, T. (2022): More than trace elements – New applications for ICP-MS to investigate the chemical Anthropocene. ICP-MS Anwender\*innen Treffen. Leoben (AUT), 05.09.2022 – 08.09.2022.

Wippermann, D., Ebeling, A., **Przibilla, A.**, Zimmermann, T., Pröfrock, D. (2022): Analytik von Meerwasserproben aus Offshore Windparks mittels ICP-MS unter Verwendung des Aufkonzentrierungssystems seaFAST®. ICP-MS Anwender\*innen Treffen. Leoben (AUT), 05.09.2022 – 08.09.2022.

## 9.4 List of published data sets

**Przibilla, A.; Sanders, T.; Neumann, A.; Nantke, C. (2023):** Pore water nutrient concentrations from sediments sampled during RV Alkor cruise AL557 [dataset]. PANGAEA, <https://doi.org/10.1594/PANGAEA.956878>

**Siems, A.; Nantke, C.; Neumann, A.; Sanders, T.; Pröfrock, D. (2024):** Nutrient and trace metal data distribution from water samples of ALKOR cruise AL557 [dataset]. PANGAEA, <https://doi.pangaea.de/10.1594/PANGAEA.967370>

**Siems, A.; Sanders, T.; Pröfrock, D. (2024):** Nutrient and trace metal data distribution from water samples of HEINCKE cruise HE586 [dataset]. PANGAEA, <https://doi.pangaea.de/10.1594/PANGAEA.967369>

**Siems, A.; Metzke, M.; Pröfrock, D.; Sanders, T.; Zimmermann, T. (2024):** Sediment core and pore water data for HE586 [dataset]. PANGAEA, <https://doi.pangaea.de/10.1594/PANGAEA.967504>

**Siems, A.; Metzke, M.; Pröfrock, D.; Sanders, T.; Zimmermann, T. (2024):** Sediment core and pore water data for AL557 [dataset]. PANGAEA, <https://doi.pangaea.de/10.1594/PANGAEA.967500>

## 9.5 List of research cruises and sampling campaigns

|                    |  |
|--------------------|--|
| <b>LP202105</b>    | Elbe River; RV Ludwig Prandtl; May 2 <sup>nd</sup> – 5 <sup>th</sup> , 2021            |
| <b>HE586</b>       | North Sea and Skagerrak, RV Heincke; October 4 <sup>th</sup> – 11 <sup>th</sup> , 2021 |
| <b>CARWatt2021</b> | Dangast Wadden Sea sampling; September 22 <sup>nd</sup> , 2021                         |
| <b>CARWatt2022</b> | Dangast and Janssand Wadden Sea sampling; January, April, June, October 2022           |





## 9.6 Supplementary Figures

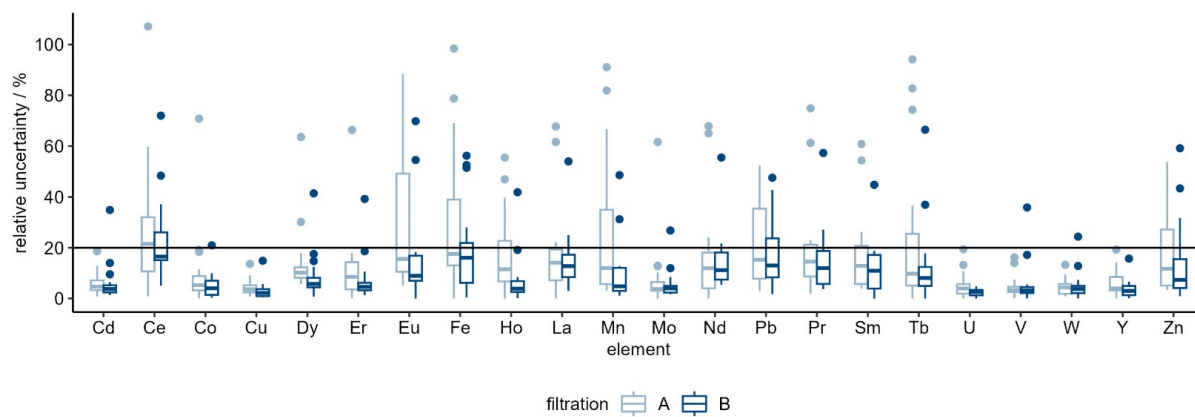


Figure A 1 Relative uncertainty ( $2 \cdot SD$ ) of the filtration triplicates for the respective elements and filtration methods ( $n=18$ ).

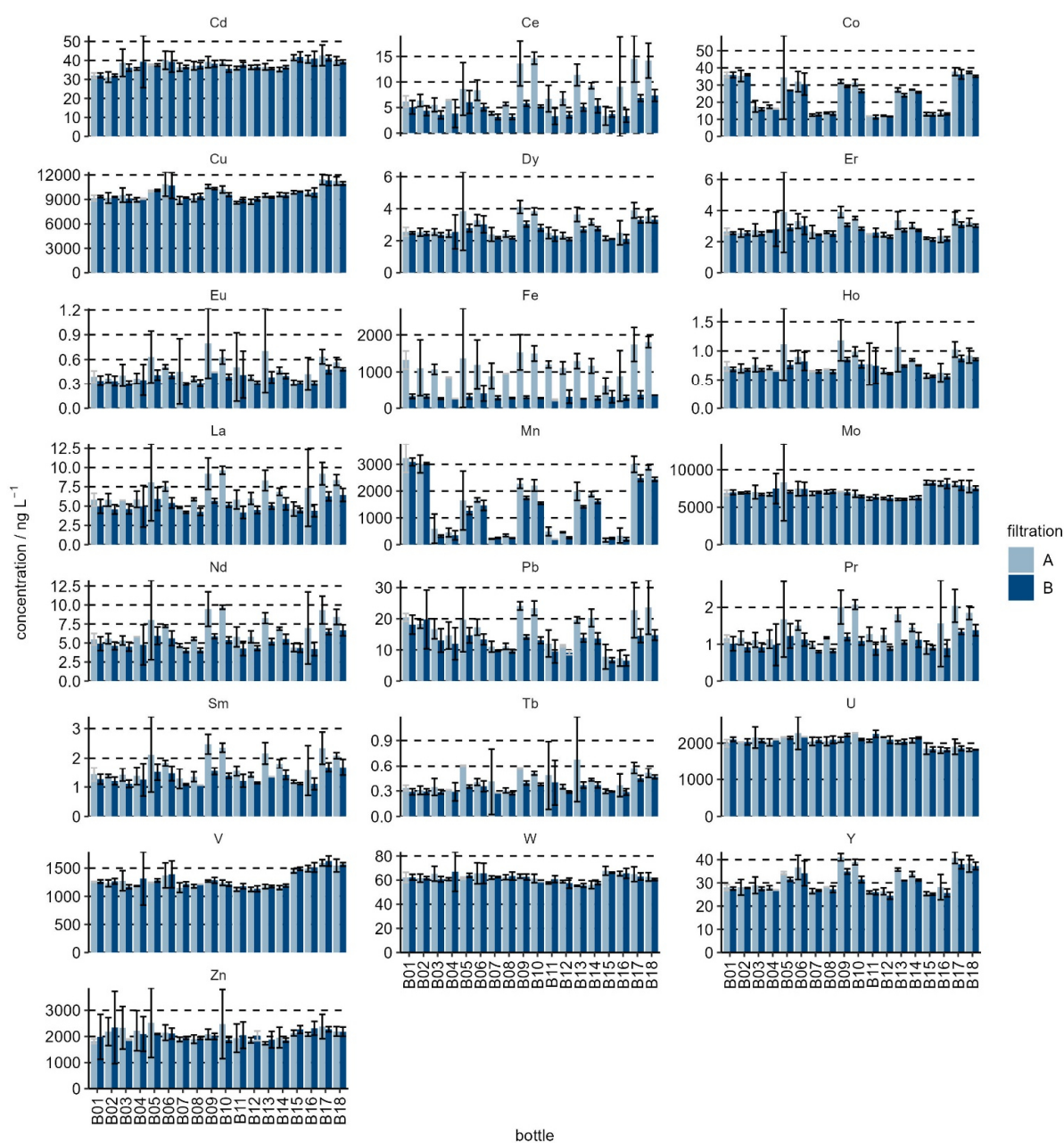


Figure A 2 Concentrations of all investigated elements in filtrates of each sample bottle for both filtration setups. Each pair of bars corresponds to one sample bottle that was either directly filtered (B01, B02), cooled or frozen (B03-B18) before filtration. Error bars correspond to  $2*SD$  ( $n=3$ , except for grey error bars with  $n=2$  after Dean-Dixon test). Description of samples for respective bottle numbers are listed in Table A 3.

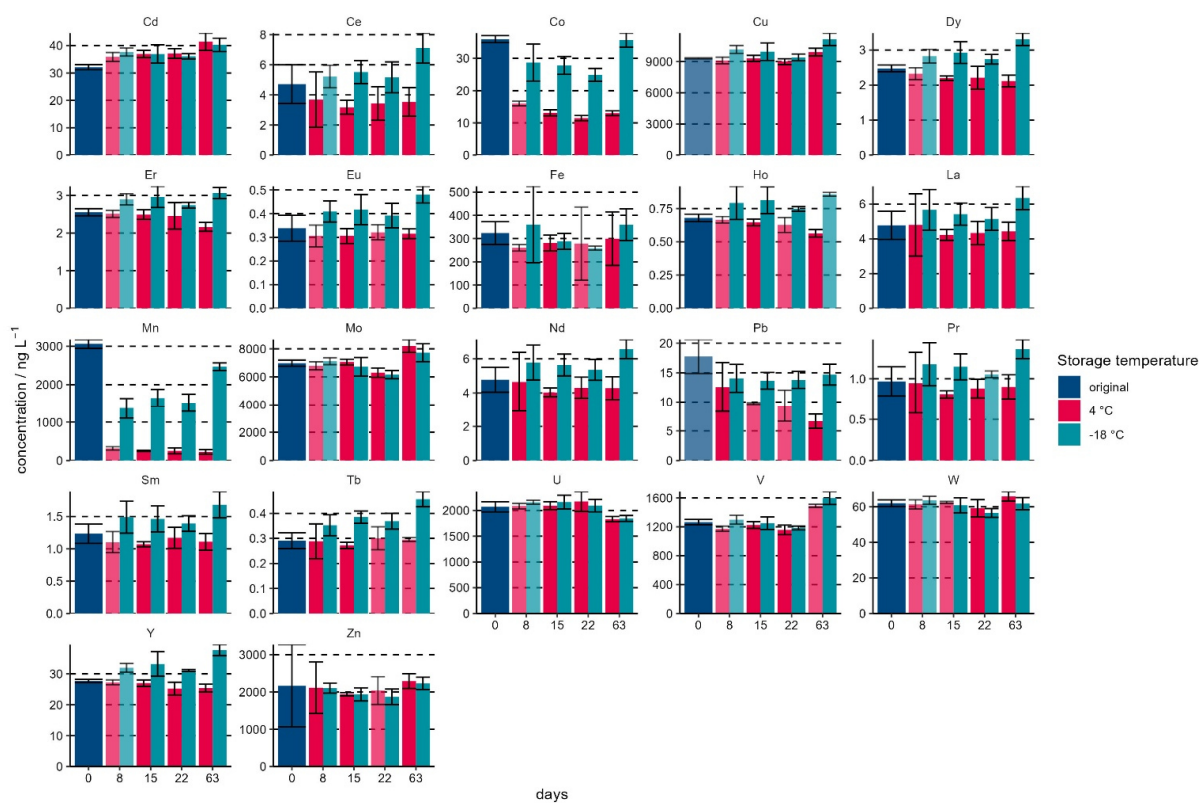


Figure A 3 Temporal trend of all investigated elemental concentrations in the filtrates obtained using filtration setup B. Error bars correspond to 2\*SD with  $n=6$  (except for pale-colored bars with  $n=5$  after Dean-Dixon test). Please note that the x-axis is not chronologically spaced.

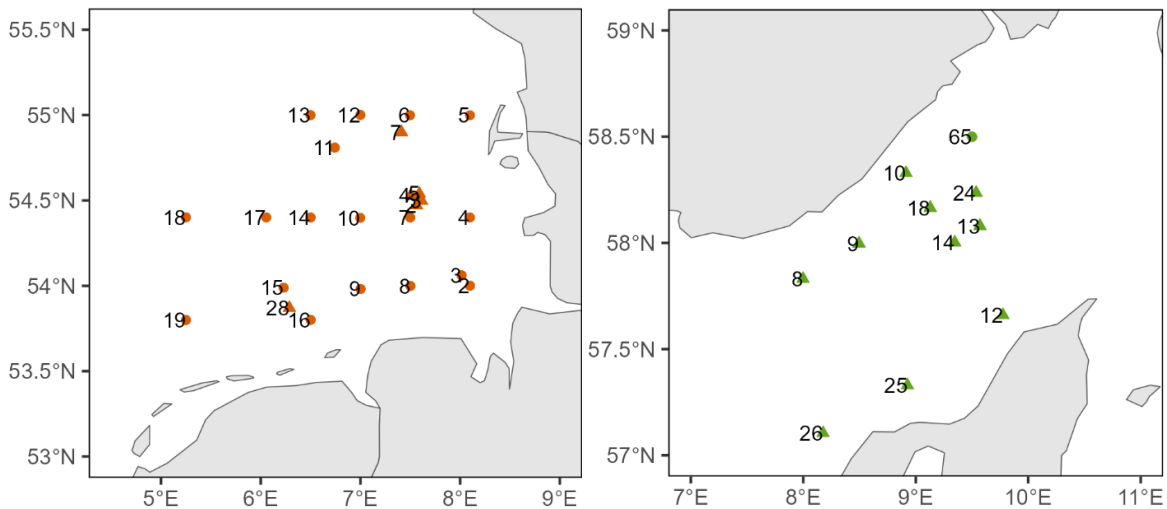
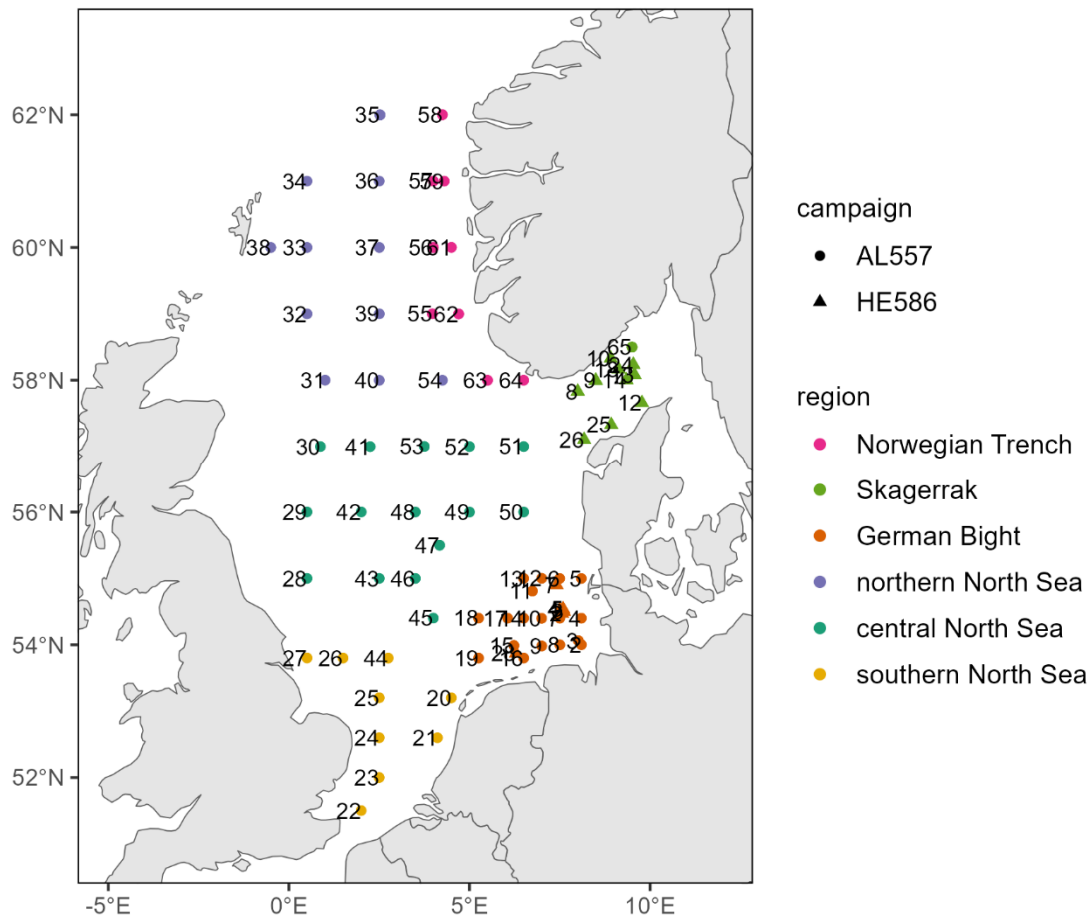


Figure A 4 Water sampling stations and regions for data interpretation in the North Sea. The circles indicate AL557 samples, triangles indicate HE586 samples. The maps on the bottom show the stations in the German Bight (left) and Skagerrak (right).

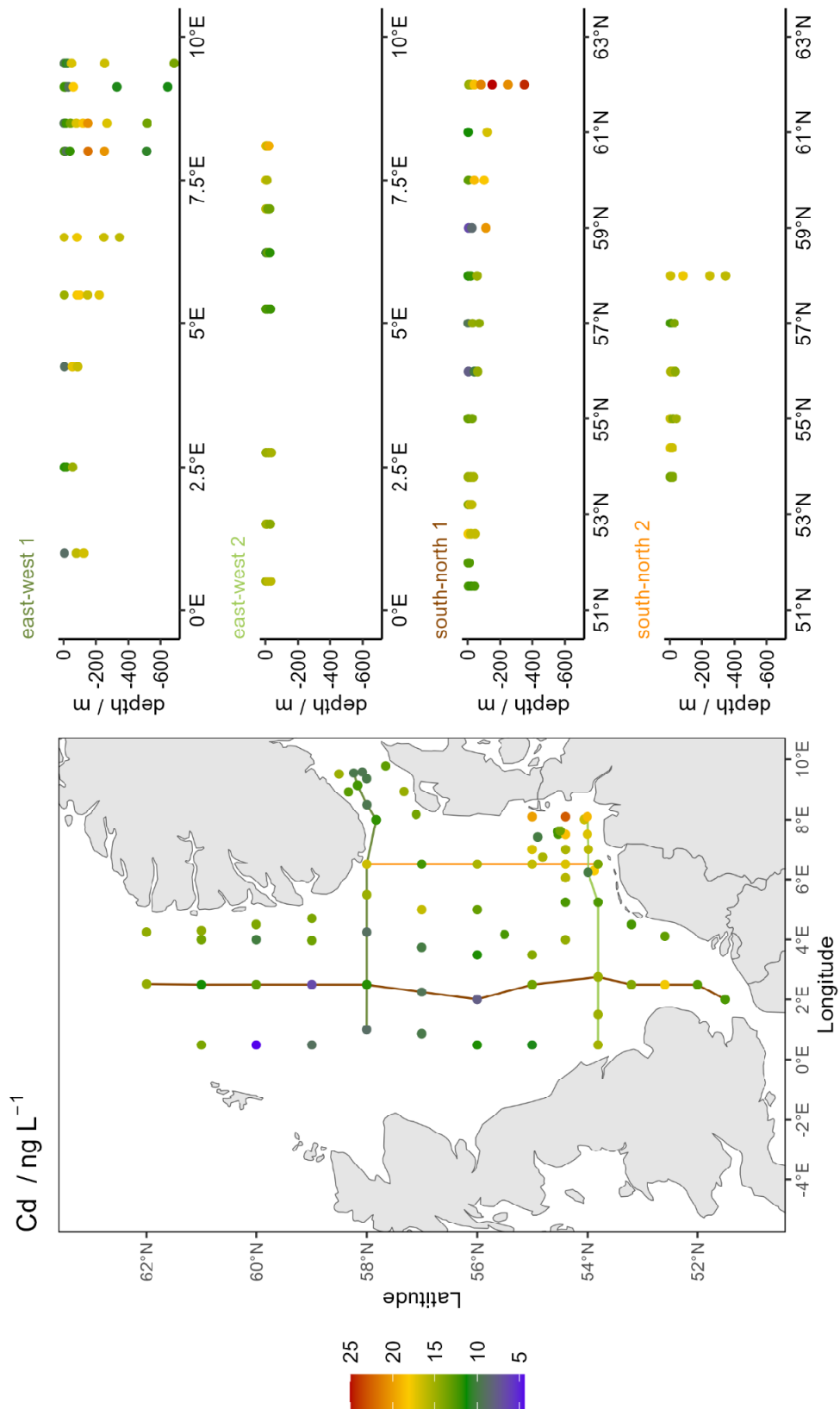


Figure A 5 Surface concentrations and depth profiles of Cd across two south-north and two east-west transects. The northernmost transect is east-west 1 and the westernmost transect is south-north 1.  $x$  indicates concentrations below the LOD, and faint points indicate concentrations between LOD and LOQ.

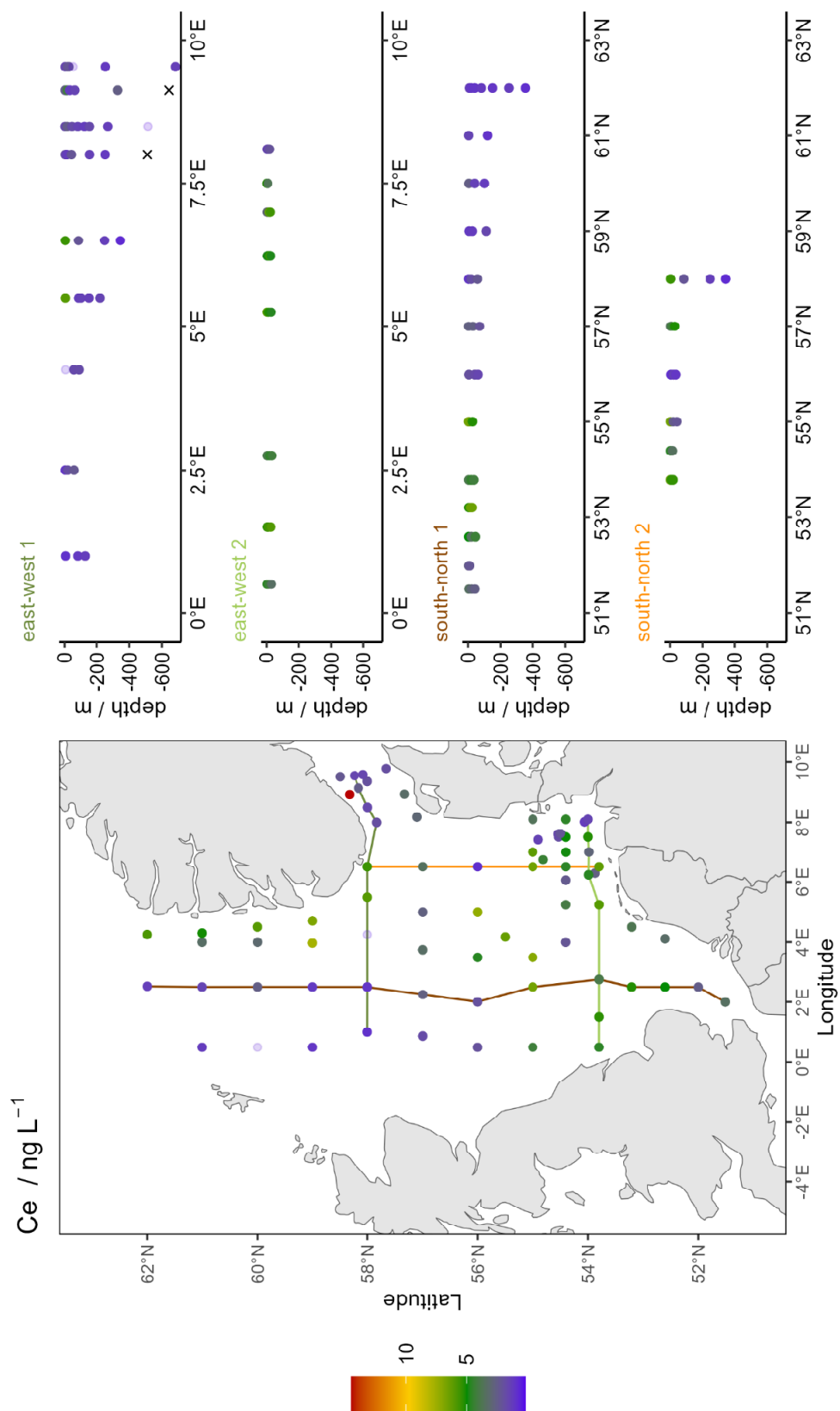


Figure A 6 Surface concentrations and depth profiles of Ce across two south-north and two east-west transects. The northernmost transect is east-west 1 and the westernmost transect is south-north 1. x indicates concentrations below the LOD, and faint points indicate concentrations between LOD and LOQ.

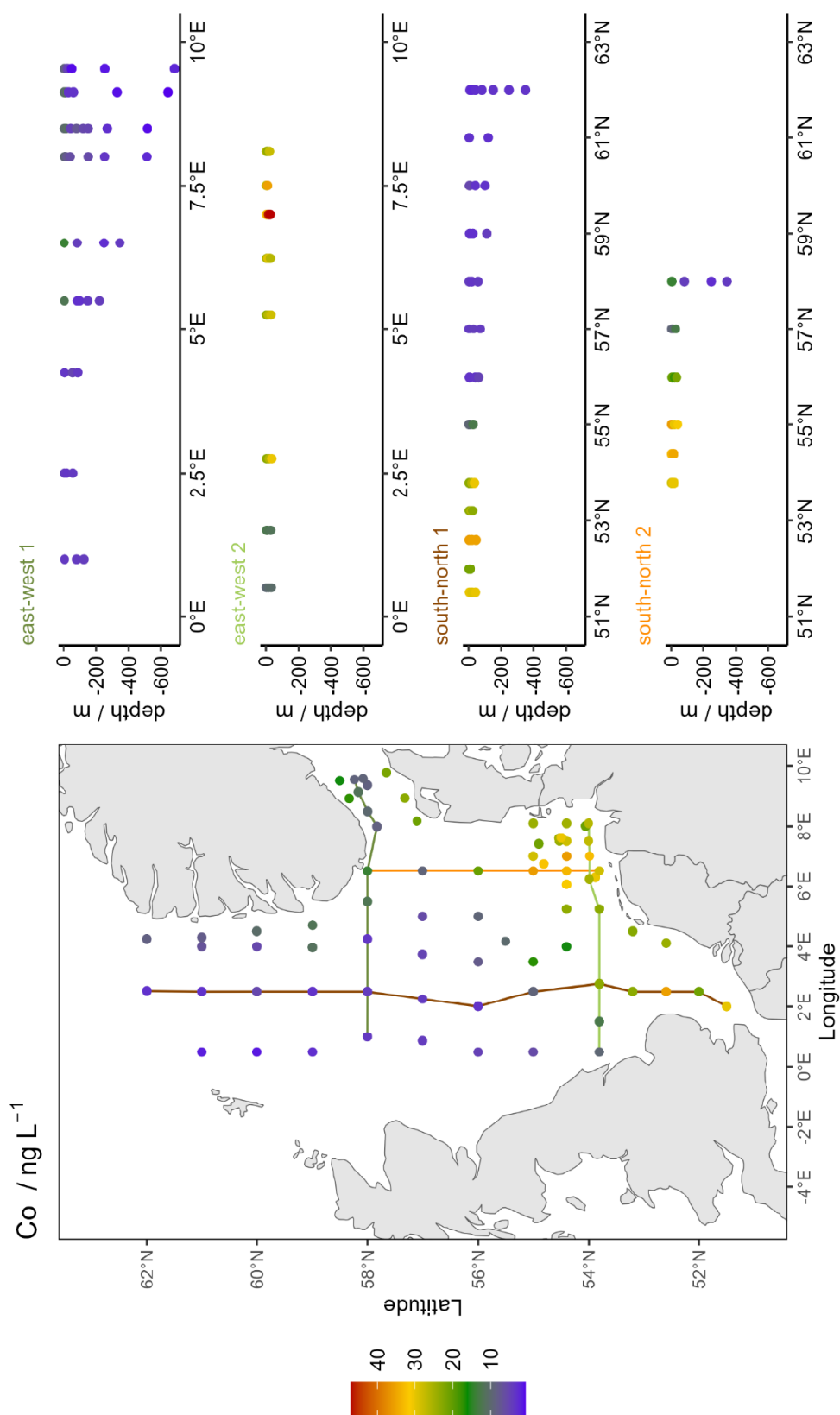


Figure A 7 Surface concentrations and depth profiles of Co across two south-north and two east-west transects. The northernmost transect is east-west 1 and the westernmost transect is south-north 1.  $x$  indicates concentrations below the LOD, and faint points indicate concentrations between LOD and LOQ.

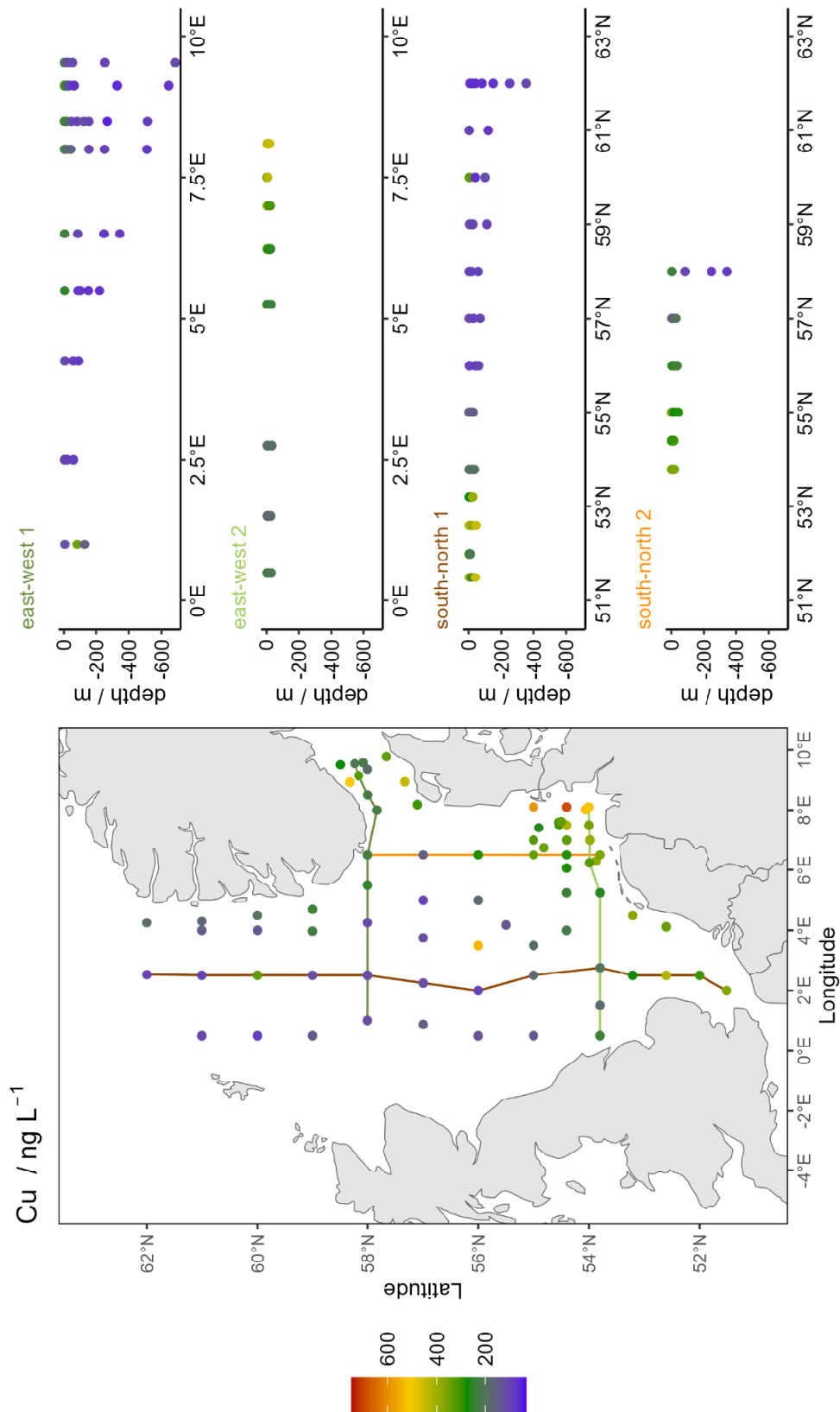


Figure A 8 Surface concentrations and depth profiles of Cu across two south-north and two east-west transects. The northernmost transect is east-west 1 and the westernmost transect is south-north 1. x indicates concentrations below the LOD, and faint points indicate concentrations between LOD and LOQ.



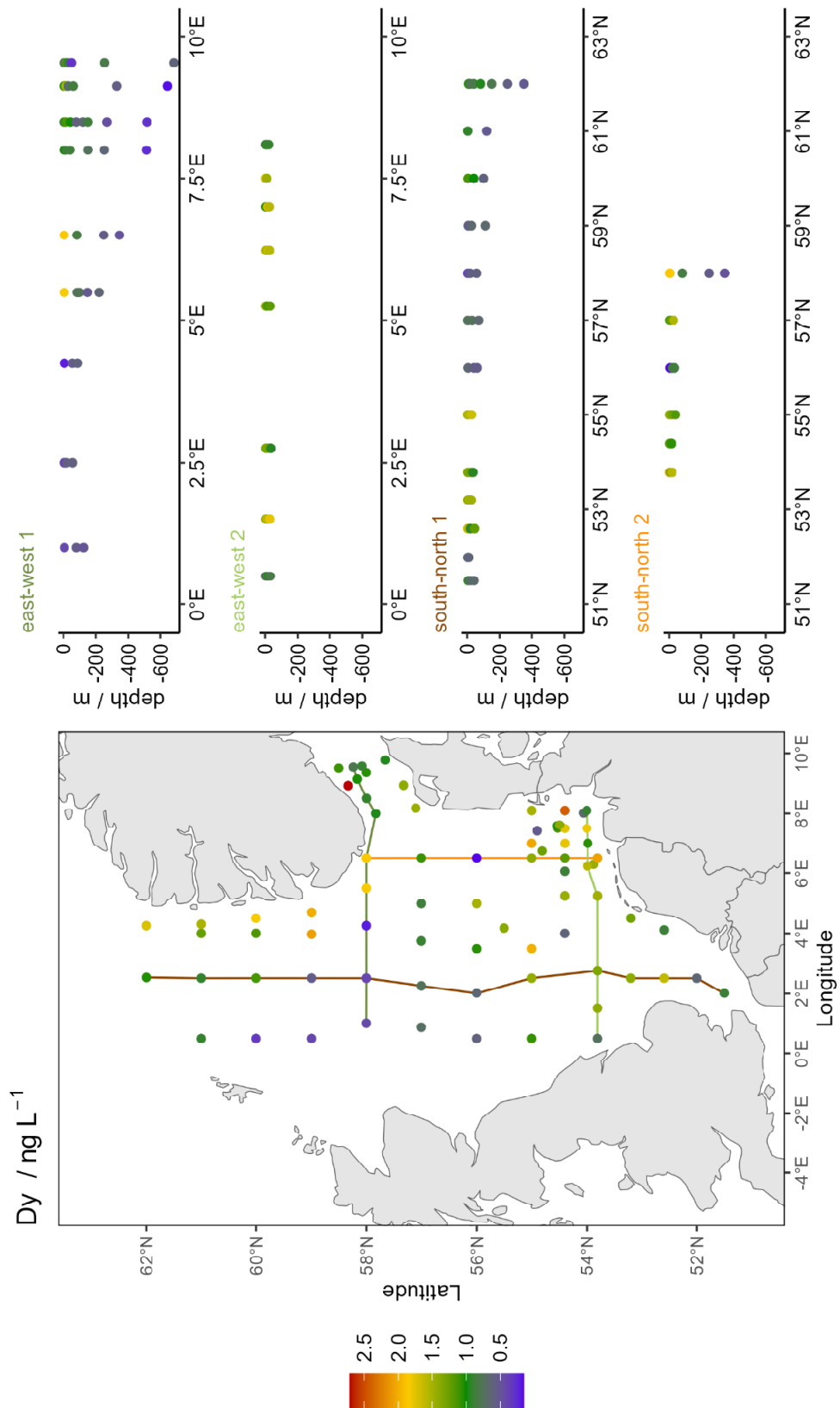


Figure A 9 Surface concentrations and depth profiles of Dy across two south-north and two east-west transects. The northernmost transect is east-west 1 and the westernmost transect is south-north 1.  $x$  indicates concentrations below the LOD, and faint points indicate concentrations between LOD and LOQ.

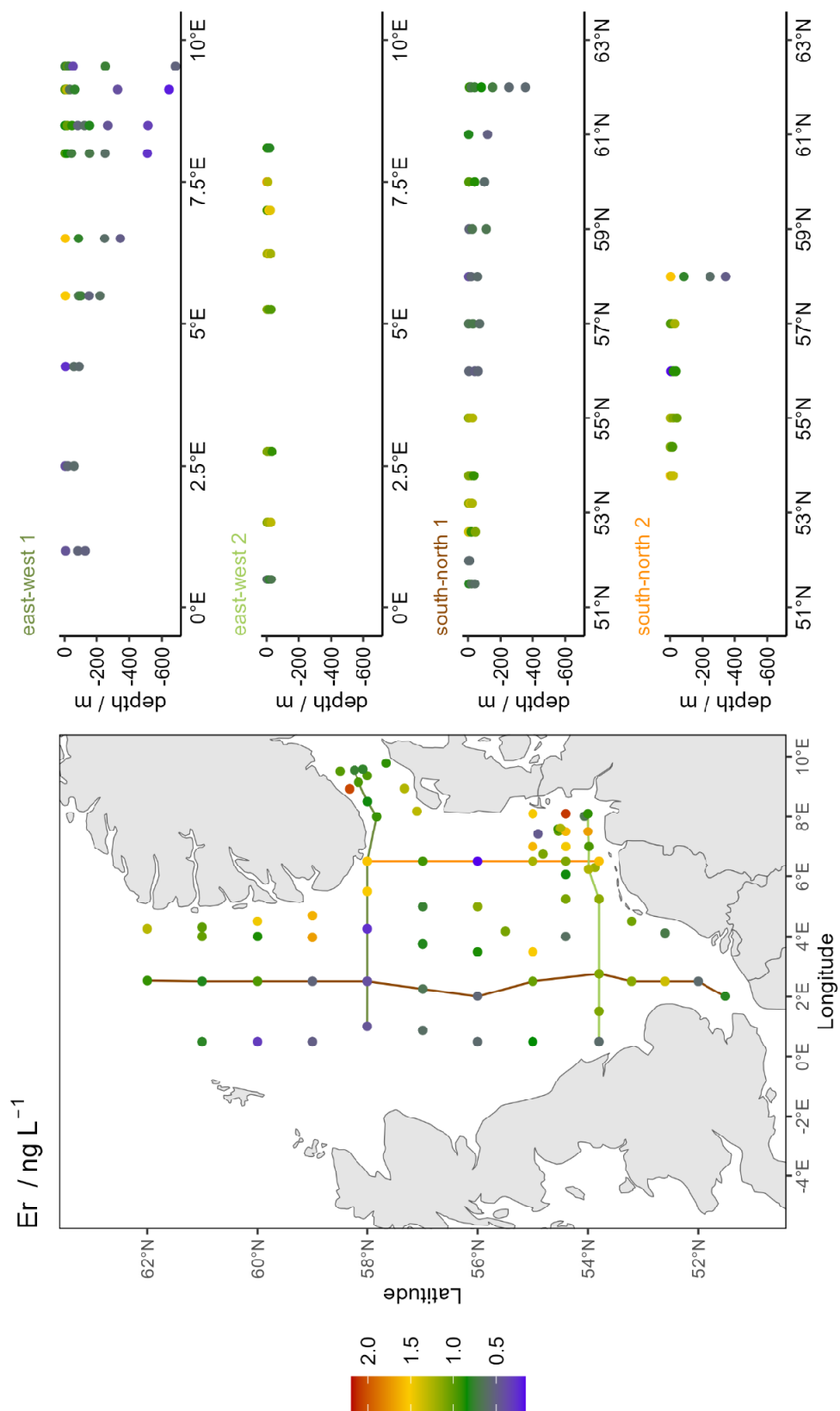


Figure A 10 Surface concentrations and depth profiles of  $Er$  across two south-north and two east-west transects. The northernmost transect is east-west 1 and the westernmost transect is south-north 1. x indicates concentrations below the LOD, and faint points indicate concentrations between LOD and LOQ.

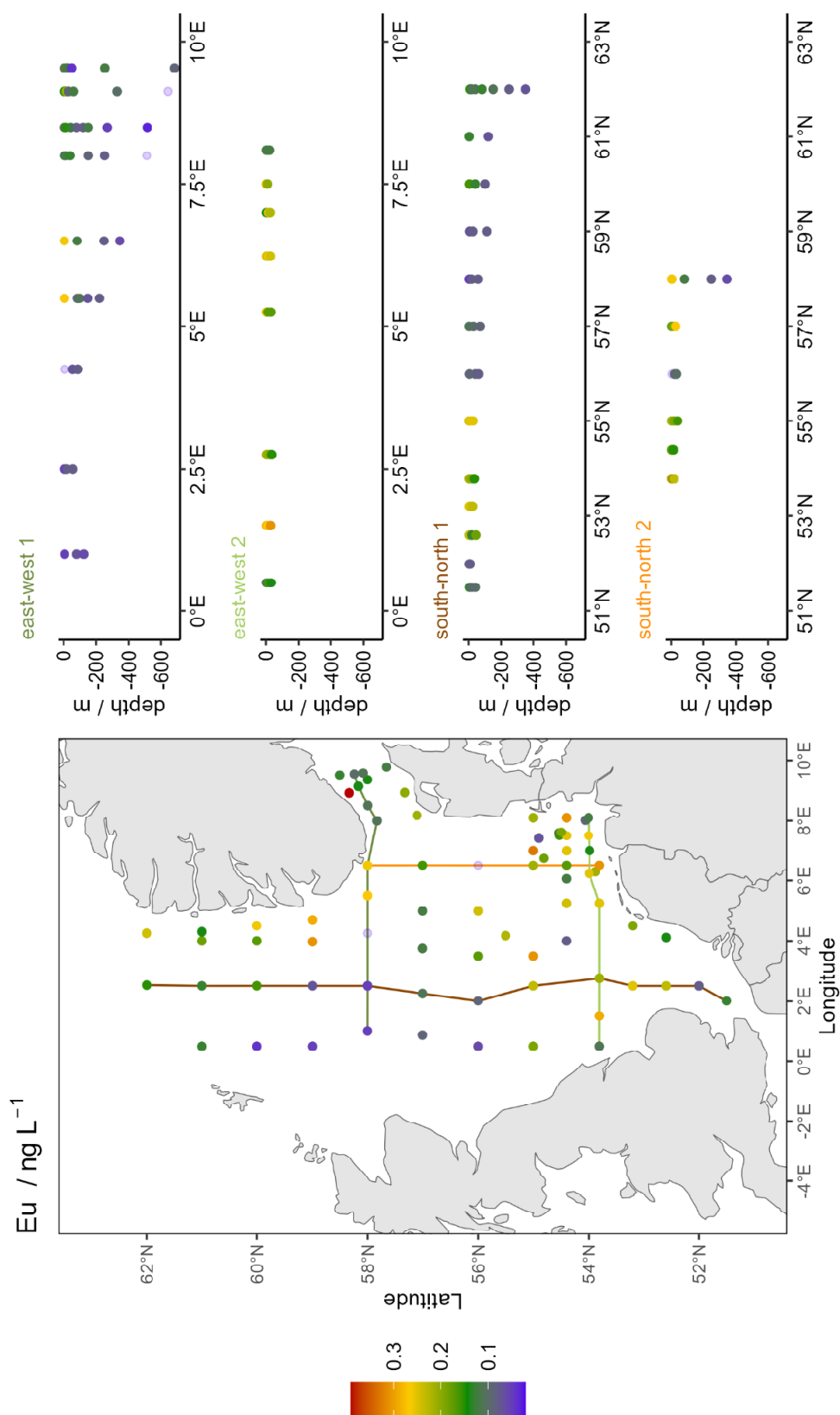


Figure A 11 Surface concentrations and depth profiles of Eu across two south-north and two east-west transects. The northernmost transect is east-west 1 and the westernmost transect is south-north 1. x indicates concentrations below the LOD, and faint points indicate concentrations between LOD and LOQ.

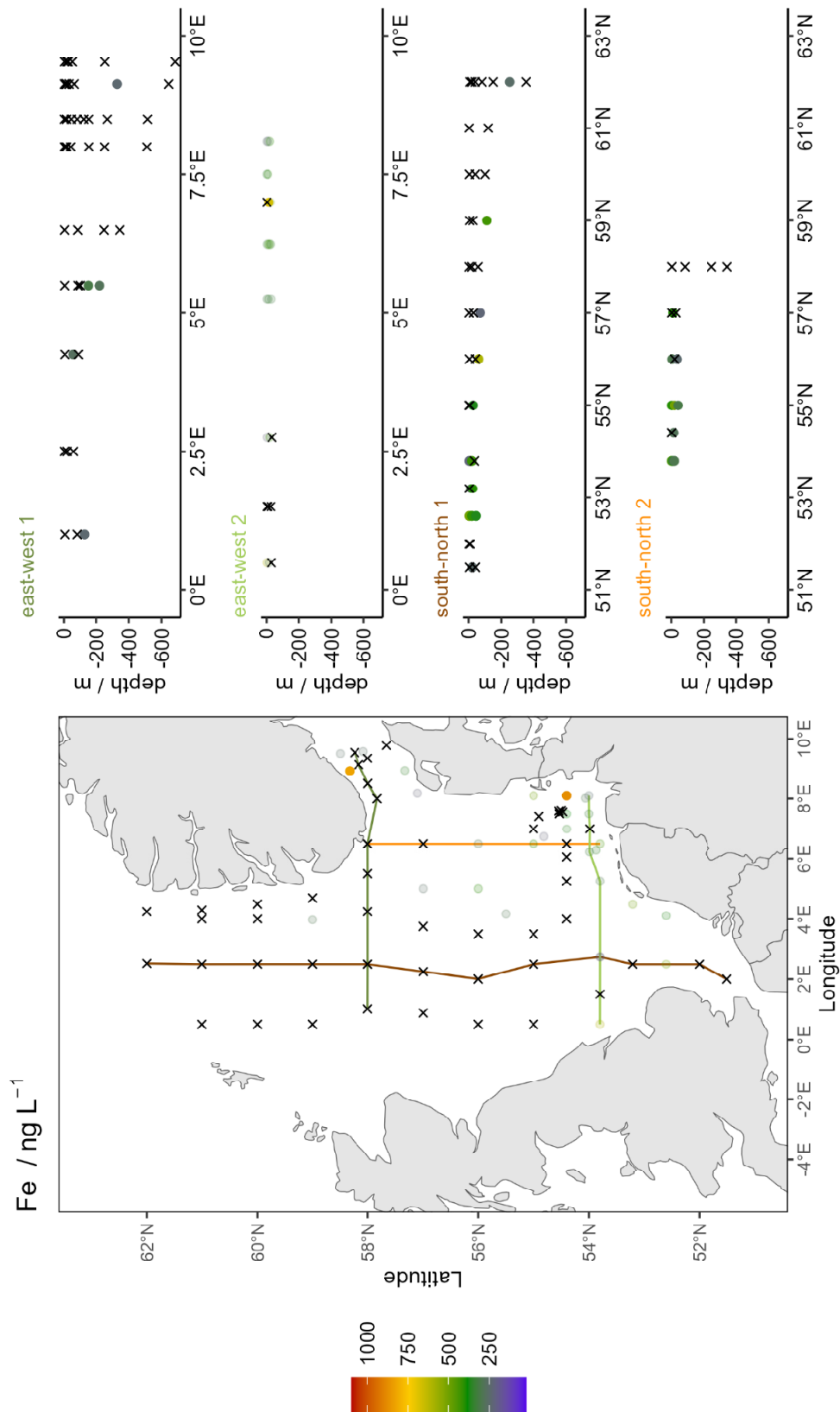


Figure A 12 Surface concentrations and depth profiles of Fe across two south-north and two east-west transects. The northernmost transect is east-west 1 and the westernmost transect is south-north 1. x indicates concentrations below the LOD, and faint points indicate concentrations between LOD and LOQ

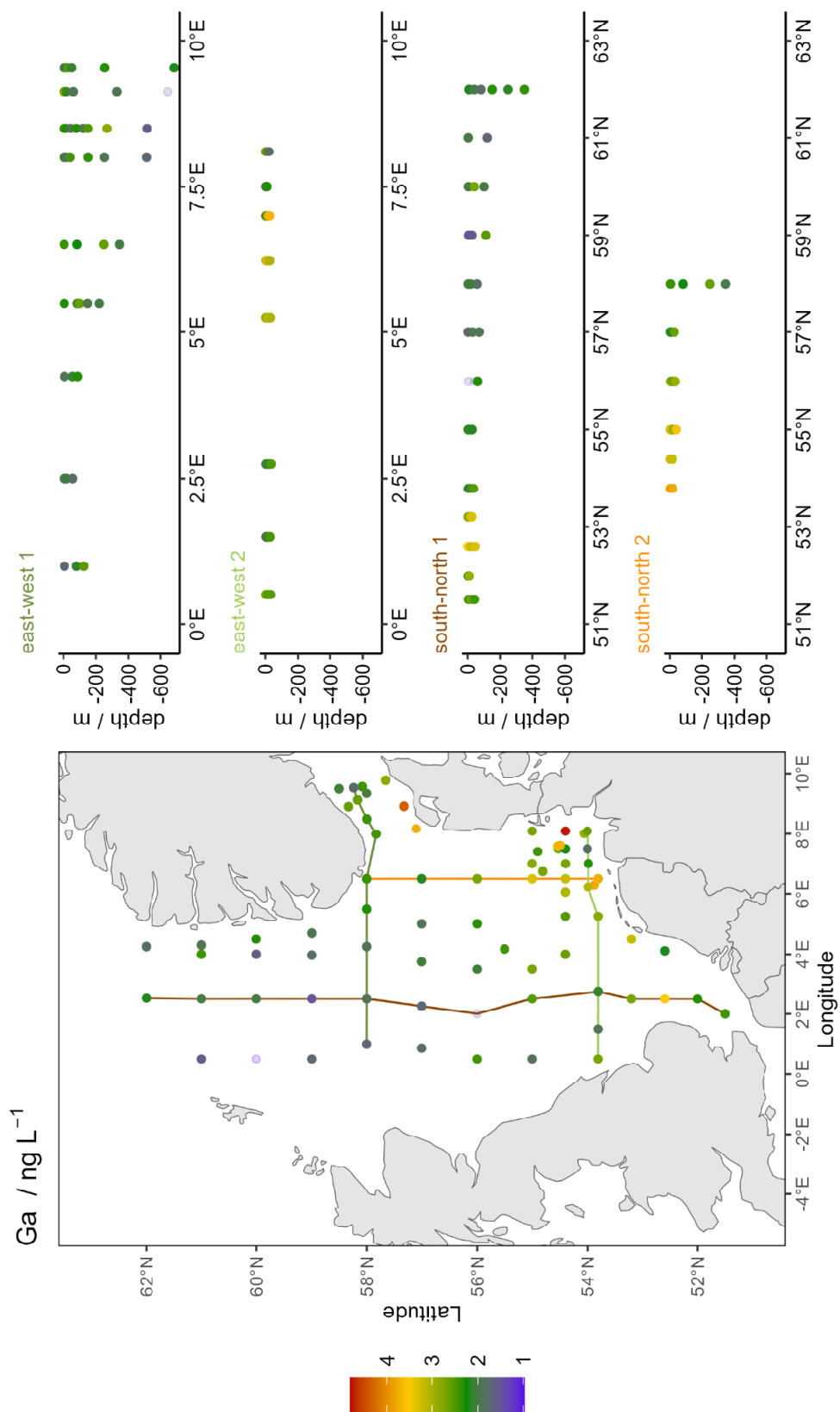


Figure A 13 Surface concentrations and depth profiles of Ga across two south-north and two east-west transects. The northernmost transect is east-west 1 and the westernmost transect is south-north 1.  $x$  indicates concentrations below the LOD, and faint points indicate concentrations between LOD and LOQ.

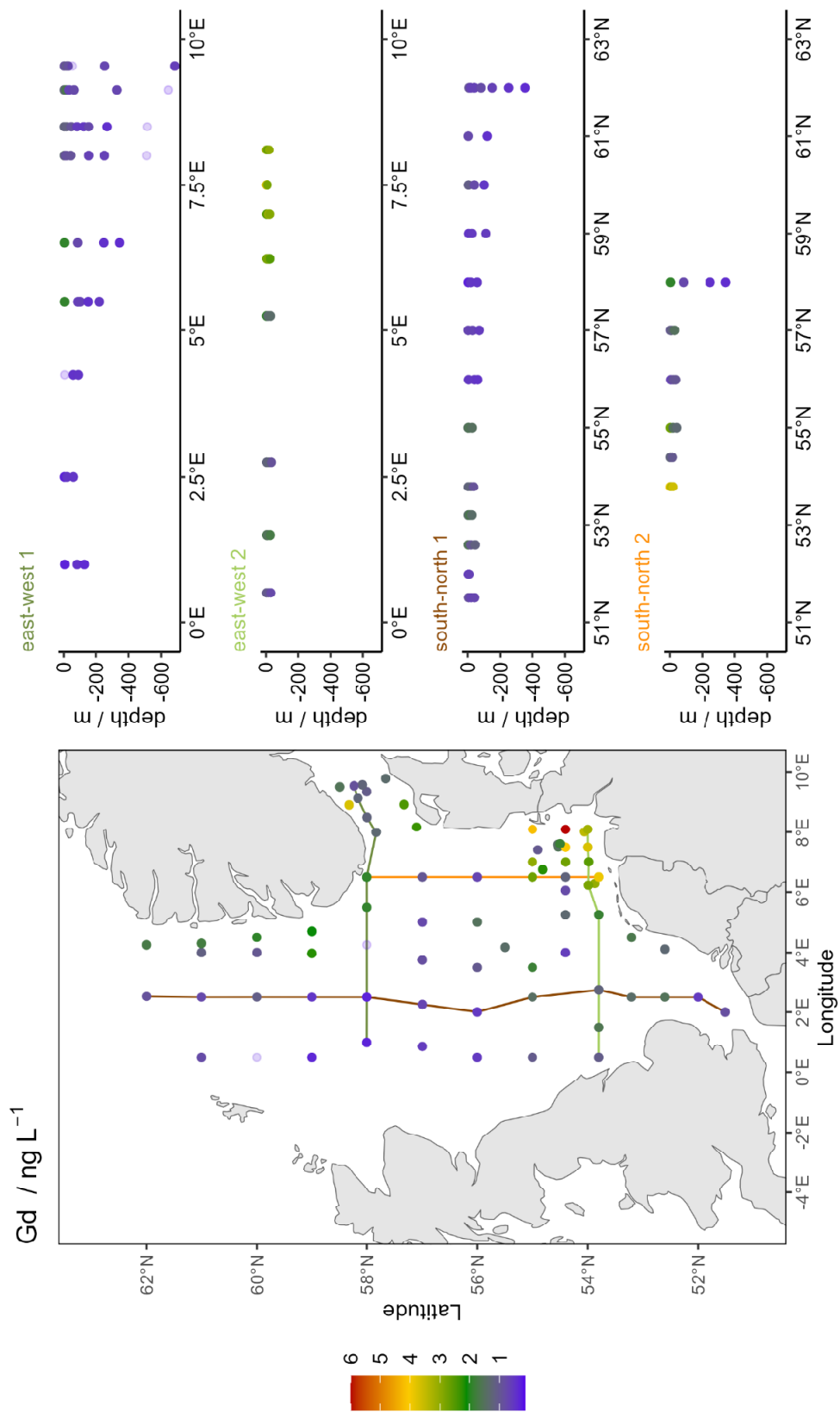


Figure A 14 Surface concentrations and depth profiles of Gd across two south-north and two east-west transects. The northernmost transect is east-west 1 and the westernmost transect is south-north 1. x indicates concentrations below the LOD, and faint points indicate concentrations between LOD and LOQ.

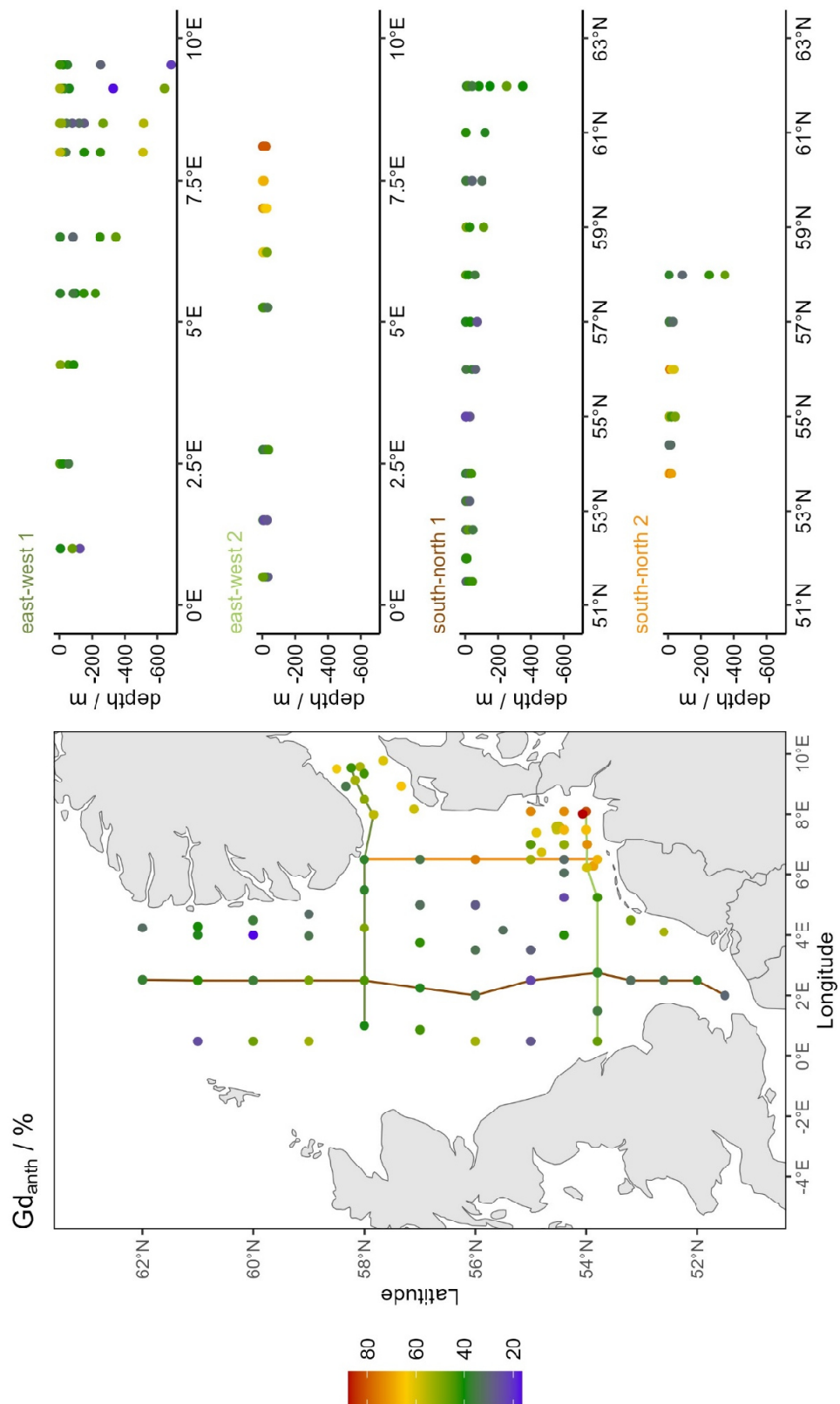


Figure A 15 Surface concentrations and depth profiles of  $Gd_{anth}$  across two south-north and two east-west transects. The northernmost transect is east-west 1 and the westernmost transect is south-north 1. x indicates concentrations below the LOD, and faint points indicate concentrations between LOD and LOQ.

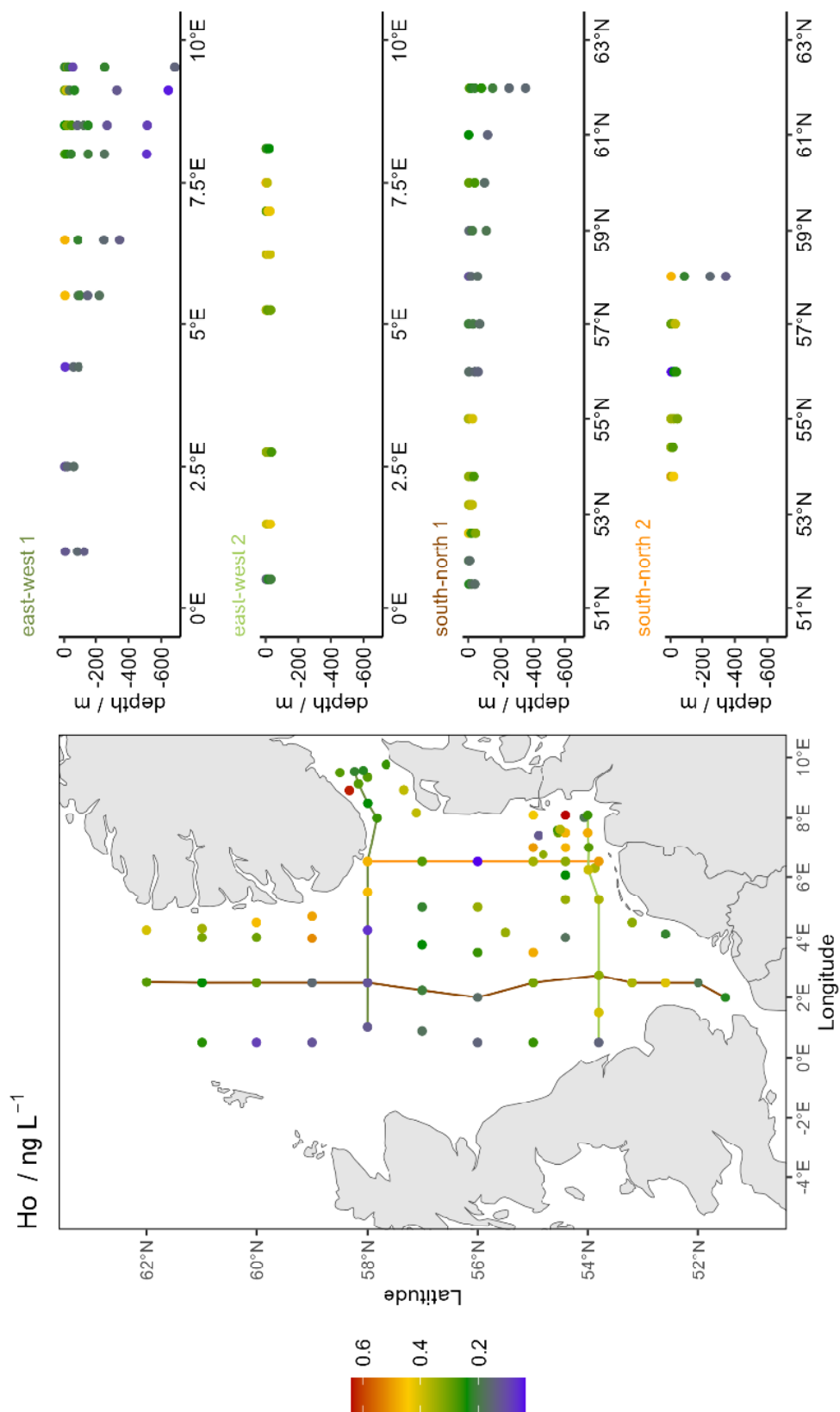


Figure A 16 Surface concentrations and depth profiles of  $Ho$  across two south-north and two east-west transects. The northernmost transect is east-west 1 and the westernmost transect is south-north 1. x indicates concentrations below the LOD, and faint points indicate concentrations between LOD and LOQ.



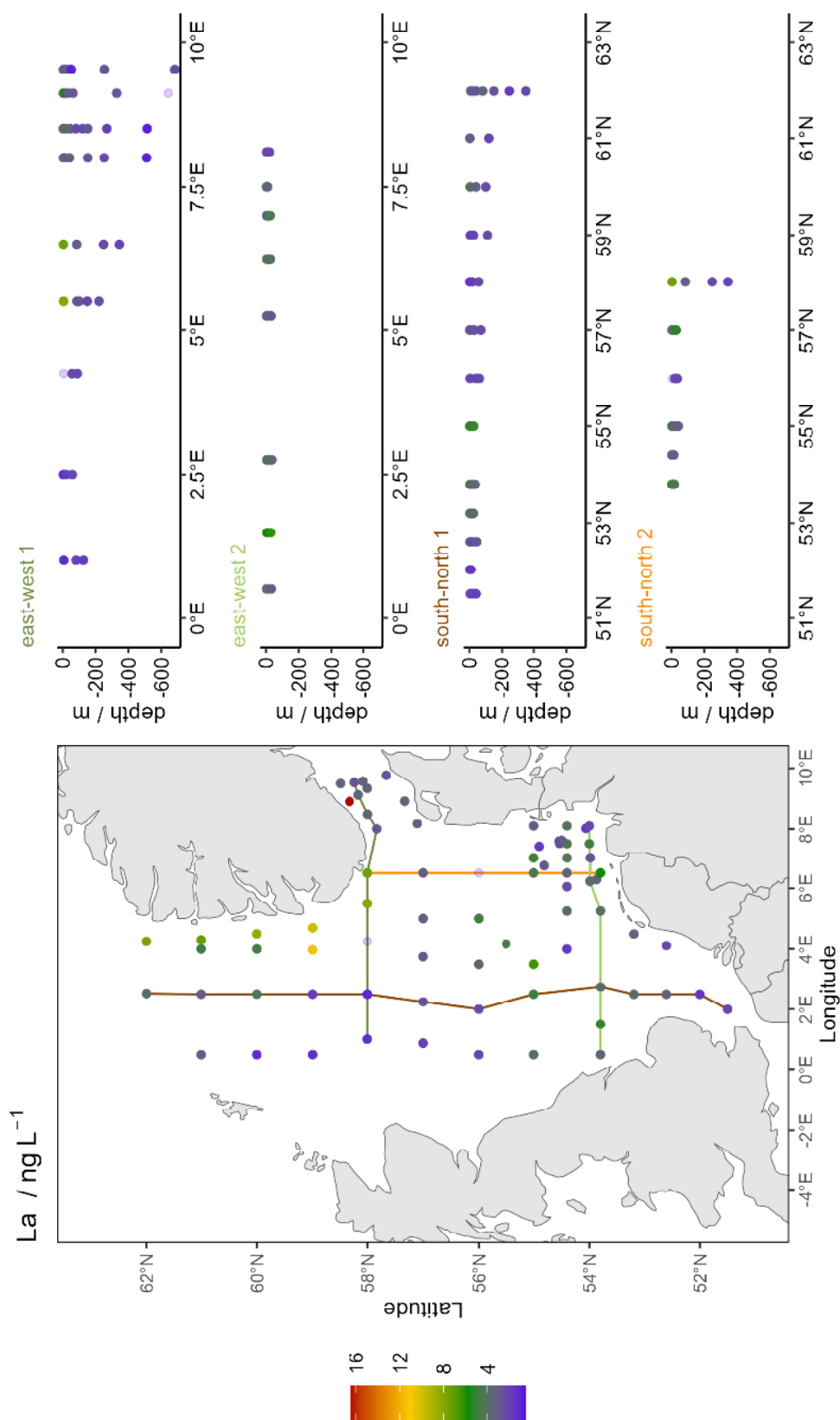


Figure A 17 Surface concentrations and depth profiles of  $La$  across two south-north and two east-west transects. The northernmost transect is east-west 1 and the westernmost transect is south-north 1.  $x$  indicates concentrations below the LOD, and faint points indicate concentrations between LOD and LOQ.

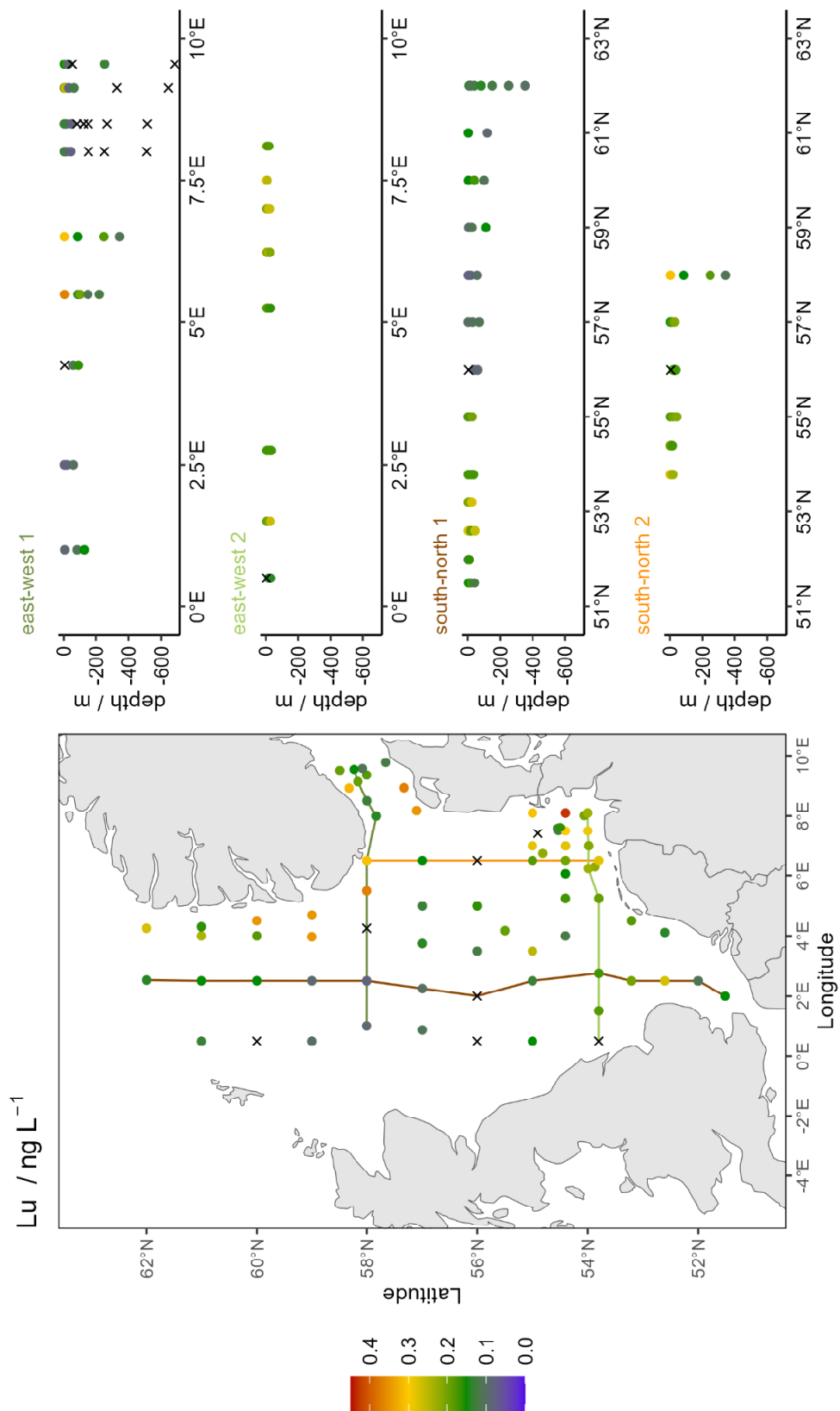


Figure A 18 Surface concentrations and depth profiles of Lu across two south-north and two east-west transects. The northernmost transect is east-west 1 and the westernmost transect is south-north 1. x indicates concentrations below the LOD, and faint points indicate concentrations between LOD and LOQ.

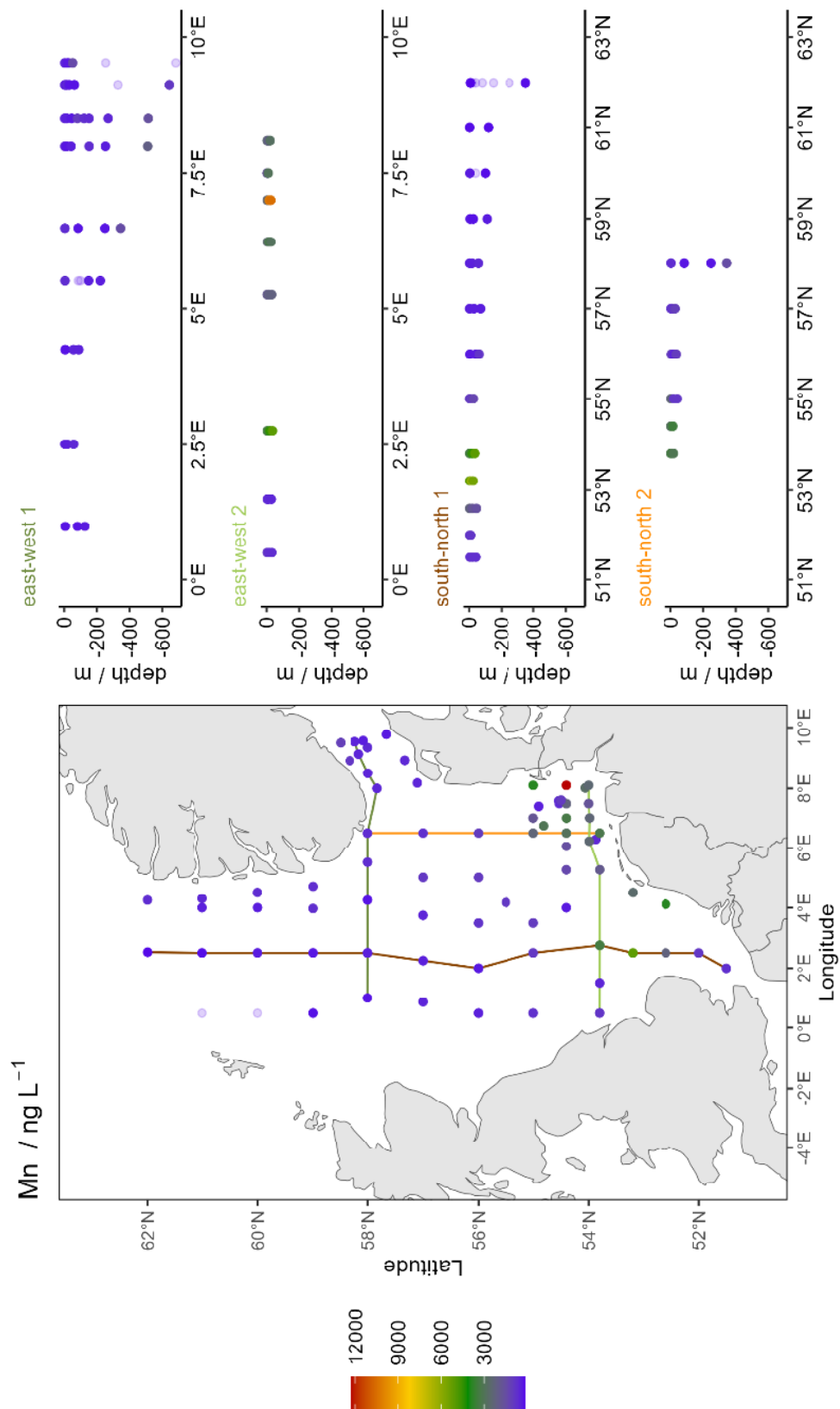


Figure A 19 Surface concentrations and depth profiles of Mn across two south-north and two east-west transects. The northernmost transect is east-west 1 and the westernmost transect is south-north 1. x indicates concentrations below the LOD, and faint points indicate concentrations between LOD and LOQ.

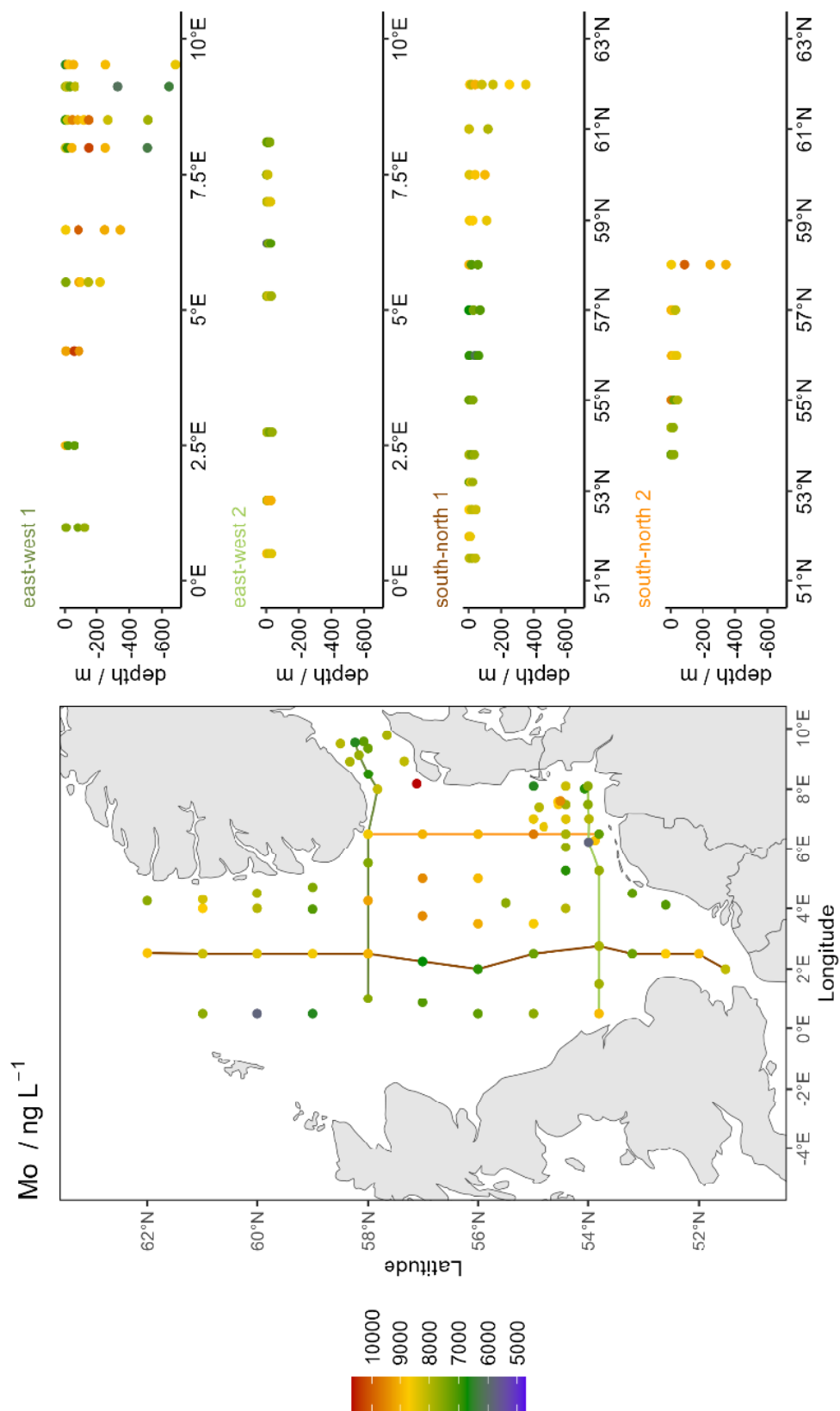


Figure A 20 Surface concentrations and depth profiles of Mo across two south-north and two east-west transects. The northernmost transect is east-west 1 and the westernmost transect is south-north 1. x indicates concentrations below the LOD, and faint points indicate concentrations between LOD and LOQ.

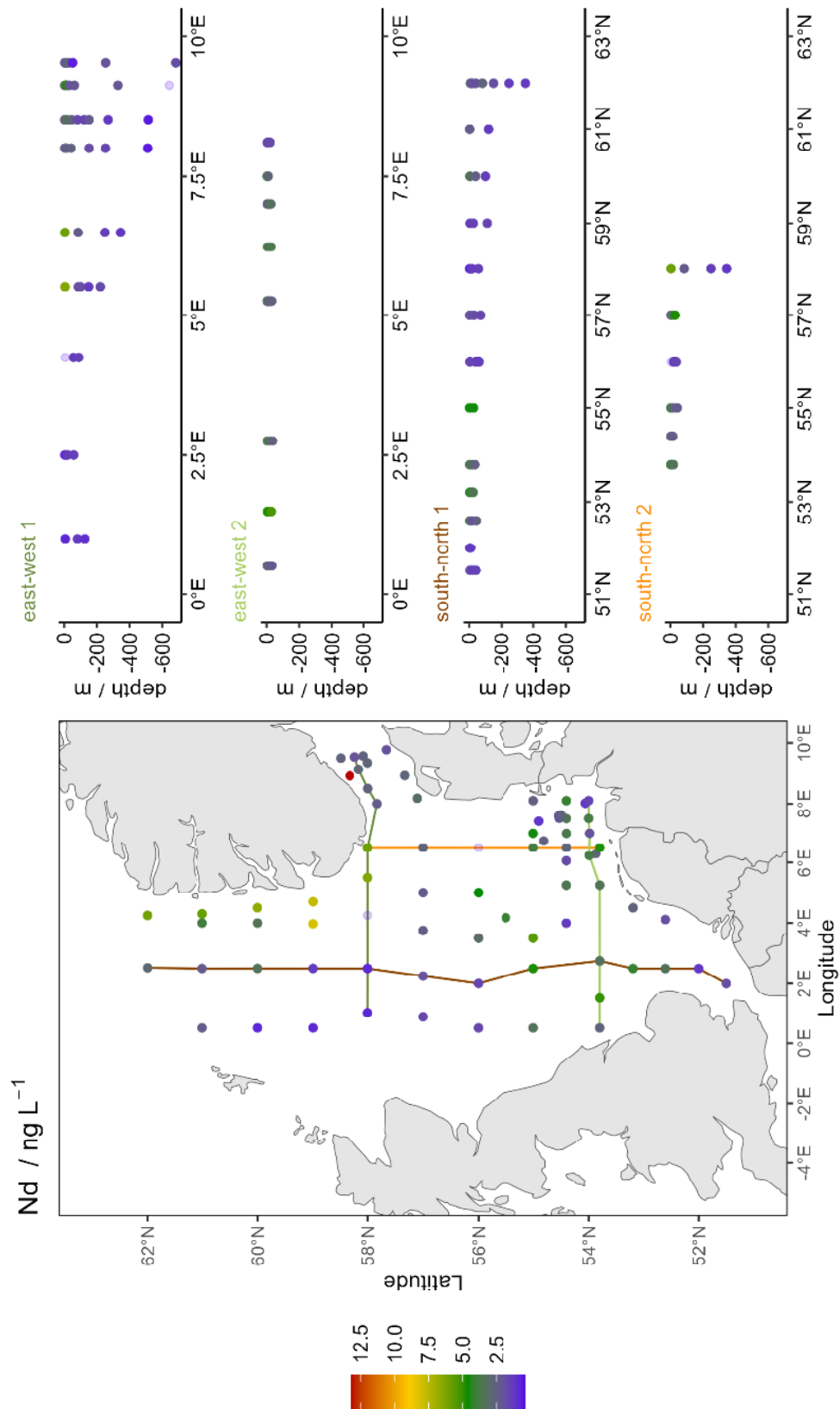


Figure A 21 Surface concentrations and depth profiles of Nd across two south-north and two east-west transects. The northernmost transect is east-west 1 and the westernmost transect is south-north 1. x indicates concentrations below the LOD, and faint points indicate concentrations between LOD and LOQ.

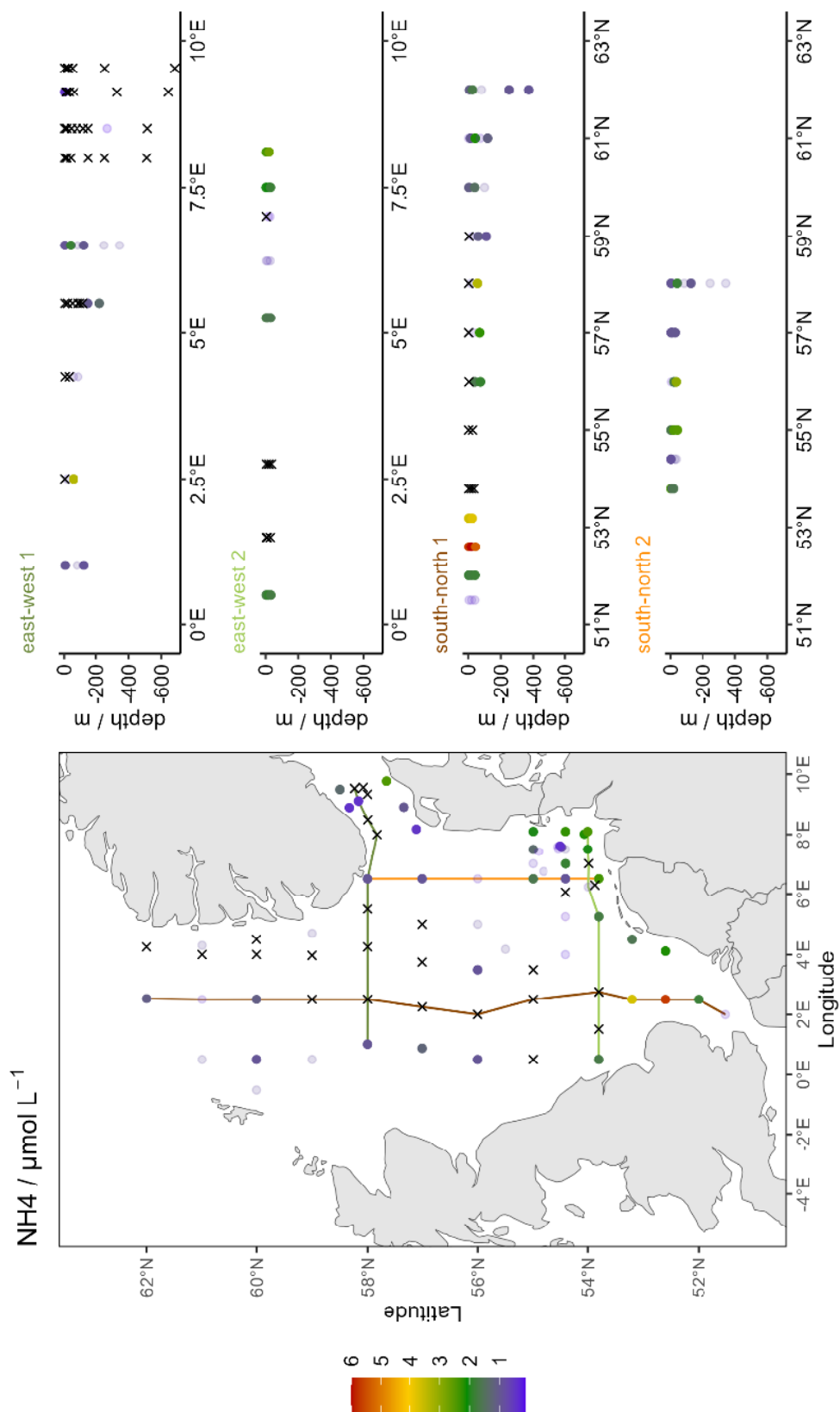


Figure A 22 Surface concentrations and depth profiles of  $\text{NH}_4^+$  across two south-north and two east-west transects. The northernmost transect is east-west 1 and the westernmost transect is south-north 1. x indicates concentrations below the LOD, and faint points indicate concentrations between LOD and LOQ.

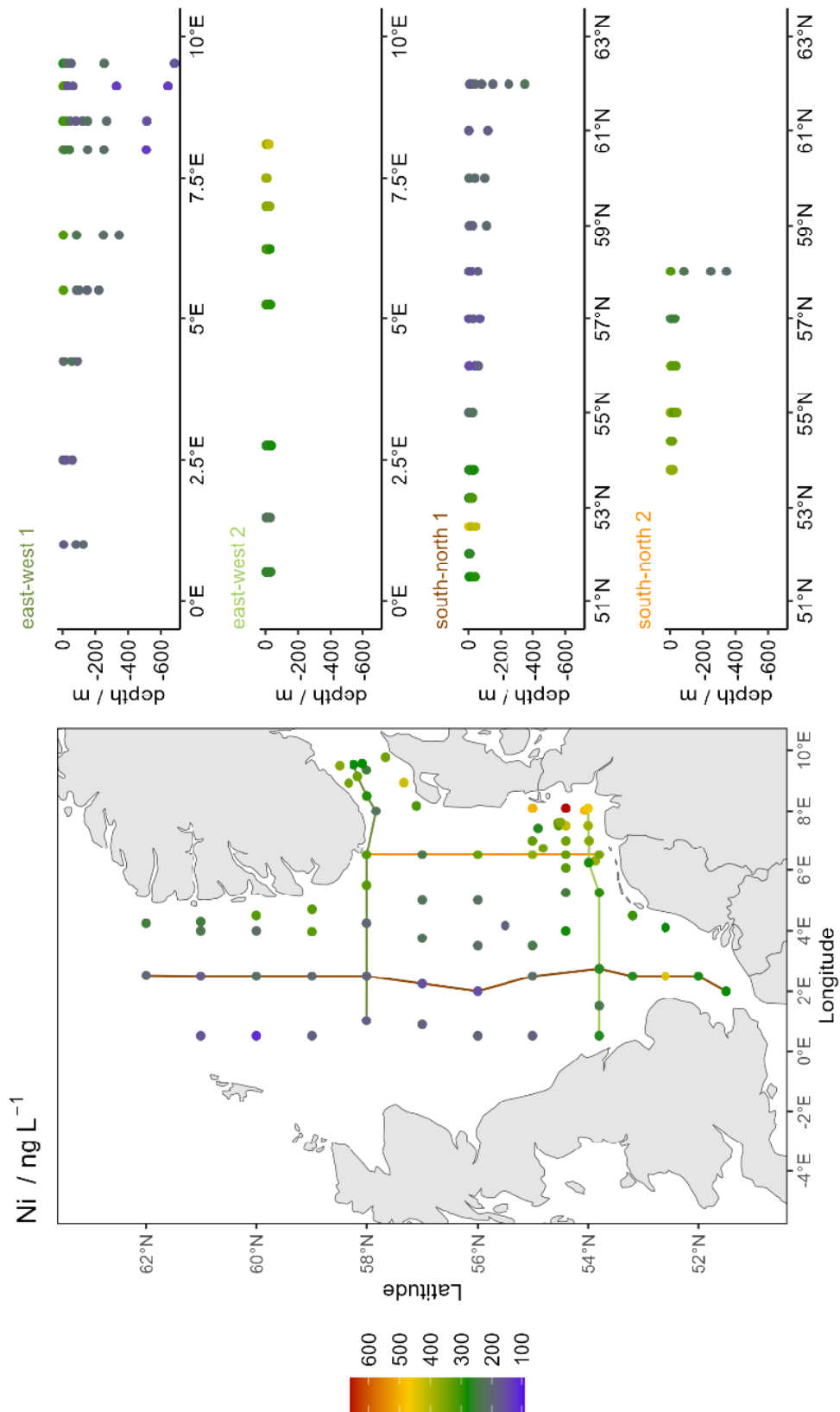


Figure A 23 Surface concentrations and depth profiles of Ni across two south-north and two east-west transects. The northernmost transect is east-west 1 and the westernmost transect is south-north 1. x indicates concentrations below the LOD, and faint points indicate concentrations between LOD and LOQ.

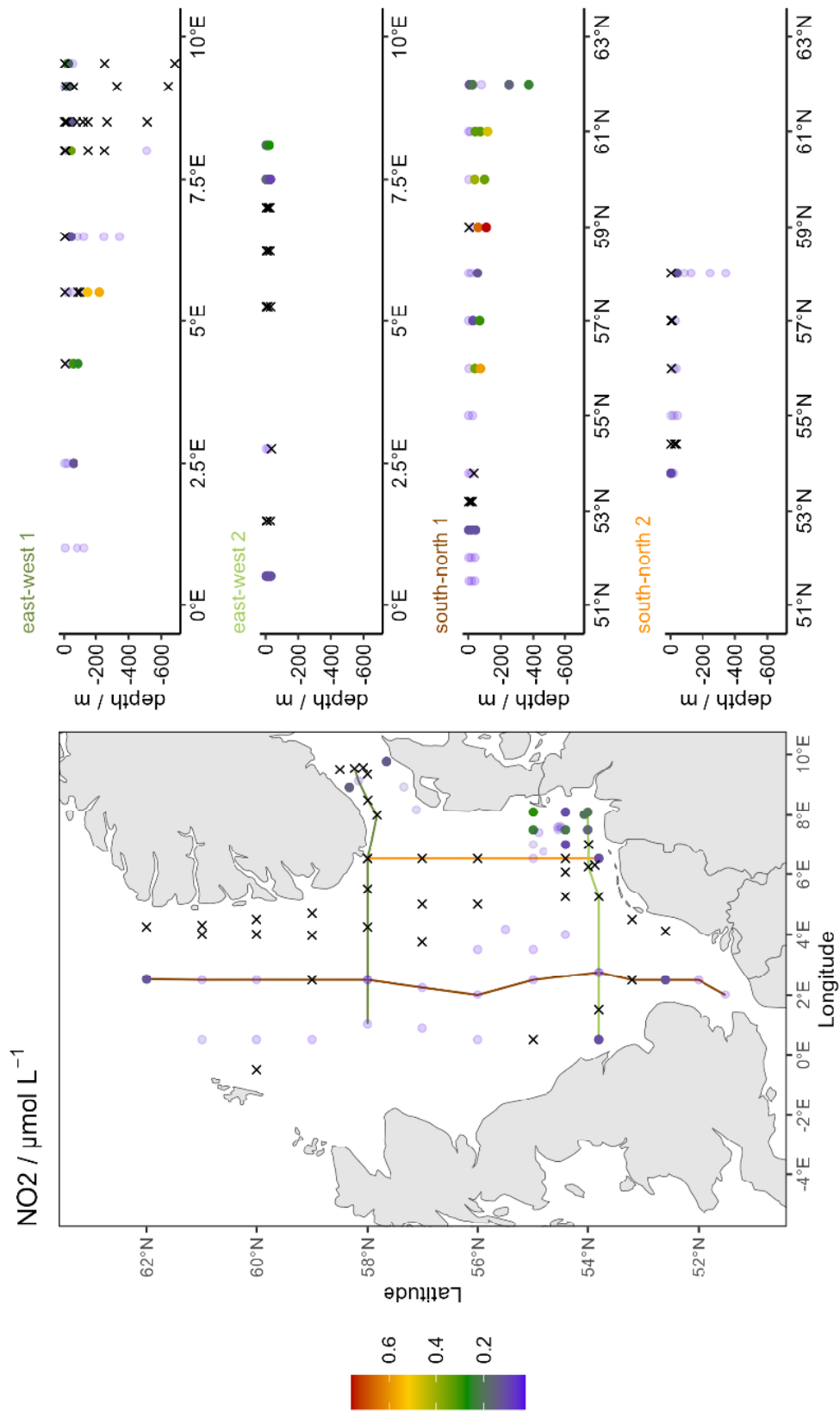


Figure A 24 Surface concentrations and depth profiles of  $\text{NO}_2^-$  across two south-north and two east-west transects. The northernmost transect is east-west 1 and the westernmost transect is south-north 1. x indicates concentrations below the LOD, and faint points indicate concentrations between LOD and LOQ.



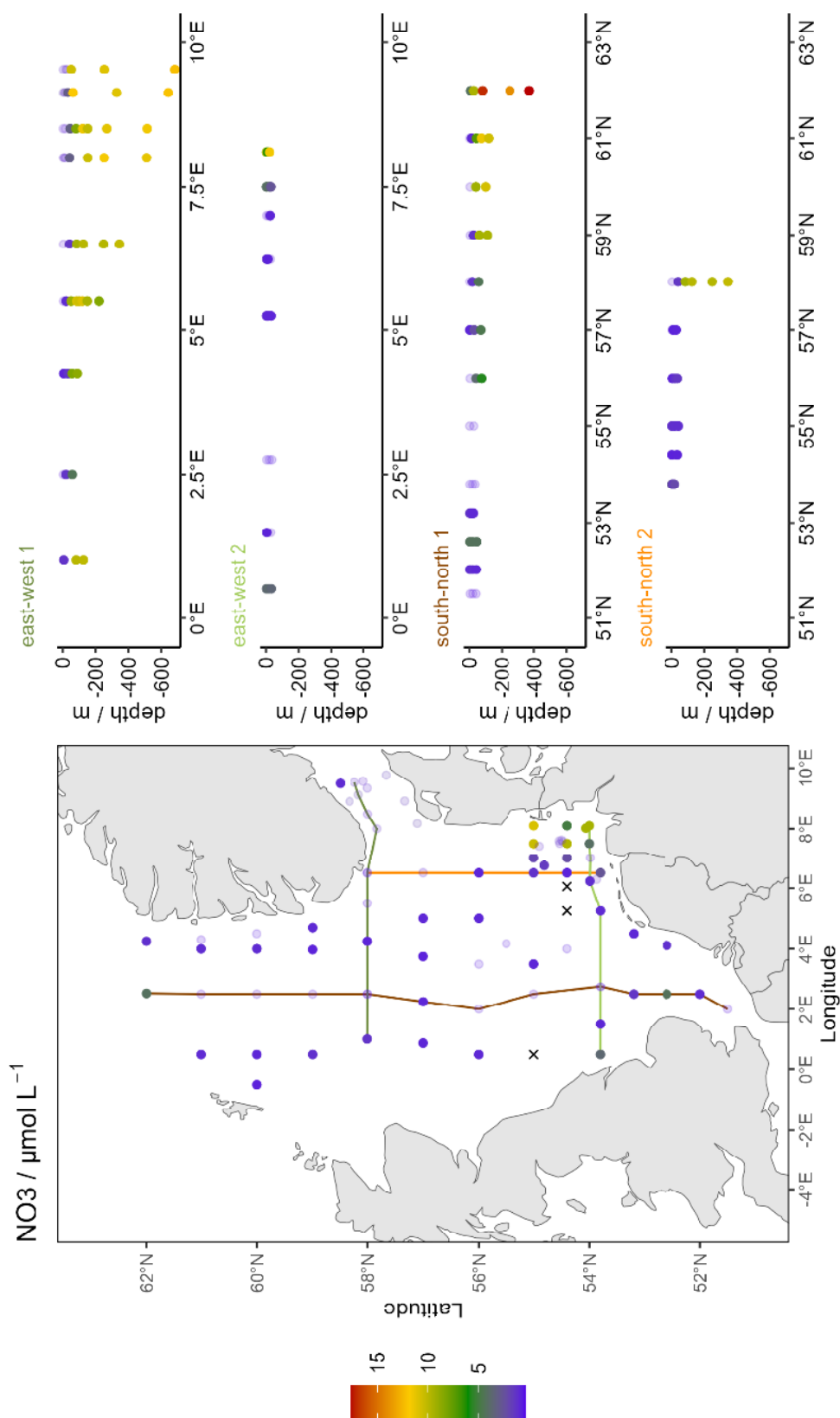


Figure A 25 Surface concentrations and depth profiles of  $\text{NO}_3^-$  across two south-north and two east-west transects. The northernmost transect is east-west 1 and the westernmost transect is south-north 1. x indicates concentrations below the LOD, and faint points indicate concentrations between LOD and LOQ.

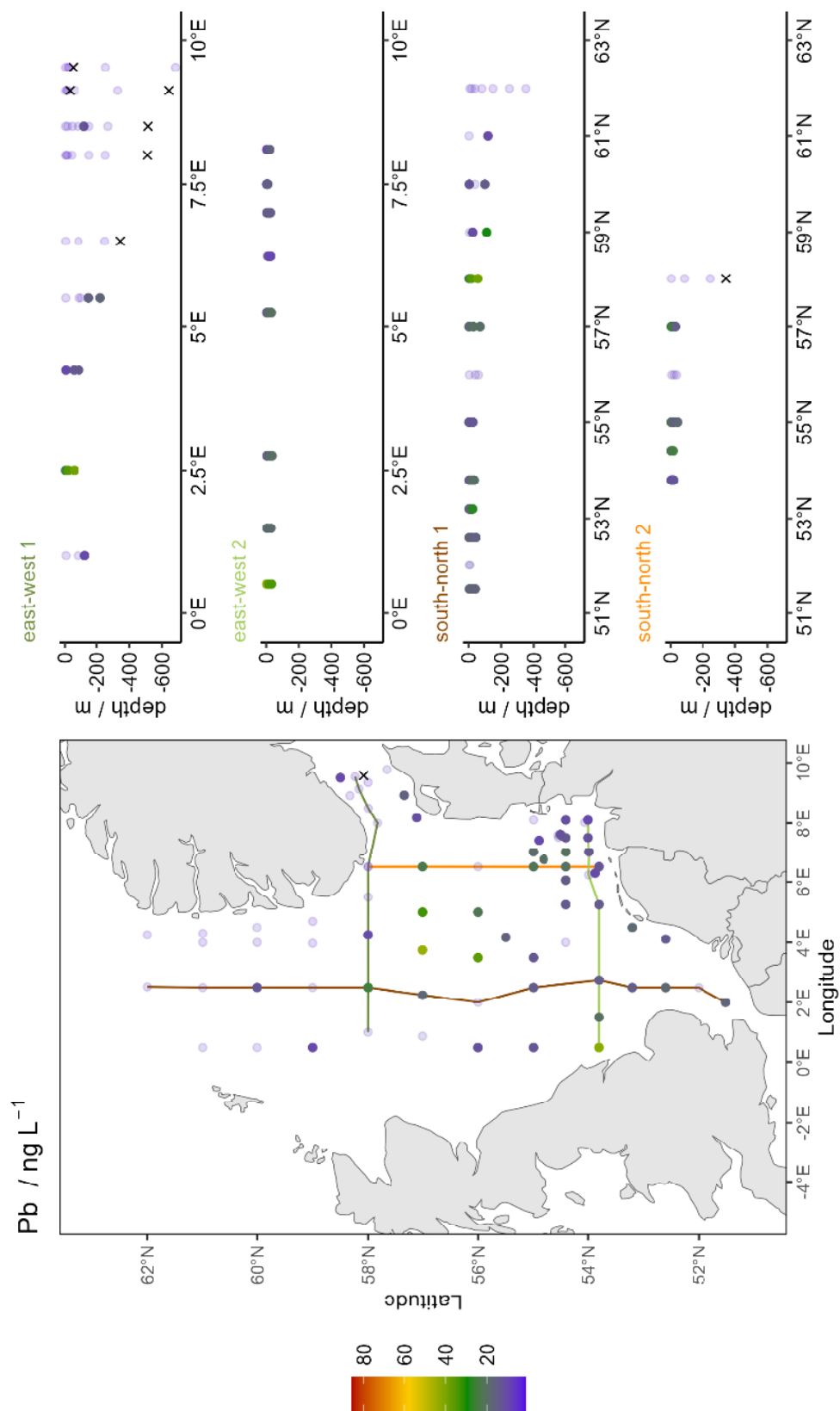


Figure A 26 Surface concentrations and depth profiles of Pb across two south-north and two east-west transects. The northernmost transect is east-west 1 and the westernmost transect is south-north 1. x indicates concentrations below the LOD, and faint points indicate concentrations between LOD and LOQ.

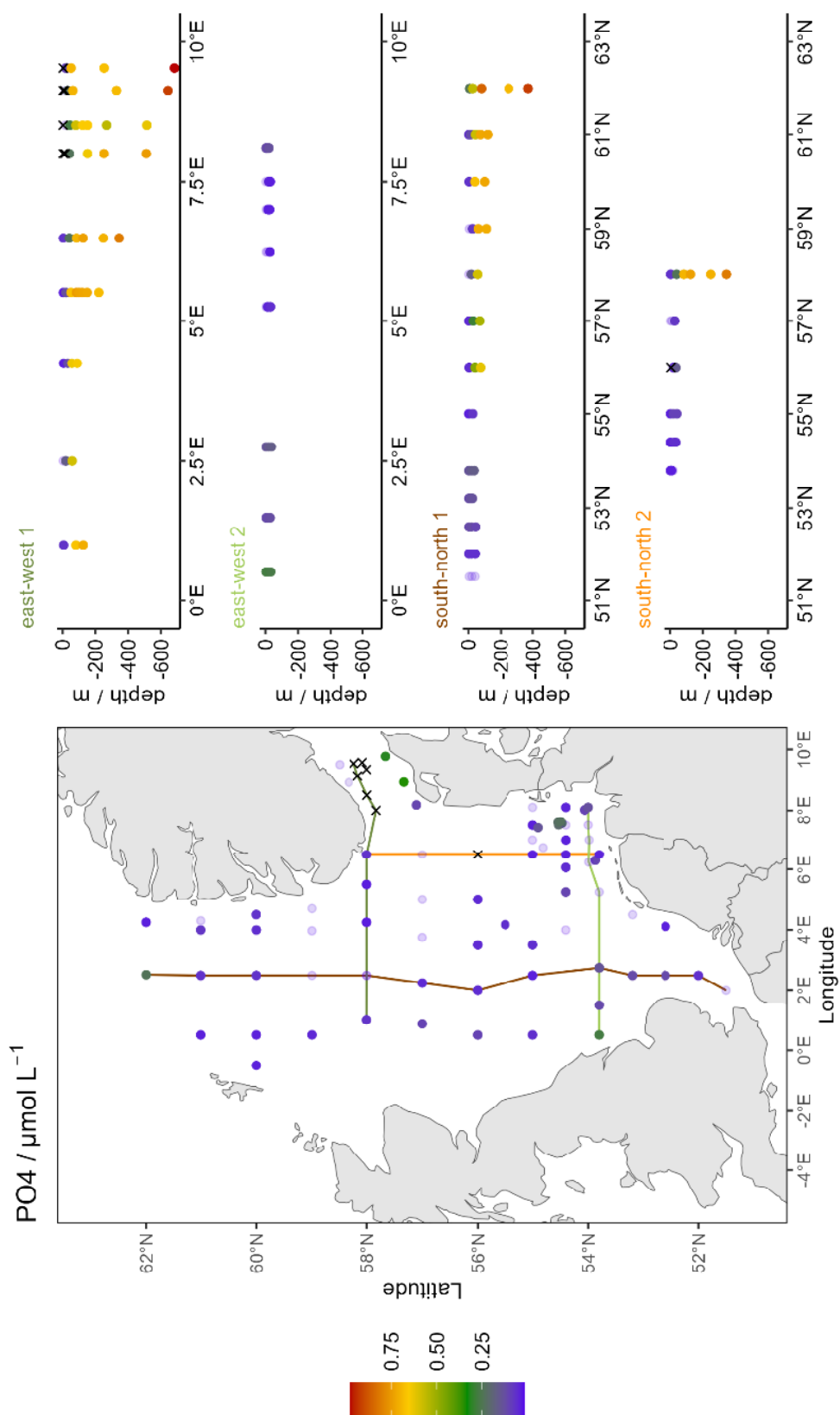


Figure A 27 Surface concentrations and depth profiles of  $PO_4^{3-}$  across two south-north and two east-west transects. The northernmost transect is east-west 1 and the westernmost transect is south-north 1. x indicates concentrations below the LOD, and faint points indicate concentrations between LOD and LOQ.

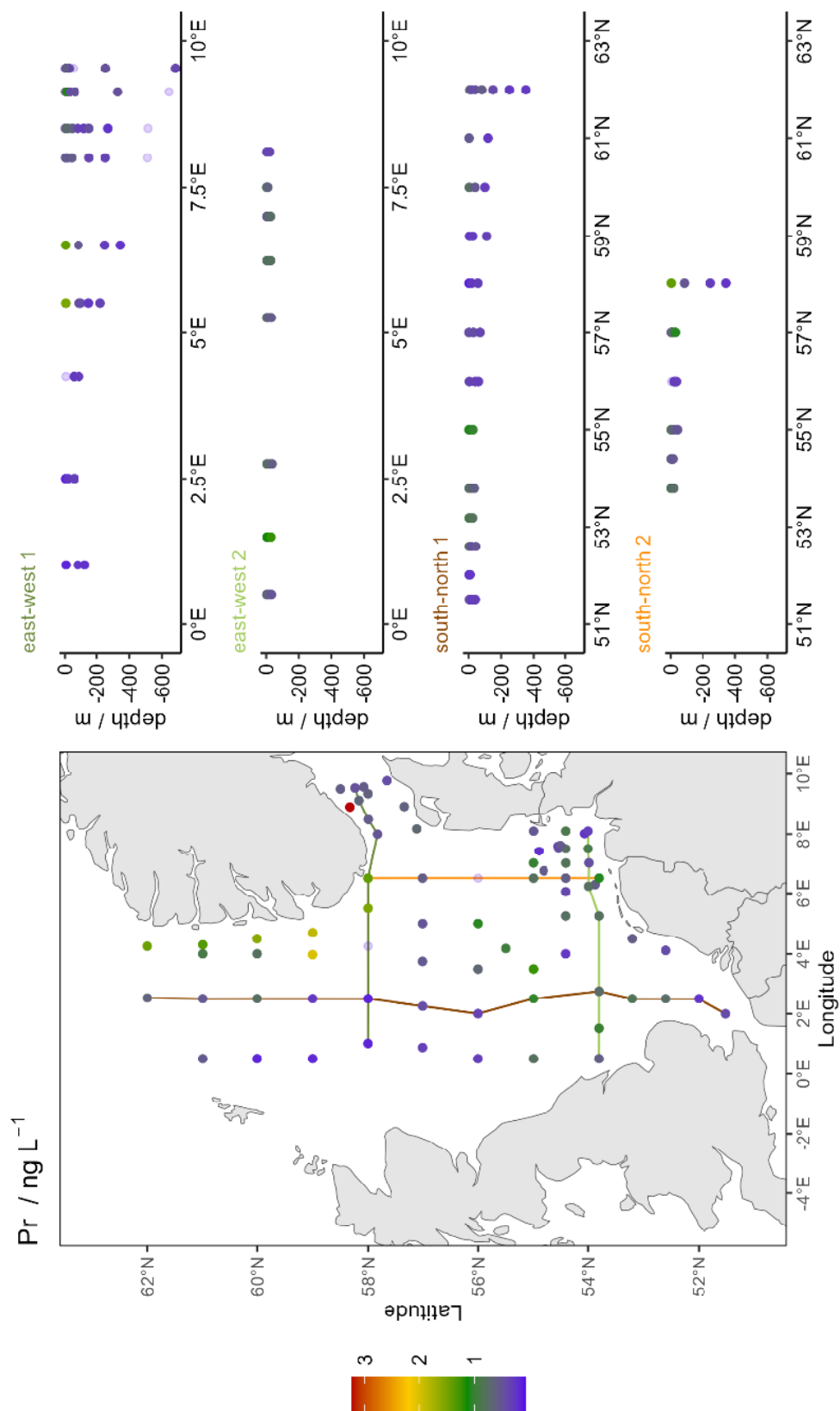


Figure A 28 Surface concentrations and depth profiles of Pr across two south-north and two east-west transects. The northernmost transect is east-west 1 and the westernmost transect is south-north 1. x indicates concentrations below the LOD, and faint points indicate concentrations between LOD and LOQ.

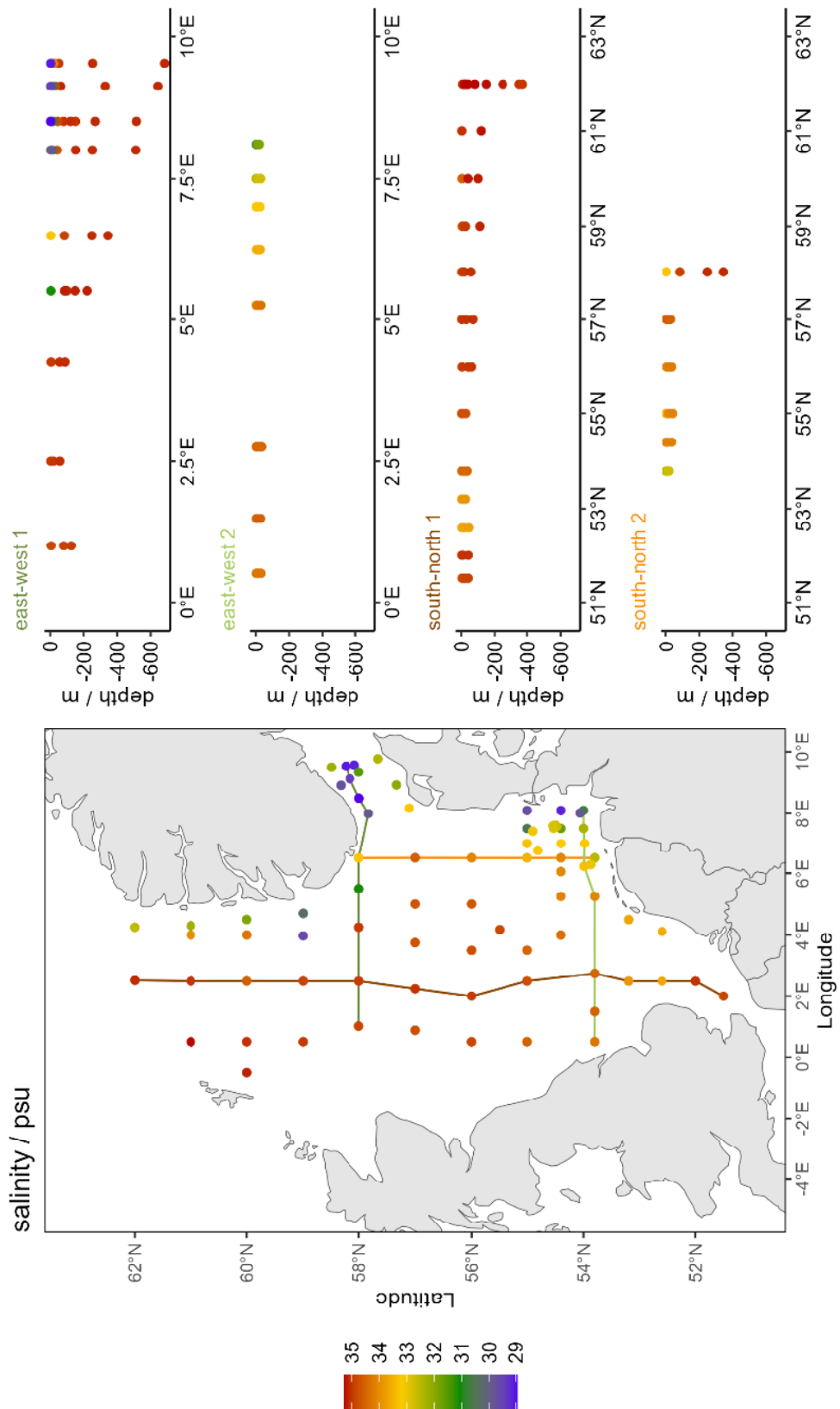


Figure A 29 Surface concentrations and depth profiles of salinity across two south-north and two east-west transects. The northernmost transect is east-west 1 and the westernmost transect is south-north 1. x indicates concentrations below the LOD, and faint points indicate concentrations between LOD and LOQ.

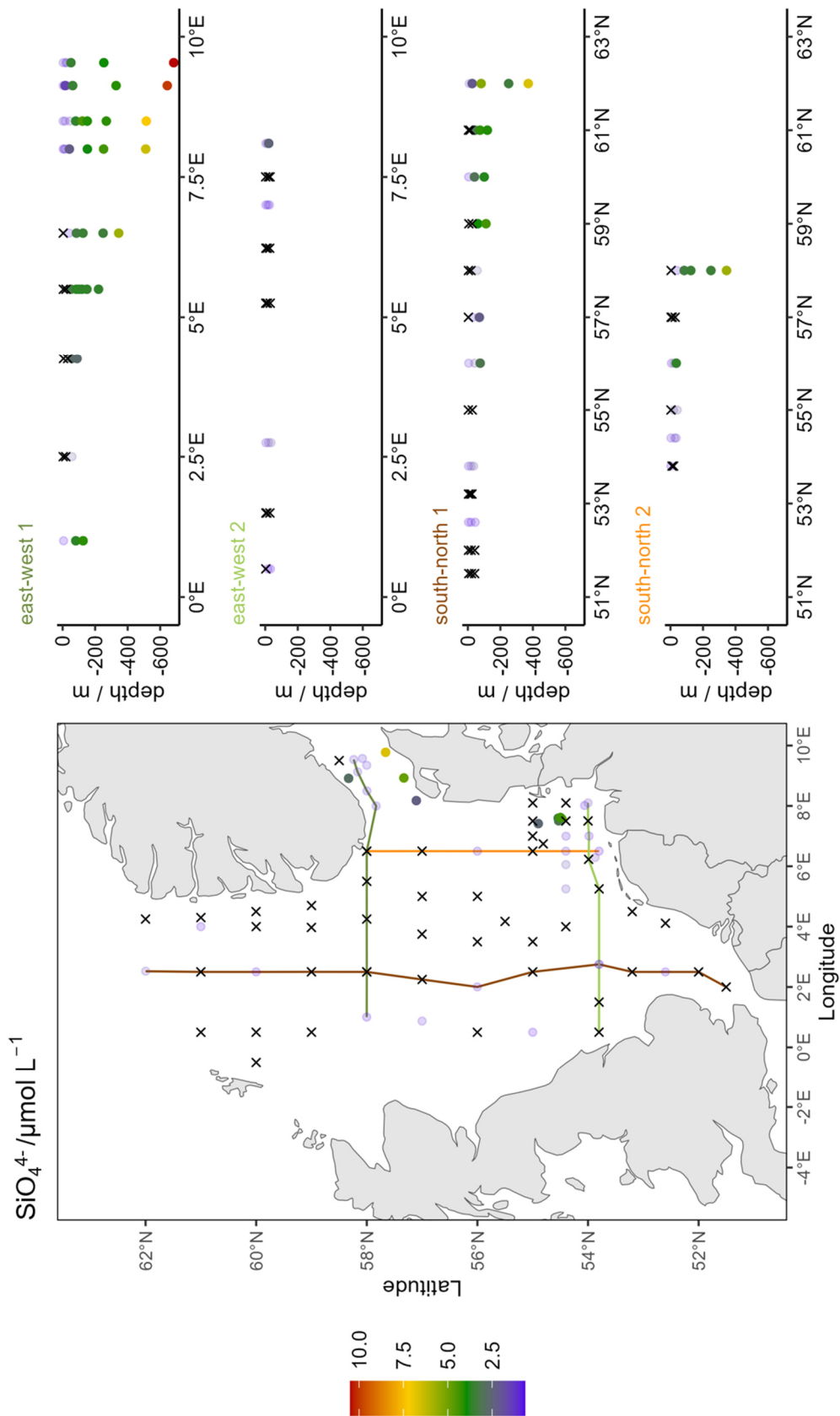


Figure A 30 Surface concentrations and depth profiles of  $\text{SiO}_4^{4-}$  across two south-north and two east-west transects. The northernmost transect is east-west 1 and the westernmost transect is south-north 1. x indicates concentrations below the LOD, and faint points indicate concentrations between LOD and LOQ.

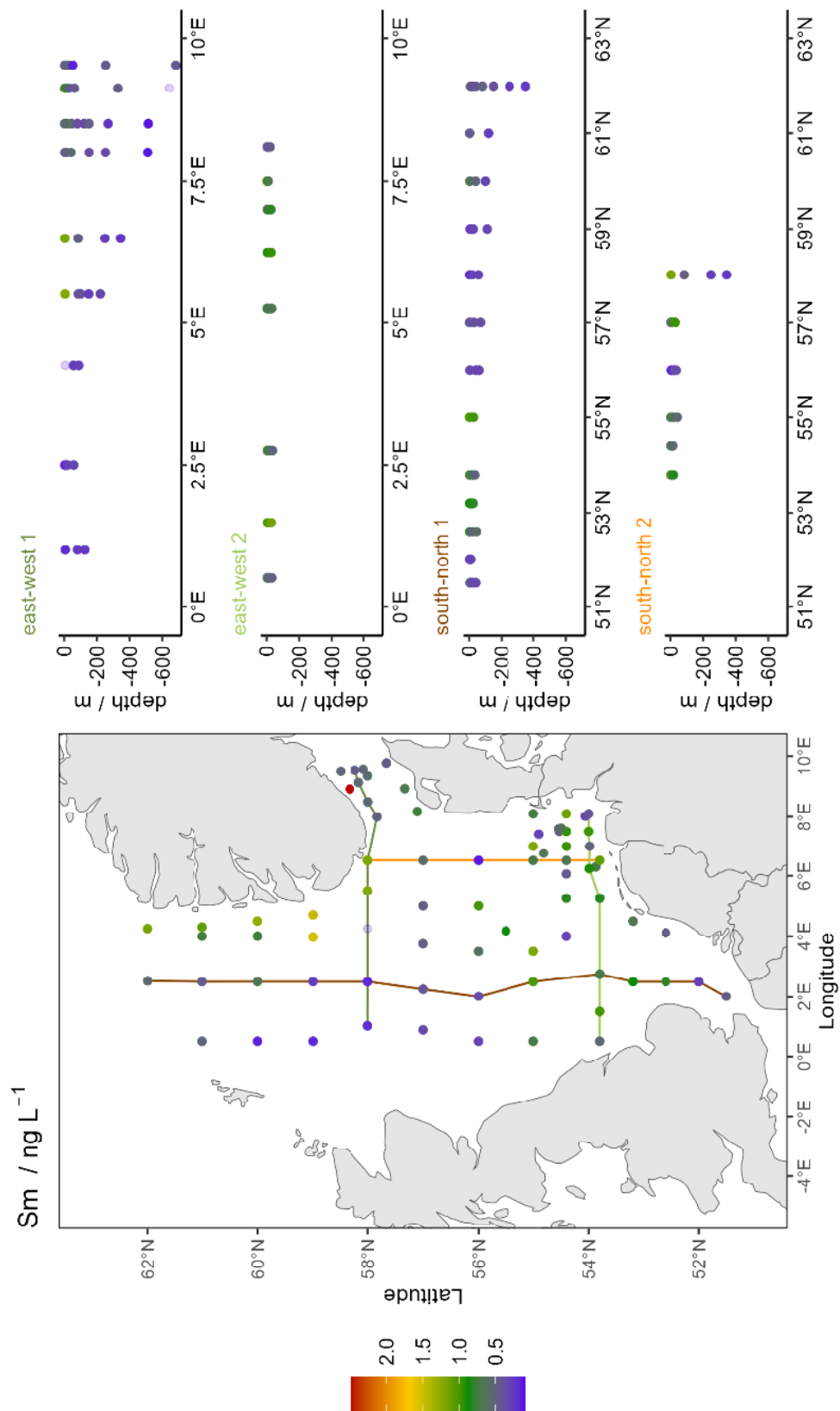


Figure A 31 Surface concentrations and depth profiles of *Sm* across two south-north and two east-west transects. The northernmost transect is east-west 1 and the westernmost transect is south-north 1. *x* indicates concentrations below the LOD, and faint points indicate concentrations between LOD and LOQ.

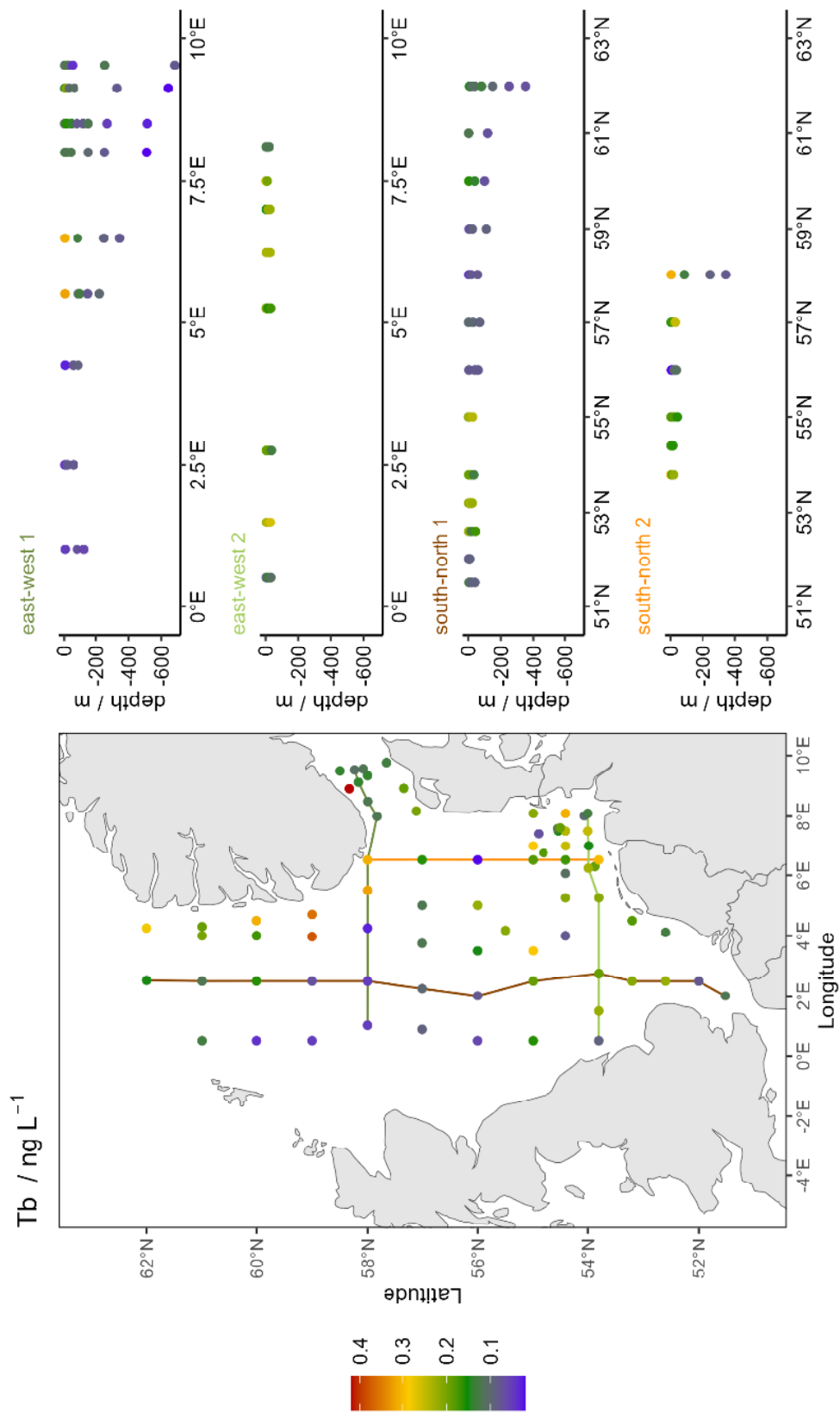


Figure A 32 Surface concentrations and depth profiles of *Tb* across two south-north and two east-west transects. The northernmost transect is east-west 1 and the westernmost transect is south-north 1. x indicates concentrations below the LOD, and faint points indicate concentrations between LOD and LOQ.



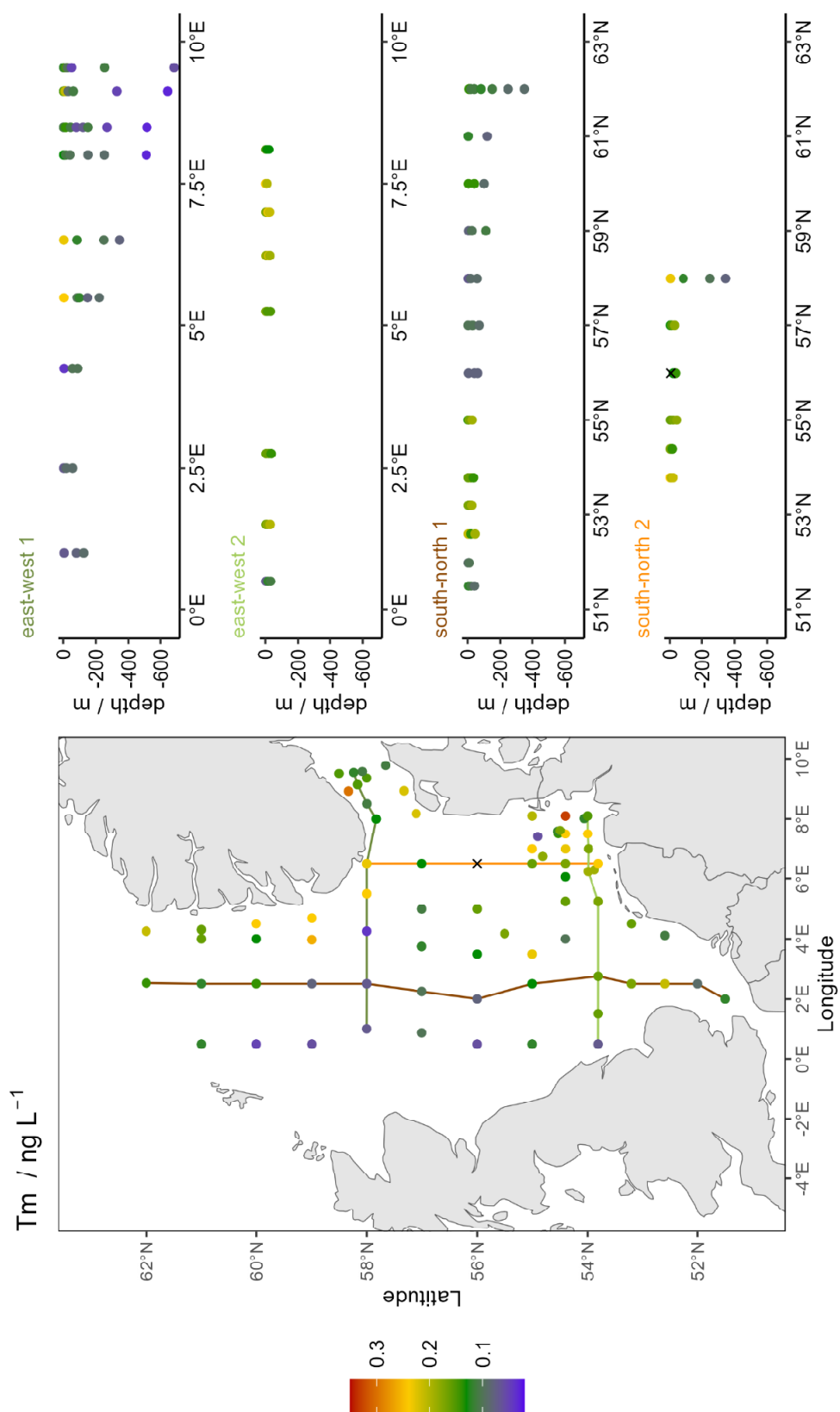


Figure A 33 Surface concentrations and depth profiles of  $T_m$  across two south-north and two east-west transects. The northernmost transect is east-west 1 and the westernmost transect is south-north 1.  $x$  indicates concentrations below the LOD, and faint points indicate concentrations between LOD and LOQ.

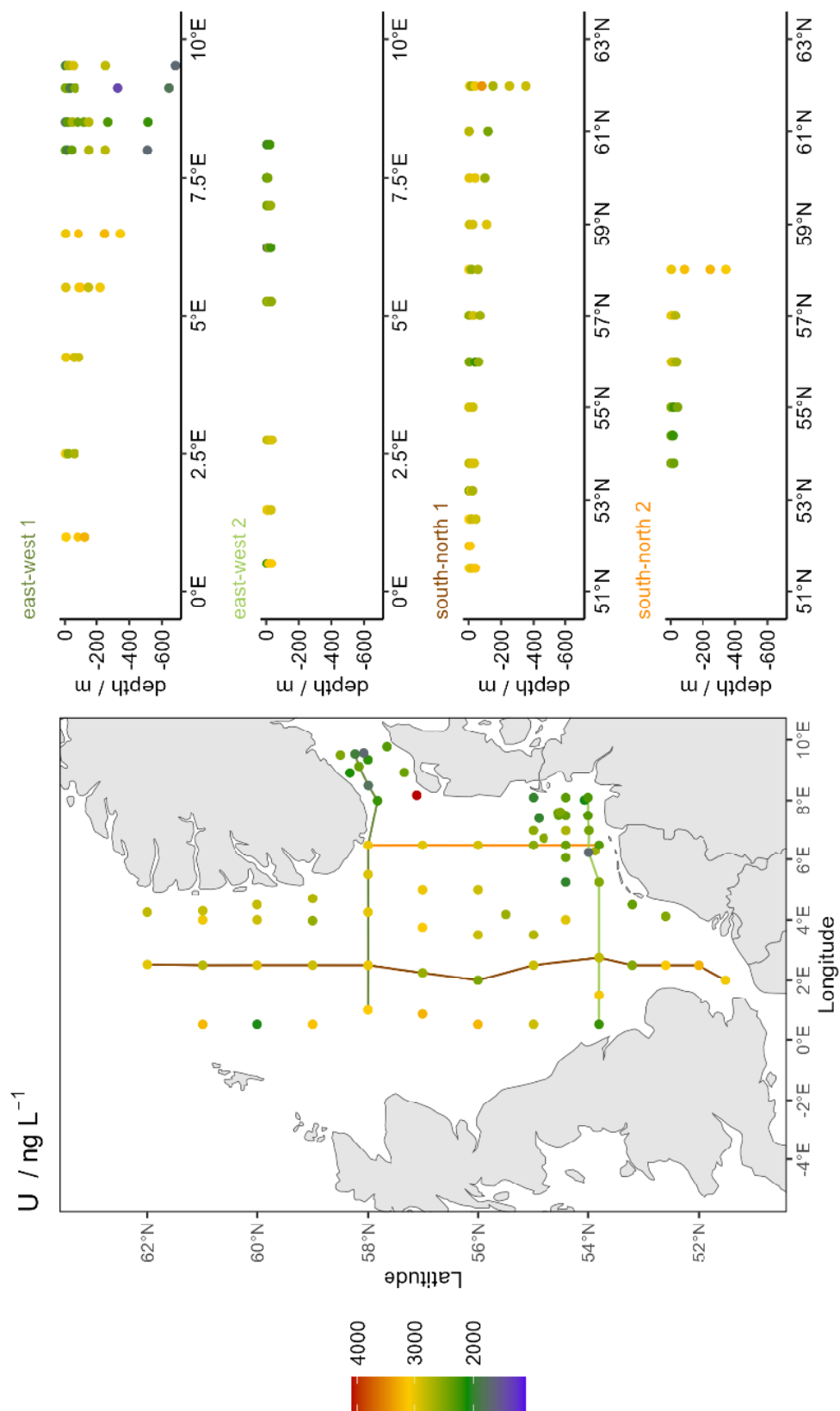


Figure A 34 Surface concentrations and depth profiles of  $U$  across two south-north and two east-west transects. The northernmost transect is east-west 1 and the westernmost transect is south-north 1.  $x$  indicates concentrations below the LOD, and faint points indicate concentrations between LOD and LOQ.

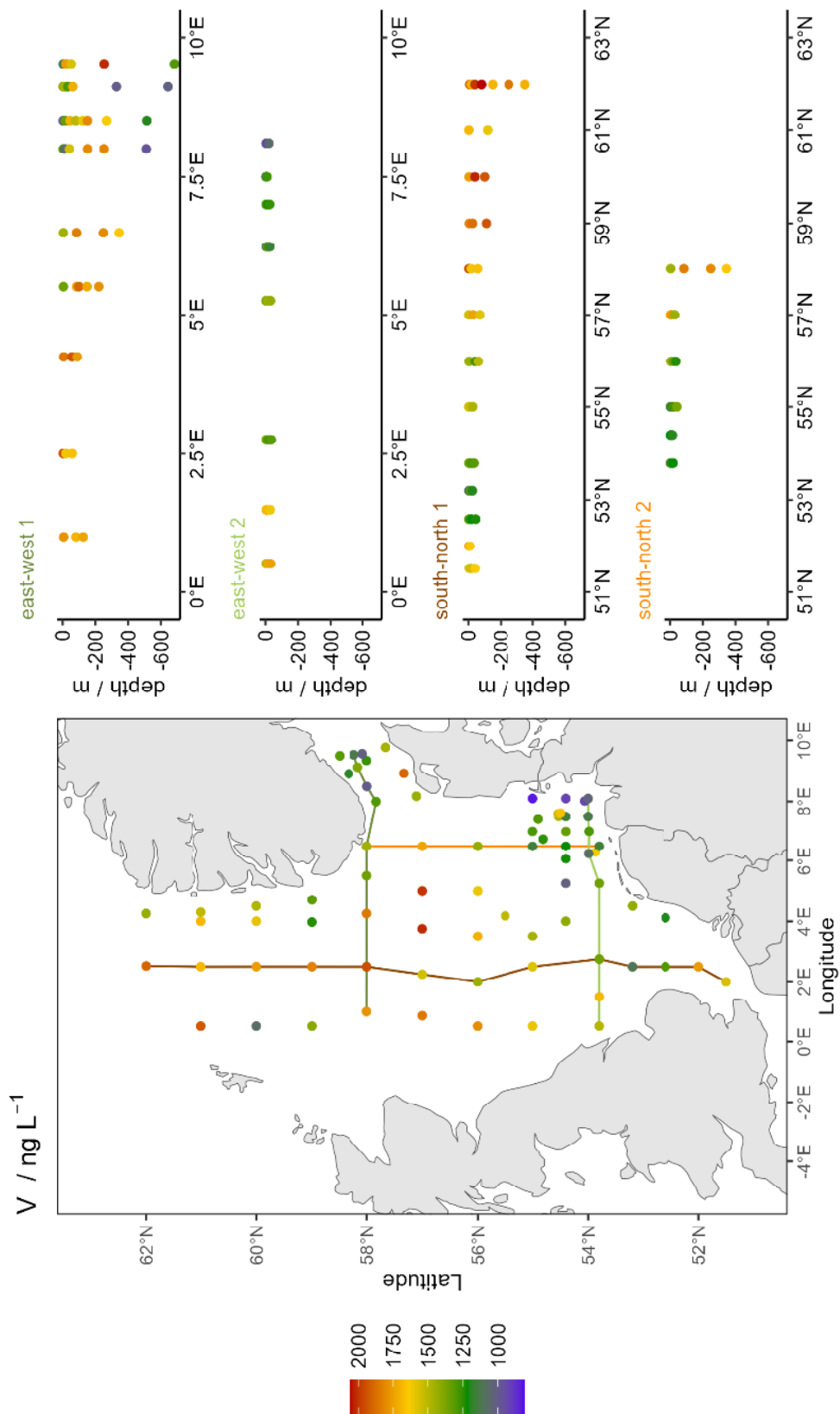


Figure A 35 Surface concentrations and depth profiles of  $V$  across two south-north and two east-west transects. The northernmost transect is east-west 1 and the westernmost transect is south-north 1.  $x$  indicates concentrations below the LOD, and faint points indicate concentrations between LOD and LOQ.

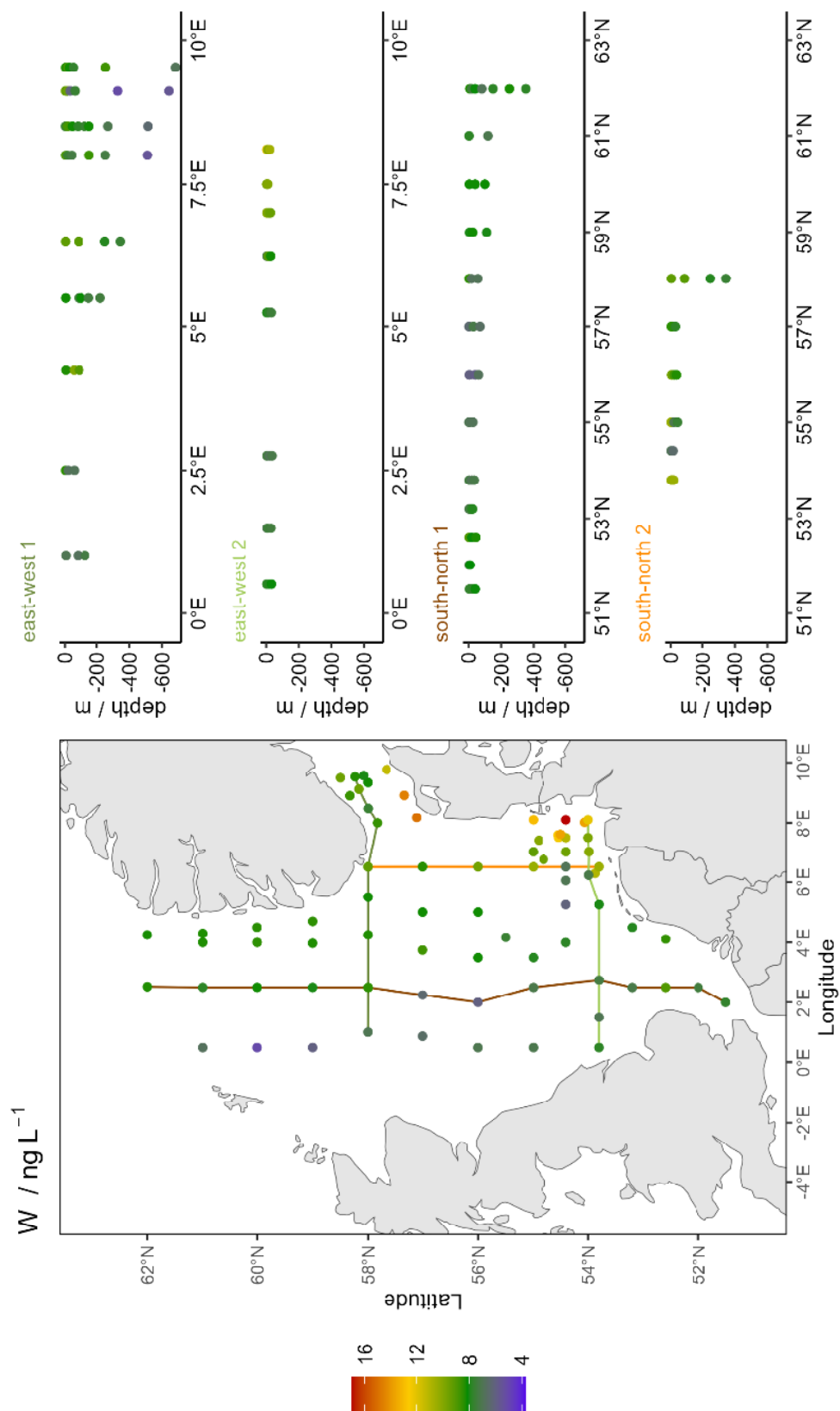


Figure A 36 Surface concentrations and depth profiles of  $W$  across two south-north and two east-west transects. The northernmost transect is east-west 1 and the westernmost transect is south-north 1.  $x$  indicates concentrations below the LOD, and faint points indicate concentrations between LOD and LOQ.

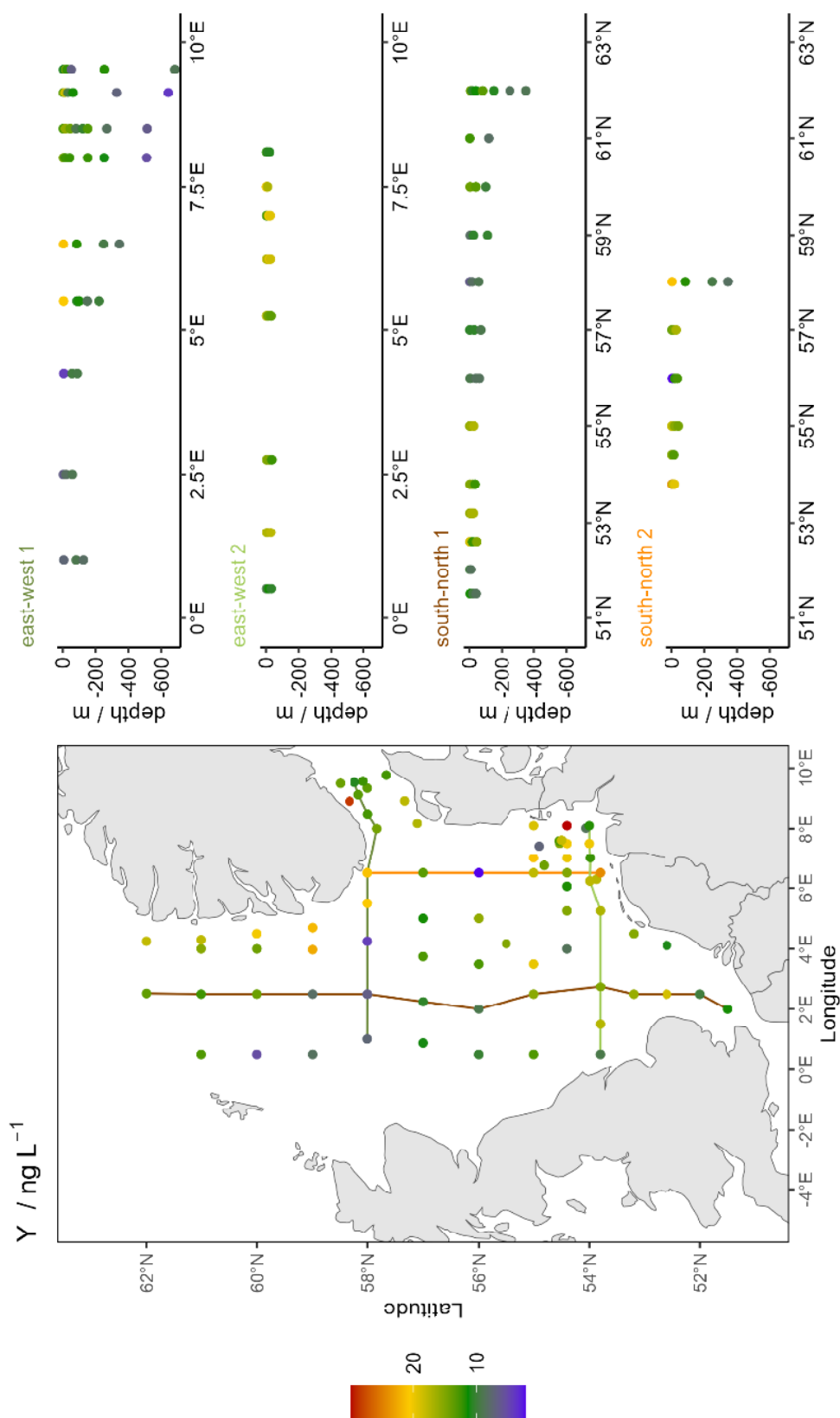


Figure A 37 Surface concentrations and depth profiles of Y across two south-north and two east-west transects. The northernmost transect is east-west 1 and the westernmost transect is south-north 1.  $x$  indicates concentrations below the LOD, and faint points indicate concentrations between LOD and LOQ.

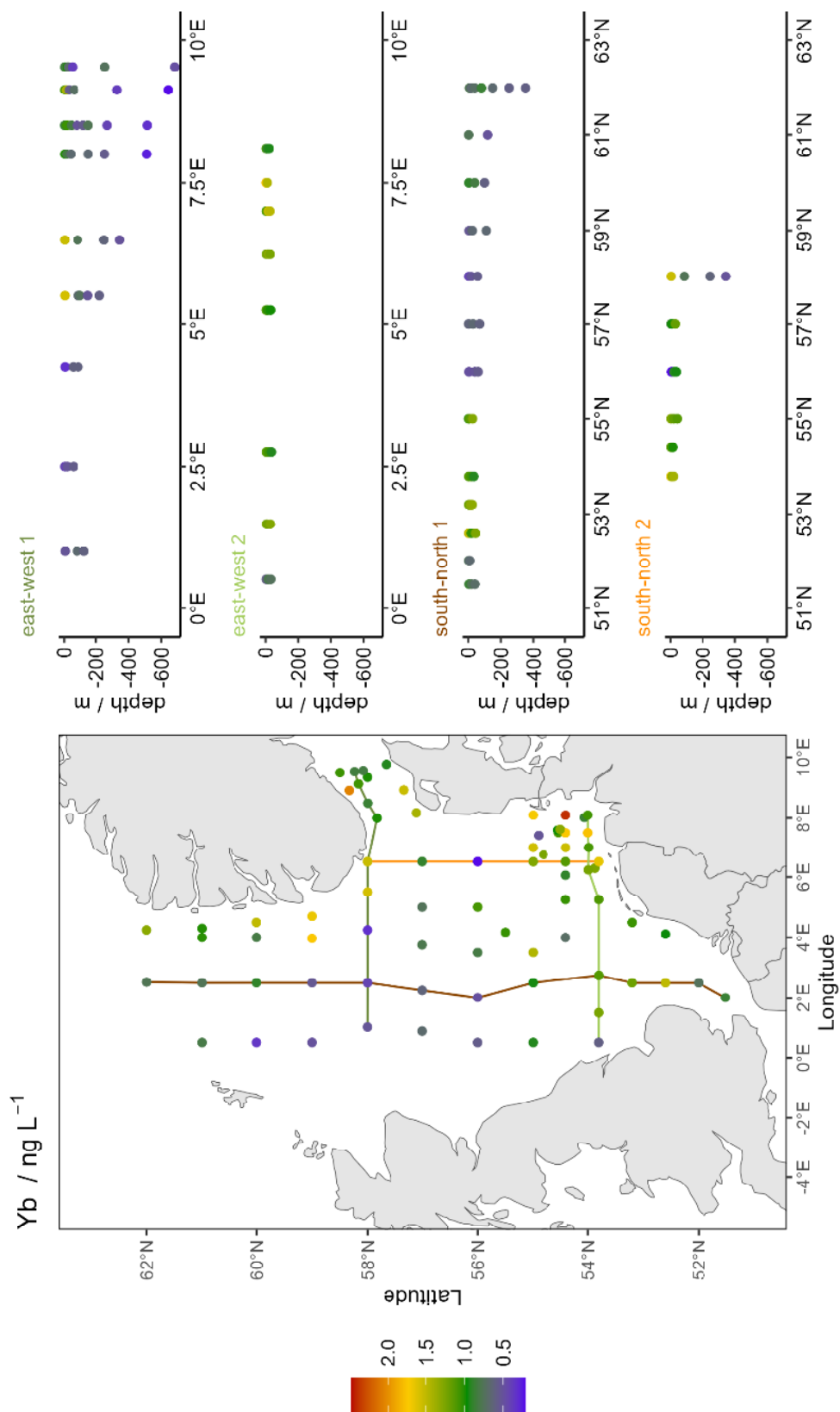


Figure A 38 Surface concentrations and depth profiles of Yb across two south-north and two east-west transects. The northernmost transect is east-west 1 and the westernmost transect is south-north 1. x indicates concentrations below the LOD, and faint points indicate concentrations between LOD and LOQ.

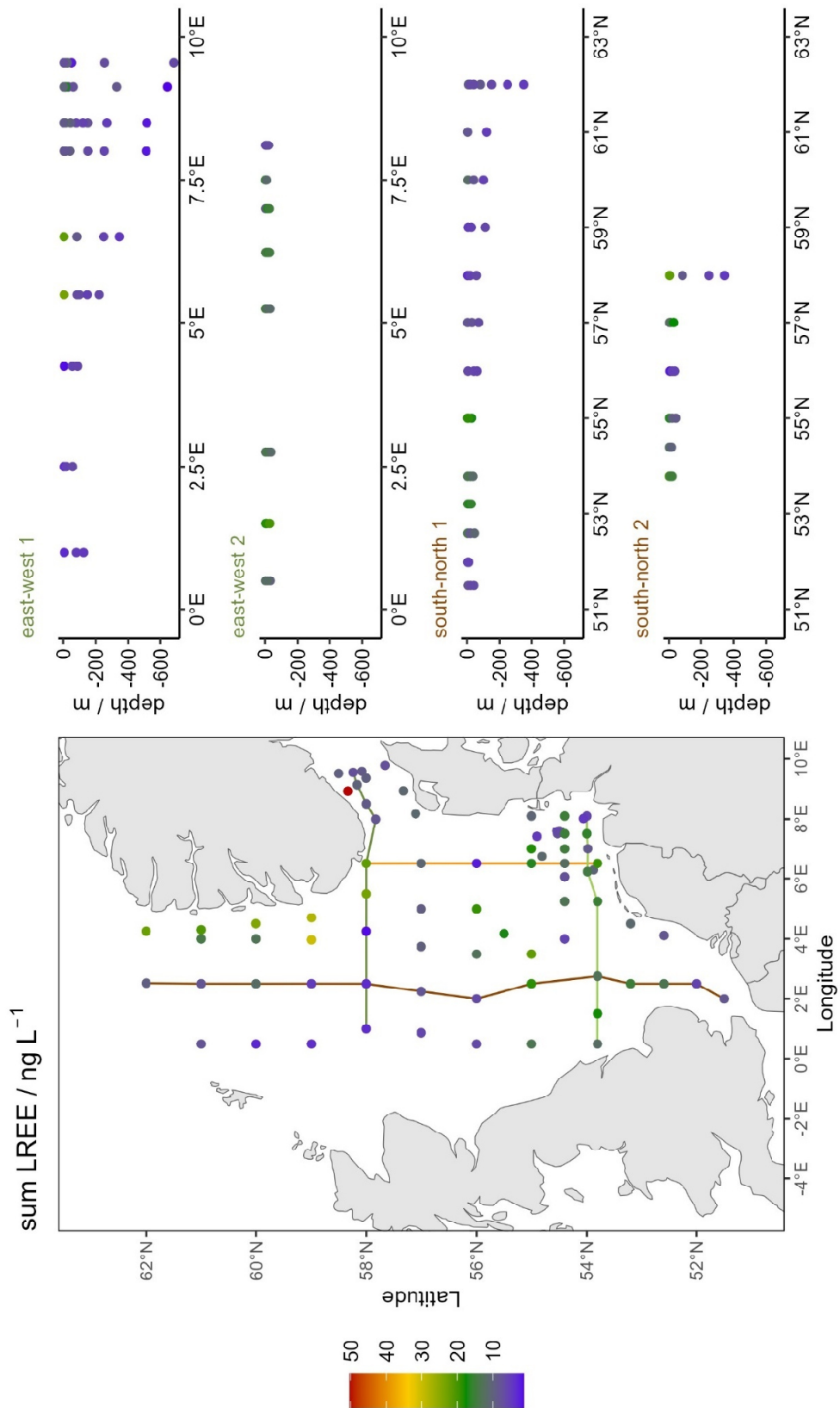


Figure A 39 Surface concentrations and depth profiles of the sum of LREE across two south-north and two east-west transects. The northernmost transect is east-west 1 and the westernmost transect is south-north 1.

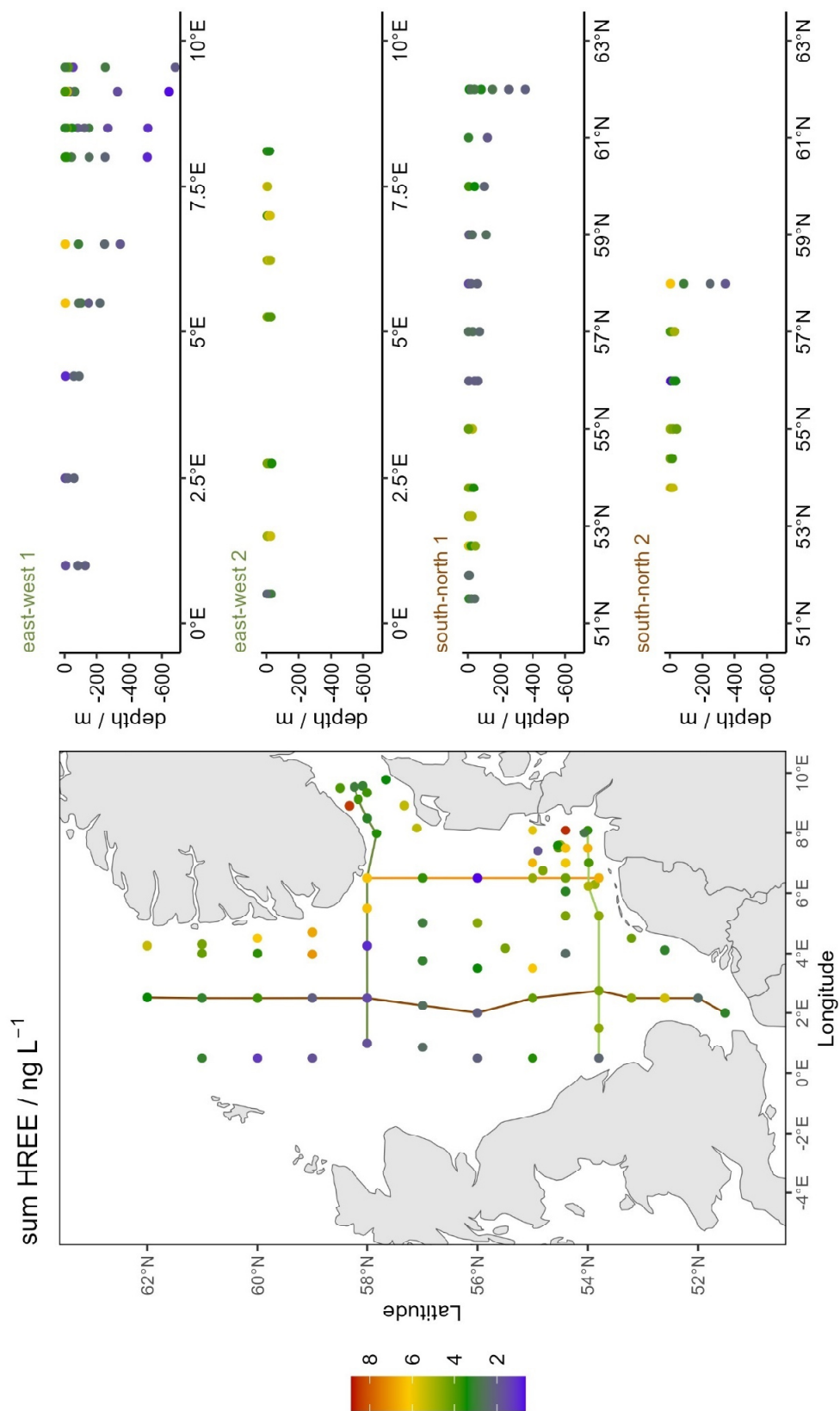


Figure A 40 Surface concentrations and depth profiles of the sum of HREE across two south-north and two east-west transects. The northernmost transect is east-west 1 and the westernmost transect is south-north 1.



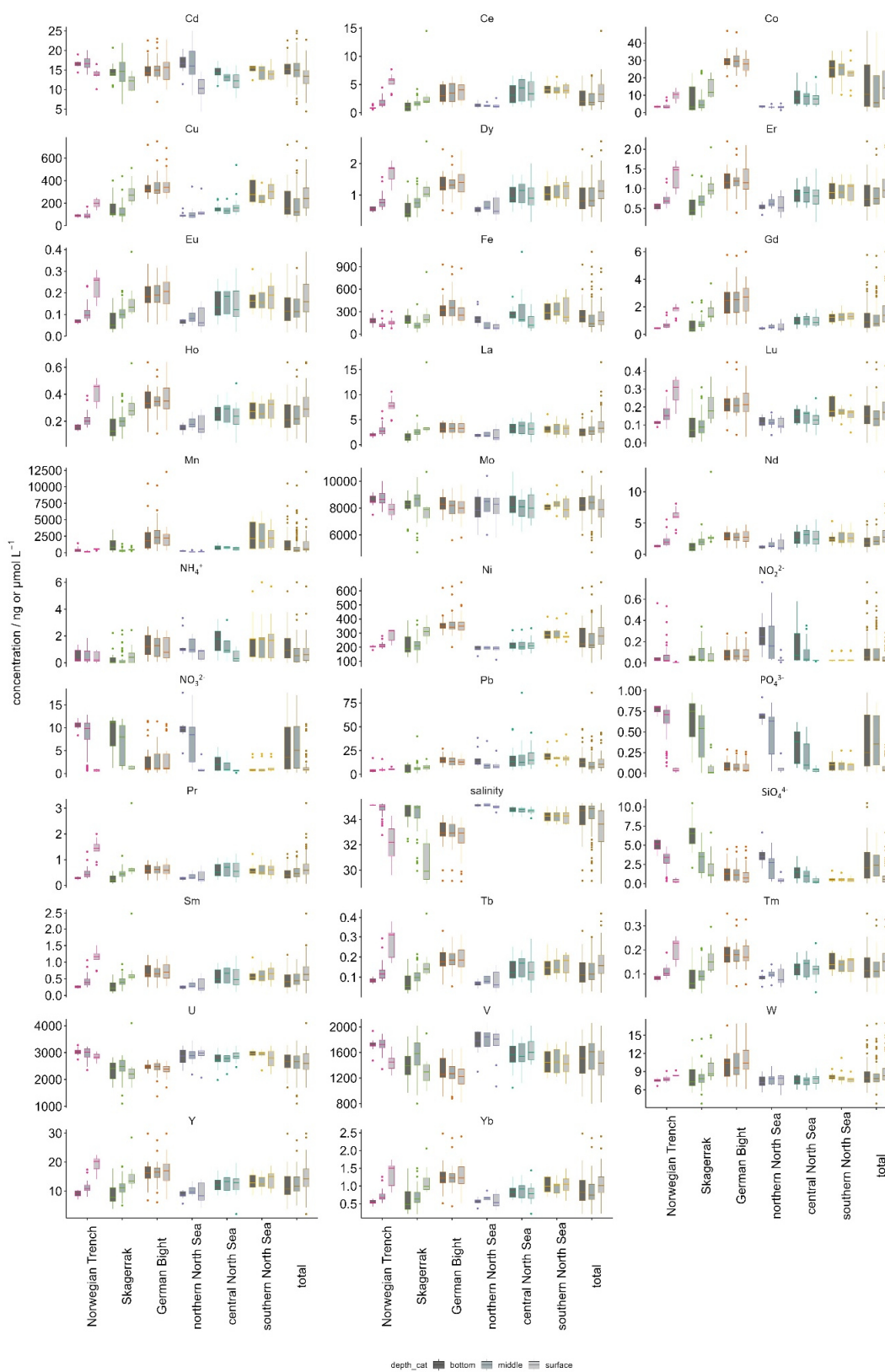


Figure A 41 Boxplot of salinity and all analytes in the North Sea (total) and six regions of the North Sea. The three boxplots per region indicate bottom (dark grey), intermediate depth (medium grey) and surface (light grey) samples.

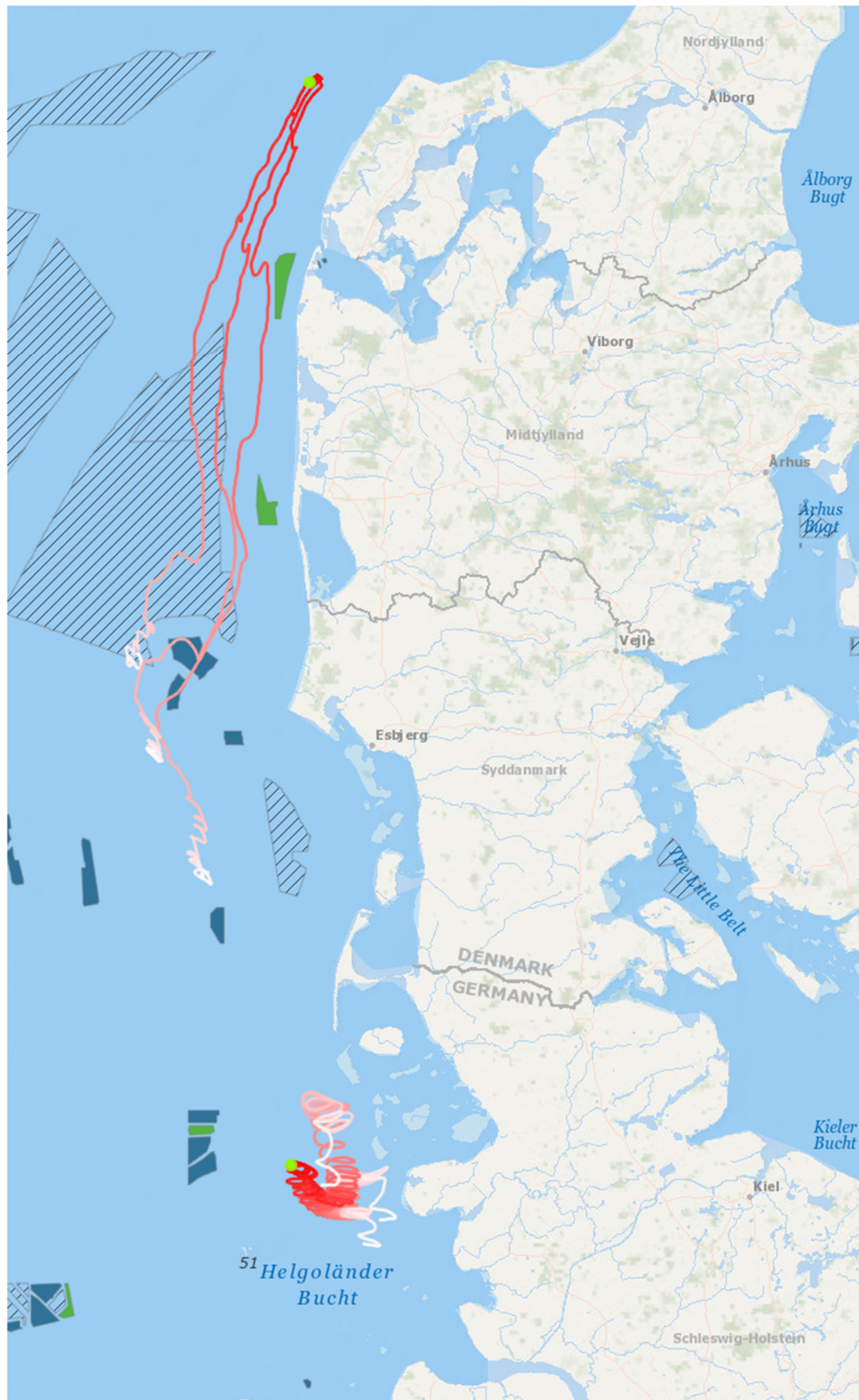


Figure A 42 Drift results for AL557 st.4 and HE586 st.26 2 weeks back with vertical mean marine currents and top layer marine currents without and with (factor 0.6) wind drag.

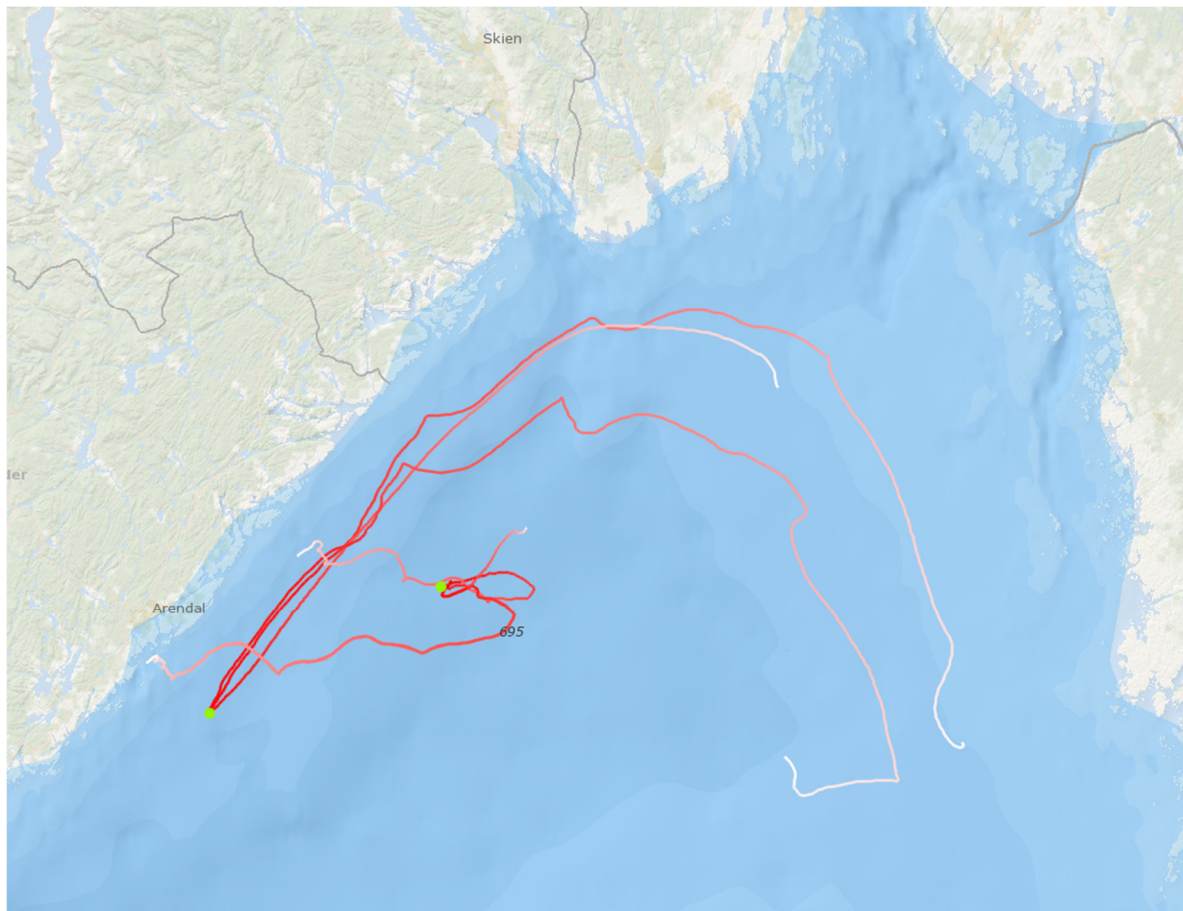


Figure A 43 Drift results for HE586 st.10 (left) and AL557 st.65 (right) from two weeks before sampling (white) to sampling time (dark red) for three different model settings: vertical mean marine currents, top layer marine currents without and with (factor 0.6) wind drag.



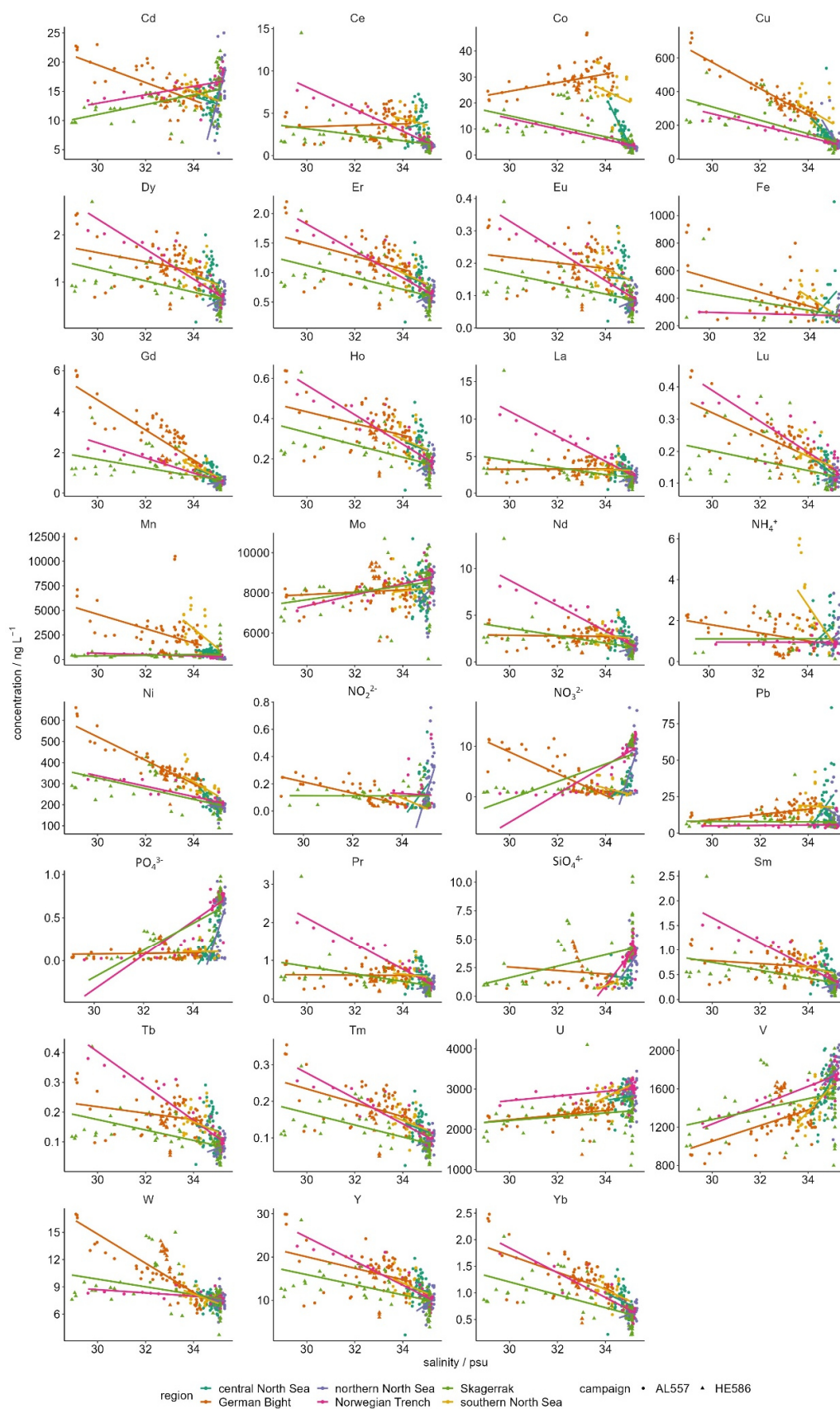


Figure A 44 Correlation plot of all dissolved analytes with salinity for the six regions of the North Sea (see legend) and campaigns AL557 (dot) and HE586 (triangle).

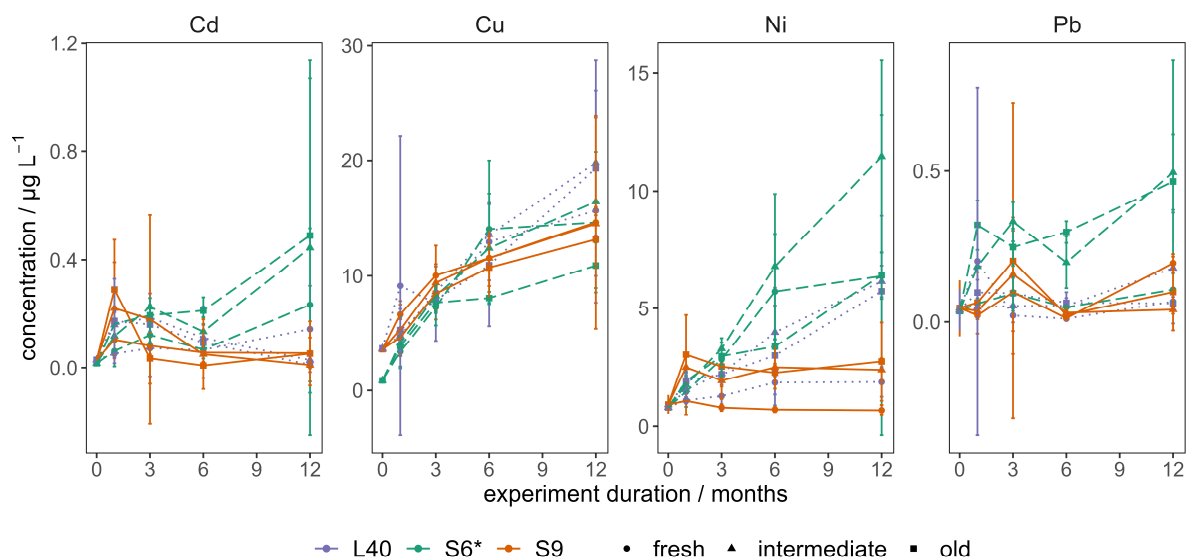


Figure A 45 Dissolved concentrations of Cd, Cu, Ni and Pb in aerobic incubations of fresh (circle), intermediate (triangle) and old (square) sediments from stations L40 (purple, dotted), S6\* (green, dashed) and S9 (orange, solid). Error bars correspond to the expanded uncertainty  $U(k=2)$ .

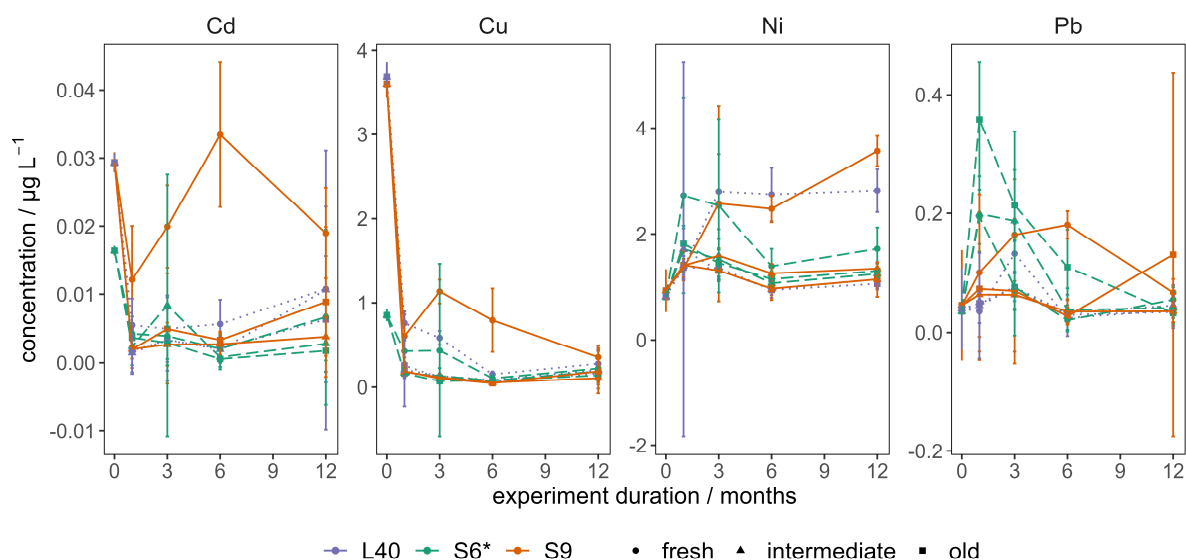


Figure A 46 Dissolved concentrations of Cd, Cu, Ni and Pb in anaerobic incubations of fresh (circle), intermediate (triangle) and old (square) sediments from stations L40 (purple, dotted), S6\* (green, dashed) and S9 (orange, solid). Error bars correspond to the expanded uncertainty  $U(k=2)$ .



## 9.7 Supplementary Tables

Table A 1 Blanks, LODs and LOQs for trace metal analysis in chapter 6.1. BEC, LOD and LOQ of measurement (pre-concentration, ICP-MS; n=6) as well as means and LOD of filtration blanks (n=14 for setup A, n=8 for setup B; \* indicates that n is lower as one outlier was removed after Dean-Dixon test). The last column contains the seawater concentrations from the initial filtrates from filtration B (n=6, uncertainty is 2\*SD).

| element | BEC /<br>ng L <sup>-1</sup> | LOD<br>(seaFAST)<br>/ ng L <sup>-1</sup> | LOQ<br>(seaFAST)<br>/ ng L <sup>-1</sup> | mean<br>blank<br>(setup A)<br>/ ng L <sup>-1</sup> | mean<br>blank<br>(setup B)<br>/ ng L <sup>-1</sup> | LOD<br>(setup A)<br>/ ng L <sup>-1</sup> | LOD<br>(setup B)<br>/ ng L <sup>-1</sup> | initial<br>filtrate<br>(setup B)<br>/ ng L <sup>-1</sup> |
|---------|-----------------------------|--|--|--|--|--|--|--|
| Cd      | 0.009                       | 0.02                                     | 0.06                                     | 0.8 ± 2.5  | 0.04 ±<br>0.05                                     | 8*                                       | 0.17                                     | 32.1 ± 0.9   |
| Ce      | 0.009                       | 0.0008                                   | 0.0023                                   | 0.11 ±<br>0.21                                     | 0.03 ±<br>0.05                                     | 0.7                                      | 0.18                                     | 4.7 ± 1.3  |
| Co      | 0.19                        | 0.013                                    | 0.04                                     | 0.06 ± 0.1   | 0.04 ±<br>0.04                                     | 0.4                                      | 0.16                                     | 36.0 ± 1.1   |
| Cu      | 0.4                         | 0.064                                    | 0.19                                     | 10 ± 50  | 3 ± 3  | 160                                      | 12                                       | 9320 ± 50  |
| Dy      | 0.0015                      | 0.0014                                   | 0.004                                    | 0.006 ±<br>0.014                                   | 0.003 ±<br>0.004                                   | 0.05                                     | 0.016                                    | 2.48 ±<br>0.10   |
| Er      | 0.0005                      | 4x10-06                                  | 1.1x10 <sup>-5</sup>                     | 0.004 ±<br>0.006                                   | 0.0014 ±<br>0.0018                                 | 0.022                                    | 0.007                                    | 2.55 ±<br>0.10   |
| Eu      | 0.0005                      | 0.001                                    | 0.0029                                   | 0.002 ±<br>0.004                                   | 0.001 ±<br>0.0021                                  | 0.013                                    | 0.007                                    | 0.34 ±<br>0.05   |
| Fe      | 40                          | 0.7                                      | 1.9                                      | 30 ± 40  | 13 ± 17  | 150*                                     | 70                                       | 320 ± 50   |
| Ho      | 0.0005                      | 0.0005                                   | 0.0015                                   | 0.0012 ±<br>0.002                                  | 0.0006 ±<br>0.0010                                 | 0.007*                                   | 0.004                                    | 0.679 ±<br>0.029   |
| La      | 0.004                       | 0.0028                                   | 0.008                                    | 0.06 ±<br>0.12                                     | 0.019 ±<br>0.03                                    | 0.4                                      | 0.11                                     | 4.8 ± 0.8  |
| Mn      | 0.5                         | 0.07                                     | 0.19                                     | 7 ± 17   | 3 ± 3  | 60                                       | 13                                       | 3060 ±<br>120  |
| Mo      | 0.3                         | 0.094                                    | 0.26                                     | 0.2 ± 0.3  | 0.14 ±<br>0.29                                     | 1  | 1*                                       | 6980 ±<br>220  |
| Nd      | 0.0023                      | 0.0022                                   | 0.006                                    | 0.03 ±<br>0.05                                     | 0.012 ±<br>0.018                                   | 0.17                                     | 0.06                                     | 4.8 ± 0.7  |
| Pb      | 0.05                        | 0.006                                    | 0.019                                    | 3 ± 8  | 0.35 ±<br>0.24                                     | 27*                                      | 1.1*                                     | 17.8 ± 2.9   |
| Pr      | 0.0005                      | 0.0005                                   | 0.0015                                   | 0.009 ±<br>0.014                                   | 0.0034 ±<br>0.0025                                 | 0.05                                     | 0.011*                                   | 0.97 ±<br>0.18   |
| Sm      | 0.0017                      | 0.005                                    | 0.014                                    | 0.006 ±<br>0.012                                   | 0.002 ±<br>0.004                                   | 0.04                                     | 0.015                                    | 1.23 ±<br>0.15   |
| Tb      | 0.0005                      | 0.0006                                   | 0.0016                                   | 0.002 ±<br>0.003                                   | 0.0006 ±<br>0.0015                                 | 0.012                                    | 0.005                                    | 0.29 ±<br>0.03   |
| U       | 0.008                       | 0.02                                     | 0.06                                     | 0.02 ±<br>0.04                                     | 0.01 ±<br>0.04                                     | 0.13                                     | 0.14                                     | 2070 ±<br>100  |
| V       | 0.13                        | 0.05                                     | 0.13                                     | 0.2 ± 0.4  | 0.6 ± 1.3  | 1.5                                      | 4  | 1270 ± 40  |
| W       | 0.06                        | 0.021                                    | 0.06                                     | 0.07 ±<br>0.06                                     | 0.07 ±<br>0.08                                     | 0.24                                     | 0.3                                      | 62.1 ± 1.9   |
| Y       | 0.0016                      | 0.0012                                   | 0.003                                    | 0.06 ±<br>0.14                                     | 0.014 ±<br>0.022                                   | 0.5                                      | 0.08                                     | 27.7 ± 0.5   |
| Zn      | 2.4                         | 0.3                                      | 0.8                                      | 300 ± 700  | 110 ± 180  | 2400*                                    | 700                                      | 2200 ±<br>1100   |

Table A 2 Validation of trace metal analysis in chapter 6.1. The in-house quality control standard (QC, n=24) and NASS-7 certified seawater (n=11) were measured. The NASS-7 reference values were taken from a) Nadeau et al. (2016) and b) Ebeling et al. (2022). The measured values do not differ significantly from the reference values (t-test, p=0.05).

| element | isotope | QC                                   |                                     |              | NASS-7                               |                                     |              |
|---------|---------|--------------------------------------|-------------------------------------|--------------|--------------------------------------|-------------------------------------|--------------|
|         |         | reference value / ng L <sup>-1</sup> | measured value / ng L <sup>-1</sup> | recovery / % | reference value / ng L <sup>-1</sup> | measured value / ng L <sup>-1</sup> | recovery / % |
| Cd      | 111     | 25 ± 2.5                             | 24.4 ± 1.2                          | 98 ± 5       | 16.1 ± 1.6 <sup>a</sup>              | 15.4 ± 0.7                          | 96 ± 5       |
| Ce      | 140     | 25 ± 2.5                             | 23.2 ± 1.1                          | 93 ± 5       | 3.48 ± 0.62 <sup>b</sup>             | 3.5 ± 0.17                          | 101 ± 5      |
| Co      | 59      | 25 ± 2.5                             | 24.2 ± 0.8                          | 97 ± 3       | 14.6 ± 1.4 <sup>a</sup>              | 14.4 ± 0.5                          | 99 ± 4       |
| Cu      | 65      | 25 ± 2.5                             | 23.9 ± 1.0                          | 96 ± 4       | 199 ± 14 <sup>a</sup>                | 188 ± 7                             | 94 ± 4       |
| Dy      | 163     | 25 ± 2.5                             | 21.4 ± 1.8                          | 86 ± 8       | 1.51 ± 0.22 <sup>b</sup>             | 1.55 ± 0.12                         | 102 ± 8      |
| Er      | 166     | 25 ± 2.5                             | 21.5 ± 1.8                          | 86 ± 9       | 1.3 ± 0.2 <sup>b</sup>               | 1.31 ± 0.08                         | 101 ± 6      |
| Eu      | 153     | 25 ± 2.5                             | 21.3 ± 1.9                          | 85 ± 9       | 0.230 ± 0.047 <sup>b</sup>           | 0.243 ± 0.021                       | 106 ± 9      |
| Fe      | 56      | 250 ± 25                             | 180 ± 40                            | 73 ± 19      | 351 ± 26 <sup>a</sup>                | 358 ± 13                            | 102 ± 4      |
| Ho      | 165     | 25 ± 2.5                             | 21.9 ± 1.7                          | 88 ± 8       | 0.394 ± 0.056 <sup>b</sup>           | 0.41 ± 0.03                         | 105 ± 8      |
| La      | 139     | 25 ± 2.5                             | 24.1 ± 1.0                          | 96 ± 4       | 9.8 ± 1.7 <sup>b</sup>               | 10.0 ± 0.4                          | 102 ± 4      |
| Mn      | 55      | 25 ± 2.5                             | 24.1 ± 0.8                          | 96 ± 3       | 750 ± 60 <sup>a</sup>                | 754 ± 25                            | 101 ± 3      |
| Mo      | 95      | 25 ± 2.5                             | 26.6 ± 2.5                          | 107 ± 9      | 9290 ± 400 <sup>a</sup>              | 7960 ± 200                          | 85.7 ± 2.5   |
| Nd      | 146     | 25 ± 2.5                             | 22.7 ± 1.3                          | 91 ± 6       | 6.09 ± 0.85 <sup>b</sup>             | 6.04 ± 0.30                         | 99 ± 5       |
| Pb      | 208     | 25 ± 2.5                             | 24.2 ± 1.0                          | 97 ± 4       | 2.6 ± 0.8 <sup>a</sup>               | 2.59 ± 0.14                         | 100 ± 5      |
| Pr      | 141     | 25 ± 2.5                             | 22.9 ± 1.2                          | 92 ± 5       | 1.38 ± 0.25 <sup>b</sup>             | 1.40 ± 0.06                         | 102 ± 5      |
| Sm      | 147     | 25 ± 2.5                             | 21.4 ± 1.8                          | 86 ± 8       | 1.06 ± 0.14 <sup>b</sup>             | 1.06 ± 0.05                         | 100 ± 5      |
| Tb      | 159     | 25 ± 2.5                             | 22.2 ± 2.1                          | 89 ± 10      | 0.202 ± 0.028 <sup>b</sup>           | 0.236 ± 0.019                       | 117 ± 8      |
| U       | 238     | 25 ± 2.5                             | 21.8 ± 2.9                          | 87 ± 13      | 2870 ± 160 <sup>a</sup>              | 2430 ± 210                          | 85 ± 8       |
| V       | 51      | 25 ± 2.5                             | 23.9 ± 1.6                          | 95 ± 7       | 1300 ± 80 <sup>a</sup>               | 1300 ± 120                          | 100 ± 9      |
| W       | 182     | 25 ± 2.5                             | 25.9 ± 1.0                          | 104 ± 4      | 9.1 ± 2.1 <sup>b</sup>               | 8.8 ± 0.7                           | 97 ± 8       |
| Y       | 89      | 25 ± 2.5                             | 23 ± 1.7                            | 92 ± 7       | 18 ± 5.2 <sup>b</sup>                | 19.6 ± 0.3                          | 108.5 ±      |
| Zn      | 66      | 250 ± 25                             | 252 ± 13                            | 101 ± 5      | 420 ± 80 <sup>a</sup>                | 427 ± 24                            | 102 ± 6      |

Table A 3 Bottle numbers, storage time and storage temperature for chapter 6.1.

| bottle | storage | storage days | bottle | storage | storage days |
|--------|---------|--------------|--------|---------|--------------|
| B01    | none    | 0            | B10    | -18 °C  | 15           |
| B02    | none    | 0            | B11    | 4 °C    | 22           |
| B03    | 4 °C    | 8            | B12    | 4 °C    | 22           |
| B04    | 4 °C    | 8            | B13    | -18 °C  | 22           |
| B05    | -18 °C  | 8            | B14    | -18 °C  | 22           |
| B06    | -18 °C  | 8            | B15    | 4 °C    | 63           |
| B07    | 4 °C    | 15           | B16    | 4 °C    | 63           |
| B08    | 4 °C    | 15           | B17    | -18 °C  | 63           |
| B09    | -18 °C  | 15           | B18    | -18 °C  | 63           |



Table A 4 Validation, blanks, LOD and LOQ for trace metal analysis in chapter 6.2. For the reference materials (QC, NASS-7), the SDs are given and for the blanks, the medians and MAD are given from which the LOD and LOQ were calculated. The number of measurements is given in parentheses. \*indicates that BEC (background equivalent concentration) was higher than the LOD and hence the BEC is shown.

| element | isotope | QC / ng L <sup>-1</sup> | NASS-7 / ng L <sup>-1</sup> | blank / ng L <sup>-1</sup> | LOD / ng L <sup>-1</sup> | LOQ / ng L <sup>-1</sup> |
|---------|---------|-------------------------|-----------------------------|----------------------------|--------------------------|--------------------------|
| V       | 51      | 28.7 ± 2.9 (138)        | 1420 ± 50 (33)              | 0.11 ± 0.17 (35)           | 1.48*                    | 1.8                      |
| Mn      | 55      | 24.9 ± 0.8 (137)        | 782 ± 20 (33)               | 11 ± 10 (35)               | 41                       | 111                      |
| Fe      | 56      | 218 ± 22 (137)          | 360 ± 40 (33)               | 60 ± 60 (35)               | 230                      | 610                      |
| Co      | 59      | 25.9 ± 0.9 (138)        | 15 ± 0.4 (33)               | 0.07 ± 0.04 (35)           | 0.18                     | 0.44                     |
| Ni      | 60      | 24.6 ± 1.6 (138)        | 255 ± 8 (33)                | 2.8 ± 2.9 (35)             | 11.6                     | 32.2                     |
| Cu      | 65      | 24.8 ± 1.6 (138)        | 201 ± 6 (33)                | 3.5 ± 2.5 (35)             | 10.9                     | 28.2                     |
| Y       | 89      | 24.5 ± 1.3 (138)        | 19.4 ± 0.5 (33)             | 0.07 ± 0.07 (35)           | 0.29                     | 0.79                     |
| Mo      | 95      | 28 ± 2.6 (129)          | 8000 ± 700 (33)             | 0.5 ± 0.5 (35)             | 2.3*                     | 5.7                      |
| Cd      | 111     | 24.9 ± 0.9 (138)        | 15.6 ± 0.5 (33)             | 0.07 ± 0.08 (35)           | 0.33                     | 0.92                     |
| La      | 139     | 24.6 ± 0.9 (138)        | 9.7 ± 0.4 (33)              | 0.06 ± 0.05 (35)           | 0.23                     | 0.61                     |
| Ce      | 140     | 24.3 ± 1.2 (138)        | 3.48 ± 0.17 (33)            | 0.08 ± 0.07 (35)           | 0.28                     | 0.77                     |
| Pr      | 141     | 24.2 ± 1.3 (138)        | 1.38 ± 0.07 (33)            | 0.014 ± 0.013 (35)         | 0.053                    | 0.145                    |
| Nd      | 146     | 23.7 ± 1.4 (138)        | 5.95 ± 0.23 (33)            | 0.05 ± 0.05 (35)           | 0.2                      | 0.54                     |
| Sm      | 147     | 23.4 ± 1.8 (138)        | 1.04 ± 0.06 (33)            | 0.009 ± 0.009 (35)         | 0.035                    | 0.095                    |
| Eu      | 153     | 23.7 ± 1.8 (138)        | 0.24 ± 0.04 (33)            | 0.0017 ± 0.0026 (35)       | 0.0097*                  | 0.027                    |
| Gd      | 157     | 23.6 ± 1.7 (138)        | 1.47 ± 0.08 (33)            | 0.024 ± 0.027 (35)         | 0.104                    | 0.292                    |
| Tb      | 159     | 24.5 ± 2.4 (138)        | 0.23 ± 0.03 (32)            | 0.0007 ± 0.001 (35)        | 0.0089*                  | 0.011                    |
| Dy      | 163     | 23.6 ± 1.7 (138)        | 1.53 ± 0.1 (33)             | 0.006 ± 0.007 (35)         | 0.028                    | 0.081                    |
| Ho      | 165     | 23.9 ± 1.7 (138)        | 0.41 ± 0.04 (33)            | 0.0011 ± 0.0017 (35)       | 0.0097*                  | 0.018                    |
| Er      | 166     | 23.7 ± 1.8 (138)        | 1.29 ± 0.09 (33)            | 0.003 ± 0.004 (35)         | 0.015                    | 0.044                    |
| Tm      | 169     | 23.4 ± 2 (138)          | 0.21 ± 0.04 (33)            | 0 ± 0 (35)                 | 0.023*                   |                          |
| Yb      | 172     | 23.1 ± 2.8 (138)        | 1.25 ± 0.1 (33)             | 0 ± 0 (35)                 | 0.04*                    |                          |
| Lu      | 175     | 23.5 ± 3.4 (138)        | 0.23 ± 0.07 (32)            | 0 ± 0 (35)                 | 0.07*                    |                          |
| W       | 182     | 25 ± 1.8 (138)          | 8.1 ± 0.5 (33)              | 0.06 ± 0.07 (35)           | 0.4*                     | 0.73                     |
| Pb      | 208     | 24.2 ± 1.2 (138)        | 2.66 ± 0.26 (30)            | 1 ± 0.8 (35)               | 3.5                      | 9.3                      |
| U       | 238     | 23 ± 2.7 (138)          | 2360 ± 160 (33)             | 0.1 ± 0.09 (35)            | 0.39                     | 1.05                     |

Table A 5 Validation of nutrient analysis in chapter 6.2. LOD and LOQ were calculated from the calibration line ( $n=4$ ). The standard concentrations were measured in the VKI standards ( $n=8$  for AL557,  $n=4$  for HE586) for the nutrient analysis. Values were calculated for each campaign separately.

| campaign | analyte             | LOD / $\mu\text{mol L}^{-1}$ | LOQ / $\mu\text{mol L}^{-1}$ | standard / $\mu\text{mol L}^{-1}$ |
|----------|---------------------|------------------------------|------------------------------|-----------------------------------|
| AL557    | $\text{NH}_4^+$     | 0.28                         | 0.9                          | $2.42 \pm 0.13$                   |
| AL557    | $\text{NO}_2^-$     | 0.023                        | 0.09                         | $1.306 \pm 0.023$                 |
| AL557    | $\text{PO}_4^{3-}$  | 0.007                        | 0.028                        | $2.18 \pm 0.03$                   |
| AL557    | $\text{SiO}_4^{4-}$ | 0.6                          | 2                            | $16.1 \pm 0.9$                    |
| AL557    | $\text{NO}_3^-$     | 0.17                         | 0.6                          | $10.85 \pm 0.18$                  |
| HE586    | $\text{NH}_4^+$     | 0.11                         | 0.4                          | $2.17 \pm 0.03$                   |
| HE586    | $\text{NO}_2^-$     | 0.03                         | 0.11                         | $1.278 \pm 0.007$                 |
| HE586    | $\text{PO}_4^{3-}$  | 0.017                        | 0.06                         | $2.034 \pm 0.017$                 |
| HE586    | $\text{SiO}_4^{4-}$ | 0.4                          | 1.5                          | $14.50 \pm 0.10$                  |
| HE586    | $\text{NO}_3^-$     | 0.5                          | 1.9                          | $10.515 \pm 0.016$                |

Table A 6 Results of the PCA with varimax rotation in chapter 6.2. The given numbers are the loadings of the analytes on the four rotated components. Blue colors indicate negative correlation, red colors positive correlations. Bold numbers indicate changes in the assignment of the variables to the components when the measurement uncertainties were added. See text for further information.

|                     | varimax with measured concentrations |        |        |        | varimax with concentrations + uncertainty |        |        |        | varimax with concentrations - uncertainty |        |        |        |
|---------------------|--------------------------------------|--------|--------|--------|---|--------|--------|--------|---|--------|--------|--------|
|                     | comp 1                               | comp 2 | comp 3 | comp 4 | comp 1                                    | comp 2 | comp 3 | comp 4 | comp 1                                    | comp 2 | comp 3 | comp 4 |
| salinity            | 0.44                                 | 0.19   | -0.81  | -0.06  | 0.43                                      | 0.19   | -0.81  | -0.09  | 0.40                                      | 0.18   | -0.83  | -0.01  |
| $\text{NO}_3^-$     | 0.07                                 | 0.85   | -0.28  | -0.13  | 0.10                                      | 0.86   | -0.24  | -0.16  | 0.05                                      | 0.85   | -0.33  | -0.04  |
| $\text{NO}_2^-$     | -0.18                                | 0.60   | 0.06   | 0.19   | -0.24                                     | 0.62   | 0.03   | 0.21   | -0.13                                     | 0.63   | 0.09   | 0.20   |
| $\text{SiO}_4^{4-}$ | 0.07                                 | 0.73   | -0.26  | -0.40  | 0.11                                      | 0.74   | -0.24  | -0.37  | 0.05                                      | 0.73   | -0.30  | -0.42  |
| $\text{PO}_4^{3-}$  | 0.28                                 | 0.66   | -0.49  | -0.20  | 0.32                                      | 0.67   | -0.45  | -0.20  | 0.23                                      | 0.65   | -0.53  | -0.17  |
| $\text{NH}_4^+$     | -0.01                                | 0.15   | 0.11   | 0.80   | -0.06                                     | 0.17   | 0.09   | 0.80   | 0.03                                      | 0.15   | 0.15   | 0.78   |
| V                   | 0.86                                 | 0.09   | -0.29  | -0.14  | 0.81                                      | 0.11   | -0.33  | -0.14  | 0.88                                      | 0.05   | -0.22  | -0.10  |
| Mn                  | -0.28                                | -0.12  | 0.48   | 0.57   | -0.26                                     | -0.14  | 0.48   | 0.57   | -0.22                                     | -0.12  | 0.55   | 0.51   |
| Fe                  | -0.15                                | 0.06   | 0.32   | 0.70   | 0.01                                      | -0.03  | 0.31   | 0.67   | -0.26                                     | 0.17   | 0.30   | 0.60   |
| Co                  | -0.24                                | -0.17  | 0.76   | 0.41   | -0.25                                     | -0.19  | 0.73   | 0.45   | -0.15                                     | -0.14  | 0.83   | 0.32   |
| Ni                  | -0.10                                | 0.08   | 0.89   | 0.25   | -0.10                                     | 0.09   | 0.86   | 0.27   | 0.02                                      | 0.09   | 0.89   | 0.21   |
| Cu                  | -0.28                                | -0.13  | 0.79   | 0.33   | -0.29                                     | -0.13  | 0.76   | 0.35   | -0.19                                     | -0.08  | 0.84   | 0.26   |
| Mo                  | 0.74                                 | 0.27   | 0.27   | -0.20  | 0.73                                      | 0.20   | 0.36   | -0.21  | 0.72                                      | 0.20   | 0.22   | -0.16  |
| Cd                  | 0.38                                 | 0.65   | 0.09   | 0.29   | 0.44                                      | 0.62   | 0.14   | 0.26   | 0.44                                      | 0.60   | 0.11   | 0.28   |
| W                   | 0.18                                 | 0.20   | 0.84   | 0.00   | 0.17                                      | 0.18   | 0.85   | 0.00   | 0.28                                      | 0.23   | 0.77   | -0.03  |
| Pb                  | 0.15                                 | -0.25  | 0.22   | 0.73   | 0.08                                      | -0.26  | 0.20   | 0.74   | 0.25                                      | -0.27  | 0.18   | 0.71   |
| U                   | 0.80                                 | -0.15  | -0.23  | 0.18   | 0.79                                      | -0.10  | -0.27  | 0.17   | 0.81                                      | -0.15  | -0.13  | 0.19   |
| Y                   | 0.03                                 | -0.24  | 0.83   | 0.16   | 0.02                                      | -0.25  | 0.83   | 0.15   | 0.09                                      | -0.20  | 0.83   | 0.12   |
| sum LREE            | -0.03                                | -0.38  | 0.72   | 0.28   | -0.03                                     | -0.38  | 0.71   | 0.27   | 0.00                                      | -0.36  | 0.72   | 0.25   |
| sum HREE            | -0.03                                | -0.25  | 0.84   | 0.24   | -0.05                                     | -0.28  | 0.83   | 0.24   | 0.02                                      | -0.20  | 0.86   | 0.19   |

Table A 7 Metadata for the incubated sediments in chapter 6.3.

| station | sampling date and time                       | depth category | mixed samples [cm] | month | aerobic |      |      | anaerobic |       |       |
|---------|--|----------------|--------------------|-------|---------|------|------|-----------|-------|-------|
|         |  |                |                    |       | rep1    | rep2 | rep3 | rep1      | rep2  | rep3  |
| S6*     | Oct 8, 2021, 8:33 (UTC), 58.0799°N, 9.5746°E | surface        | 0-10               | 1     | 6.06    | 5.52 | 6.16 | 15.19     | 15.48 | 15.43 |
|         |  |                |                    | 3     | 5.70    | 5.45 | 5.39 | 15.48     | 15.25 | 15.95 |
|         |  |                |                    | 6     | 6.05    | 5.52 | 5.65 | 15.68     | 15.33 | 15.25 |
|         |  |                |                    | 12    | 6.14    | 6.00 | 5.74 | 15.63     | 15.99 | 15.19 |
|         |  | middle         | 11-20              | 1     | 5.77    | 5.47 | 6.19 | 15.63     | 15.11 | 15.37 |
|         |  |                |                    | 3     | 6.35    | 5.96 | 5.63 | 15.64     | 16.41 | 15.88 |
|         |  |                |                    | 6     | 5.75    | 5.69 | 6.75 | 15.45     | 16.62 | 16.95 |
|         |  |                |                    | 12    | 5.35    | 6.06 | 6.50 | 16.37     | 15.41 | 16.19 |
|         |  | bottom         | 21-32              | 1     | 5.82    | 5.99 | 5.45 | 16.78     | 15.82 | 15.69 |
|         |  |                |                    | 3     | 6.44    | 5.52 | 5.37 | 16.21     | 15.57 | 15.62 |
|         |  |                |                    | 6     | 5.62    | 5.92 | 5.60 | 16.27     | 16.51 | 15.92 |
|         |  |                |                    | 12    | 6.05    | 5.80 | 5.32 | 15.58     | 15.98 | 16.43 |
| S9      | Oct 9, 2021, 7:39 (UTC), 58.2349°N, 9.5346°E | surface        | 0-12               | 1     | 5.62    | 6.78 | 6.97 | 15.73     | 15.79 | 15.35 |
|         |  |                |                    | 3     | 6.76    | 6.26 | 6.89 | 15.63     | 15.92 | 15.63 |
|         |  |                |                    | 6     | 6.40    | 6.27 | 6.73 | 16.22     | 17.00 | 16.21 |
|         |  |                |                    | 12    | 6.53    | 6.77 | 6.64 | 16.43     | 16.32 | 16.15 |
|         |  | middle         | 13-24              | 1     | 6.22    | 6.56 | 6.30 | 15.00     | 15.60 | 15.50 |
|         |  |                |                    | 3     | 5.33    | 6.00 | 5.42 | 15.34     | 15.68 | 16.48 |
|         |  |                |                    | 6     | 6.90    | 5.10 | 6.23 | 16.10     | 15.72 | 15.06 |
|         |  |                |                    | 12    | 6.29    | 6.21 | 6.89 | 15.17     | 15.52 | 15.85 |
|         |  | bottom         | 25-36              | 1     | 5.55    | 6.84 | 6.81 | 15.53     | 16.13 | 15.71 |
|         |  |                |                    | 3     | 5.75    | 5.63 | 5.94 | 15.33     | 15.22 | 16.56 |
|         |  |                |                    | 6     | 6.58    | 6.01 | 5.10 | 15.84     | 15.11 | 15.92 |
|         |  |                |                    | 12    | 5.41    | 6.10 | 5.25 | 16.27     | 15.73 | 16.53 |
| L40     | Oct 7, 2021, 7:53 (UTC), 57.8304°N, 7.9981°E | surface        | 0-10               | 1     | 5.50    | 5.70 | 5.90 | 15.67     | 15.83 | 16.42 |
|         |  |                |                    | 3     | 6.08    | 5.04 | 6.97 | 15.86     | 16.08 | 15.39 |
|         |  |                |                    | 6     | 5.54    | 8.00 | 5.64 | 15.55     | 16.20 | 16.20 |
|         |  |                |                    | 12    | 6.16    | 6.69 | 5.39 | 16.07     | 16.93 | 16.44 |
|         |  | middle         | 11-20              | 1     | 5.75    | 5.40 | 5.76 | 15.25     | 16.84 | 16.30 |
|         |  |                |                    | 3     | 6.16    | 5.59 | 7.00 | 15.11     | 15.03 | 16.47 |
|         |  |                |                    | 6     | 6.08    | 6.54 | 5.52 | 15.00     | 15.34 | 15.38 |
|         |  |                |                    | 12    | 6.53    | 6.91 | 5.22 | 16.66     | 15.78 | 16.42 |
|         |  | bottom         | 21-30              | 1     | 6.46    | 5.30 | 5.62 | 15.46     | 16.47 | 16.10 |
|         |  |                |                    | 3     | 6.69    | 5.59 | 6.64 | 16.58     | 16.36 | 15.49 |
|         |  |                |                    | 6     | 6.18    | 6.10 | 5.45 | 15.24     | 15.40 | 15.21 |
|         |  |                |                    | 12    | 5.83    | 6.73 | 5.60 | 15.55     | 16.59 | 16.62 |

Table A 8 Validation of trace metal analysis in sediments for chapter 6.3.

|                        | element                                    | As                    | Cu                  | Fe                            | Mn                      | Mo                    | Ni                  | Pb                    |
|------------------------|--|-----------------------|---------------------|-------------------------------|-------------------------|-----------------------|---------------------|-----------------------|
|                        | isotope                                    | 75                    | 65                  | 56                            | 55                      | 95                    | 60                  | 208                   |
| blanks<br>(n=42)       | blank /<br>$\mu\text{g L}^{-1}$            | 200 $\pm$<br>130      | 400 $\pm$<br>1100   | 30000 $\pm$<br>90000          | 300 $\pm$<br>700        | 24 $\pm$ 14           | 130 $\pm$<br>160    | 100 $\pm$<br>180      |
|                        | LOD /<br>$\mu\text{g kg}^{-1}$             | 600                   | 2500                | 300000                        | 2300                    | 65                    | 600                 | 640                   |
|                        | LOQ /<br>$\mu\text{g kg}^{-1}$             | 1520                  | 10900               | 900000                        | 6900                    | 162                   | 1700                | 1900                  |
| BCR-<br>2<br>(n=53)    | reference<br>value / $\mu\text{g kg}^{-1}$ | --                    | 19000 $\pm$<br>2000 | 9650000<br>0 $\pm$<br>1500000 | 1520000<br>$\pm$ 60000  | 248000 $\pm$<br>17000 | --                  | 11000 $\pm$<br>2000   |
|                        | measured<br>value / $\mu\text{g kg}^{-1}$  | --                    | 15200 $\pm$<br>1900 | 9000000<br>0 $\pm$<br>7000000 | 1540000<br>$\pm$ 130000 | 268000 $\pm$<br>25000 | --                  | 10400 $\pm$<br>1000   |
|                        | recovery / %                               | --                    | 80 $\pm$ 10         | 93 $\pm$ 7                    | 101 $\pm$ 9             | 108 $\pm$ 10          | --                  | 95 $\pm$ 9            |
| GBW<br>07311<br>(n=51) | reference<br>value / $\mu\text{g kg}^{-1}$ | 188000 $\pm$<br>13000 | 79000 $\pm$<br>3000 | --                            | 2490000<br>$\pm$ 84000  | 5900 $\pm$<br>600     | 14300 $\pm$<br>1000 | 636000 $\pm$<br>22000 |
|                        | measured<br>value / $\mu\text{g kg}^{-1}$  | 185000 $\pm$<br>12000 | 68000 $\pm$<br>7000 | --                            | 2420000<br>$\pm$ 180000 | 7000 $\pm$<br>400     | 13800 $\pm$<br>1700 | 670000 $\pm$<br>60000 |
|                        | recovery / %                               | 98 $\pm$ 6            | 86 $\pm$ 9          | --                            | 97 $\pm$ 7              | 119 $\pm$ 7           | 97 $\pm$ 12         | 105 $\pm$ 9           |
| QC<br>(n=56)           | reference<br>value / $\mu\text{g L}^{-1}$  | 250.0 $\pm$<br>12.5   | 25.0 $\pm$<br>1.3   | 250 $\pm$ 13                  | 25.0 $\pm$<br>1.3       | 25.0 $\pm$<br>1.3     | 25.0 $\pm$<br>1.3   | 25.0 $\pm$<br>1.3     |
|                        | measured<br>value / $\mu\text{g L}^{-1}$   | 235 $\pm$ 19          | 22.9 $\pm$<br>2.5   | 224 $\pm$ 18                  | 23.1 $\pm$<br>2.2       | 23.9 $\pm$<br>1.6     | 23 $\pm$ 3          | 24.6 $\pm$<br>2.4     |
|                        | recovery / %                               | 94 $\pm$ 8            | 92 $\pm$ 10         | 90 $\pm$ 7                    | 92 $\pm$ 9              | 96 $\pm$ 6            | 92 $\pm$ 12         | 98 $\pm$ 10           |

Table A 9 Validation of trace metal analysis in seawater for chapter 6.3. Two different concentrations of QC in-house multi-element standard were measured.

|                    | element                                | Cd                 | Cu                 | Fe                | Mn                | Mo                 | Ni                | Pb                 |
|--------------------|--|--------------------|--------------------|-------------------|-------------------|--------------------|-------------------|--------------------|
|                    | isotope                                | 111                | 65                 | 56                | 55                | 95                 | 60                | 208                |
| aerobic<br>(n=3)   | blank / $\text{ng L}^{-1}$             | 9.4 $\pm$ 0.8      | 246.8 $\pm$<br>1.3 | 164 $\pm$ 9       | 73.2 $\pm$<br>1.3 | 13.7 $\pm$<br>1.1  | 11.3 $\pm$<br>0.5 | 3.56 $\pm$<br>0.22 |
|                    | LOD / $\text{ng L}^{-1}$               | 11.8               | 250.7              | 191               | 77.1              | 16.9               | 12.8              | 4.22               |
|                    | LOQ / $\text{ng L}^{-1}$               | 17.3               | 259.8              | 252               | 86.1              | 24.3               | 16.1              | 5.75               |
| anaerobic<br>(n=3) | blank / $\text{ng L}^{-1}$             | 0.70 $\pm$<br>0.08 | 32.9 $\pm$<br>1.2  | 111 $\pm$ 9       | 10.6 $\pm$<br>0.6 | 5.02 $\pm$<br>0.27 | 6.6 $\pm$ 1.0     | 4.08 $\pm$<br>0.05 |
|                    | LOD / $\text{ng L}^{-1}$               | 0.94               | 36.5               | 139               | 12.4              | 5.82               | 9.5               | 4.22               |
|                    | LOQ / $\text{ng L}^{-1}$               | 1.49               | 44.8               | 203               | 16.4              | 7.69               | 16.1              | 4.54               |
| QC low             | measured<br>value / $\text{ng L}^{-1}$ | 25.2 $\pm$<br>1.4  | 25.0 $\pm$<br>1.4  | 250 $\pm$ 40      | 26.9 $\pm$<br>2.4 | 26.8 $\pm$<br>2.1  | 25.7 $\pm$<br>1.1 | 26.0 $\pm$<br>0.8  |
|                    | recovery / %                           | 101 $\pm$ 6        | 100 $\pm$ 6        | 99 $\pm$ 14       | 107 $\pm$ 10      | 107 $\pm$ 8        | 103 $\pm$ 5       | 104 $\pm$ 3        |
|                    | n                                      | 18                 | 18                 | 17                | 16                | 18                 | 18                | 18                 |
| QC high            | measured<br>value / $\text{ng L}^{-1}$ | 257 $\pm$ 11       | 255 $\pm$ 14       | 2500 $\pm$<br>170 | 258 $\pm$ 14      | 266 $\pm$ 15       | 257 $\pm$ 13      | 256 $\pm$ 14       |
|                    | recovery / %                           | 103 $\pm$ 5        | 102 $\pm$ 6        | 100 $\pm$ 7       | 103 $\pm$ 6       | 106 $\pm$ 6        | 103 $\pm$ 5       | 103 $\pm$ 6        |
|                    | n                                      | 56                 | 56                 | 56                | 56                | 56                 | 56                | 55                 |
| NASS-7             | measured<br>value / $\text{ng L}^{-1}$ | 14.9 $\pm$<br>0.7  | 195 $\pm$ 11       | 375 $\pm$ 25      | 790 $\pm$ 40      | 8200 $\pm$<br>300  | 253 $\pm$ 15      | 2.61 $\pm$<br>0.12 |
|                    | recovery / %                           | 92 $\pm$ 4         | 98 $\pm$ 5         | 107 $\pm$ 7       | 105 $\pm$ 5       | 88 $\pm$ 4         | 102 $\pm$ 6       | 100 $\pm$ 5        |
|                    | n                                      | 15                 | 15                 | 15                | 15                | 15                 | 15                | 15                 |

Table A 10  $\delta^{98/95}\text{Mo}$  values for the analyzed reference materials in chapter 6.3.

| reference material | $\delta^{98/95}\text{Mo} / \text{‰}$ | SD / ‰ | <i>n</i> |
|--------------------|--------------------------------------|--------|----------|
| GBW07311           | 0.31                                 | 0.08   | 3        |
| BCR-2              | -0.10                                | 0.06   | 3        |
| IAPSO              | 1.90                                 | 0.05   | 5        |
| SRM 3134           | -0.04                                | 0.10   | 4        |

Table A 11 Validation of porewater analysis for chapter 6.3.

|                      | Element                                | As          | Fe          | Mn          | Mo            |
|----------------------|--|-------------|-------------|-------------|---------------|
|                      | isotope                                | 75          | 56          | 55          | 95            |
|                      | LOD / $\mu\text{g L}^{-1}$             | 0.10        | 1.0         | 0.8         | 0.16          |
|                      | LOQ / $\mu\text{g L}^{-1}$             | 0.32        | 3.2         | 2.2         | 0.48          |
| QC ( <i>n</i> =8)    | reference value / $\mu\text{g L}^{-1}$ | 250 ± 12.5  | 250 ± 12.5  | 25 ± 1.25   | 25 ± 1.25     |
|                      | measured value / $\mu\text{g L}^{-1}$  | 237 ± 20    | 237 ± 23    | 25.1 ± 2.4  | 24 ± 3        |
|                      | recovery / %                           | 95 ± 8      | 95 ± 9      | 101 ± 9     | 97 ± 12       |
| CASS6 ( <i>n</i> =3) | reference value / $\mu\text{g L}^{-1}$ | 1.04 ± 0.1  | 1.56 ± 0.12 | 2.22 ± 0.12 | 9.15 ± 0.52   |
|                      | measured value / $\mu\text{g L}^{-1}$  | 1.07 ± 0.17 | 2.26 ± 0.22 | 2.80 ± 0.27 | 13.8 ± 0.7    |
|                      | recovery / %                           | 103 ± 17    | 145 ± 14    | 126 ± 12    | 151 ± 8       |
| SLRS6 ( <i>n</i> =3) | reference value / $\mu\text{g L}^{-1}$ | 0.57 ± 0.08 | 84.3 ± 3.6  | 2.12 ± 0.1  | 0.215 ± 0.018 |
|                      | measured value / $\mu\text{g L}^{-1}$  | 0.71 ± 0.08 | 86 ± 13     | 2.2 ± 0.3   | 0.219 ± 0.028 |
|                      | recovery / %                           | 125 ± 14    | 102 ± 15    | 105 ± 15    | 102 ± 13      |



## 10 Danksagungen

Beim Schreiben dieser Arbeit haben mich viele Kollegen, Freunde und Familienmitglieder unterstützt, mich ermutigt und mir immer wieder gezeigt, was möglich ist. An dieser Stelle möchte ich die Gelegenheit nutzen, mich bei einigen dieser Personen zu bedanken.

Mein erster Dank geht an Dr. Daniel Pröfrock für die Möglichkeit, in einer wunderbaren Abteilung zu arbeiten und zu promovieren. Vielen Dank, dass du bei Problemen und Fragen immer direkt unterstützt hast, sowohl im Labor als auch beim Schreiben. Du hast mir viele Freiräume gegeben und es immer möglich gemacht, an Konferenzen, Forschungsaufenthalten und Kampagnen teilzunehmen. Ich weiß, dass das nicht selbstverständlich ist und habe mich daher umso mehr über diese vielfältigen Möglichkeiten gefreut.

Vielen Dank an Dr. Tina Sanders für die Co-Betreuung meiner Arbeit. Danke, dass du mit mir durch die Höhen und Tiefen von CARBOSTORE gegangen bist. Du hattest es nicht immer einfach mit uns Chemikern, aber du hast mir die Möglichkeit gegeben, über den Tellerrand der Metalle hinauszuschauen.

An dieser Stelle möchte ich mich auch bei Prof. Dr. Michael Steiger, Dr. Kirstin Dähnke und Assoz. Prof. Dr. Johanna Irrgeher für die konstruktiven Diskussionen bei meinen Panel Meetings bedanken.

Danke Dr. Tristan Zimmermann, dass du immer einen realistischen Blick auf meine Zeitplanung und ein offenes Ohr für meine Fragen hattest. Ohne die zahlreichen Diskussionen über Abstracts, Publikationen, Daten und Präsentationen hätte ich mich oft verloren gefühlt.

Danke Dr. Ole Klein, dass du immer zur Stelle warst, wenn auf der Strecke zwischen vorbereiteter Probe und statistisch korrekt ausgewertetem Datensatz irgendwas nicht funktioniert hat. Du warst immer zur Stelle, egal ob das Problem vor oder hinter dem Bildschirm saß.

KUA, jede und jeder einzelne von euch hat dazu beigetragen, dass ich mich von Anfang an bei euch wohlfühlt habe. Danke, dass ihr immer ein offenes Ohr hattet und bereit wart, mir zu helfen. Dabei war es egal, ob ich Proben aus der letzten Ecke des Kühlraums brauchte oder ein Gerät ebendiese Proben nicht messen wollte. Es hat mir Spaß gemacht, mit euch zu arbeiten! Insbesondere möchte ich mich bei Andrea Pieper, Svenja Faust und Bettina Rust

bedanken. Ihr habt mir immer mit Rat und Tat zur Seite gestanden, auch wenn ich die 15. Person war, die in eurer Tür stand. Als kurzzeitige Mitglieder von KUA möchte ich mich auch bei Clara Witthoff, Beatrice Aleksiejus, Maurice Brogmus und Süeda Öztürk bedanken. Ihr habt mir geholfen, durch den undurchdringbaren Dschungel von CARBOSTORE-Proben zu kommen.

Außerdem möchte ich mich bei den Menschen bedanken, die mich in ihren Laboren aufgenommen oder bei Probenahmen begleitet haben. Hierzu zählt die Abteilung KCN, da ich mit meinen Inkubationen bei euch arbeiten durfte und Leon Schmidt, da du die zahlreichen Nährstoffproben gemessen hast. Außerdem danke ich Carola Lehnert und Matthias Birkicht für die Unterstützungen bei meinen Messungen und Prof. Dr. Michael Wieser für die wunderbare Zeit im Isotopenlabor in Calgary. Natürlich dürfen hier auch die CARBOSTORE Mitglieder nicht fehlen – vielen Dank Andrea, Carla, Micha und Wiebke für die großartigen Probenahmen im Watt.

Paddy, du warst seit dem ersten Tag des Studiums immer an meiner Seite und hast die Erfolge mit mir gefeiert. Aber noch viel wichtiger ist, dass du auch an allen anderen Tagen – den langen, stressigen, verzweifelten und aussichtslosen – an meiner Seite warst. Du hast für mich gekocht und mich immer wieder aus dem Trott geholt, um mit mir den Alltag zu feiern. Und du bist sogar bei den meisten Probevorträgen überwiegend wach geblieben. Ich danke dir!

Am Ende möchte ich mich noch bei den Menschen bedanken, die sich nicht wirklich vorstellen können, womit ich die letzten Jahre verbracht habe, die aber trotzdem immer für mich da waren. Dazu gehören die vielen Freunde, mit denen ich so viele schöne Momente erlebt habe und neue Kraft tanken konnte. Danke an meine Geschwister, die Rostocker, an Amrei, Nele, Patricia und Sofia. Außerdem möchte ich mich an dieser Stelle bei meinen Eltern und Großeltern bedanken. Ihr habt mich immer meinen Weg gehen lassen und an mich geglaubt. Danke, dass ich mich auf eure Unterstützung verlassen kann und dass ihr mir den Rücken stärkt.



## 11 Eidesstattliche Versicherung

Hiermit erkläre ich, Anna Theresa Siems, geb. Przibilla, an Eides statt, dass ich die vorliegende Dissertationsschrift mit dem Titel „*A trace metal perspective on biogeochemical processes in the North Sea*“ selbst verfasst und keine anderen als die angegebenen Quellen und Hilfsmittel benutzt habe. Ich versichere, dass die gebundenen Exemplare der Dissertation und das in elektronischer Form eingereichte Dissertationsexemplar und das bei der Fakultät zur Archivierung eingereichte gedruckte gebundene Exemplar der Dissertationsschrift identisch sind. Diese Arbeit ist in gleicher oder ähnlicher Form an keiner anderen Universität als Promotionsarbeit eingereicht worden und es wurden zuvor keine weiteren Promotionsversuche von mir vorgenommen.

Anna Theresa Siems

*A. Siems*

---

Geesthacht, den 09.07.2024